Università degli Studi di Palermo

AREA RICERCA E TRASFERIMENTO TECNOLOGICO
SETTORE DOTTORATI E CONTRATTI PER LA RICERCA
U. O. DOTTORATI DI RICERCA

Matematica e Scienze Computazionali

Dipartimento di Matematica e Informatica

MAT 07

Models for charge transport in semiconductors

LA DOTTORESSA: **Giorgia Vitanza**

COORDINATRICE: **Prof.ssa Maria Carmela Lombardo**

TUTOR: **Prof. Vittorio Romano**

CO RELATORE: **Dott. Vito Dario Camiola**

Ciclo XXXVI

ANNO ACCADEMICO 2022/2023

Contents

Acknowledgements

I would like to thank my supervisor Prof. Vittorio Romano to give me the opportunity to undertake this path and to improve my knowledges and my managment and organization skills. A big thanks to my colleagues Giovanni Nastasi, Dario Camiola, Giulia Aliffi and Carla Perrone to share with me their knolwedges and to support me in good and bad situations.

I feel grateful for each person I met during these almost four years, for all the moments spent together, for all the beautiful places I visited, for everything I learned, for everything I taught with the hope to have left something of me in each of you.

The PhD experience is not always easy, but for each failure something good follows, therefore never give up! Thank you to my friends and to my family, always besides me. Last, but not least, thank you to my self for going on against everything and everyone overcoming big and small obstacles and reaching my goal with determination. I tried to take the maximum from this experience and now I feel to be a new person, with more awareness but always full of will to go forward towards new aims.

List of Symbols.

$[\cdot,\cdot]$	commutator.
$\{\cdot,\cdot\}$	Poisson parenthesis.
$C^\infty(\mathbb{R})$	the set of infinitely derivable functions with domain $\mathbb{R}$.
$\langle\cdot,\cdot\rangle$	scalar product.
$Dom(A)$	domain of a function A associated to an operator.
$L^2(A,B)$	set of summable square functions $f : A \longrightarrow B$, for Lebesgue measure theory.
$\hbar$	reduced Planck constant.
k_B	Boltzmann constant.
∇	gradient.
$\nabla\cdot$	divergence.

Introduction

In the last years, the miniaturization of the electronic devices became a very challenging topic. So, the mathematical models that describe transport phenomena in semiconductors have a crucial role and are the focus of this thesis. In particular semiclassical and quantum hydrodynamical, drift diffusion and energy transport models will be devised and discussed.

The structure of the thesis is the following: in Chapter 1 we introduce the Weyl Quantization and the Moyal Calculus; in Chapter 2 the main features of solid state matter are recalled, in particular the crystal properties with a special focus on graphene; in Chapter 3 phonons and electrons transport is introduced and in Chapter 4 the maximum entropy approach to close the moments equations is explained. The original contribution starts from the Chapter 5 in which an optimized hydrodynamical model is presented. In Chapter 6 there is the original part regarding a quantum corrected transport model for phonons obtained from the Wigner equation. In Chapter 7 the Wigner approach is used also for electrons transport. In Chapter 8 there are original results about an optimized quantum drift diffusion model for a Resonant Tunneling Diode.

The papers strictly related to the thesis and already published are the following:

- *Camiola, V.D., Nastasi, G., Romano, V., Vitanza, G. (2022), "Optimized Hydrodynamical Model for Charge Transport in Graphene" In: Ehrhardt, M., Günther, M. (eds) Progress in Industrial Mathematics at ECMI 2021. ECMI 2021. Mathematics in Industry(), vol 39. Springer, Cham. https://doi.org/10.1007/978-3-031-11818-0_37* (see Chapter 5);

- *Camiola, V.D., Romano, V. & Vitanza, G., "Wigner Equations for Phonons Transport and Quantum Heat Flux" J Nonlinear Sci 34, 10 (2024). https://doi.org/10.1007/s00332-023-09993-z* (see Chapter 6);

- *Muscato, O., Nastasi, G., Romano, V., Vitanza, G., (2024), "Optimized quantum drift diffusion model for a resonant tunneling diode", Journal of Non-Equilibrium Thermodynamics, 2024. https://doi.org/10.1515/jnet-2023-0059.* (see Chapter 8).

In addition also other two topics have been developed during my Ph.D. course. The first one is a model to fit a real dataset about infected, susceptible and recovered people, considering the vaccine effect and comparing the different measures taken by the governments during the COVID pandemic (see chapter 9, first section). This work has been published in *Nastasi, G.; Perrone, C.; Taffara, S.; Vitanza, G. "A Time-Delayed Deterministic Model for the Spread of COVID-19 with Calibration on a Real Dataset" Mathematics 2022, 10, 661. https://doi.org/10.3390/math10040661.* The second one is an accepted paper developed during my period in STMicroelectronics, in Prague. The subject of this last work is the development of an automated flow, implemented in Python, to appropriately place the analog and digital devices in integrated circuits, trying to optimize the area utilization and to respect all the constraints given for the electric components inside the circuits. Usually, this procedure is performed by hand in the engineering design centers. We have improved this approach by using machine learning and artificial intelligence techniques. This activity has been developed within the European MSCA-Raise project *AMBEATion* (see chapter 9, second section).

The content of chapter 7 is the matter of a preprint.

Chapter 1

From Weyl Quantization to Moyal calculus

The use of the Wigner function is one of the most promising ways to study quantum transport. Its main advantage is that a description similar to the classical or semiclassical transport is obtained in a suitable phace-space. The mean values are expectation values with respect to the Wigner function as it would be a probability density and the semiclassical limit of the Wigner transport equation recovers, at least formally, the Boltzmann transport one. There is a huge body of literature regarding the Wigner equation and the way to numerically solve it (see for example [1–3] and references therein). However, the most part of the works in the subject consider a quadratic dispersion relation for the energy. Instead, for several material like semiconductors or semimetal, e.g. graphene, other dispersion relations must be considered [4, 5, 7, 8]. From the Wigner transport equation quantum hydrodynamical models have been obtained in [9] for charge transport in silicon in the case of parabolic bands, while in [10] the same has been devised for electrons moving in graphene including quantum effects as second order corrections in the scaled Planck constant arising from the equilibrium Wigner function at the same temperature of a thermal bath of phonons.

To treat the Wigner function one has to start with the Weyl's quantization scheme [11], that is a corrispondence between quantum-mechanical operators in Hilbert space and ordinary functions in phase space.

There are also alternative paths to deal with the quantization: the standard one utilizing operators in Hilbert space, developed by Heisenberg, Schrödinger, Dirac, and others in the 1920s; another one was introduced by Dirac and constructed by Feynman and it is based on path integrals [12].

But which are the advantages of following the Wigner-Weyl approach? As it is known, the usual procedure (map) which associates to a classic function

defined on the phase space a quantum operator is affected by ambiguity problems. Indeed it's not enough to think that to solve this association we simply can correlate a classic function to an operator, beacause this procedure leads to a partially correct theory. The minimal requests on the previous map are:

- the map is linear in its arguments;
- the identical operator is associated to the constant function of value one;
- the map returns a self-adjoint operator;

In addition to these simple rules, we would like to verify that our quantization hypothesis are physically meaningful. From a methematical point of view, the Weyl map is properly an original and mathematically rigorous solution to these requests, in particular thanks to its invertibility and to the Moyal product that allows to expand and to generalize the Poisson parenthesis in the quantum theory.

At the end, to summarize, we can say that the Weyl quantization has several advantages:

- Preservation of Symmetry: Weyl quantization preserves the symmetries of the classical system. In particular, it respects the symplectic structure of the classical phase space. This is important because symmetries often play a crucial role in the understanding of physical systems.
- Compatibility with Canonical Commutation Relations: The Weyl quantization naturally leads to quantum operators that satisfy the canonical commutation relations. This is essential for maintaining consistency with the fundamental principles of quantum mechanics.
- Correspondence Principle: The Weyl quantization satisfies the correspondence principle, which states that quantum mechanics should reduce to classical mechanics in the limit of large quantum numbers or high energies. This makes Weyl quantization a suitable framework for connecting classical and quantum descriptions of a system.
- Unitary Equivalence: Operators obtained through Weyl quantization are unitarily equivalent to the corresponding classical observables. This means that the transformation preserves the inner product structure of the Hilbert space, which is a desirable property in quantum mechanics.
- Mathematical Simplicity: The Weyl quantization procedure is mathematically straightforward and elegant. It provides a clear and systematic way to map classical functions on phase space to quantum operators.

- Generalization to Higher Dimensions: Weyl quantization can be easily extended to systems with higher dimensions, making it versatile for applications in various physical scenarios.
- Applications in Quantum Field Theory: Weyl quantization is often employed in the quantization of classical field theories, providing a bridge between classical and quantum descriptions of fields.

Despite all these advanteges, the choice of quantization method often depends on the specific properties of the system under consideration and the mathematical convenience of the chosen approach. In our case, the Weyl's quantization and the Wigner function will be crucial for the development of this thesis, then in the following we will introduce some preliminary definitions and theorems, in order to explain in a rigorous way all the advantages already listed.

In particular, the comparison with some common quantization schemes will be analyzed in Section 1.1 and in Section 1.2 the Weyl quantization will be deeply explained, with a special focus on the Moyal product.

1.1 Some Common Quantization Schemes

The first point to clarify before moving on is: "What does the word quantization mean?". In few and simple words, the quantization is the mathematical procedure that maps a classic state (information about the system given by the measurements of this one) into a quantum state, that is represented by a unit vector ψ in an appropriate Hilbert space H. If ψ_1 and ψ_2 are two unit vectors in H with $\psi_2 = c\psi_1$ for some constant $c \in \mathbb{C}$, then ψ_1 and ψ_2 represent the same quantum physical state. This last sentence could be translated mathematically in different ways, then the answer exists but it's not unique! Actually there are different definitions for the quantization scheme (see [13]), but only the most common ones will be reported here.

The most common possible descriptions of a system in quantum mechanics are in terms of coordinates or in terms of momentum [14].

Definition 1 Coordinates representation *For a particle moving in $\mathbb{R}^3$, let the quantum Hilbert space be $L^2(\mathbb{R}^3)$ and define the position and momentum operators X_j and P_j, $j = 1, 2, 3$, by*

$$X_j\psi(\mathbf{x}) = x_j\psi(\mathbf{x}), \quad P_j\psi(\mathbf{x}) = -i\hbar\frac{d\psi(\mathbf{x})}{dx_j}. \tag{1.1}$$

Definition 2 Momentum representation *For a particle moving in $\mathbb{R}^3$, let the quantum Hilbert space be $L^2(\mathbb{R}^3)$ and define the position and momentum operators X_j and P_j, $j = 1, 2, 3$, by*

$$P_j\psi(\mathbf{p}) = p_j\psi(\mathbf{p}), \quad X_j\psi(\mathbf{p}) = -i\hbar\frac{d\psi(\mathbf{p})}{dp_j}. \tag{1.2}$$

By the von Neumann Stone theorem, these representations are unitarily equivalent; that is, there is a unitary transformation

$$\psi(\mathbf{x}) \xrightarrow{W} \psi(\mathbf{p})$$

such that the operators defined by (1.2) are transformed into the operators (1.1). It is not hard to see that the Fourier transformation

$$\psi(\mathbf{x}) = \left(\frac{1}{2\pi h}\right)^{\frac{3}{2}} \int_{\mathbb{R}^3} e^{\frac{i}{h}\mathbf{px}}\psi(\mathbf{p})d\mathbf{p},$$
$$\psi(\mathbf{p}) = \left(\frac{1}{2\pi h}\right)^{\frac{3}{2}} \int_{\mathbb{R}^3} e^{-\frac{i}{h}\mathbf{px}}\psi(\mathbf{x})d\mathbf{x}.$$

is such a transformation (see [14]). Neither the position nor the momentum operator is defined as mapping the entire Hilbert space $L^2(\mathbb{R}^3)$ into itself. Indeed, for $\psi \in L^2(\mathbb{R}^3)$, the function $x_j\psi(\mathbf{x})$ may fail to be in $L^2(\mathbb{R}^3)$. Similarly, a function $\psi \in L^2(\mathbb{R}^3)$ may fail to be differentiable, and even if it is differentiable, the derivative may fail to be in $L^2(\mathbb{R}^3)$. This means that X_j and P_j are unbounded operators [1]. They are defined on suitable dense subspaces $Dom(X_j)$ and $Dom(P_j)$ of $L^2(\mathbb{R}^3)$. A vitally important property of this pair of operators is that they do not commute.

Proposition 1 *The position and momentum operators X_i and P_j do not commute, but satisfy the relation*

$$X_iP_j - P_jX_i = i\hbar\delta_{ij}, \tag{1.3}$$

This relation is known as the canonical commutation relation.

Given that, the easiest systems with one degree of freedom and with classic observables, that are polynomials in x (position) and p (momentum), will be presented. The domain for all of our operators is $C^\infty(\mathbb{R})$.

One of the problems that arises from the definition of quantization scheme is that we are considering operators that may not to be essentially self-adjoint and this could lead to not real eigenvalues, even if they are symmetric, therefore the definitions has to take into account this issue. For example, the operator $P^2 - cX^4$, for $c > 0$, is not essentially self-adjoint on $C^\infty(\mathbb{R})$.

The simplest approach to quantization is to choose which operator put first, the position or the momentum operator. If we put the momentum operators to the right, it is acting first, and the position operators to the left it is acting second. In this approach, a polynomial in x and p will be quantized to a differential operator in "standard form", with all the derivatives acting first, followed by multiplication operators.

[1] An operator A is unbounded if there is no constant C such that $||A\psi|| \leq C||\psi|| \quad \forall\psi$.

In harmonic analysis, there is a method for extending this quantization scheme to more-or-less arbitrary symbols[2], f. For a general (nonpolynomial) symbol f, the resulting operator $\hat{f}$ is known as a pseudodifferential operator.

Let's analyze some quantization definition:

Definition 3 Pseudodifferential operator quantization:

$$Q(x^j p^k) = X^j P^k.$$

The limit of this definition is that even when the symbol f is real-valued, the operator $\hat{f}$ is typically not self-adjoint (or even symmetric). If, for example, $f(x,p) = xp$, then the associated operator is XP, the adjoint of which is PX, which is not equal to XP. The simplest way to fix this problem is to symmetrize the operator by taking half the sum of the operator and its adjoint. From this idea arises the following definition:

Definition 4 Symmetrized pseudodifferential operator quantization:

$$Q(x^j p^k) = \frac{1}{2}(X^j P^k + P^k X^j).$$

But also in this case, we don't have a definition general enough. The Weyl quantization, instead, takes into account all possible orderings of X and P. For example, x^2p^2 will be quantized by the Weyl quantization as follows

$$\frac{1}{6}(X^2P^2 + XPXP + XP^2X + PX^2P + PXPX + P^2X^2).$$

For a general monomial, the Weyl quantization similarly averages all the possible orderings of the position and momentum operators.

Definition 5 Weyl quantization:

By starting from a scheme that is uniquely determined-as a map from polynomials on $\mathbb{R}^2$ into operators on $C^\infty(\mathbb{R})$, we can define the Weyl quantization:

$$Q(x^j p^k) = \frac{1}{(j+k)!} \sum_{\sigma \in S_{j+k}} \sigma(X, X, ..., X, P, P, ..., P),$$

where for any operators $A_1, A_2, ..., A_n$ and any $\sigma \in S_n$, we define

$$\sigma(A_1, A_2, ..., A_n) = A_{\sigma(1)} A_{\sigma(2)} \cdots A_{\sigma(n)}. \tag{1.4}$$

where S_n is the set of the all possible orderings of n operators.

In the applications, the most useful quantization scheme is Weyl scheme and in the following we will see the advantages of this approach. All of the definitions of quantization schemes, except for the pseudodifferential operator quantization, have the property of mapping real-valued polynomials to symmetric operators on $C^\infty(\mathbb{R})$.

[2]phase-space functions.

Observation 1 *It is important to recognize that two different expressions may describe the same operator. We may calculate, for example, that*

$$\frac{1}{2}(XP^2 + P^2X) = \frac{1}{2}(PXP + [X,P]P + PXP - P[X,P]) = PXP,$$

since $[X,P]$ *is a multiple of the identity and thus commutes with* P*. As a result, we can eliminate the* PXP *term in the Weyl quantization of* xp^2*, with the result that*

$$Q(xp^2) = \frac{1}{3}(XP^2 + PXP + P^2X) = \frac{1}{2}(XP^2 + P^2X), \tag{1.5}$$

which coincides, in this very special case, with the symmetrized pseudodifferential quantization of xp^2*.*

$Op_\hbar$ indicates the Weyl quantization, in order to underline the operatorial nature of the "object" with which we are dealing and also the dependence on the constant $\hbar$ (Planck reduced constant) that will be useful when we will use the expansion of quantum operator and the Moyal calculus.

Proposition 2 *The Weyl quantization -viewed as a linear map of the space of polynomials on* $\mathbb{R}^2$ *into operators on* $C^\infty(\mathbb{R})$*- is uniquely characterized by the following identity:*

$$Op_\hbar((ax+bp)^j) = (aX+bP)^j \tag{1.6}$$

for all non-negative integers j *and all* $a, b \in \mathbb{C}$*.*

The proof is taken from [13].

Proof. The Weyl quantization satisfies the identity

$$Op_\hbar((a_1x+b_1p)\cdots(a_jx+b_jp)) = \frac{1}{j!}\sum_{\sigma\in S_j}\sigma(a_1X+b_1P, ..., a_jX+b_jP), \tag{1.7}$$

for all sequences $a_1, ..., a_j$ and $b_1, ..., b_j$ of complex numbers, where the expression $\sigma(\cdot,\cdot,...,\cdot)$ is defined by (1.4). Specializing to the case where all the a_j's are equal to a and all the b_j's are equal to b gives (1.6).

Conversely, suppose that Q is any linear map of polynomials into operators on $C^\infty(\mathbb{R})$ satisfying $Q((ax+bp)^j) = (aX+bP)^j$ for all a, b, and j. For each j, let V_j denote the space of homogeneous polynomials f of degree j such that $Q(f) = Op_\hbar(f)$. Then V_j contains all polynomials of the form $(ax+bp)^j$, and thus, V_j consists of all homogeneous polynomials of degree j, so that $Q = Op_\hbar$. □

Proposition 3 *The Weyl quantization satisfies*

$$Op_\hbar(xg) = Op_\hbar(x)Op_\hbar(g) - \frac{i\hbar}{2}Op_\hbar\left(\frac{\partial g}{\partial p}\right) \tag{1.8}$$

$$= Op_\hbar(g)Op_\hbar(x) + \frac{i\hbar}{2}Op_\hbar\left(\frac{\partial g}{\partial p}\right) \tag{1.9}$$

and

$$Op_\hbar(pg) = Op_\hbar(p)Op_\hbar(g) + \frac{i\hbar}{2}Op_\hbar\left(\frac{\partial g}{\partial x}\right) \tag{1.10}$$

$$= Op_\hbar(g)Op_\hbar(p) - \frac{i\hbar}{2}Op_\hbar\left(\frac{\partial g}{\partial x}\right) \tag{1.11}$$

for all polynomials g in x and p.

Observation 2 *The formulas for the Weyl quantization in Proposition 3 may not give the same "expression" for $Op_\hbar(f)$ as does Definition 5, but it gives the same operator.*

The proof is extracted from [13].

Proof. Suppose $A = (a_1X + b_1P)$ and $B = (a_2X + b_2P)$. Then $[A, B]$ is a multiple of I, from which we can easily verify that

$$AB^j = B^kAB^{j-k} + k[A, B]B^{j-1}, \quad 0 \le k \le j.$$

If we sum this relation over k and divide by $j + 1$, we obtain

$$AB^j = \frac{1}{j+1}\sum_{k=0}^{j} B^kAB^{j-k} + \frac{1}{j+1}\frac{j(j+1)}{2}[A, B]B^{j-1}. \tag{1.12}$$

Now, A is the Weyl quantization of (a_1x+b_1p) and B^j is the Weyl quantization of $(a_2x+b_2p)^j$, and both terms on the right-hand side of (1.12) are easily recognized as Weyl quantizations. Thus, after rearranging the terms and evaluating the commutator, (1.12) becomes,

$$Op_\hbar((a_1x + b_1p)(a_2x + b_2p)^j) = Op_\hbar(a_1x + b_1p)Op_\hbar((a_2x + b_2p)^j)$$

$$-\frac{i\hbar j}{2}(a_1b_2 - a_2b_1)Op_\hbar((a_1x + b_1p)^{j-1}). \tag{1.13}$$

Meanwhile, if we run the same argument starting with B^jA we obtain a similar result:

$$Op_\hbar((a_1x + b_1p)(a_2x + b_2p)^j) = Op_\hbar((a_2x + b_2p)^j)Op_\hbar(a_1x + b_1p)$$

$$+\frac{i\hbar j}{2}(a_1b_2 - a_2b_1)Op_\hbar((a_1x + b_1p)^{j-1}). \tag{1.14}$$

If we specialize to the case $(a_1, b_1) = (1, 0)$ and $(a_2, b_2) = (a, b)$, we get

$$Op_\hbar(x(ax + bp)^j) = Op_\hbar(x)Op_\hbar((ax + bp)^j) - \frac{i\hbar j}{2}bOp_\hbar((ax + bp)^{j-1}), \tag{1.15}$$

where the last term on the right-hand side of (1.15) is $-i\hbar/2$ times the Weyl quantization of $\partial(ax+bp)^j/\partial p$. Thus, (1.15) is precisely (1.8) in the case $g(x, p) = (ax + bp)^j$. We can then see that (1.8) holds for all polynomials g. The proofs of (1.9), (1.10), and (1.11) are similar.□

1.2 The Weyl Quantization for $\mathbb{R}^{2d}$

At this point, we could wonder if the definitions and results obtained until now in the simplest case of polynomials on $\mathbb{R}^2$, can be generalized for a much larger class of symbols. We can start by generalizing from symbols defined on $\mathbb{R}^2$ to symbols defined on $\mathbb{R}^{2d}$, but before proceeding we need some preliminary theorems and observations.

1.2.1 Stone's Theorem

The commutation relation in exponential form is one of the crucial point for the Weyl's quantization: precisely the assumption of this different point of view will allow the resolution of a certain number of problems of the standard formulation of quantum mechanics. However, this exponential version only makes sense in light of Stone's theorem. Stone's result concerns one-parameter unitary groups and strongly continuous groups.

Definition 6 *Called H a generic Hilbert space and $U(H)$ the set of unitary operators acting on it, given the application U such that $U : \mathbb{R} \to U(H)$, U defines a* **unitary group with one parameter** *if $\forall t \in \mathbb{R}$ then $U(t)$ is unitary and $U(t+s) = U(t)U(s)$ $\forall s; t \in \mathbb{R}$, with the additional requirement that $U(0) = I$. Furthermore U is* **strongly continuous** *if $\forall \phi \in H$ it is true that*

$$U(t)\phi \to U(t_0)\phi,$$

when $t \to t_0$.

If U is a strongly continuous one-parameter unitary group, the infinitesimal generator of U is the operator A given by

$$A\phi = \lim_{t\to 0} \frac{1}{i} \frac{U(t)\phi - \phi}{t}, \tag{1.16}$$

with the domain of the operator A, $Dom(A)$, consisting of the set of $\phi \in H$ for which the limit in (1.16) exists in the norm topology on H. It is now possible to state Stone's theorem.

Theorem 1 *(Stone's) Suppose U is a strongly continuous one-parameter unitary group on H. Then the infinitesimal generator A of U is densely defined and self-adjoint, and $U(t) = \exp(itA)$ $\forall t \in \mathbb{R}$.*

This theorem introduce the idea of exponential operators, and this is the way that we want to follow to generalize the quantization procedure to more generic symbols. In the following, the idea will be explained in detail.

1.2.2 Some prelimanary observations to generalize the quantization procedure

For all $\mathbf{a}, \mathbf{b} \in \mathbb{R}^d$ and all non-negative integers j, we can easily think that the generalized Weyl quantization is defined as follows

$$Op_\hbar((\mathbf{a}\cdot\mathbf{x}+\mathbf{b}\cdot\mathbf{p})^j) = (\mathbf{a}\cdot\mathbf{X}+\mathbf{b}\cdot\mathbf{P})^j \tag{1.17}$$

If we want to extend $Op_\hbar$ to certain non polynomial symbols, we can use the concepts introduced in the previous paragraph and we will start to do some considerations on the complex exponentials, to explain the link between the generalization procedure and the Stone's theorem.

If we multiply (1.17) by $(i)^j/j!$ and sum on j, we would expect to have

$$Op_\hbar(\exp(i(\mathbf{a}\cdot\mathbf{x}+\mathbf{b}\cdot\mathbf{p}))) = \exp(i(\mathbf{a}\cdot\mathbf{X}+\mathbf{b}\cdot\mathbf{P})). \tag{1.18}$$

Now, if f is any sufficiently regular function on $\mathbb{R}^{2d}$, we can write f by using the Fourier anti-transform that involves functions like $\exp(i(\mathbf{a}\cdot\mathbf{x}+\mathbf{b}\cdot\mathbf{p}))$:

$$f(\mathbf{x},\mathbf{p}) = (2\pi)^{-n}\int_{\mathbb{R}^{2d}} \hat{f}(\mathbf{a},\mathbf{b})\exp(i(\mathbf{a}\cdot\mathbf{x}+\mathbf{b}\cdot\mathbf{p}))d\mathbf{a}d\mathbf{b},$$

where $\hat{f}$ is the Fourier transform of f. Putting together the (1.18) and this last expression of f, it seems natural to define

$$Op_\hbar(f) = (2\pi)^{-n}\int_{\mathbb{R}^{2d}} \hat{f}(\mathbf{a},\mathbf{b})\exp(i(\mathbf{a}\cdot\mathbf{X}+\mathbf{b}\cdot\mathbf{P}))d\mathbf{a}d\mathbf{b}, \tag{1.19}$$

Before proceeding, we will try to compute the operator $\exp(i(\mathbf{a}\cdot\mathbf{X}+\mathbf{b}\cdot\mathbf{P}))$.

If A and B are bounded operators that commute with their commutator (i.e., such that $[A,[A,B]] = [B,[A,B]] = 0$), then

$$\exp(A+B) = \exp(-[A,B]/2)\exp(A)\exp(B). \tag{1.20}$$

If we formally apply (1.20) with $A = i\mathbf{a}\cdot\mathbf{X}$ and $B = i\mathbf{b}\cdot\mathbf{P}$ (even though these are unbounded operators), we obtain

$$\exp(i(\mathbf{a}\cdot\mathbf{X}+\mathbf{b}\cdot\mathbf{P})) = \exp(i\hbar(\mathbf{a}\cdot\mathbf{b})/2)\exp(i\mathbf{a}\cdot\mathbf{X})\exp(i\mathbf{b}\cdot\mathbf{P}). \tag{1.21}$$

Meanwhile, we know that

$$(\exp(i\mathbf{b}\cdot\mathbf{P})\phi)(\mathbf{x}) = \phi(\mathbf{x}+\hbar\mathbf{b}).$$

Thus, we may deduce that

$$(\exp(i(\mathbf{a}\cdot\mathbf{X}+\mathbf{b}\cdot\mathbf{P}))\phi)(\mathbf{x}) = \exp(i\hbar(\mathbf{a}\cdot\mathbf{b})/2)\exp(i\mathbf{a}\cdot\mathbf{x})\phi(\mathbf{x}+\hbar\mathbf{b}). \tag{1.22}$$

Now we have to remember that we have used unbounded operators instead of bounded ones but we can prove that, in this particular case, the result of the formal calculation is correct. Thus, to prove it we can use the following Proposition (the interested reader can find more details in [13]).

Proposition 4 *For all* $\mathbf{a}$ *and* $\mathbf{b}$ *in* $\mathbb{R}^d$*, the operators* $U_{\mathbf{a},\mathbf{b}}(t)$ *on* $L^2(\mathbb{R}^d, \mathbb{C})$ *given by*

$$(U_{\mathbf{a},\mathbf{b}}(t)\phi)(\mathbf{x}) = \exp(it^2\hbar(\mathbf{a}\cdot\mathbf{b})/2)\exp(it\mathbf{a}\cdot\mathbf{x})\phi(\mathbf{x}+t\hbar\mathbf{b}) \tag{1.23}$$

form a strongly continuous one-parameter unitary group. The infinitesimal generator of this group coincides with $\mathbf{a}\cdot\mathbf{X}+\mathbf{b}\cdot\mathbf{P}$ *on* $C^\infty(\mathbb{R}^d)$ *and is essentially self-adjoint on this domain. Thus, if* $\mathbf{a}\cdot\mathbf{X}+\mathbf{b}\cdot\mathbf{P}$ *denotes the unique self-adjoint extension of the infinitesimal generator on* $C^\infty(\mathbb{R}^d)$*, it follows from Stone's theorem that*

$$\exp(it(\mathbf{a}\cdot\mathbf{X}+\mathbf{b}\cdot\mathbf{P})) = \exp(it^2\hbar(\mathbf{a}\cdot\mathbf{b})/2)\exp(it\mathbf{a}\cdot\mathbf{X})\exp(it\mathbf{b}\cdot\mathbf{P})$$

$\forall\ t\in\mathbb{R}$*. In particular, (1.21) and (1.22) hold.*

With the computation of the operator $\exp(i(\mathbf{a}\cdot\mathbf{X}+\mathbf{b}\cdot\mathbf{P}))$ in hand, we return to our analysis of the proposed formula (1.19) for the general Weyl quantization. For our purposes, it is convenient to think of operators on $L^2(\mathbb{R}^{2d},\mathbb{C})$ as integral operators and to write down a formula for the integral kernel of $Op_\hbar(f)$ in terms of f itself. At a formal level, the operator mapping ϕ to $\exp(i\hbar(\mathbf{a}\cdot\mathbf{b})/2)\exp(i\mathbf{a}\cdot\mathbf{x})\phi(\mathbf{x}+\hbar\mathbf{b})$ may be thought as an "integral" operator, with integral kernel given by

$$\exp(i\hbar(\mathbf{a}\cdot\mathbf{b})/2)\exp(i\mathbf{a}\cdot\mathbf{x})\delta_n(\mathbf{x}+\hbar\mathbf{b}-\mathbf{y}), \tag{1.24}$$

where δ_n is a n-dimensional δ function. Thus, it should be possible to obtain the integral kernel of $Op_\hbar(f)$ by integrating the previous expression against $\hat{f}(\mathbf{a},\mathbf{b})$. To evaluate the resulting integral, we make the change of variable $\mathbf{c}=\hbar\mathbf{b}$, from which we obtain

$$\begin{aligned}&(2\pi\hbar)^{-n}\int_{\mathbb{R}^d}\int_{\mathbb{R}^d}\exp(i(\mathbf{a}\cdot\mathbf{c})/2)\exp(i\mathbf{a}\cdot\mathbf{x})\delta_n(\mathbf{x}+\mathbf{c}-\mathbf{y})\hat{f}(\mathbf{a},\mathbf{c}/\hbar)d\mathbf{c}d\mathbf{a}\\ &=\hbar^{-n}(2\pi)^{-n/2}\left[(2\pi)^{-n/2}\int_{\mathbb{R}^d}\exp(i\mathbf{a}\cdot(\mathbf{x}+\mathbf{y})/2)\hat{f}(\mathbf{a},(\mathbf{y}-\mathbf{x})/\hbar)d\mathbf{a}\right].\end{aligned} \tag{1.25}$$

We may recognize the integral in square brackets in (1.25) as undoing the Fourier transform of f in the $\mathbf{x}$-variable, leaving us with the partial Fourier transform of f in the $\mathbf{p}$ variable, evaluated in $((\mathbf{x}+\mathbf{y})/2,\ (\mathbf{y}-\mathbf{x})/\hbar)$. Thus, we expect that $Op_\hbar(f)$ should be the integral operator with integral kernel k_f given by

$$k_f(\mathbf{x},\mathbf{y}) = (2\pi\hbar)^{-n}\int_{\mathbb{R}^d} f((\mathbf{x}+\mathbf{y})/2,\mathbf{p})\exp(-i(\mathbf{y}-\mathbf{x})\cdot\mathbf{p}/\hbar)d\mathbf{p}. \tag{1.26}$$

1.2.3 Weyl Quantization for L^2 symbols

What we have discussed in the previous section will help us to define $Op_\hbar(f)$ as the integral operator with kernel k_f, beginning with the case in which f belongs to $L^2(\mathbb{R}^{2d},\mathbb{C})$. The resulting operators will turn out to be Hilbert-Schmidt

operators on $L^2(\mathbb{R}^d, \mathbb{C})$. If H is a Hilbert space and $A \in B(H)$ is a non-negative self-adjoint operator on H, then it can be shown that A has a well-defined trace, that is to say the value of

$$\mathrm{tr}(A) := \sum_j \langle e_j, Ae_j \rangle$$

is the same for each orthonormal basis $\{e_j\}$ of H.

Observation 3 *Since A is a non-negative operator, $\langle e_j, Ae_j \rangle$ is a non-negative real number, so that the sum is always defined, but may have the value $+\infty$.*

We would like to avoid infinity values, so it is natural to introduce the following definition. Given that if A is any bounded operator, then A^*A is self-adjoint and nonnegative.

Definition 7 *We say that A is Hilbert–Schmidt if*

$$tr(A^*A) < \infty.$$

Given two Hilbert-Schmidt operators A and B, it can be shown that AB is a trace-class operator, namely

$$\mathrm{tr}(A^*B) := \sum_{j=1}^{\infty} \langle e_j, A^*Be_j \rangle$$

is absolutely convergent and the value of the sum is independent of the choice of orthonormal basis.

Definition 8 *We define the Hilbert-Schmidt inner product of A and B and the associated Hilbert-Schmidt norm of A by*

$$\langle A, B \rangle_{HS} := tr(A^*B)$$

$$||A||_{HS} := \sqrt{tr(A^*A)}.$$

It can be demonstrated that the space of Hilbert-Schmidt operators on H forms a Hilbert space with respect to the Hilbert-Schmidt inner product. We denote the space of Hilbert-Schmidt operators on H by $HS(H)$. We will make use of the following standard result characterizing Hilbert-Schmidt operators on $L^2(\mathbb{R}^d, \mathbb{C})$ in terms of integral operators.

Proposition 5 *If k is in $L^2(\mathbb{R}^{2d}, \mathbb{C})$ then for every $\phi \in L^2(\mathbb{R}^d, \mathbb{C})$, the integral*

$$A_k(\phi)(\mathbf{x}) := \int_{\mathbb{R}^d} k(\mathbf{x}, \mathbf{y})\phi(\mathbf{y})d\mathbf{y} \tag{1.27}$$

is absolutely convergent for almost every $\mathbf{x} \in \mathbb{R}^d$, and $A_k(\phi)$ also belongs to $L^2(\mathbb{R}^d, \mathbb{C})$. Furthermore, the operator A_k is a Hilbert-Schmidt operator on $L^2(\mathbb{R}^d, \mathbb{C})$ and

$$||A_k||_{HS} = ||k||_{L^2(\mathbb{R}^{2d}, \mathbb{C})}.$$

Conversely, for any Hilbert-Schmidt operator A on $L^2(\mathbb{R}^d, \mathbb{C})$, there exists a unique $k \in L^2(\mathbb{R}^{2d}, \mathbb{C})$ such that $A = A_k$.

We are now ready to define the Weyl quantization of L^2 symbols.

Definition 9 *For all $f \in L^2(\mathbb{R}^{2d}, \mathbb{C})$, define $k_f : \mathbb{R}^{2d} \to \mathbb{C}$ by*

$$k_f(\mathbf{x}, \mathbf{y}) = (2\pi\hbar)^{-n} \int_{\mathbb{R}^d} f((\mathbf{x}+\mathbf{y})/2, \mathbf{p}) \exp(-i(\mathbf{y}-\mathbf{x}) \cdot \mathbf{p}/\hbar) d\mathbf{p}, \tag{1.28}$$

and define the **Weyl quantization** *of f, as an operator on $L^2(\mathbb{R}^d, \mathbb{C})$, by*

$$Op_\hbar(f) = A_{k_f},$$

where A_{k_f} is defined by (1.27).

The integral in (1.28) is not necessarily absolutely convergent, and should be understood as computing a partial Fourier transform. Thus, we should replace the right-hand side of (1.28) with

$$\lim_{R\to\infty} (2\pi\hbar)^{-n} \int_{|\mathbf{p}|\leq R} f((\mathbf{x}+\mathbf{y})/2, \mathbf{p}) \exp(-i(\mathbf{y}-\mathbf{x}) \cdot \mathbf{p}/\hbar) d\mathbf{p}, \tag{1.29}$$

where the limit is in the norm topology of $L^2(\mathbb{R}^{2d}, \mathbb{C})$. In few words, we may describe the procedure for computing k_f at a point $(\mathbf{x}^1, \mathbf{x}^2)$ in $\mathbb{R}^{2d}$ in three steps:

1. compute the partial Fourier transform $\mathcal{F}_p$ of $f(\mathbf{x}, \mathbf{p})$ in the $\mathbf{p}$-variable, resulting in the function $(\mathcal{F}_\mathbf{p} f)(\mathbf{x}, \xi)$;
2. evaluate $\mathcal{F}_\mathbf{p} f$ at the point $\mathbf{x} = (\mathbf{x}^1 + \mathbf{x}^2)/2, \xi = (\mathbf{x}^2 - \mathbf{x}^1)/\hbar$;
3. multiply the result by $\hbar^{-n}(2\pi)^{-n/2}$ to get

$$k_f(\mathbf{x}^1, \mathbf{x}^2) = \hbar^{-n}(2\pi)^{-n/2} (\mathcal{F}_\mathbf{p} f)((\mathbf{x}^1 + \mathbf{x}^2)/2, (\mathbf{x}^2 - \mathbf{x}^1)/\hbar). \tag{1.30}$$

Definition 10 *The inverse map $Op_\hbar^{-1} : HS(L^2(\mathbb{R}^d)) \to L^2(\mathbb{R}^{2d})$ is given by*

$$Op_\hbar^{-1}(A)(\mathbf{x}, \mathbf{p}) = \hbar^d \int_{\mathbb{R}^d} k(\mathbf{x} - \mathbf{y}/2, \mathbf{x} + \mathbf{y}/2) e^{i\mathbf{y}\cdot\mathbf{p}} d\mathbf{y},$$

where k is the integral kernel of A and $HS(L^2(\mathbb{R}^d))$ is the Hilbert-Schmidt space. The latter integral is called ***symbol*** *of the operator A.*

Theorem 2 *The map $Op_\hbar$ is a constant multiple of a unitary map of $L^2(\mathbb{R}^{2d}, \mathbb{C})$ onto $HS(L^2(\mathbb{R}^d, \mathbb{C}))$. The inverse map $Op_\hbar^{-1} : HS(L^2(\mathbb{R}^d, \mathbb{C})) \to L^2(\mathbb{R}^{2d}, \mathbb{C})$ is given by*

$$Op_\hbar^{-1}(A)(\mathbf{x}, \mathbf{p}) = \hbar^n \int_{\mathbb{R}^d} k(\mathbf{x} - \hbar\mathbf{b}/2, \mathbf{x} + \hbar\mathbf{b}/2) \exp(i\mathbf{b} \cdot \mathbf{p}) d\mathbf{b},$$

where k is the integral kernel of A as in Proposition 5. Furthermore, for all $f \in L^2(\mathbb{R}^{2d}, \mathbb{C})$, we have $Op_\hbar(\overline{f}) = Op_\hbar(f)^*$; in particular, $Op_\hbar(f)$ is self-adjoint if f is real valued.

Observation 4 *The integral in the theorem should be understood as an L^2 limit, as in (1.29). The fact that $Op_\hbar$ is unitary (up to a constant) tells us that for an appropriate constant c, the operators $c\exp(i(\mathbf{a}\cdot\mathbf{X}+\mathbf{b}\cdot\mathbf{P}))$ form an "orthonormal basis in the continuous sense" for the Hilbert space $HS(L^2(\mathbb{R}^d,\mathbb{C}))$.*

The following proof is taken from [13].

Proof. Proposition 5 gives a unitary identification of $HS(L^2(\mathbb{R}^d,\mathbb{C}))$ with $L^2(\mathbb{R}^{2d},\mathbb{C})$. Thus, it suffices to show that the map $f\to k_f$ is a multiple of a unitary map. This result holds because the partial Fourier transform is a unitary map of $L^2(\mathbb{R}^{2d},\mathbb{C})$ to itself and composition with an invertible linear map is a constant multiple of a unitary map. The inverse of the map $f\to k_f$ is obtained by inverting the linear map and undoing the partial Fourier transform. Finally, it is apparent from (1.28) that

$$k_{\overline{f}}(\mathbf{x},\mathbf{y})=\overline{k_f(\mathbf{y},\mathbf{x})}.$$

This shows that $Op_\hbar(\overline{f})=Op_\hbar(f)^*$. □

1.2.4 The Moyal Product

Until now, we have demonstrated the strength of the Weyl corrispondence thanks to its ivertibility. But another advantage of the Weyl approach is introduced in this paragraph and it is to have an expansion in powers of $\hbar$ of the product of two operators, under certain hypothesis that will lead us to consider in particular the Hilbert-Schmidt operators.

Let consider $f,g\in L^2(\mathbb{R}^{2d},\mathbb{C})$, then $Op_\hbar(f)$ and $Op_\hbar(g)$ are Hilbert- Schmidt operators, in which case their product is again Hilbert-Schmidt. Thus, since $Op_\hbar$ is a bijection of $L^2(\mathbb{R}^{2d},\mathbb{C})$ with $HS(L^2(\mathbb{R}^d,\mathbb{C}))$, there is a unique L^2 function, which we denote by $f*g$, such that

$$Op_\hbar(f)Op_\hbar(g)=Op_\hbar(f*g). \tag{1.31}$$

Since we know that the Weyl quantization is characterized by the Fourier transform, it's natural to state the following proposition.

Proposition 6 *The Moyal product $f*g$ may be characterized in terms of the Fourier transform as*

$$\widehat{(f*g)}(\mathbf{a},\mathbf{b})=(2\pi)^{-n}\int_{\mathbb{R}^d}\int_{\mathbb{R}^d}\exp(-i\hbar(\mathbf{a}\cdot\mathbf{b}'-\mathbf{b}\cdot\mathbf{a}')/2)\times\hat{f}(\mathbf{a}-\mathbf{a}',\mathbf{b}-\mathbf{b}')\hat{g}(\mathbf{a}',\mathbf{b}')d\mathbf{a}'d\mathbf{b}',$$

where the symbol $\widehat{f}$ on a function f is the Fourier transform.

Observation 5 *If we set $\hbar=0$ in the above formula, $\widehat{f*g}$ reduces to $(2\pi)^{-n}$ times the convolution of $\hat{f}$ and $\hat{g}$, which is the Fourier transform of fg. It is thus not difficult to show that*

$$\lim_{\hbar\to 0^+} f*g=fg.$$

That is to say, the Moyal product $f * g$ is a "deformation" of the ordinary pointwise product of functions on $\mathbb{R}^{2d}$.

Observation 6 *The Moyal product can be expanded in an asymptotic expansion in powers of $\hbar$. This expansion terminates in the case that f and g are both polynomials. This expansion will be crucial for the Wigner equation that will be introduced later.*

Proof. The easier way to work is to consider (1.19), which can be shown to give the same result as Definition 9 when f is a Schwartz function. We assume standard properties of the Bochner integral[3] for functions with values in a Banach space $(B(H))$, which are similar to those of the Lebesgue integral. We have, then,

$$Op_\hbar(f)Op_\hbar(g) = (2\pi)^{-n}\int_{\mathbb{R}^{2d}} \hat{f}(\mathbf{a},\mathbf{b})\exp(i(\mathbf{a}\cdot\mathbf{X}+\mathbf{b}\cdot\mathbf{P}))d\mathbf{a}d\mathbf{b} \tag{1.32}$$

$$\times(2\pi)^{-n}\int_{\mathbb{R}^{2d}} \hat{g}(\mathbf{a}',\mathbf{b}')\exp(i(\mathbf{a}'\cdot\mathbf{X}+\mathbf{b}'\cdot\mathbf{P}))d\mathbf{a}'d\mathbf{b}'.$$

Now, it is an easy calculation to verify, using Proposition 4, that

$$\exp(i(\mathbf{a}\cdot\mathbf{X}+\mathbf{b}\cdot\mathbf{P}))\exp(i(\mathbf{a}'\cdot\mathbf{X}+\mathbf{b}'\cdot\mathbf{P})) =$$
$$\exp(-i\hbar(\mathbf{a}\cdot\mathbf{b}'-\mathbf{b}\cdot\mathbf{a}')/2)\exp(i((\mathbf{a}+\mathbf{a}')\cdot\mathbf{X}+(\mathbf{b}+\mathbf{b}')\cdot\mathbf{P})), \tag{1.33}$$

which is what one obtains by formally applying the special case of the Baker-Campbell-Hausdorff formula in (1.20). Thus, we may combine the integrals in (1.32) to obtain

$$Op_\hbar(f)Op_\hbar(g) = \frac{1}{(2\pi)^{2n}}\int_{\mathbb{R}^{4d}} [\exp(-i\hbar(\mathbf{a}\cdot\mathbf{b}'-\mathbf{b}\cdot\mathbf{a}')/2)\exp(i((\mathbf{a}+\mathbf{a}')\cdot\mathbf{X}+(\mathbf{b}+\mathbf{b}')\cdot\mathbf{P}))\times$$
$$\hat{f}(\mathbf{a},\mathbf{b})\hat{g}(\mathbf{a}',\mathbf{b}')\Big]\, d\mathbf{a}d\mathbf{b}d\mathbf{a}'d\mathbf{b}'.$$

By introducing new variables $\mathbf{c}=\mathbf{a}+\mathbf{a}'$ and $\mathbf{d}=\mathbf{b}+\mathbf{b}'$ in the $\mathbf{a}$ and $\mathbf{b}$ integrals and reversing the order of integration, we obtain, after simplifying the exponent,

$$Op_\hbar(f)Op_\hbar(g) = \frac{1}{(2\pi)^{n}}\int_{\mathbb{R}^{2d}} [(2\pi)^{-n}\int_{\mathbb{R}^{2d}} \exp(-i\hbar(\mathbf{c}\cdot\mathbf{b}'-\mathbf{d}\cdot\mathbf{a}')/2) \tag{1.34}$$

$$\times\hat{f}(\mathbf{c}-\mathbf{a}',\mathbf{d}-\mathbf{b}')\hat{g}(\mathbf{a}',\mathbf{b}')d\mathbf{a}'d\mathbf{b}']\exp(i(\mathbf{c}\cdot\mathbf{X}+\mathbf{d}\cdot\mathbf{P}))d\mathbf{c}d\mathbf{d}.$$

From this and (1.19), we see that $Op_\hbar(f)Op_\hbar(g)$ is the Weyl quantization of the function whose Fourier transform is the quantity in square brackets above, which is what we wanted to show.□

[3] it extends the definition of Lebesgue integral to functions that take values in a Banach space, as the limit of integrals of simple functions.

Proposition 7 *The Moyal product $f*g$ extends to a continuous map of $L^2(\mathbb{R}^{2d},\mathbb{C})\times L^2(\mathbb{R}^{2d},\mathbb{C})$ into $L^2(\mathbb{R}^{2d},\mathbb{C})$ and the composition formula (1.31) holds for all f and g in $L^2(\mathbb{R}^{2d},\mathbb{C})$.*

Proof. A standard inequality asserts that for any two Hilbert-Schmidt operators A and B, we have

$$||AB||_{HS} \leq ||A||_{HS}||B||_{HS}.$$

It follows that the product map $(A,B)\to AB$ is a continuous map of $HS(L^2(\mathbb{R}^d,\mathbb{C}))\times HS(L^2(\mathbb{R}^d,\mathbb{C}))$ to $HS(L^2(\mathbb{R}^d,\mathbb{C}))$. Meanwhile, the Weyl quantization is a constant multiple of a unitary map from $L^2(\mathbb{R}^{2d},\mathbb{C})$ to $HS(L^2(\mathbb{R}^d,\mathbb{C}))$. For Schwartz functions f and g, the Moyal product is nothing but

$$f*g = Op_\hbar^{-1}(Op_\hbar(f)Op_\hbar(g)). \tag{1.35}$$

The right-hand side of (1.35) provides the desired continuous extension of $f*g$. Clearly, the composition formula (1.31) holds for this extension.□

The Moyal product, under suitable regularity assumptions (see [15]), possesses the following formal semiclassical expansion

$$f*g(\mathbf{a},\mathbf{b}) = \sum_{\alpha,\beta}\left(\frac{i\hbar}{2}\right)^{|\alpha|+|\beta|}\frac{(-1)^{|\beta|}}{\alpha!\beta!}\partial_{\mathbf{a}}^{\alpha}\partial_{\mathbf{b}}^{\beta}f(\mathbf{a},\mathbf{b})\partial_{\mathbf{a}}^{\beta}\partial_{\mathbf{b}}^{\alpha}g(\mathbf{a},\mathbf{b}) \tag{1.36}$$

where $\alpha=(\alpha_1,...,\alpha_d)\in\mathbb{N}^d$ is a multi-index, $|\alpha|=\sum_i\alpha_i$, $\alpha!=\prod_i\alpha_i!$, $\partial_{\mathbf{a}}^{\alpha}=\prod_i\partial_{a_i}^{\alpha_i}$ and similarly for $\partial_{\mathbf{b}}^{\beta}$.

The expansion (1.36) can be rewritten as

$$f*g(\mathbf{a},\mathbf{b}) = \sum_{n=0}^{\infty}\hbar^n f*_n g \tag{1.37}$$

where

$$f*_n g(\mathbf{a},\mathbf{b}) = \sum_{\alpha,\beta,|\alpha|+|\beta|=n}\left(\frac{i}{2}\right)^{n}\frac{(-1)^{|\beta|}}{\alpha!\beta!}\partial_{\mathbf{a}}^{\alpha}\partial_{\mathbf{b}}^{\beta}f(\mathbf{a},\mathbf{b})\partial_{\mathbf{a}}^{\beta}\partial_{\mathbf{b}}^{\alpha}g(\mathbf{a},\mathbf{b}) \tag{1.38}$$

It is easy to see that

$$f*_n g(\mathbf{a},\mathbf{b}) = (-1)^n g*_n f(\mathbf{a},\mathbf{b}),$$

that is the operation $*_n$ is commutative (respectively anticommutative) when n is even (respectively odd).

These properties will be crucial for the following chapters of the thesis.

1.2.5 Commutation Relations

The last step that will be useful for writing the Wigner equations, it's to discuss the commutation relations, in light of what we have said until now about Weyl

quantization. Indeed, in quantum mechanics, the commutator of two operators (divided by $i\hbar$) plays a role similar to that of the Poisson bracket in classical mechanics, that are fundamental to write the equations that describe the changing in time of the system states. Thus, we may naturally ask: How does the Weyl quantization map Poisson brackets? Are the commutation relations mantained after the quantization? The answer is: not always; such an exact correspondence holds only for special classes of symbols. If we consider, for example, the class of symbols that depend only on $\mathbf{x}$ and not on $\mathbf{p}$, then on the classical side, all such functions Poisson commute. The Weyl quantization maps such functions $f(\mathbf{x})$ to the operator of multiplication by $f(\mathbf{x})$, and thus the quantizations of any two such functions commute. A more interesting (in particular, noncommutative) example is the following.

Proposition 8 *Suppose f is a polynomial in $\mathbf{x}$ and $\mathbf{p}$ of degree at most 2 and g is an arbitrary polynomial in $\mathbf{x}$ and $\mathbf{p}$. Then*

$$\frac{1}{i\hbar}[Op_\hbar(f), Op_\hbar(g)] = Op_\hbar(\{f, g\}), \tag{1.39}$$

where $\{f, g\}$ is the Poisson bracket of f and g.

Observation 7 *We define the Weyl quantization by the obvious n-variable extension of Definition 5, and we regard all operators as operating on $C^\infty(\mathbb{R}^d)$.*

The following proof is present in [13].

Proof. If f has degree zero, then both sides of the desired equality are zero. Turning to case in which f has degree 1, we use the n-variable extension of Proposition 3, the proof of which is essentially the same as the 1-variable result. The result is as follows:

$$Op_\hbar(x_j g) = Op_\hbar(x_j)Op_\hbar(g) - \frac{i\hbar}{2}Op_\hbar\left(\frac{\partial g}{\partial p_j}\right) = Op_\hbar(g)Op_\hbar(x_j) + \frac{i\hbar}{2}Op_\hbar\left(\frac{\partial g}{\partial p_j}\right).$$

By subtracting these two formulas and rearranging, we get

$$\frac{1}{i\hbar}[Op_\hbar(x_j), Op_\hbar(g)] = Op_\hbar\left(\frac{\partial g}{\partial p_j}\right) = Op_\hbar(\{x_j, g\}).$$

A very similar argument establishes the desired result when $f = p_j$ and thus for all homogeneous polynomials of degree 1. Suppose now that f_1 and f_2 are homogeneous polynomials of degree 1 in $\mathbf{x}$ and $\mathbf{p}$. Then it follows easily from Proposition 3 that for any polynomial h, we have

$$Op_\hbar(f_j h) = \frac{1}{2}(Op_\hbar(f_j)Op_\hbar(h) + Op_\hbar(h)Op_\hbar(f_j)), \quad j = 1, 2. \tag{1.40}$$

In particular, we have

$$Op_\hbar(f_1 f_2) = \frac{1}{2}(Op_\hbar(f_1)Op_\hbar(f_2) + Op_\hbar(f_2)Op_\hbar(f_1)). \tag{1.41}$$

Using (1.41) and the product rule for commutators, we have

$$\frac{1}{i\hbar}[Op_\hbar(f_1 f_2), Op_\hbar(g)] = \frac{1}{2i\hbar}([Op_\hbar(f_1), Op_\hbar(g)]Op_\hbar(f_2)+Op_\hbar(f_1)[Op_\hbar(f_2), Op_\hbar(g)]$$
$$+[Op_\hbar(f_2), Op_\hbar(g)]Op_\hbar(f_1) + Op_\hbar(f_2)[Op_\hbar(f_1), Op_\hbar(g)]).$$

Using the degree-1 case of the result we are trying to prove, along with (1.40), we get

$$\begin{aligned}\frac{1}{i\hbar}[Op_\hbar(f_1 f_2), Op_\hbar(g)] &= \frac{1}{2}(Op_\hbar(\{f_1, g\})Op_\hbar(f_2) + Op_\hbar(f_1)Op_\hbar(\{f_2, g\}) \\ &\quad + Op_\hbar(\{f_2, g\})Op_\hbar(f_1) + Op_\hbar(f_2)Op_\hbar(\{f_1, g\})) \\ &= Op_\hbar(f_2\{f_1, g\}) + Op_\hbar(f_1\{f_2, g\}) = Op_\hbar(\{f_1 f_2, g\}),\end{aligned} \tag{1.42}$$

where in the last equality we have used the product rule for the Poisson bracket. We have now established the desired result when f is a homogeneous polynomial of degree 0, 1, or 2. □

It could appear that the result is valid also in the case where f has degree 3, by considering three homogenous polynomials f_1, f_2, and f_3 of degree 1 and symmetrizing. The argument breaks down, however, because the $Op_\hbar(f_j)$'s do not commute. The $Op_\hbar(f_j)$'s will not always occur in the correct order to allow us to pull the f_j's back inside the Weyl quantization. Indeed, an elementary calculations shows that

$$\frac{1}{i\hbar}[Op_\hbar(x^2 p), Op_\hbar(xp^2)] = 3X^2P^2 - 6i\hbar XP - \hbar^2 I,$$

whereas

$$Op_\hbar(\{x^2 p, xp^2\}) = 3X^2P^2 - 6i\hbar XP - \frac{3}{2}\hbar^2 I,$$

so that the two expressions differ by $\hbar^2 I/2$.

This last observation won't be a problem for the development of the thesis, because the operators considered are not of higher degree than two.

Chapter 2

Solid state physics basic concepts

Solid state physics is one of the branch of physics and it deals with properties of solid matter. Solid materials are made of a huge amount of atoms interacting each other. From these interactions the mechanical, thermal, electrical, magnetic and optical properties of solids are deduced. A particular class of solids material is that one constitued by the crystals [5].

This chapter is organized as follows: in Section 2.1 the crystal lattice structure is presented and then the properties and the structure of phonons and electrons will be introduced in Section 2.2 and 2.3, respectively. In the last section the structure of graphene is briefly treated.

2.1 Crystal lattice

In this section we want to introduce some definitions about a crystal lattice before going into details of crystal vibrations. Crystals are made of atoms, and atoms are relatively complex systems with nuclei and electrons around them. Nevertheless, many features of crystal vibrations are reasonably well described considering atoms simply as single particles located at the lattice points. This is the result of the adiabatic approximation, introduced by Born and Oppenheimer in 1927 and well verified in most cases. Crystals constitute a particular class of solids; its characteristic is that they are made of repeated identical building blocks of atoms or group of atoms. The sinlgle block of atoms or group of atoms that is reapeted is called *primitive cell* or *unit cell* and it's described mathematically by three vectors linearly indipendent and not orthogonal. These vectors are called *primitive vectors* and by translating them, without rotating them, all the space will be filled.

If we call $\mathbf{a}_1, \mathbf{a}_2, \mathbf{a}_3$ the primitive vectors and $n_1, n_2, n_3 \in \mathbb{Z}$, the set of all locations of the unit cells is given by

$$\mathbf{R} = n_1\mathbf{a}_1 + n_2\mathbf{a}_2 + n_3\mathbf{a}_3,$$

and this set is called *Bravais lattice* of the crystal.

Observation 8 *In a crystal all the points transformed by* $\mathbf{R}$ *are equivalent. More in details, if*

$$\mathbf{x}' = \mathbf{x} + \mathbf{R},$$

then $\mathbf{x}' \equiv \mathbf{x}$ *and all physical quantities assume the same value both in* $\mathbf{x}$ *and in* $\mathbf{x}'$*.*

The primitive cell that is copied throughout space can assume any shape but the most natural choice is a parallelepiped with three edges equal to the primitive vectors. Thanks to the fact that the primitive vectors generate the Bravais lattice, we can define the concept of *basis* as the set of vectors giving the location of the atoms relative to the origin of each cell.

Another important definition is the *Wigner-Seitz primitive cell*, that is a particular primitive cell which is formed by all points closer to one of the lattice points than to any other.

The *reciprocal lattice* is a fundamental concept in the whole theory of solid state. Given a direct lattice with primitive vectors $\mathbf{a}_1, \mathbf{a}_2, \mathbf{a}_3$, the corresponding reciprocal lattice is defined in the space of wavevectors by the three unit vectors $\mathbf{b}_1, \mathbf{b}_2, \mathbf{b}_3$ such that $\mathbf{a}_i \cdot \mathbf{b}_j = 2\pi\delta_{ij}$, where δ_{ij} is the Kronecker symbol. The reciprocal lattice is itself a Bravais lattice.

The *First Brillouin Zone* (FBZ) of a lattice is formed by all points of the reciprocal space closer to one of the points of the reciprocal lattice than to any other. It is the analogous, in the reciprocal space, of the Wigner-Seitz cell of direct space. The center of the FBZ is called Γ point.

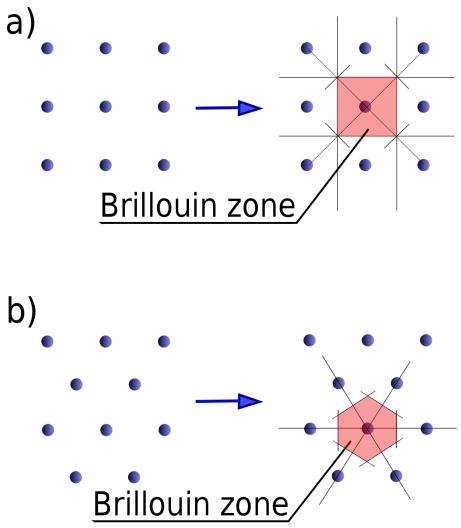

Figure 2.1: The reciprocal lattices (dots) and corresponding FBZs of (a) square lattice and (b) hexagonal lattice. (Picture from Wikipedia)

2.2 Crystal Vibrations and Phonons

The concept of phonons was introduced in 1932 by the soviet physicist Igor Tamm. The name phonon comes from the Greek word $\phi\omega\nu\eta'$ (phonē), which translates "to sound" or "voice", because long-wavelength phonons give rise to sound. There is a strong link between the vibrations of the lattice and the phonons; indeed, the phonons are produced when more atoms interact, therefore it doesn't make sense to consider phonons when we don't have any interactions. The crystal temperature is also involved in these interactions because the higher is the temperature and the higher will be the amount of interactions and vibrations in the crystal. In particular, in solids, under the adiabatic approximation[1], thermal motion of atoms around their equilibrium positions can be described as an ensemble of normal modes (branches) of the crystal lattice vibration [17]. The interactions among the atoms depend on the specific chemical bond, e.g. ionic or covalent. As first approximation they can be considered as elastic interactions and this approximation allows us to use the Hooke's law to describe their behavior.

Let discuss different situations in which phonons and crystal vibrations are involved.

[1] According to this approximation, since the electrons are much lighter than the nuclei, they can follow their nuclei, at least the most internal ones closer to the nuclei, without internal energy change, i.e., adiabatically.

2.2.1 Chain of N equal particles of mass m

We can start from a chain of N equal particles of mass m, connected by equal massless springs with elastic constant k. This model is only a simplified case that will be generalized later. The lattice constant a is the physical dimension that determine the geometry of the unit cells in a crystal lattice, but since we are in 1D case it represents the distance from the equilibrium position (see Fig. 2.2).

The particles can vibrate along the direction of the chain producing longitudinal waves or along the perpendicular directions producing transversal waves (see Fig. 2.2). For simplicity, we will assume that the particles can vibrate only along the longitudinal direction.

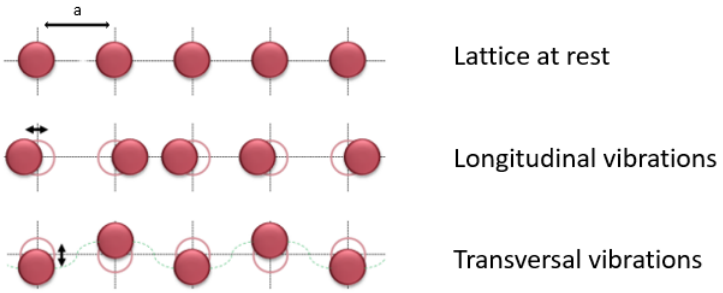

Figure 2.2: Types of vibrations in a crystal lattice.

Let x_j be the displacement of the j-th particle from its equilibrium position. If cyclic boundary conditions are imposed we will deal with an infinite chain,

$$x_{j+N}(t) = x_j(t), \quad t > 0,$$

where t is time and $N \in \mathbb{N}$ is the period. We are assuming that only the interactions of each atom with the nearest neighbors are taken into account. Under such hypothesis one gets the following motion equations

$$mx_j'' = k(x_{j+1} + x_{j-1} - 2x_j), \quad j = 1, 2, ..., N. \tag{2.1}$$

To solve these equations, we want to look for solutions of the type

$$x_j = \xi \exp(i(ljа - \omega(l)t)),$$

where ξ is the amplitude and l the (1D) wave vector. The solution represents a plane wave. After substituing x_j in (2.1), we have non trivial solutions if and only if the angular frequency $\omega(l)$ satisfies the dispersion relation

$$\omega(l) = 2\sqrt{k/m}\left|\sin\left(\frac{la}{2}\right)\right|.$$

By imposing the boundary conditions introduced previously, one has

$$\exp(ilNa) = 1 \Longrightarrow l = \frac{2\pi}{Na}n = \frac{2\pi}{L}n, \quad n \in \mathbb{Z},$$

where $L = Na$ is the length of the portion of chain made of the N atoms. The distance between two consecutive wave vectors is $\frac{2\pi}{L}$ and therefore the density of states, that is the number of wave-vectors per unit-length, is $d(l) = \frac{L}{2\pi}$. Since under the transformation $l \mapsto l + l\frac{2\pi}{a}$, $l \in \mathbb{Z}$, the solution does not change, it is enough to let vary $l \in [-\pi/a, \pi/a]$ which is the first Brillouin zone for the considered case. There are exactly N distinct modes. Of course the solutions are periodic with the FBZ as interval of periodicity.

When the wavelength is much longer than the interatomic distance,

$$|la| << 1,$$

the frequency is approximately given by the linear relation

$$\omega(l) = \sqrt{\frac{k}{m}}a|l|.$$

Note that in this limit the waves are not dispersive and the group velocity (equal to the phase velocity) is $\sqrt{\frac{k}{m}}a$ which represents the sound velocity of the crystal in the continuum limit. The solutions considered are plane waves, but we can see these waves like particles with energy and momentum that follow the Bose Einstein statistic. These particles are the phonons, that have a double nature as particles and waves, in analogy with photons.

2.2.2 Linear chain with two different types of particles

Let us now consider a linear chain composed of two different types of particles, with alternate masses m_1 and m_2 (see Fig. 2.3). This one could be considered as a simple model to describe a one-dimensional crystal with two atoms in each unit cell. Let us assume that the lattice distance is $a = 2b$, b being the equilibrium distance betweeen two adjacent atoms.

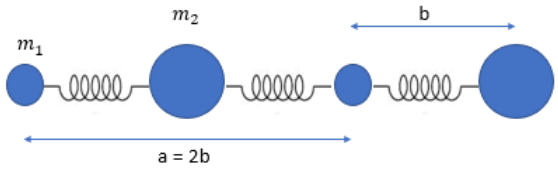

Figure 2.3: Schematic representation of a biatomic linear chain.

The motion equations are the following

$$\begin{cases} m_1 x''_{2j+1} = k(x_{2j+2} + x_{2j} - 2x_{2j+1}), \\ m_2 x''_{2j} = k(x_{2j+1} + x_{2j-1} - 2x_{2j}). \end{cases} \tag{2.2}$$

Also in this case, to solve the system we look for solutions of the following type

$$x_{2j+1} = \xi \exp(i((2j+1)bl - \omega(l)t)),$$
$$x_{2j} = \eta \exp(i(2jbl - \omega(l)t)).$$

distinguish between even and odd indices that represent particles with mass m_1 and m_2, respectively. Proceeding as in the previous case, one gets the dispersion relation

$$\omega^2(l) = k\left(\frac{1}{m_1} + \frac{1}{m_2}\right)\left[1 \mp \sqrt{1 - \frac{4m_1 m_2}{(m_1+m_2)^2}\sin^2(bl)}\right].$$

In the limit $|bl| << 1$, it becomes

$$\omega^2(l) = \begin{cases} \frac{2k}{m_1+m_2} b^2 l^2, & \text{acoustic branch,} \\ 2k\left(\frac{1}{m_1} + \frac{1}{m_2}\right), & \text{optical branch.} \end{cases} \tag{2.3}$$

Note that near to $l = 0$ the acoustic branch is almost linear (Debye approximation), while the optical branch is almost flat (Einstein approximation). Therefore, near to $l = 0$, the optical branch has a negligible group velocity and does not transport energy.

It is meaningful to analyze also the ratio of the displacements

$$\frac{\xi}{\eta} = \frac{2k\cos(lb)}{2k - m_1\omega^2} \sim \begin{cases} 1, \text{for acoustic modes (branches)} \\ -\frac{m_2}{m_1}, \text{for optical modes (branches)} \end{cases} \qquad \text{as} \quad l \mapsto 0.$$

Therefore, the acoustic modes produce oscillations along the same direction, while the optical modes produce oscillations in opposite directions.

2.2.3 Three dimensional case

In the 3D situation we have different directions of polarization with longitudinal and transversal oscillations, for both optical and acoustic modes, that in term of particles are considered as different branches of phonons. Each unit (primitive) cell generally consists of more than one atom, which is therefore characterized by four numbers. The first three, $\mathbf{n} = (n_1, n_2, n_3)$, with $n_i \in \mathbb{Z}$, $i = 1, 2, 3$, identify the cell to which it belongs and the fourth, $s \in \mathbb{N}$, represents its number in the cell and runs from 1 to the number of atoms in each primitive cell.

Let $\mathbf{u}_s(\mathbf{n})$ be the displacements of the atoms in their vibrations. The Lagrangian of a crystal lattice, considered as a mechanical system of particles vibrating around their equilibrium positions, by retaining in the potential only up to the quadratic terms in the displacements (harmonic approximation), is given by

$$\mathcal{L} = \frac{1}{2}\sum_{\mathbf{n},s} m_s |\mathbf{u'}_s(\mathbf{n})|^2 - \frac{1}{2}\sum_{\mathbf{n},\mathbf{n'},s,s'} \langle \Lambda^{ss'}(\mathbf{n}-\mathbf{n'})\mathbf{u}_s(\mathbf{n}), \mathbf{u}_{s'}(\mathbf{n'})\rangle, \tag{2.4}$$

where the m_s are the masses of the atoms and the matrices $\Lambda^{ss'}$ depend only on the differences $\mathbf{n}-\mathbf{n'}$, since the interaction forces depend only on the relative position of the atoms. The $\Lambda^{ss'}$'s satisfy the simmetry relation

$$\Lambda^{ss'}(\mathbf{n}) = (\Lambda^{s's}(-\mathbf{n})^T), \tag{2.5}$$

along with some further relations which descend from the fact that a parallel displacement or a rotation of the lattice as a whole give rise to no forces. In (2.5) the upper-script T indicates transposition.

The Lagrange equations of motion read

$$m_s \mathbf{u''}_s(\mathbf{n}) = -\sum_{\mathbf{n'},s'} \Lambda^{ss'}(\mathbf{n}-\mathbf{n'})\mathbf{u}_{s'}(\mathbf{n'}). \tag{2.6}$$

Let us look for solutions in the form of plane waves

$$\mathbf{u}_s(\mathbf{n}) = \mathbf{e}_s(\mathbf{l})\exp[i(\mathbf{l}\cdot\mathbf{r}_\mathbf{n} - \omega t)], \tag{2.7}$$

with $\mathbf{r}_\mathbf{n}$ the radius vector of any particular vertex of the cell $\mathbf{n}$, which can be used to define its position, ω the angular frequency, $\mathbf{l}$ the wave vector and $\mathbf{e}_s$ the polarization vector, which is the same for equivalent atoms in different cells. Substituing (2.7) into (2.6), after some algebra one gets

$$\sum_{s'} \tilde{\Lambda}^{ss'}(\mathbf{l})\mathbf{e}_{s'} - \omega^2 m_s \mathbf{e}_s = 0, \tag{2.8}$$

where

$$\tilde{\Lambda}^{ss'}(\mathbf{l}) := \sum_{\mathbf{n}} \Lambda^{ss'}(\mathbf{n})\exp(-i\mathbf{l}\cdot\mathbf{r}_\mathbf{n}). \tag{2.9}$$

System (2.8) has non trivial solutions if and only if

$$\det|\tilde{\Lambda}^{ss'}(\mathbf{l}) - \omega^2 m_{s'}\delta_{ss'}| = 0, \tag{2.10}$$

is satisfied. If ν is the number of atoms per cell, the order of the determinant is 3ν, therefore (2.10) is an algebric equation of degree 3ν in the unknown ω^2.

Each solution determines ω as a function of the wave vector $\mathbf{l}$, which means that there are 3ν branches of such function

$$\omega = \omega_\mu(\mathbf{l}), \quad \mu = 1, ..., 3\nu,$$

which, as said, is called dispersion relation, μ labelling the various branches. From definition (2.9) and property (2.5), it follows that

$$\tilde{\Lambda}^{ss'}(\mathbf{l}) = \tilde{\Lambda}^{s's}(-\mathbf{l}) = [\tilde{\Lambda}^{s's}(\mathbf{l})]^*, \tag{2.11}$$

where * indicates complex conjugation. As a consequence, the $\tilde{\Lambda}^{ss'}(\mathbf{l})$'s form an Hermitian matrix, whose eigenvectors corresponding to different eigenvalues are orthogonal, that is

$$\sum_{s=1}^{\nu} m_s \mathbf{u}_s^{(\mu)} \cdot \mathbf{u}_s^{(\mu')*} = 0, \quad \text{for} \quad \mu \neq \mu', \tag{2.12}$$

Due to the symmetry of the mechanical equations of motion under time reversal, the dispersion relation has to be even

$$\omega(\mathbf{l}) = \omega(-\mathbf{l}).$$

Moreover, the wave vector $\mathbf{l}$ appears in (2.7) only in the exponential factor $\exp(i\mathbf{l} \cdot \mathbf{r_n})$, which does not change under the substitution

$$\mathbf{l} \mapsto \mathbf{l} + \mathbf{G}, \quad \mathbf{G} = n_1\mathbf{a}_1^* + n_2\mathbf{a}_2^* + n_3\mathbf{a}_3^*, \quad n_1, n_2, n_3 \in \mathbb{Z}, \tag{2.13}$$

where $\mathbf{G}$ is an arbitrary vector of the reciprocal lattice. Therefore, the wave vector is phisically indeterminate, meaning that values of $\mathbf{l}$ differing by $\mathbf{G}$ are phisically equivalent. This implies that the function $\omega(\mathbf{l})$ is periodic in the reciprocal lattice

$$\omega(\mathbf{l} + \mathbf{G}) = \omega(\mathbf{l}), \tag{2.14}$$

and can be restricted to a single cell. From a geometrical point of view, the dispersion relation $\omega(\mathbf{l})$ is represented by a finite four dimensional hypersurface, with 3ν layers, corresponding to the various branches, which may intersect.

As seen for the simple 1D chain, it is possible to ensure also in the 3D case that some of the branches of the vibrational spectrum, for wavelengths large with respect to the physical dimension of a unit cell, correspond to sound waves in the crystal and for them the dispersion relation is a first order homogeneous function of the components of the wave vector, for $\mathbf{l}$ small enough. These waves are called acoustic waves.

In lattices with more than one atom per cell, there are $3(\nu - 1)$ further types of waves, whose frequency does not vanish at $\mathbf{l} = 0$, but tends to a finite constant.

Such vibrations are called optical vibrations, and for them the atoms in each cell are in relative motion[16].

For example, in silicon and gallium arsenide there are two atoms per cell and, therefore, six types of elastic waves: three acoustic modes and three optical modes. Among the three acoustic modes, one is longitudinal (LA), that is to say the atoms are displaced in the direction of the wave propagation, and two are transverse (TA), in which the atoms are displaced in an orthogonal direction. The same is true for the optical phonons (LO and TO). The transversal modes are doubly degenerate.

What said above is strictly valid only in the harmonic approximation, in which the various monochromatic waves freely propagate through the crystal, without interacting. Higher order terms are taken into account as various processes of decay and scattering among these waves. Their description is rather complex. A simplified approach based on a relaxation time approximation is usually adopted in the device simulations. Recently, other methods based on molecular dynamics simulations have been adopted for studying the anharmonic effects.

2.2.4 Phonons

The description of the lattice vibrations in nanoelectronics needs a quantum approach, because of very small dimensions that are involved in the analysis. Since $\tilde{\Lambda}^{ss'}(\mathbf{l})$'s are Hermitian matrices, it is possible to write the classical equations of motion in canonical coordinates decoupling them in indipendent harmonic oscillators. As a consequence, the analogous quantum Hamiltonian is the sum of the Hamiltonians of $3\nu N$ indipendent quantum oscillators, with N total number of cells, each of them having quantized energy levels given by

$$\varepsilon_n = \hbar\omega\left(n + \frac{1}{2}\right), \quad n = 0, 1, 2, ...$$

From the particle point of view, each quantum state can be considered as formed by n fictitious particles called *phonons* having energy $\hbar\omega$. The processes which change the state from the energy level ε_n to ε_{n+1} (respectively ε_{n-1}) can be interpreted as the *creation* (respectively *annihilation*) of a phonon.

The quasi-momentum

$$\mathbf{q} = \hbar\mathbf{l}$$

is associated to phonons. It is almost analogous to the ordinary momentum, with the important difference that it is defined up to an arbitrary constant vector $\hbar\mathbf{G}$, with $\mathbf{G}$ belonging to the reciprocal lattice. In the continuum, the phonon velocity is given by the group velocity of the corresponding classical waves, $\mathbf{v} = \frac{\partial\omega}{\partial\mathbf{l}}$, which can be rewritten in the form

$$\mathbf{v} = \frac{\partial \varepsilon(\mathbf{q})}{\partial \mathbf{q}},$$

where $\varepsilon(\mathbf{q})$ is the energy.

In the approximation successive to the harmonic one, various elastic and inelastic phonon collision processes occur. The latter tend to drive the system toward equilibrium. In these processes, the energy and momentum conservation laws must be satisfied, the latter up to an additive vector of the form $\hbar\mathbf{G}$

$$\sum \mathbf{q} = \sum \mathbf{q}' + \hbar\mathbf{G},$$

where $\mathbf{q}$ and $\mathbf{q}'$ are the momenta of the phonons before and after the collision.

An arbitrary number of identical phonons can be created simultaneously in the lattice, which means that the phonon gas obeys the Bose statistics. Since the total number of phonons is determined by the equilibrium conditions, the phonon chemical potential is zero. Therefore, the equilibrium occupation number $\overline{g}(\mathbf{p})$ of a quantum state with momentum $\mathbf{q}$ and energy $\varepsilon(\mathbf{q})$ is determined by the Planck distribution function

$$\overline{g}(\mathbf{q}) = \frac{1}{\exp(\varepsilon(\mathbf{q})/T_L) - 1},$$

where T_L is the lattice temperature.

If the typical phonon wavelength is much shorter than the phonon mean free path, phonons can be treated as semi-classical particles that obey, as said, the Bose statistics. In this case, the state of the phonon gas can be described through the distribution function $g^\mu(\mathbf{q})$, whose time evolution is governed by the Boltzmann-Peierls (BP) equation in the semiclassical approximation [17]

$$\frac{\partial g^\mu}{\partial t} + \mathbf{v}_\mu \cdot \nabla_{\mathbf{x}} g^\mu = \sum_\eta \mathcal{C}^\mu_\eta(g^\mu) + \mathcal{C}^\mu_{oth}(g^\mu), \tag{2.15}$$

the index μ labeling the several branches. The right-hand side is the collision operator. The term $\sum_\eta \mathcal{C}^\mu_\eta(g^\mu)$ represents the phonon-phonon collisions, and collisions of phonons with impurities, boundaries and defects. The index η labels the various types of scattering. The other contributions in the collision operator are due to the interaction of phonons with other particles, e.g. electrons and photons.

2.3 Electrons and energy band structure

The electrons are the particles responsible for charge transport in solids. A correct analysis of the electron dynamics in crystals requires the application of advanced many-body techniques. For the present purpose, however, we may limit ourselves to consider a single electron subject to the potential due to the nuclei,

to the core electrons and to the average interaction with all the other external electrons. Let us then consider the Schrödinger equation for the Hamiltonian eigenfunctions of a particle of mass m subject to a potential $V_L(\mathbf{x})$ with the periodicity of the direct lattice:

$$i\hbar\partial_t\psi(\mathbf{x},t) = H\psi(\mathbf{x},t) \tag{2.16}$$

where $\psi(\mathbf{x},t)$ is the wave function, and H is the Hamiltonian, that physically represents the energy of the system and mathematically is an operator that reads as follows:

$$H = -\frac{\hbar^2}{2m}\Delta - eV_L. \tag{2.17}$$

Here eV_L is the potential energy. If we assume that the solution of the equation is $\psi(\mathbf{x},t) = \psi(\mathbf{x})\exp(-\frac{iEt}{\hbar})$, by separating the variables, we will get the time-independent Schrödinger equation:

$$H\psi(\mathbf{x}) = E\psi(\mathbf{x}) \tag{2.18}$$

The solutions of this last equation are expressed by the Bloch Theorem:

Theorem 3 *Let V_L be a periodic potential of period $\mathbf{T} \in L$ then the eigenvalue problem for the Schrödinger operator*

$$H = -\frac{\hbar^2}{2m}\Delta - eV_L, \quad \mathbf{x} \in \mathbb{R}^3,$$

can be reduced to an infinite set of eigenvalue problems for the Schrödinger equation on the primitive cell D of the lattice, indexed by $\mathbf{k} \in B$ (the Brillouin zone),

$$H\psi_{\mathbf{k}} = E\psi_{\mathbf{k}} \quad \text{in } D, \quad \psi_{\mathbf{k}}(\mathbf{x}+\mathbf{T}) = \exp(i\mathbf{k}\cdot\mathbf{T})\psi_{\mathbf{k}}(\mathbf{x}), \quad \mathbf{x} \in D, \mathbf{T} \in L. \tag{2.19}$$

For each $\mathbf{k} \in B$, there exists a sequence $E_n(\mathbf{k}), n \geq 1$, of eigenvalues with associated eigenfunctions $\psi_{n,\mathbf{k}}(\mathbf{x}) = \exp(i\mathbf{k}\cdot\mathbf{x})u_{n,\mathbf{k}}(\mathbf{x})$ (named Bloch functions) where $u_{n,\mathbf{k}}(\mathbf{x})$ is a periodic function. The eigenvalues $E_n(\mathbf{k})$ are real functions of $\mathbf{k}$, periodic and symmetric on B. The spectrum of H is given by the union of the closed intervals

$$\{E_n(\mathbf{k}) : \mathbf{k} \in B\}$$

for $n \geq 1$. The Bloch functions are modulated plane waves. The vector $\mathbf{k}$ is the wave-vector.

Observation 9 *The function $E_n(\mathbf{k})$ is called* **dispersion relation**.

For a proof of Bloch's theorem see [5]. The hypothesis of periodicity of the potential with the same periodicity of the lattice is important because a function with the periodicity of the direct lattice can be expanded in Fourier series with wavevectors of the reciprocal lattice. Inversely, if the Fourier expansion of a function contains only wavevectors of the reciprocal lattice, the function is periodic with the periodicity of the direct lattice.

The differential Schrödinger equation has been therefore transformed into an infinite set of eigenvalue problems, one set for each $\mathbf{k}$. We may therefore consider wavefunctions whose Fourier series contains only one $\mathbf{k}$ and all the vectors of the type $\mathbf{k}+\mathbf{G}$, where $\mathbf{G}$ is an arbitrary vector of the reciprocal lattice. Therefore, the Bloch functions can be written as

$$\psi_{\mathbf{k}}(\mathbf{x}) = u_{\mathbf{k}}(\mathbf{x})e^{i\mathbf{k}\cdot\mathbf{x}}$$

where

$$u_{\mathbf{k}}(\mathbf{x}) = \sum_{\mathbf{G}} C(\mathbf{k}+\mathbf{G})e^{i\mathbf{G}\cdot\mathbf{x}}. \tag{2.20}$$

Since the Fourier series in (2.20) contains only wavevectors of the reciprocal lattice, $u_{\mathbf{k}}(\mathbf{x})$ is a periodic function with the period of the direct lattice. The Fourier expansion of $u_{\mathbf{k}}(\mathbf{x})$ may be truncated at values of $\mathbf{G}$ large enough for all the oscillations of the wavefunction to be correctly accounted for. The infinite system is then reduced to a finite system, and the solutions of the secular equation are the energy eigenvalues $E_n(\mathbf{k})$ of our Hamiltonian, corresponding to the vector $\mathbf{k}$.

If all $\mathbf{k}$'s are considered, the eigenvalues $E_n(\mathbf{k})$ distribute themselves in intervals of allowed values called **energy bands**, separated by gaps, called **energy band gaps**.

If we assume periodic boundary conditions for our Bloch states, we can calculate the density of states. The latter can be calculated by knowing the distance $\delta\mathbf{k}$, between $\mathbf{k}'s$ in the reciprocal axis. The density is

$$g(\mathbf{k}) = \frac{1}{\delta\mathbf{k}}$$

and for example in three dimensional case we have $g(\mathbf{k}) = \frac{V}{(2\pi)^3}$. In addition, we have a factor of 2 in the density of states for the spin degeneracy [4]. Infact according to the Pauli principle each eigenstate of the Hamiltonian may contain at most two electrons.

2.3.1 Tight-Binding Approach

Electrons in the deepest atomic levels, forming the so-called atomic cores, can be described as occupying their atomic levels without big modifications, since their wave functions do not reach in an appreciable way the neighboring atoms.

More external electron states, in particular those that participate in the chemical bond, cannot be described in this simple way and require a study that takes into account the presence of the nearby atoms. There is a very intuitive approach to the problem of electron states, called tight-binding approach, which exploits the above idea: let us consider, as a starting point, a fictitious crystal that has the same structure of the real one, but with an arbitrarily large lattice constant. Such a system can be described as a set of isolated atoms, so that atomic wavefunctions represent exact states for all electrons. We then let the lattice constant decrease. At a certain distance, the most external electrons start to feel the presence of the neighboring atoms. The atomic wavefunctions overlap and form states extended over the entire crystal. Equivalent atomic orbitals, which are degenerate when far apart, split into different levels as consequence of the interaction. Starting from the most outer states, as the atoms get closer, single levels become narrow energy bands that increase and eventually overlap. The actual lattice constant is determined by the minimum of the total energy of the crystal.

2.3.2 Band structure calculations

As indicated above, the calculation of the eigenvalues and eigenstates of the Hamiltonian of the electrons in a crystal is the first basic step for the theoretical understanding of most properties of a solid. Many methods have been developed for the solution of such a problem. Here, we can only mention the most important of them since this subject is somewhat outside of our scope. In general terms, the first problem to solve consists in the reduction of the many-body problem to a one-particle equation. For this purpose, some sort of mean-field approximation is to be performed, where the effect of all "other" electrons is embodied in an effective potential acting on each single electron. Self-consistency is obviously required, since the solution of the single-particle equation for one electron will affect the mean field acting on the others. Often the potential to use in the one-particle Schrödinger equation is given a particular analytical form on the basis of general theoretical considerations, with some parameters fixe a posteriori by the comparison of the theoretical results with experimental data. Many computer programs have been developed for band-structure calcu lations, some of which are commercially available.

The most used techinque to perform the band calculatios are:

- LCAO method (the method of linear combination of atomic orbitals, that is the immediate quantitative application of the idea of tight binding introduced above, and, in fact, the two phrases are often used as synonyms);
- the $\mathbf{k} \cdot \mathbf{p}$ method (the states obtained with this method are rather good for small $\mathbf{k}$, although the method can be extended to expand the band

structure around any given value $\mathbf{k_0}$);

- pseudeopotential method (it was proposed for solids by Phillips and Kleinman in 1959, it generated a significant improvement in the calculations of band structures and it is today the approach most used for this purpose).

For further details the interested reader is referred to [4].

2.3.3 Effective mass approximation

Near a minimum of the energy of a band, the energy $\epsilon(\mathbf{k})$ can be approximated by a quadratic form:

$$\epsilon(\mathbf{k}) = \frac{1}{2}\hbar^2 \sum_{ij} \left(\frac{1}{m}\right)_{ij} k_i k_j, \tag{2.21}$$

where $\left(\frac{1}{m}\right)_{ij}$ is the inverse effective-mass tensor. In case of spherical symmetry, we have a simple effective mass m defined by

$$\epsilon(\mathbf{k}) = \frac{\hbar^2 k^2}{2m}.$$

We should note, however, that this approximation is extensively used in the theory of electron transport in semiconductors [4].

2.3.4 Bloch Wavepackets and group velocity

Before leaving the subject of Bloch states, let us analyze the properties of wavepackets formed by superpositions of such states, representing electrons moving inside a crystal. For simplicity, we shall assume here that the states forming the wavepackets belong to one single band and shall omit the band index in the equations. With the inclusion of the time dependence, a wavepacket formed by the superposition of Bloch states has the form

$$\psi_{\mathbf{k_0}}(\mathbf{x}, t) = \sum_{\mathbf{k}} a_{\mathbf{k_0}}(\mathbf{k}) u_{\mathbf{k}}(\mathbf{x}) e^{i[\mathbf{k}\cdot\mathbf{x} - \epsilon(\mathbf{k})t/\hbar]}. \tag{2.22}$$

To have a well-defined wavepacket, we assume that the coefficients of the superposition are given by a function $a_{\mathbf{k_0}}(\mathbf{k})$ strongly peaked around a value $\mathbf{k_0}$. At the same time, we wish the wavepacket itself to be significantly different from zero in a limited region of space. From the theory of Fourier analysis, we know that the group velocities of our wavepackets are given by

$$\mathbf{v}(\mathbf{k_0} + \mathbf{G}) = \frac{1}{\hbar}\nabla_{\mathbf{k}}\epsilon(\mathbf{k})_{|\mathbf{k}=\mathbf{k_0}+\mathbf{G}}. \tag{2.23}$$

Owing to the periodicity of the energy function, however, all these group velocities are equal, so that all the wave packets travel jointly with group velocity

$$\mathbf{v}(\mathbf{k_0}) = \frac{1}{\hbar}\nabla_{\mathbf{k}}\epsilon(\mathbf{k})_{|\mathbf{k}=\mathbf{k_0}} \tag{2.24}$$

which is therefore the velocity of our original wave packet in (2.22). Note that the above expression for the electron wave packet is formally identical to that for free electrons but, now, the momentum $\hbar\mathbf{k}$ is actually the crystal momentum of the electron, and $\epsilon(\mathbf{k})$ indicates its band energy [4].

2.4 Semiconductors

2.4.1 Free dynamics of Bloch electrons

Under rather general conditions, the crystal momentum of a Bloch state subject to an external force $\mathbf{F}$ changes according to the semiclassical law

$$\frac{d(\hbar\mathbf{k})}{dt} = \mathbf{F}. \tag{2.25}$$

This result is to some extent amazing if we consider that the dynamics of the electron wave is continuously affected by the interaction with the atoms of the crystal. The effect of the crystal periodic potential lies in the fact that $\hbar\mathbf{k}$ appearing in (2.25) is the crystal momentum, not the real momentum, and its relation with the energy is given by the band function $\epsilon(\mathbf{k})$. If an electric field is applied, an electron will continuously change its $\mathbf{k}$, according to (2.25), in absence of collisions. Its velocity, given by the derivative of the band, will also change continuously, increasing as long as the crystal momentum lies in the lower, concave, part of the band. When the electron reaches the upper, convex, part of the band, the velocity starts to decrease, and this is a crucial effect of the crystal potential. When $\mathbf{k}$ reaches the energy maximum, the electron group velocity vanishes. In a simple band, this happens at the BZ edge. As the effect of the force continues, $\mathbf{k}$ surpasses the zone edge, and its velocity is reversed. Since $\mathbf{k}$ is defined to within a vector of the reciprocal lattice, it may be considered to reenter the BZ from the opposite side. Thus, the crystal momentum, in presence of a constant and homogeneous electric field, performs oscillations in the BZ, corresponding to oscillations of the wavepacket in real space, called Bloch oscillations. It is important to remember that these oscillations occur in absence of collisions, a situation practically unrealizable in bulk materials [4].

2.4.2 Insulators, Conductors and Semiconductors

The concepts before introduced are crucial for the solids classification. We know that the energy eigenvalues of electrons in perfect crystals fall in intervals, the energy bands, separated by intervals where the energy eigenvalues are absent, called band gaps.

When at zero absolute temperature the last occupied band, in the order of increasing energies, is totally occupied by electrons, it is called valence band, since the corresponding electron states are the main responsible for the bonds of

the atoms that form the crystal. The next higher band is called conduction band, since the corresponding electron states are the main responsible for electrical conduction.

What follows is a basic classification of the different materials from the point of view of their electrical properties.

- If at zero absolute temperature the highest band occupied by electrons is entirely occupied (valence band) and the energy gap between this band and the next higher band (conduction band) is much higher than $k_B T$, where k_B is the Boltzmann constant and T the room temperature, the conduction band remains empty even at room temperature since the thermal energy is not sufficient to promote electrons from the last occupied band to the next empty band. In absence of impurities, the material is an insulator. In fact, the totally occupied valence band does not conduct, and the conduction band does not conduct because it is void of electrons.

- If the energy gap between the valence band, entirely occupied at zero temperature, and the conduction band, empty at zero temperature, is comparable with $k_B T$ at room temperature, some electrons are promoted to the conduction band by the thermal energy. The conduction band contains some electrons, the valence band contains an equal number of holes, and in absence of impurities the material is an intrinsic semiconductor. It is obvious that at zero temperature any intrinsic semiconductor becomes an insulator.

- If at zero absolute temperature the last occupied band is only partially occupied, the material is a metallic conductor.

If we consider that the band gap of Si is about 1.1 eV and that of GaAs is 1.4 eV, we understand that the conductivity of the intrinsic semiconductors of most technological interest is negligible. If, however, a number of donor impurities (i.e. atoms different from the atoms which the intrinsic semiconductior is made of, with a greater number of electrons in the conduction band, that with a small thermal energy ionize the impurity with the effect of leaving a fixed positive charge in the crystal, the ionized impurity, and an electron free to move in the conduction band) are present in the material, a significant fraction of them can be ionized at lower temperature, and free electrons are available in the conduction band. The conductivity of the semiconductor is increased by orders of magnitude. Since the current is carried in this case by electrons with negative charge, the material is called a doped semiconductor of n type.

If the impurities present in the material are acceptors (i.e. atoms different from the atoms which the intrinsic semiconductior is made of, with a lower number of electrons in the conduction band, that with a small thermal energy ionize the impurity with the effect of leaving a fixed negative charge in the

crystal, the ionized impurity, and a hole free to move in the conduction band), the free carriers are positive holes and the doped semiconductor is of p type.

When both types of impurities are present, electrons may fall from donor states into acceptor states; both types of impurities become ionized, but the free charge carriers available for the conduction mechanism are reduced with respect to the case when only one type is present. The semiconductor is said to be compensated [4].

2.5 Graphene

A particular case of crystal is represented by the graphene, that will be analyzed in some works published for my thesis. Here we briefly recall its structure (for further details see [19]).

Graphene is described by a two dimensional honeycomb lattice in whose vertices are arranged the carbon atoms. The honeycomb net is classified as a triangular Bravais lattice with a two-point basis [4]. In this way it can be considered as composed by two interpenetrating nonequivalent sublattices, usually indicated by A and B. The primitive vectors are

$$\mathbf{a}_1 = \frac{a}{2}(3, \sqrt{3}), \quad \mathbf{a}_2 = \frac{a}{2}(3, -\sqrt{3}),$$

where $a \approx 1.42\mathring{A}$ is the nearest neighbor distance. Since we have a two-point basis this is not the lattice constant, that is $a\sqrt{3} \approx 2.46\mathring{A}$. Regarding the sublattice A, the nearest neighbors are located throw the vectors

$$\delta_1 = \frac{a}{2}(1, \sqrt{3}), \quad \delta_2 = \frac{a}{2}(1, -\sqrt{3}), \quad \delta_3 = -a(1, 0),$$

and, similarly, for sublattice B they are

$$\gamma_1 = -\frac{a}{2}(1, \sqrt{3}), \quad \gamma_2 = \frac{a}{2}(-1, \sqrt{3}), \quad \gamma_3 = a(1, 0).$$

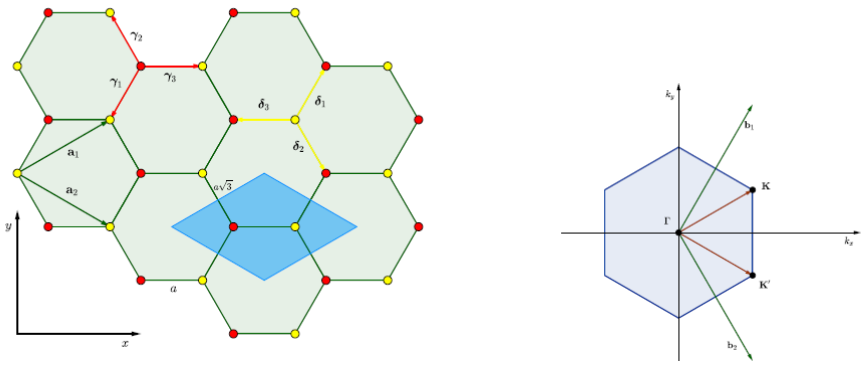

Figure 2.4: Honeycomb structure of graphene (left) and Brillouin zone (right).

In the Figure 2.4 the above mentioned properties are depicted, where the sublattices A and B are colored in yellow and red respectively and the unit cell is highlighted in blue. The primitive reciprocal vectors are

$$\mathbf{b}_1 = \frac{2\pi}{3a}(1, \sqrt{3}), \quad \mathbf{b}_2 = \frac{2\pi}{3a}(1, -\sqrt{3}).$$

They define an hexagonal Brillouin zone, represented in Figure 2.4. Let we consider a reference frame whose origin is the G point, that is the center of the Brillouin zone. The vertices of the latter, indicated by K e K' and called *Dirac points*, are located in

$$\mathbf{K} = \left(\frac{2\pi}{3a}, \frac{2\pi}{3\sqrt{3}a}\right), \quad \mathbf{K}' = \left(\frac{2\pi}{3a}, -\frac{2\pi}{3\sqrt{3}a}\right).$$

2.5.1 The electronic band structure

The energy bands are derived from the tight-binding Hamiltonian for electrons in graphene, considering that electrons can hop to both nearest- and next-nearest-neighbor atoms [42]. They have the form

$$E_{\pm}(\mathbf{k}) = \pm\gamma_1\sqrt{3 + f(\mathbf{k})} - \gamma_2 f(\mathbf{k}) \tag{2.26}$$

with

$$f(\mathbf{k}) = 2\cos\left(\sqrt{3}k_y a\right) + 4\cos\left(\frac{\sqrt{3}}{2}k_y a\right)\cos\left(\frac{3}{2}k_x a\right), \tag{2.27}$$

where $\gamma_1 \approx 2.8\ eV$ is the nearest-neighbor hopping energy and $\gamma_2 \approx 0.1\ eV$ is the next nearest-neighbor hopping energy. We remark that the coordinates of $\mathbf{k}$ are expressed with respect to the Γ point. In the Equation (2.26) the plus sign corresponds to the conduction band and the minus sign refers to the valence band. If we neglect the next nearest-neighbor hopping energy, that is we assume $\gamma_2 = 0$, the two bands appear to be symmetrical. In this case by simple calculation we can assert that the two energy bands touches at the Dirac points. It means that there is no energy gap in graphene.

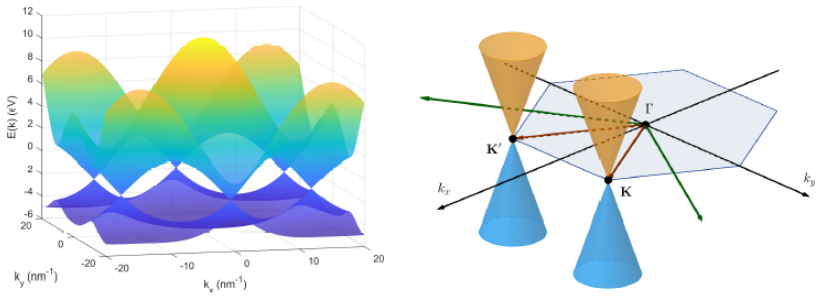

Figure 2.5: Electronic dispersion in the honeycomb lattice. The full expression is reproduced on the left, the zoom in close the Dirac points is shown on the right.

Moreover, by expanding the full band structure (2.26) close to $\mathbf{K}$ (or $\mathbf{K}'$) the dispersion relation reduces to

$$E_{\pm}(\mathbf{k}) \approx \pm\hbar v_F|\mathbf{k}| + O(|\mathbf{k}|^2), \tag{2.28}$$

where v_F is the Fermi velocity, given by

$$v_F = \frac{3\gamma_1 a}{2\hbar}, \tag{2.29}$$

with a value of $v_F \approx 10^6 m/s$. Therefore we remark that the dispersion relation shape is conic near the Dirac points. A plot is shown in Figure 2.5.

Chapter 3

Phonons and electrons transport

In this section we are going to deal with phonons and electrons transport. The phonons transport regards only the energy, instead the electrons are responsible of the charge transport. Phonons and electrons interact and through the scattering terms these interactions are described.

In few words, if a semiconductor is subject to an external electric field, the electrons will gain energy from the latter and they will produce phonons, by losing energy. Thus, phonons and electrons will interact and from this exchange of energy, other phonons will be generated until will be reached a balance between lost and gained energy and the charges will move with a constant velocity, called saturation velocity. The phonons are also linked to the temperature of the semiconductor, through the crystal vibrations, and therefore to the heat flux.

In this chapter we will focus on both the phonons and electrons transport. In particular, in Section 3.1 the semiclassical phonons transport will be explained and in Section 3.2 the Wigner equation will be introduced. In Section 3.3 we will see the Boltzmann equation and the electron transport.

3.1 Phonons transport

The phonons vary from a material to another but in any case they are grouped in acoustic and optical phonon branches which, in turn, can oscillate in the longitudinal or transversal direction, as already said. The complete dispersion relations can be usually obtained by a numerical approach in the FBZ, $\mathcal{B}$. However, in the applications some standard approximations are often adopted, for dispersion relations.

For the acoustic phonons, the Debye approximation for the dispersion relation

$\varepsilon_\mu(\mathbf{q})$ is usually assumed, $\varepsilon_\mu(\mathbf{q}) = c_\mu|\mathbf{q}|$, $\mu = LA, TA$, where $\mathbf{q}$ is the phonon momentum. c_μ is the sound speed of the μ-branch. Consistently, the FBZ is extended to $\mathbb{R}^d$. Here d is the dimension of the space; $d = 3$ for bulk crystal while $d = 2$ for graphene or similar 2D material like dichalcogenides. Sometimes also the case $d = 1$ is considered but it represents an oversimplification from a physical point of view. We remark that the standard way to express the dispersion relation is in terms of wave-vector. However, in view of the quantum kinetic formulation which will be devised in the next sections, the phonon momentum is a more appropriate variable.

For the longitudinal optical and the transversal optical phonon, the Einstein dispersion relation, $\varepsilon_\mu(\mathbf{q}) \approx$ const, with $\mu = LO, TO$, is usually adopted. Note that under such an assumption, the group velocity of the optical phonons is negligible.

In some peculiar materials like graphene, it is customary to introduce also a fictitious branch called K-phonons constituted by the phonons having wave vectors close to the Dirac points, K or K', in the FBZ (taking the origin in the center Γ of FBZ). Also in this case the Einstein approximation is used on account of the limited variability of the phonon energy near those points. Moreover, in graphene the phonons are classified as in-plane, representing vibration parallel to the material, and out of plane, representing vibrational mode orthogonal to the material. The LA, TA, LO, TO and K phonons are in plane. The out of plane phonons belong to the acoustic branch and are named ZA phonons. For them a quadratic dispersion relation is a good approximation: $\varepsilon_{ZA}(\mathbf{q}) = \overline{\alpha}|\mathbf{q}|^2$, where $\overline{\alpha} = \alpha/\hbar$ with $\alpha = 6.2 \times 10^7 m^2/s$ (see [20]).

Observe that in all the cases considered above, the dispersion relation is isotropic. Hereafter we assume such a property for $\varepsilon_\mu(\mathbf{q})$, $\mu = LA, TA, LO, TO, K, ZA$.

The thermal transport is usually described by macroscopic models, e.g. the Fourier one, those based on the Maximum Entropy methods [17] or on phenomenological description [21]. A more accurate way to tackle the question is to resort to semiclassical transport equations, the so-called Peierls-Boltzmann equations, for each phonon branch for the phonon distributions $f_\mu(\mathbf{x}, \mathbf{q}, t)$

$$\frac{\partial f_\mu}{\partial t} + \mathbf{c}_\mu \cdot \nabla_{\mathbf{x}} f_\mu = C_\mu, \quad \mu = LA, TA, \ldots, \tag{3.1}$$

where $\mathbf{c}_\mu = \nabla_{\mathbf{q}}\, \varepsilon_\mu(\mathbf{q})$ is the group velocity of the μ-th phonon specie.

The phonon collision term C_μ splits into two terms

$$C_\mu = C_\mu^\mu + \sum_{\nu, \nu \neq \mu} C_\mu^\nu, \quad \mu = LA, TA, \ldots. \tag{3.2}$$

C_μ^μ describes the phonon interaction within the same branch while C_μ^ν describes the phonon-phonon interaction between different species. To deal with the complete expressions of the C_μ's is a very complicated task even from a numerical

point of view [22]. So, they are usually simplified by the relaxation time approximation

$$C_\mu = -\frac{f_\mu - f_\mu^{LE}}{\tau_\mu},$$

which mimics the relaxation of each phonon branch towards a common local equilibrium condition, characterised by a local equilibrium temperature T_L that is the same for each phonon population. The τ_μ's are the phonon relaxation times.

The local equilibrium phonon distributions are given by the Bose-Einstein distributions

$$f_\mu^{LE} = \left[\exp(\varepsilon_\mu(\mathbf{q})/k_B T_L) - 1\right]^{-1}, \tag{3.3}$$

where k_B is the Boltzmann constant.

The modern devices, e.g. the electron ones like double gate MOSFETs (see [17]), are undergoing more and more miniaturization. This implies that the characteristic scales are of the same order as the typical lengths where quantum effects become more and more relevant. Therefore, quantum effects must be included and the semiclassical phonon transport equations must be replaced by a more accurate model.

A huge literature has been devoted to the application of the Wigner equations to charge transport (see [1–3]) but a limited use has been made for phonon transport. This original contribute will be presented in the Chapter 6.

3.2 Wigner equation

In the previous section, Weyl's quantization and a set of rules to pass directly from the mathematical world description of classical physical quantities (the phase space) to that of quantum variables (set of operators acting in a Hilbert space) and vice versa has been introduced. It is also underlined how the advantage of this formalism lies precisely in its success to give a description of two very different theories on the same geometric structure, allowing us to fully grasp similarities and differences. To put this program into practice, it will be necessary to identify that quantum operator which, among all, is full of informative content about the state of our system and which, therefore, also allows to express the expectation values of all the relevant physical parameters of the same. What we are essentially looking for is the analogue of the probability function distribution associated with a classical ensemble, which lives in the phase space.

One of the main point of this thesis is the kinetic description of a one-particle quantum statistical state, given in terms of one-particle Wigner functions. Then we want to briefly recall the basic definitions and properties (see chapter 1).

A mixed (statistical) one-particle quantum state for an ensemble of scalar particles in $\mathbb{R}^d$ is described by a density operator $\hat{\rho}$, i.e. a bounded non-negative

operator with unitary trace, acting on $L^2(\mathbb{R}^d, \mathbb{C})$. Given the density operator $\hat{\rho}$ on $L^2(\mathbb{R}^d, \mathbb{C})$, the associated Wigner function, $w = w(\mathbf{x}, \mathbf{p})$, $(\mathbf{x}, \mathbf{p}) \in \mathbb{R}^{2d}$, is the inverse Weyl quantization of $\hat{\rho}$,

$$w = Op_{\hbar}^{-1}(\hat{\rho}). \tag{3.4}$$

We recall that the Weyl quantization of a phase-space function (a *symbol*) $a = a(\mathbf{x}, \mathbf{p})$ is the (Hermitian) operator $Op_{\hbar}(a)$ formally defined by Definition 9. The inverse quantization of $\hat{\rho}$ can be written as the *Wigner transform*

$$w(\mathbf{x}, \mathbf{p}) = \int_{\mathbb{R}^d} \rho(\mathbf{x} + \nu/2, \mathbf{x} - \nu/2) \exp(i\mathbf{p} \cdot \nu/\hbar) d\nu, \tag{3.5}$$

of the kernel $\rho(\mathbf{x}, \mathbf{y})$ of the density density operator. The dynamics of the time-dependent Wigner function $w(\mathbf{x}, \mathbf{p}, t)$, steams directly from the dynamics of the corresponding density operator $\hat{\rho}(t)$, i.e. from the Von Neumann or quantum Liouville equation

$$i\hbar\partial_t \hat{\rho}(t) = [\hat{H}, \hat{\rho}(t)] := \hat{H}\hat{\rho}(t) - \hat{\rho}(t)\hat{H}, \tag{3.6}$$

where $\hat{H}$ denotes the Hamiltonian operators of the particle considered and $[\cdot, \cdot]$ the commutator. If $h = Op_{\hbar}^{-1}(\hat{H})$ is the symbol associated to $\hat{H}$, then, from Eq.s (3.6), we obtain the *Wigner equation*

$$i\hbar\partial_t w(\mathbf{x}, \mathbf{p}, t) = \{h, w(\mathbf{x}, \mathbf{p}, t)\}_* := h * w(\mathbf{x}, \mathbf{p}, t) - w(\mathbf{x}, \mathbf{p}, t) * h. \tag{3.7}$$

Since in the following we will use the limit for $\hbar \to 0$ we need to rescale the previous equation to make $\hbar$ dimensionless. Let $\tilde{\hbar} = \frac{\hbar}{k_B T_L \bar{t}}$ where $\bar{t}$ is a characteristic time and $\tilde{h} = \frac{h}{k_B T_L}$. Dividing both terms of (3.7) by $k_B T_L$ and multiplying and dividing the first member by $\bar{t}$ we get

$$i\frac{\hbar\bar{t}}{k_B T_L \bar{t}}\partial_t w(\mathbf{x}, \mathbf{p}, t) = \frac{h * w(\mathbf{x}, \mathbf{p}, t)}{k_B T_L} - \frac{w(\mathbf{x}, \mathbf{p}, t) * h}{k_B T_L}.$$

Renaming the new quantities by using the tilde symbol we have

$$i\tilde{\hbar}\partial_{\tilde{t}} w(\mathbf{x}, \mathbf{p}, t) = \tilde{h} * w(\mathbf{x}, \mathbf{p}, t) - w(\mathbf{x}, \mathbf{p}, t) * \tilde{h}. \tag{3.8}$$

that has the same form of the Wigner equation from which we start, but rescaled. Since $\hbar = 6.582 \times 10^{-16} eVs$ and $k_B T_L \bar{t} \approx 0.0259 \times 10^{-12} eVs$ at room temperature $T_L = 300K$ and with a characteristic time of $\bar{t} = 10^{-12}s$, the ratio $\hbar/k_B T_L \bar{t}$ is small enough to justify the limit for $\hbar \to 0$ and consequently the expansion in $\hbar$. In the following, for saking of semplicity, we will omit the tilde for this equation but the previous transformation is intended to hold.

The procedure described in this paragraph is used both for phonons and for electrons.

3.3 Electrons transport

In this section we will introduce the charge transport in solids. In particular, the Boltzmann equation will be presented. This last is fundamental for the following developments, but it is also very complex to solve, for this reason the moments equations will be introduced.

This last procedure simplifies the equations on one hand and creates some issues on the other hand. For this reason we need to introduce also the Maximum Entropy method. The plan of this section is to present the equations that describe the electron transport and then to introduce the moments equations in the last subsection. A whole chapter will be dedicated for the Maximum Entropy Method.

3.3.1 Boltzmann equation

First, we would like to specify the meaning of semiclassical and quantum approach. We know that the classical physics is not enough to describe all the complex situations that can occur, because of the assumptions that characterize this branch of physics: it is accurate only for large objects that are not extremely massive and with speeds far from the light speed. When very small devices are considered, the classical mechanics fails, so a semiclassical or quantum approach is used.

The Boltzmann equation is an example of the semiclassical approach: indeed, this equation describes a system of many particles using a distribution function. It leads to a macroscopic semiclassical charge transport model as we will see in the next paragraphs.

Let $f(\mathbf{x}, \mathbf{k}, t)$ be the distribution function that represents the number of particles per state in $\mathbf{x}$ and in $\mathbf{k}$ at time t. Then, if we consider a system made by N particles, the normalization condition has to be satisfied:

$$\frac{2}{(2\pi)^3} \int_B \int_{\mathbb{R}^3} f(\mathbf{x}, \mathbf{k}, t) d\mathbf{k} d\mathbf{x} = N, \tag{3.9}$$

while if we integrate only over $d\mathbf{k}$ we obtain the particle space density at time t. Under this condition, the semiclassical Boltzmann equation for electrons in the conduction band is

$$\frac{\partial f}{\partial t} + \mathbf{v}(\mathbf{k}) \cdot \nabla_{\mathbf{x}} f - \frac{e}{\hbar} \mathbf{E} \cdot \nabla_{\mathbf{k}} f = C[f], \tag{3.10}$$

where $\mathbf{v}$ is the electron velocity, $\mathbf{E}$ is the electric field and $C[f]$ is the collision term that describes the interactions between electrons and impurites or phonons or electrons them selves. Since the expression of the collision term is rather complex, some collisions that don't give a big contribution to the collisional term are usually neglected and only the phonons-electrons collisions are taken into account. The collisions can be intra or inter valley if after the collision the

electrons remain in the same valley or in another one, respectively; they can be classified also as intra or inter band for reasons analogous to the previous explained for valleys.

Mathematically, these interactions can be expressed by using the Fermi's golden rule: for a generic intravalley and intraband collision, we get

$$C[f] = \frac{1}{(2\pi)^3} \int_B [P(\mathbf{k}, \mathbf{k}')f(\mathbf{k}')(1 - f(\mathbf{k})) - P(\mathbf{k}, \mathbf{k}')f(\mathbf{k})(1 - f(\mathbf{k}'))]d^3\mathbf{k}', \tag{3.11}$$

where $P(\mathbf{k}, \mathbf{k}')$ is the transition probability per unit time from the state $\mathbf{k}$ to the state $\mathbf{k}'$ and the two terms of the difference are respectively the gain and the loss term, and they describe the Pauli exclusion principle.

Observation 10 *The factor $\frac{1}{(2\pi)^3}$ is not multiplied by 2 because the collisions doesn't change the spin of the electron. In the normalization condition, it is multiplied by 2 because the spin electron is taken into account.*

Under the assumption that $f << 1$ we can linearize the collision term. Substituing f with f_{eq} that is the equilibrium state distribution (as Fermi-Dirac distribution) and using the balance principle (for which the gain and the loss term have to be equal), the transition rate for the scattering between electrons and phonons can be deduced. It will depends on the dispersion relation and different expression for each different branch of phonons will be used. Sometimes the collision term could be calculated in the relaxation time approximation, by introducing the relaxation time τ and it reads

$$C[f] = -\frac{f - f_{eq}}{\tau}. \tag{3.12}$$

Since the Boltzmann equation is an integro-differential equation not easy to solve, both analitically and numerically, some macroscopic quantities can be introduced to simplify the equation and to obtain an equivalent system of equations easier to solve. In this way, the microscopic and the macroscopic quantities of the physical system are linked. The number of equations and moments introduced depend on the model that we want to consider: if we consider the energy density and the energy flux density we obtain an energy-transport model; if we introduce charge density, velocity, energy and energy flux we obtain an hydrodynamical model. In the next paragraph we will introduce them.

3.3.2 Moments equations

Starting from the Boltzmann equation (3.10) the moments equations can be deduced, multiplying it by the weight functions and integrating over $d\mathbf{k}$. But,

how a moment is defined? Let us consider a weight function, regular enough, $\Psi(\mathbf{k})$. We define the moments as follows:

$$M_\Psi = M_\Psi(\mathbf{x}, t) := \frac{2}{(2\pi)^3} \int_B \Psi(\mathbf{k}) f(\mathbf{x}, \mathbf{k}, t) d\mathbf{k}. \tag{3.13}$$

In this way, the macroscopic quantites we need for our model by varying the weights are obtained. Of course one of the weights is $\Psi(\mathbf{k}) = 1$ to obtain the electron density.

The next step is to use these weights to get the moments equations as follows:

$$\frac{\partial M}{\partial t} + \int_B \frac{2\Psi(\mathbf{k})}{(2\pi)^3} \mathbf{v}(\mathbf{k}) \cdot \nabla_{\mathbf{x}} f d\mathbf{k} - \frac{e}{\hbar} \mathbf{E} \cdot \int_B \frac{2\Psi(\mathbf{k})}{(2\pi)^3} \nabla_{\mathbf{k}} f d\mathbf{k} = \int_B \frac{2\Psi(\mathbf{k})}{(2\pi)^3} C[f] d\mathbf{k}. \tag{3.14}$$

Then, a system of some equations is obtained. Formally in number equal to the number of the moments introduced but, by developing the calculation of the integrals we can observe that some additional quantites appear. So the advantage of this approach is that integrating over $\mathbf{k}$ a variable from the equation is "eliminated" and we will deal with some easier equation to solve by getting some macroscopic quantities that have a specific physical meaning. The price to pay is that new additional quantities appear and then the system obtained is not closed. The good news is that this issue is solvable in different ways. The two most used solutions are the drift-diffusion approach or the Maximum entropy principle.

The first approach has some limitations because it holds only for low fields and for constant temperatures. Sometimes it could be a good compromise to solve the closure issue by introducing a constitutive relation in which a term of drift and a term of diffusion appear (from which the name of this approach).

The solution based on the Maximum Entropy Principle is more complex but more general and it will be introduced in the next chapter.

Chapter 4

Maximum Entropy Principle

Before showing the method to close the previous system, the definition of entropy has to be introduced, together with its properties and how to use them to infer a distribution. We will distinguish between the discrete and continuous case, even if for this thesis only the second case will be used. The procedure based on the maximum entropy principle could seem complex, but will be clarified in the next sections, also through some examples to get the Fermi-Dirac distribution and the Bose-Einstein distribution that are fundamental to describe the fermions and the bosons transport, respectively. The difference between fermions and bosons is that for the first ones the Pauli exclusion principle doesn't hold, while for the bosons it has to be taken into account. The particles that we will consider for our work are electrons and phonons and they are particular cases of fermions and bosons, respectively. For these reasons this chapter is crucial for the charge transport and to understand the link between the particles and their dynamics by using the statistical mechanics and its main distributions. The interested reader is referred to [17] for more details.

4.1 Entropy and its properties

The concept of entropy was introduced by Boltzmann in the statistic mechanics, by Clausius in thermodynamics like a thermodynamical potential and by Jaynes and Shannon in the information theory.

Mathematically the formulation of Boltzmann entropy is expressed by

$$S = k_B \log W$$

where W is a quantity proportional to the number of microstates of the system.

This formula could be seen as a link between microscopic and macroscopic physical worlds.

From now on, we will focus on the Jaynes-Shannon definition of entropy. The idea under the maximum entropy approach is to maximize the entropy, that in the information theory represents the amount of ignorance of the system by the observer. This is the crucial difference: for Boltzmann-Clausius the entropy is a property of the system, while for Jaynes-Shannon the entropy is a property of the observer. By maximizing this last amount of ignorance, under certain constraints, the expressions of statistical mechanics are obtained.

There are three axioms underlie this theory. Let us consider first the discrete case of a random variable X which takes the values in the set $\Omega = \{x_1, x_2, ..., x_n\}$ with a priori probability $p_1, p_2, ..., p_n$, satisfying, of course, the condition

$$\sum_{i=1}^{n} p_i = 1.$$

Let consider the function $S(p_1, ..., p_n)$ as the measure of the uncertainty associated to the system, where $(p_1, ..., p_n)$ is the probability distribution that we know only partially. The first axiom guarantees the continuity of the function in its variables, for technical reasons. The second axiom explains, intuitively, that if we have more possible outcomes, we will have more uncertainty. The third axiom is not very intuitive, but it is related to the conditional probability.

Formally, the axioms are expressed as follows:

- **Continuity** The function that represents the information entropy is continuos;
- **Equally likely cases** If all p_i are equal, the quantity $S(\frac{1}{n}, ..., \frac{1}{n})$ is a monotonically increasing function of its number of arguments;
- **Grouping axiom** If the values of a discrete random variable X are grouped in m disjoint sets $\{x_{11}, ..., x_{1k_1}\}$,$\{x_{21}, ..., x_{2k_2}\}$,...,$\{x_{m1}, ..., x_{mk_m}\}$, the probabilities of these events are $w_j = p_{j1} + p_{j2} + ... + p_{jk_j}$, $j = 1, ..., m$. The grouping axiom requires

$$S(p_1, p_2, ..., p_n) = S(w_1, ..., w_m) + w_1 S\left(\frac{p_{11}}{w_1}, ..., \frac{p_{1k_1}}{w_1}\right) + ... + w_m S\left(\frac{p_{m1}}{w_m}, ..., \frac{p_{mk_m}}{w_m}\right).$$

These three axioms are fundamental to recover the expression of the information entropy that is the following:

$$S(p_1, p_2, ..., p_n) = -C \sum_{i=1}^{n} p_i \log p_i, \tag{4.1}$$

where the constant $C > 0$ depends on the unit used.

The expression of S is valid also if $p_i = 0$ for some i, formally setting $0 \log 0 := 0$ which preserves also the continuity of $S(p_1, ..., p_n)$.

It is possible to prove the following results:

Theorem 4 *Let us define*

$$H(n) = S\left(\frac{1}{n}, \frac{1}{n}, ..., \frac{1}{n}\right), \quad n = 1, 2, ...$$

then $H(n) = C \log n$ *with* $C > 0$.

Theorem 5 *The only function that satisfies the three axioms before introduced is the (4.1).*

The Shannon-Jaynes Entropy has the following properties:

Property 1

The information entropy has $\left(\frac{1}{n}, \frac{1}{n}, ..., \frac{1}{n}\right)$ as point of maximum.

Property 2

The information entropy is not affected by the events of zero probability.

Property 3

The information entropy of a system is correlated to the information entropy of its parts.

The random variable X before considered was discrete, if we consider a continuos variable X with a probability density $p(x), x \in \mathbb{R}^d$, we can generalize the previous definition of entropy as follows:

$$S[p(x)] = -C \int_{\mathbb{R}^d} p(x) \log \left[\frac{p(x)}{m(x)}\right] dx. \tag{4.2}$$

where we have introduced the measure $m(x)$ to let be the entropy invariant for coordinates transformation; indeed a relative entropy is obtained, in this way. There is also the analougus relative entropy in the discrete case. The difference between the two cases is that the entropy in the continuous case is not always defined in sign and can be considered only for the calculation of decreasing or increansing of uncertainty.

4.2 Inference of a distribution

In this section the Maximum Entropy Principle (MEP) will be introduced in detail. Since the entropy is different if the random variable is continuos or discrete, also for the MEP we should distinguish between these two cases. The main goal in this procedure is to find a distribution that maximizes the entropy under certain constraints. This procedure described mathematically, assumes the physical meaning of maximizing the amount of ignorance of the observer by knowing only partially the system and this information will be expressed by some

mean values functions, that will be the constraints of our optimization problem. From a statistical point of view, we want to find the least biased estimator of our random variable X, that could be discrete or continuous [17].

4.2.1 Discrete case

Let us consider a discrete random variable X with n possible outcomes $x_1, x_2, ..., x_n$. Let suppose that r avarage of functions are known

$$\langle f_r(x) \rangle = \sum_{i=1}^{n} p_i f_r(x_i), \quad r = 1, ..., m.$$

where $f_r : \{x_1, x_2, ..., x_n\} \longrightarrow \mathbb{R}$ are assigned.

The goal is to estimate the probabilities $p_1, p_2, ..., p_n$ associated to the different n outcomes, with $p_i = p(x_i)$. To solve this problem the following procedure will be used:

the least biased estimator of p_i, $i =, ..., n$, with respect to the only knowledge of the avarages $\langle f_r \rangle$, $r = 1, ..., m$, is given by the maximization of the entropy $S = -C \sum_i p_i \log(p_i/m_i)$ under the constraints

$$\sum_{i=1}^{n} p_i = 1,$$

$$\langle f_r(x) \rangle = \sum_{i=1}^{n} p_i f_r(x_i), \quad r = 1, ..., m.$$

The idea is to convert this constrained optimization problem to a non constrained one, by using the Lagrangian function $\mathcal{L}$ that is the difference between the objective function (the entropy in our case) and the Lagrange multipliers λ_r multiplied for each constraint:

$$\mathcal{L}(p_1, ..., p_n, \lambda_0, ..., \lambda_r) = -C \sum_i p_i \log(p_i/m_i) - \lambda_0 \left(\sum_{i=1}^{n} p_i - 1 \right) \tag{4.3}$$

$$- \sum_{r=1}^{m} \lambda_r \left[\langle f_r(x) \rangle - \sum_{i=1}^{n} p_i f_r(x_i) \right].$$

By calculating the derivative of $\mathcal{L}$ with respect to its variables and imposing that these derivatives are equal to zero, we obtain a system of $n + r + 1$ equations of which $r + 1$ are the constraints of the initial problem and by substituing them in the first n equations

$$p_i = m_i \exp\left(-\lambda_0 - \sum_{r=1}^{m} \lambda_r f_r(x_i) \right), \quad i = 1, ..., n. \tag{4.4}$$

we will obtain the general solution for the p_i:

$$p_i = \frac{m_i}{Z} \exp\left(-\sum_{r=1}^{m} \lambda_r f_r(x_i)\right), \quad \lambda_0 = \log Z, \tag{4.5}$$

where we have transformed $1+\frac{\lambda_0}{C} \mapsto \lambda_0$, $\frac{\lambda_r}{C} \mapsto \lambda_r$ and $Z = \sum_{i=1}^{n} m_i \exp\left(-\sum_{r=1}^{m} \lambda_r f_r(x_i)\right)$ is the partition function.

As known, this procedure leads to a possible relative extreme point, but to be sure that this last is the maximum for S we need a direct verification.

Substituing (4.4) in S and using the result for which if we have two probability vectors $(p_1, ..., p_n)$ and $(q_1, ..., q_n)$ then it holds the following inequality

$$-\sum_{i=1}^{n} q_i \log \frac{q_i}{m_i} \leq -\sum_{i=1}^{n} q_i \log \frac{p_i}{m_i},$$

at the end our goal is reached.

The discrete case could be divided into finite and countable case, but we will not enter into the details for this second case that is more daunting because we will have series instead of simple summations, then the problem of the convergence arises and for this reason some restrictions to the choiche of the known avarages f_r will be required.

4.2.2 Continuous case

In analogy with the discrete case, now we will speak about the continuous case. In this case we start from a continuous random variable and for this reason a distribution function $f : \mathbb{R}^d \longrightarrow \mathbb{R}_0^+$ has to be introduced. The constraints are the known information of the system and in this case are expressed as follows:

$$\langle \mu_A \rangle = \int_{\mathbb{R}^d} \mu_A(x) f(x) dx, \quad A = 1, .., N, \tag{4.6}$$

where

$$\mu_A : \mathbb{R}^d \longrightarrow \mathbb{R}^{d_A}, \quad A = 1, ..., N,$$

are called weight functions and $d_A \in \mathbb{N}$ is such that the integrals in (4.6) there exist and they are finite. The aim is to estimate the distribution function f, by knowing only the assigned functions μ_A. Also in this case we can formulate the MEP:

Maximum Entropy Principle

The least biased estimator for f by knowing only a finite number of averages functions is given by the maximization of the entropy

$$S[g] = -C \int_{\mathbb{R}^d} g(x) \log \frac{g(x)}{m(x)} dx,$$

under the constraints

$$\langle \mu_A \rangle = \int_{\mathbb{R}^d} \mu_A(x) g(x) dx, \quad A = 1, .., N,$$

by letting vary $g(x) : \mathbb{R}^d \longrightarrow \mathbb{R}_0^+$ *in the set of distribution functions that allows the integrals to exist and to be finite.*

The procedure to follow is analogous with the discrete case. We introduce the Lagrangian $\mathcal{L}$ and the Lagrange multipliers λ_A

$$\mathcal{L}(g, \lambda_1, ..., \lambda_N) = S[g] + \sum_{A=1}^{N} \lambda_A \left(\langle \mu_A \rangle - \int_{\mathbb{R}^d} \mu_A(x) g(x) dx \right). \tag{4.7}$$

Now the Lagrangian should be derived, but in this case we have a functional, not a function, so the first variation is needed:

$$\delta \mathcal{L} = - \int_{\mathbb{R}^d} \delta g \left[C \left(\log \frac{g(x)}{m(x)} + 1 \right) + \sum_{A=1}^{N} \lambda_A \mu_A(x) \right] dx = 0. \quad \forall \delta g,$$

and the solution that we get is the following:

$$f_{MEP}(x) = m(x) \exp \left(- \left(1 + \sum_{A=1}^{N} \frac{\lambda_A}{C} \mu_A(x) \right) \right)$$

under the constraints

$$\langle \mu_A \rangle = \int_{\mathbb{R}^d} \mu_A(x) f_{MEP}(x) dx, \quad A = 1, .., N.$$

Also in this case, as in the countable discrete case, we need some restrictions on the weight functions in order to have the existence and the convergence of the integrals.

4.3 Classical case: Maxwell-Boltzmann distribution

In this section, we would like to do a first example to use the above presented procedure in order to obtain the Maxwell-Boltzmann distribution. Let consider a random variable X that in this case is discrete and it represents the number of particles in a certain energy level ε_i. The corresponding probabilities are p_i and they are the variables of our optimization problem.

At this point, some information about the system under consideration are necessary to define the constraints. These information are, at thermal equilibrium, the following:

- The total number of particles in the system is N;

- the total energy of the system is E;
- n_i is the number of particles for each i-th energy level ($\sum_i n_i = N$);
- the number of quantum states available for each energy level ε_i is G_i and is called degeneracy;
- we assume that the particles are distinguishable, that they don't interact and they follow the laws of classical mechanics.

From these assumptions, we can write mathematically the optimization problem:

$$S = -k_B \sum_i p_i \log \frac{p_i}{G_i}$$

$$\sum_i p_i = 1, \quad \sum_i p_i \varepsilon_i = \overline{\varepsilon},$$

where $\overline{\varepsilon} = E/N$ and S is the entropy to maximize. The general constant C in this case is equal to k_B.

By following the procedure before introduced the Maxwell-Boltzmann distribution will be obtained:

$$p_i = \frac{G_i}{Z} \exp(-\lambda \varepsilon_i), \tag{4.8}$$

where $Z = \sum_i G_i \exp(-\lambda \varepsilon_i)$ and λ is the Lagrange multiplier relative to the energy constraint (the constant k_B is included in the multiplier as we have already seen before).

4.4 Quantum case: Fermi-Dirac and Bose-Einstein distributions

In these two examples we will consider a system that obeys to quantum mechanics and made of identical and indistinguishable particles. The difference between the two cases is that for fermions the Pauli's exclusion principle holds, instead for bosons not.

But we will start from the same hypothesis:

- The total number of particles in the system is N;
- The total energy of the system is E;
- p_{ijn} is the probability that the j-th quantum state has n particles in the i-th energy level ε_i;
- $\langle n_i \rangle = \sum_{j=1}^{G_i} \sum_n p_{ijn} n$ is the avarage number of particles in the energy level ε_i.

Known this information, the entropy to maximize is the following

$$S = -C \sum_i \sum_{j=1}^{G_i} \sum_n p_{ijn} \log p_{ijn}$$

under the constraints

$$\sum_i \langle n_i \rangle = N, \quad \sum_i \langle n_i \rangle \varepsilon_i = E.$$

The solution obtained by the MEP procedure is the following:

$$p_{ijn} = \frac{\exp(-(\lambda_1 + \lambda_2 \varepsilon_i) n)}{\sum_r \exp(-(\lambda_1 + \lambda_2 \varepsilon_i) r)},$$

where λ_1, λ_2 are the Lagrange multipliers and the constant C is included in them. Now we have to distinguish between fermions and bosons by taking into account the Pauli exclusion principle:

- Fermi-Dirac distribution:

  In this case, since the Pauli exclusion principle is valid, we can consider only $n = 0, 1$ then

  $$\langle n_i \rangle = \frac{G_i}{1 + \exp(\lambda_1 + \lambda_2 \varepsilon_i)}.$$

- Bose-Einstein distribution:

  in this case $n = 0, 1, ...$ then

  $$\langle n_i \rangle = \frac{\sum_{j=1}^{G_i} \sum_{n=0}^{+\infty} n \exp(-(\lambda_1 + \lambda_2 \varepsilon_i) n)}{\sum_{n=0}^{+\infty} \exp(-(\lambda_1 + \lambda_2 \varepsilon_i) n)},$$

  by using the known sum of the series that appear in the previous expressions we have:

  $$\langle n_i \rangle = \frac{G_i}{\exp(\lambda_1 + \lambda_2 \varepsilon_i) - 1}, \tag{4.9}$$

  with $\lambda_1 + \lambda_2 \varepsilon_i > 0$.

  To recover the expression of the statistical mechanics we impose that $\lambda_1 = -\frac{\mu}{k_B T}, \quad \lambda_2 = \frac{1}{k_B T}$ where μ is the chemical potential.

Finally, we can conclude that the Fermi-Dirac and Bose-Einstein distribuitions have been obtained and they are:

$$f(\varepsilon_i) = \frac{\langle n_i \rangle}{G_i} = \frac{1}{\exp(\frac{\varepsilon_i - \mu}{k_B T}) \pm 1} \tag{4.10}$$

where the sign "+" is for fermions and the sign "-" is for bosons.

4.5 Quantum Maximum Entropy Principle

In this section we will present the corresponding procedure for Maximum Entropy Principle in the quantum case, even if it's not trivial to extend the previous procedure. In the classical case, given a probability function $f(x)$ the entropy is defined as

$$S = -k_B \int f(x) \log f(x) dx = -k_B \langle \log f \rangle.$$

In the quantum case, the role of the distribution function f is played by the density operator $\hat{\rho}$. One defines, in analogy with the classical case, the quantum entropy as follows:

$$S(\hat{\rho}) = -k_B \mathrm{tr}(\hat{\rho} \log \hat{\rho})$$

where tr is the trace of an operator [23]. The expression above should be interpreted in the following way: let us suppose that $\hat{\rho}$ is written in terms of an orthonormal basis ψ_i (for sake of simplicity, we consider the discrete case) $i = 0, 1, 2, ...$

$$\hat{\rho} = \sum_i \rho_i P_{\psi_i} = \sum_i \rho_i |\psi_i\rangle\langle\psi_i|;$$

where

$$\sum_i \rho_i = 1, \quad \rho_i \geq 0,$$

and P_{ψ_i} is the projection on the space generated by ψ_i and then

$$S(\hat{\rho}) = -k_B \sum_i \rho_i \log \rho_i.$$

Let us suppose that the average energy of the system is known

$$\langle H \rangle = \mathrm{tr}(\hat{\rho} H).$$

We should remember that the evolution equation for $\hat{\rho}$ is given by

$$\frac{d\hat{\rho}}{dt} = \{\hat{\rho}, H\}.$$

At the equilibrium the state γ of the system doesn't change and then $\hat{\rho}$ (that it's in one-to-one correspondence with γ) doesn't depend on the time. So, it implies that $[\hat{\rho}, H] = 0$.

Proposition 9 *Let A, B be two observables. $[A, B] = 0$ if and only if there exists a basis with respect to which both A and B have a diagonal representation.*

We know that $[\hat{\rho}, H] = 0$ then it follows that there exists a basis with respect to which both $\hat{\rho}$ and H assume the same diagonal form. Called (ψ_i) this basis

$$\hat{\rho} = \sum_i \rho_i P_{\psi_i} = \sum_i \rho_i |\psi_i\rangle\langle\psi_i|$$

$$H = \sum_i \varepsilon_i \psi_i = \sum_i \varepsilon_i |\psi_i\rangle\langle\psi_i|$$

$$\langle H \rangle = \sum_i \rho_i \varepsilon_i.$$

In order to get $\hat{\rho}$ at the equilibrium $\hat{\rho}^{eq}$, we have to maximize S_Q under the constraints

$$\sum_i \rho_i^{eq} = 1; \quad \sum_i \rho_i^{eq} \varepsilon_i = \langle H \rangle,$$

where H is an assigned value. (It represents the average of the macroscopic energy), $\rho_i \geq 0 \quad i = 1, 2, ...$

$$0 = \delta \left[S(\hat{\rho}) - \alpha \left(1 - \sum_i \rho_i^{eq} \right) - \beta \left(\langle H \rangle - \sum_i \rho_i^{eq} \varepsilon_i \right) \right]$$

$$0 = \frac{\partial}{\partial \rho_j^{eq}} (S(\hat{\rho})) + \alpha + \beta \varepsilon_j = -k_B \log \rho_j^{eq} + \alpha - k_B + \beta \varepsilon_j$$

$$\rho_j^{eq} = z \exp\left(-\frac{\beta}{k_B} \varepsilon_j \right), \qquad \exp\left(-\frac{\beta}{k_B} H \right) = \sum_i \exp\left(-\frac{\beta}{k_B} \varepsilon_i \right) P_{\psi_i}.$$

z is the partition function; from the first constraint

$$z = \left(\sum_j \exp\left(-\frac{\beta}{k_B} \varepsilon_j \right) \right)^{-1} = tr\left(\exp\left(-\frac{\beta}{k_B} H \right) \right).$$

β is expressed as $\beta = \frac{1}{T}$ where T is the absolute temperature in analogy with the classical case. Therefore

$$\hat{\rho} = \frac{1}{z} \sum_j \exp\left(-\frac{\varepsilon_j}{k_B T} \right) P_{\psi_j} = \frac{1}{z} \exp\left(-\frac{1}{k_B T} H \right) = \frac{\exp\left(-\frac{H}{k_B T} \right)}{tr\left(\exp\left(-\frac{H}{k_B T} \right) \right)}.$$

The internal energy is the following:

$$U = \mathrm{tr}(\hat{\rho} H) = \frac{\sum_j \varepsilon_j \exp\left(-\frac{\varepsilon_j}{k_B T} \right)}{\sum_j \exp\left(-\frac{\varepsilon_j}{k_B T} \right)} =$$

$$= \frac{\partial}{\partial \sigma} \ln \left(\sum_j \exp(-\varepsilon_j \sigma) \right) = \frac{\partial}{\partial \sigma} \ln z,$$

where $\sigma = \frac{1}{k_B T}$.

4.5.1 Entropy including the statistics

The starting point is the entropy for the quantum system under consideration. We take as entropy a generalization of the classical one for bosons (upper sign) or fermions (lower sign). Let us introduce the operator

$$s(\hat{\rho}) = -k_B[\hat{\rho}\ln\hat{\rho} \mp (1 \pm \hat{\rho})\ln(1 \pm \hat{\rho})], \tag{4.11}$$

which must be intended in the sense of the functional calculus. The corresponding quantum entropy reads

$$S(\hat{\rho}) = \mathrm{tr}\{s(\hat{\rho})\}$$

which can be viewed as a quantum Bose-Einstein (Fermi-Dirac) entropy.

Also in this case, we estimate $\hat{\rho}$ with $\hat{\rho}^{MEP}$ which is obtained by maximizing $S(\hat{\rho})$ under the constraints that some expectation values have to be preserved.

The quantum formulation of MEP is given in terms of expectation values

$$E_1(t) = \mathrm{tr}\left\{\hat{\rho}\right\}(t) = 1, \quad E_2(t) = \mathrm{tr}\left\{\hat{\rho}H\right\}(t),$$

as follows: for fixed t

$$\hat{\rho}^{MEP} = \text{argument max}\, S(\hat{\rho}) \tag{4.12}$$

under the constraints

$$\mathrm{tr}\{\hat{\rho}^{MEP}\} = E_1(t), \quad \mathrm{tr}\{\hat{\rho}^{MEP}H\} = E_2(t), \tag{4.13}$$

in the space of the Hilbert-Schmidt operators on $L^2(\mathbb{R}^d, \mathbb{C})$ which are positive, with trace one and such that the previous expectation values there exist.

If we introduce the vector of the Lagrange multipliers

$$\eta = (\eta_0(\mathbf{x}, t), \eta_1(\mathbf{x}, t)), \tag{4.14}$$

the constrained optimization problem (4.12)-(4.13) can be rephrased as a saddle-point problem for the Lagrangian $\mathcal{L}(\hat{\rho}, \eta)$ in the space of the admissible $\hat{\rho}$ and smooth function η.

If the Lagrangian $\mathcal{L}(\hat{\rho}, \eta)$ is Gâteaux-differentiable with respect to $\hat{\rho}$, the first order optimality conditions require

$$\delta\mathcal{L}(\hat{\rho}, \eta)(\delta\hat{\rho}) = 0$$

for each Hilbert-Schmidt operators $\delta\hat{\rho}$ on $L^2(\mathbb{R}^d, \mathbb{C})$ which is positive, with trace one and such that the previous expectation values there exist.

The existence of the first order Gâteaux derivative is a consequence of the following Lemma.

Lemma 1 *If $r(x)$ is a continuously differentiable increasing function on $\mathbb{R}^+$ then $tr\{r(\hat{\rho})\}$ is Gâteaux-differentiable in the class of the Hermitian Hilbert-Schmidt positive operators on $L^2(\mathbb{R}^d, \mathbb{C})$. The Gâteaux derivative along $\delta\rho$ is given by*

$$\delta tr\{r(\hat{\rho})\}(\delta\hat{\rho}) = tr\left\{r'(\hat{\rho})\delta\hat{\rho}\right\}. \tag{4.15}$$

The extremality conditions for the unconstrained optimization problem are similar to that of the semiclassical case, as expressed by the following lemma.

Lemma 2 *The first order optimality condition for the optimization problem (4.12)-(4.13) is equivalent to*

$$\hat{\rho} = (s')^{-1}(Op_\hbar(\boldsymbol{\eta} \cdot \boldsymbol{\Psi})) \tag{4.16}$$

where $(s')^{-1}$ *is the inverse function of the first derivative of* s *and* $\boldsymbol{\Psi}$ *is the vector of weights, in our example* $\boldsymbol{\Psi} = (1, H)$.

Proof. By applying Lemma 3, the Gâteaux derivative of the Lagrangian is given by

$$\delta\mathcal{L}(\hat{\rho}, \boldsymbol{\eta})(\delta\hat{\rho}) = \operatorname{tr}\left\{(s'(\hat{\rho}) - Op_\hbar(\boldsymbol{\eta} \cdot \boldsymbol{\Psi}))\, \delta\hat{\rho}\right\}$$

$\forall \delta\hat{\rho}$ perturbation in the class of the Hermitian Hilbert-Schmidt positive operators on $L^2(\mathbb{R}^d, \mathbb{C})$. This implies

$$s'(\hat{\rho}) = Op_\hbar(\boldsymbol{\eta} \cdot \boldsymbol{\Psi}).$$

□

Since the function $s(x)$ is concave, $s'(x)$ is invertible. Explicitly we have

$$(s')^{-1}(z) = \frac{1}{\exp(z/k_B) \pm 1},$$

where we have rescaled the Lagrange multipliers including the factor $1/k_B$, and the operator solving the first order optimality condition reads

$$\hat{\rho}^* = (s')^{-1}(Op_\hbar(\boldsymbol{\eta} \cdot \boldsymbol{\Psi})) = \frac{1}{\exp(Op_\hbar(\boldsymbol{\eta} \cdot \boldsymbol{\Psi})) \pm 1}. \tag{4.17}$$

Moreover, such an operator is a point of maximum for the Lagrangian.

Now, to complete the program we have to determine, among the smooth functions, the Lagrange multipliers $\boldsymbol{\eta}$ by solving the constraints.

If the constraints equations have a solution $\boldsymbol{\eta}^*$, altogether the MEP density operator reads

$$\hat{\rho}^{MEP} = \frac{1}{\exp\left[Op_\hbar\left(\eta_0^*(\mathbf{x}, t) + \eta_1^*(\mathbf{x}, t)H\right)\right] \pm 1}. \tag{4.18}$$

To determine conditions under which the constraints equations admit solutions is a very difficult task. Even in the semiclassical case there are examples of sets of moments that cannot be moments of a MEP distribution.

We will see in the following, how to determine them, in the case of phonons and electrons transport.

Chapter 5

Optimized hydrodynamical model for charge transport in graphene

In this chapter we will present the original result [38] where an hydrodynamical model for charge transport in suspended monolayer graphene have been devised.

Some similar models have been developed in [10, 17, 27, 39–41] where closure relations have been obtained by adopting the Maximum Entropy Principle (MEP). In our work, we used some physical parameters present in the production terms such as the acoustic phonon, the optical phonon and the K-phonon coupling constants, to optimize the previous models.

They depend on the modelling of the energy band and scattering terms. Here, we try to improve the hydrodynamical model proposed in [39] by an optimisation of the parameters above through a minimisation of the difference between velocity and energy, found with the considered hydrodynamical models and the direct solution of the Boltzmann equation obtained with a Discontinuous Galerkin (DG) method.

5.1 Boltzmann Equation

In a semiclassical kinetic setting, the charge transport in graphene is described, in general, by four Boltzmann equations, one for electrons in the valence (π) band and one for electrons in the conduction (π^*) band, that in turn can belong to the K or K' valley. Here, we assume that the K and K' valleys are equivalent. Moreover, by applying a gate voltage transversal with respect to the graphene sheet, it is possible to modify the Fermi energy ε_F and therefore the charge density. As shown in [45], if the Fermi energy is high enough (more than about

0.2 eV), the contribution to the current due to holes in the valence band is negligible with respect to that of electrons in the conduction band. Therefore, only the transport equation for electrons in the conduction band is considered and interband transitions are neglected. It can be written as

$$\frac{\partial f}{\partial t} + \mathbf{v} \cdot \nabla_{\mathbf{x}} f - \frac{e}{\hbar} \mathbf{E} \cdot \nabla_{\mathbf{k}} f = \mathcal{C}(\mathbf{k}) \tag{5.1}$$

where $f = f(t, \mathbf{x}, \mathbf{k})$ represents the distribution function of electrons in the conduction band at position $\mathbf{x}$, time t and wave-vector $\mathbf{k}$. We denote by $\nabla_{\mathbf{x}}$ and $\nabla_{\mathbf{k}}$ the gradients with respect to the position and the wave vector, respectively. The group velocity $\mathbf{v}$ is related to the energy band ϵ by $\mathbf{v} = \frac{1}{\hbar} \nabla_{\mathbf{k}} \epsilon$. With a very good approximation [42], a linear dispersion relation holds for the energy bands around the Dirac points; so that, choosing the origin of the reference frame in the $\mathbf{k}$-space coinciding with a Dirac point, we have $\epsilon = \hbar \mathbf{v}_F |\mathbf{k}|$, where $\mathbf{v}_F$ is the (constant) Fermi velocity and $\hbar$ the Planck constant divided by 2π.

The Brillouin zone is extended to $\mathbb{R}^2$. The elementary (positive) charge is denoted by e. Here the electric field $\mathbf{E}$ is assumed as external, and therefore we do not include the Poisson equation. The right hand side of Eq.(5.1) is the collision term which takes into account scatterings between electrons and phonons. In suspended monolayer graphene three kinds of phonons have to be considered: acoustic, optical and K phonons. We assume that phonons are in thermal equilibrium.

The collision term can be written as

$$\mathcal{C}(\mathbf{k}) = \int_{\mathbb{R}^2} S(\mathbf{k}', \mathbf{k}) f(t, \mathbf{x}, \mathbf{k}')(1 - f(t, \mathbf{x}, \mathbf{k}))d\mathbf{k}' - \int_{\mathbb{R}^2} S(\mathbf{k}, \mathbf{k}') f(t, \mathbf{x}, \mathbf{k})(1 - f(t, \mathbf{x}, \mathbf{k}'))d\mathbf{k}' \tag{5.2}$$

where the total transition rate is given by the sum of the contributions of the above mentioned types of scatterings

$$S(\mathbf{k}', \mathbf{k}) = \sum_{\nu} |G^{(\nu)}(\mathbf{k}', \mathbf{k})|^2 \left[\left(n_{\mathbf{q}}^{(\nu)} + 1 \right) \delta \left(\epsilon(\mathbf{k}) - \epsilon(\mathbf{k}') + \hbar \omega_{\mathbf{q}}^{(\nu)} \right) + n_{\mathbf{q}}^{(\nu)} \delta \left(\epsilon(\mathbf{k}) - \epsilon(\mathbf{k}') - \hbar \omega_{\mathbf{q}}^{(\nu)} \right) \right]$$

The index ν labels the ν-th phonon mode, $|G^{(\nu)}(\mathbf{k}', \mathbf{k})|$ is the matrix element, which describes the scattering mechanism, due to phonons of type ν. The symbol δ denotes the Dirac distribution, $\omega_{\mathbf{q}}^{(\nu)}$ is the ν-th phonon frequency, $n_{\mathbf{q}}^{(\nu)}$ is the Bose-Einstein distribution for the phonons of type ν

$$n_{\mathbf{q}}^{(\nu)} = \frac{1}{e^{\hbar \omega_{\mathbf{q}}^{(\nu)} / k_B T} - 1}$$

k_B is the Boltzmann constant and T is the graphene lattice temperature which, in this article, will be assumed constant.

For acoustic phonons, one usually considers the elastic approximation [44]

$$2 n_{\mathbf{q}}^{(ac)} |G^{(ac)}(\mathbf{k}', \mathbf{k})|^2 = \frac{1}{(2\pi)^2} \frac{\pi D_{ac}^2 k_B T}{2 \hbar \sigma_m v_p^2} (1 + cos \vartheta_{\mathbf{k}, \mathbf{k}'}), \tag{5.3}$$

where D_{ac} is the acoustic phonon coupling constant, v_p is the sound speed in graphene, σ_m the graphene areal density, and $\vartheta_{\mathbf{k},\mathbf{k}'}$ is the convex angle between $\mathbf{k}$ and $\mathbf{k}'$.

There are three relevant optical phonon scatterings: the longitudinal optical (LO), the transversal optical (TO) and the K-phonons. The matrix elements are [48]

$$|G^{(LO)}(\mathbf{k}',\mathbf{k})|^2 + |G^{(TO)}(\mathbf{k}',\mathbf{k})|^2 = \frac{2}{(2\pi)^2}\frac{\pi D_O^2}{\sigma_m \omega_O}, \tag{5.4}$$

$$|G^{(K)}(\mathbf{k}',\mathbf{k})|^2 = \frac{2}{(2\pi)^2}\frac{\pi D_K^2}{\sigma_m \omega_K}(1 - cos\theta_{\mathbf{k},\mathbf{k}'}), \tag{5.5}$$

where D_O is the optical phonon coupling constant, ω_O the optical phonon frequency, D_K is the K-phonon coupling constant and ω_K the K-phonon frequency.

5.2 Hydrodynamical model - L6MM

We will investigate the model proposed in [39] which is based on the following moments

$$\begin{aligned}
\rho &= \frac{2}{(2\pi)^2}\int_{\mathbb{R}^2} f(t,\mathbf{x},\mathbf{k})d^2\mathbf{k} \quad \text{density},\\
\rho W &= \frac{2}{(2\pi)^2}\int_{\mathbb{R}^2} f(t,\mathbf{x},\mathbf{k})\epsilon(\mathbf{k})d^2\mathbf{k} \quad \text{energy density},\\
\rho \mathbf{V} &= \frac{2}{(2\pi)^2}\int_{\mathbb{R}^2} f(t,\mathbf{x},\mathbf{k})\mathbf{v}(\mathbf{k})d^2\mathbf{k} \quad \text{linear momentum density},\\
\rho \mathbf{S} &= \frac{2}{(2\pi)^2}\int_{\mathbb{R}^2} f(t,\mathbf{x},\mathbf{k})\epsilon(\mathbf{k})\mathbf{v}(\mathbf{k})d^2\mathbf{k} \quad \text{energy-flux density}.
\end{aligned}$$

The corresponding evolution equations are given by

$$\begin{aligned}
&\frac{\partial}{\partial t}\rho + \nabla_{\mathbf{x}}(\rho\mathbf{V}) = \rho C_\rho,\\
&\frac{\partial}{\partial t}(\rho W) + \nabla_{\mathbf{x}}(\rho\mathbf{S}) + e\rho\mathbf{E}\cdot\mathbf{V} = \rho C_W,\\
&\frac{\partial}{\partial t}(\rho\mathbf{V}) + \nabla_{\mathbf{x}}(\rho\mathbf{F}^{(\mathbf{0})}) + e\rho\mathbf{G}^{(\mathbf{0})} : \mathbf{E} = \rho C_{\mathbf{V}},\\
&\frac{\partial}{\partial t}(\rho\mathbf{S}) + \nabla_{\mathbf{x}}(\rho\mathbf{F}^{(\mathbf{1})}) + e\rho\mathbf{G}^{(\mathbf{1})} : \mathbf{E} = \rho C_{\mathbf{S}}.
\end{aligned}$$

Besides the average densities, velocities, energies and energy fluxes, additional

quantities appear

$$\rho C_\rho = \frac{2}{(2\pi)^2}\int_{\mathbb{R}^2} \mathcal{C}(\mathbf{k})d^2\mathbf{k}, \tag{5.6}$$

$$\rho C_{\mathbf{V}} = \frac{2}{(2\pi)^2}\int_{\mathbb{R}^2} \mathbf{v}(\mathbf{k})\mathcal{C}(\mathbf{k})d^2\mathbf{k}, \tag{5.7}$$

$$\rho C_W = \frac{2}{(2\pi)^2}\int_{\mathbb{R}^2} \epsilon(\mathbf{k})\mathcal{C}(\mathbf{k})d^2\mathbf{k}, \tag{5.8}$$

$$\rho C_{\mathbf{S}} = \frac{2}{(2\pi)^2}\int_{\mathbb{R}^2} \epsilon(\mathbf{k})\mathbf{v}(\mathbf{k})\mathcal{C}(\mathbf{k})d^2\mathbf{k}, \tag{5.9}$$

$$\rho\begin{pmatrix}\mathbf{F^{(0)}}\\ \mathbf{F^{(1)}}\end{pmatrix} = \frac{2}{(2\pi)^2}\int_{\mathbb{R}^2}\begin{pmatrix}1\\ \epsilon(\mathbf{k})\end{pmatrix}\mathbf{v}(\mathbf{k})\otimes\mathbf{v}(\mathbf{k})f(t,\mathbf{x},\mathbf{k})d^2\mathbf{k}, \tag{5.10}$$

$$\rho\begin{pmatrix}\mathbf{G^{(0)}}\\ \mathbf{G^{(1)}}\end{pmatrix} = \frac{2}{\hbar(2\pi)^2}\int_{\mathbb{R}^2} f(t,\mathbf{x},\mathbf{k})\nabla_{\mathbf{k}}\begin{pmatrix}\mathbf{v}(\mathbf{k})\\ \epsilon(\mathbf{k})\mathbf{v}(\mathbf{k})\end{pmatrix}d^2\mathbf{k}, \tag{5.11}$$

that must be expressed as functions of the basic variables ρ, W, $\mathbf{V}$, $\mathbf{S}$. Regarding the production terms, they are given by the sum of contributions arising from the different types of phonon scattering

$$C_M = C_M^{(ac)} + \sum_{\nu=LO,TO,K} C_M^{(\nu)}$$

with $M = \rho, W, \mathbf{V}, \mathbf{S}$. We recall that the generic term due to a single scattering from a state $\mathbf{k}$ to a state $\mathbf{k}'$ is given by (5.2). Explicit closure relations have been obtained in [39] by adopting MEP and by linearising the resulting distribution f_{MEP} with respect to the vectorial Lagrange multipliers. We will refer to this model as L6MM.

5.3 Formulation of the problem

By inserting f_{MEP} in the definition of the quantities appearing in L6MM one gets a closed system of hyperbolic balance equations. In particular, the production terms contain the electron-phonon coupling parameters D_{ac}, D_Γ, D_K. We try to improve the accuracy of L6MM with respect to the mean values of velocity and energy obtained by a direct solution of the Boltzmann equation, considering D_{ac}, D_Γ, D_K as fitting parameters which are allowed to vary with respect to the values present in the Boltzmann equation.

So, in the equations (5.7)-(5.10), instead of $D_{ac}, D_\Gamma^2, D_K^2$, we consider $a_1\, D_{ac}$, $a_2\, D_\Gamma^2$, $a_3\, D_K^2$ where the coefficients a_i belong to a suitable admissible set we specify below. In the case $a_1 = a_2 = a_3 = 1$ one has the value used in the Boltzmann equation which will be assumed as initial guess in the optimisation procedure.

Several 1D space homogeneous solutions with different values of the only significant component of the electric field E and Fermi energy ε_F have been

considered. In this case the density is constant and depends on ε_F (see [43, 45]). The steady state solutions are compared.

We take the following objective function

$$f_{obj}(\mathbf{a}) = \alpha \left[\sum_{i,j} |V_{L6MM}(\mathbf{a}, E_i, \varepsilon_{F_j}, t) - V_{DG}|^2 \right]^{1/2} + \beta \left[\sum_{i,j} |W_{L6MM}(\mathbf{a}, E_i, \varepsilon_{F_j}, t) - W_{DG}|^2 \right]^{1/2}, \tag{5.12}$$

where $V_{L6MM}(\mathbf{a}, E_i, \varepsilon_{F_j}, t)$ and $W_{L6MM}(\mathbf{a}, E_i, \varepsilon_{F_j}, t)$ are velocity and energy at time t, electric field E_i and Fermi level ε_{F_j} computed with L6MM, respectively; these functions depend on $\mathbf{a} = [a_1, a_2, a_3]$. V_{DG} and W_{DG} are the reference values calculated with the DG method.

In order to considered the steady state, we have fixed $t = 3$ ps. Moreover, we have set $\alpha = 1$ and $\beta = 0.1$ to give more weight to the velocity with the aim to get an improvement of the current. The parameters a_i are allowed to vary in the range $[0.4 - 2.5]$.

The complete formulation of the problem is as follows:

$$\begin{cases} \min f_{obj}(\mathbf{a}) \\ \mathbf{a}_0 = [1, 1, 1] \\ 0.4 \leq a_k \leq 2.5 \qquad k = 1, 2, 3. \end{cases} \tag{5.13}$$

Ten values of the electric field have been considered, from 0.1 V/μm to 1 V/μm with increments of 0.1 V/μm, and three Fermi levels, 0.4 eV, 0.5 eV and 0.6 eV.

To solve this constrained optimization problem we have adopted three approaches: the MATLAB optimization function `fmincon` [78], the genetic algorithm, and the simulated annealing method.

5.4 Numerical Results

In this section we show the numerical results and highlight the difference between three models: L6MM, DG and the Hydrodynamical model optimized with the new constants $a_1 D_{ac}$, $a_2 D_\Gamma^2$ and $a_3 D_K^2$. The value of the objective function in the initial guess $\mathbf{a}_0$ is $f_{obj}(\mathbf{a}_0) = 2.819$.

By using the MATLAB function `fmincon`, the optimum is given by the vector $\mathbf{a} = [0.400, 2.115, 0.400]$ with $f_{obj}(\mathbf{a}) = 2.067$. The genetic algorithm with the number of maximum generation set equal to 100, gives as optimum point $\mathbf{a} = [0.399, 2.088, 0.399]$ with $f_{obj}(\mathbf{a}) = 2.082$, while the simulated annealing furnishes the optimal solution $\mathbf{a} = [0.401, 2.093, 0.434]$, with $f_{obj}(\mathbf{a}) = 2.084$. The numerical results in the different cases are very similar, but the genetic algorithm and simulated annealing are more expensive computationally than the function `fmincon`.

In Fig. 5.1 the transient solutions obtained with the direct solution of the Boltzmann equation with the DG method, the original L6MM model and the optimized L6MM model are compared. We get a noticeable improvement of the asymptotic value of the velocity, at the expenses of a slight worsening of the asymptotic values of the energy (note that the scales are different between velocity and energy). However, from the point of view of the steady electric current, the overall performance of the the improved L6MM is better than the original L6MM.

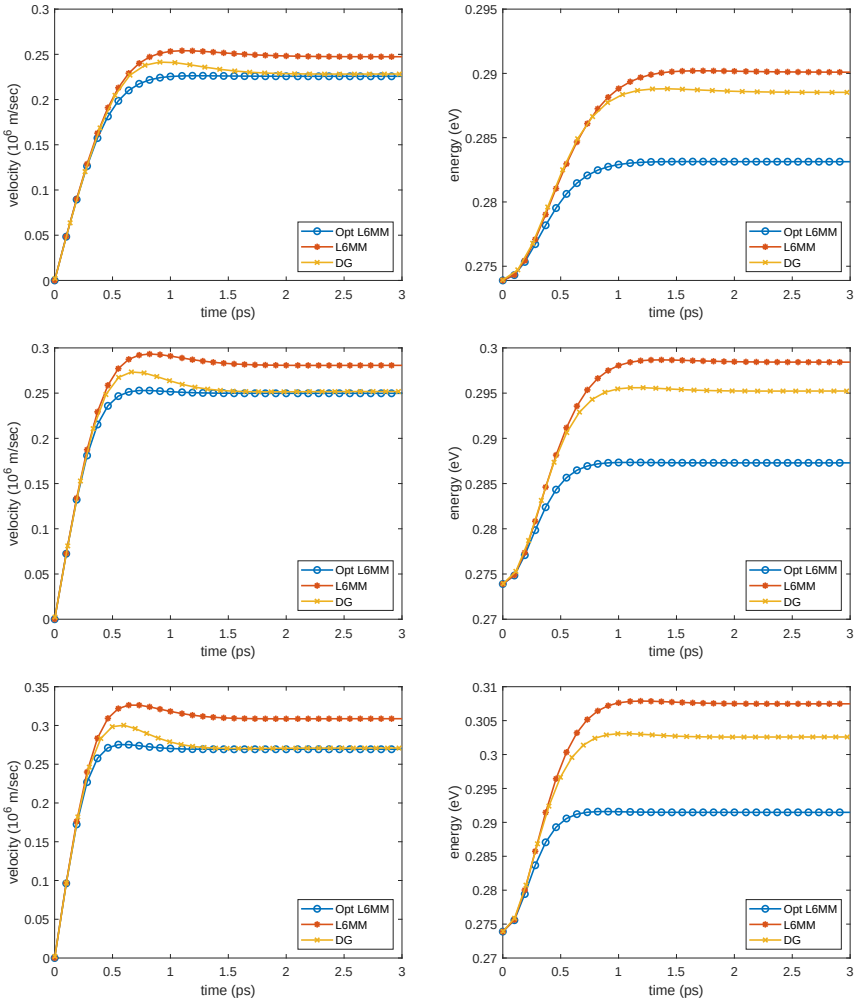

Figure 5.1: Velocity (on the left) and Energy (on the right) of charges in graphene, calculated by DG, L6MM and compared with the optimized L6MM (blue line) in the cases $\varepsilon_F = 0.4$eV and $E = 0.2$ V/μm (top), $E = 0.3$ V/μm (middle), $E = 0.4$ V/μm (bottom).

Chapter 6

Wigner equations for phonons transport and quantum heat flux

In this chapter we will apply the equations and the concepts introduced before to the phonons transport. In particular, starting from the quantum Liouville equation for the density operator and applying the Weyl quantization, Wigner equations for the acoustic, optical and Z phonons are deduced. The equations are valid for any solid, including 2D crystals like graphene. With the use of Moyal's calculus and its properties the pseudo-differential operators are expanded up to the second order in $\hbar$ (see (3.8) for details about the justification of the expansion in $\hbar$).

An energy transport model is obtained by using the moment method with closure relations based on a quantum version of the Maximum Entropy Principle by employing a relaxation time approximation for the production terms of energy and energy flux. An explicit form of the thermal conductivity with quantum correction up to $\hbar^2$ order is obtained under a long time scaling for the most relevant phonon branches.

In this chapter, the focus is on the acoustic and optical phonons dynamics with a general dispersion relation. In order to get insights into the quantum corrections, moment equations are deduced from the corresponding Wigner equation. As in the classical case, one is led to a system of balance equations that are not closed. So, the well-known problem of getting closure relations arises, that is the issue to express the additional fields appearing in the moment equations in terms of a set of fundamental variables. A sound way to accomplish this task is resorting to a quantum formulation of the maximum entropy principle [24] (hereafter QMEP), formulated for the first time by Jaynes [23]. Recently, a

more formal theory has been developed in a series of papers [25, 26] with several applications, for example for charge transport in semiconductors [9, 27–29]. The interested reader is also referred to [17].

We apply QMEP to the Wigner equations assuming the energy density and the energy flux for each species of phonons as basic fields. By expanding up to the second order in $\hbar$, quantum corrections to the semiclassical case [30] are deduced. In particular, in a long time scaling an asymptotic expression for the heat flux is obtained. The latter consists of a Fourier-like part with a highly nonlinear second order correction in the temperature gradient. Explicit formulas for acoustic phonons in the Debye approximation are written.

The plan of the chapter is as follows. In section 6.1 we write down the Wigner equations for phonons. Section 6.2 is dedicated to deducing the moment equations whose closure relations are achieved by QMEP in section 6.3. In section 6.4 a definition of local temperature is introduced by generalizing what has been proposed in [30] and in the last section an asymptotic expression of the quantum correction to the heat flux is obtained for the most relevant branches of phonons. We remark that the results of this chapter are original and have been presented in [31].

6.1 Phonon Wigner functions

By following the equations introduced in the Section 1.2, here we will describe the dynamics of the time-dependent phonon Wigner functions for the several phonon branches $g_\mu(\mathbf{x}, \mathbf{q}, t)$, $\mu = LA, TA, \dots$ steams directly from the dynamics of the corresponding density operator $\hat{\rho}_\mu(t)$, i.e. from the Von Neumann or quantum Liouville equation

$$i\hbar\partial_t\hat{\rho}_\mu(t) = [\hat{H}_\mu, \hat{\rho}_\mu(t)] := \hat{H}_\mu\hat{\rho}_\mu(t) - \hat{\rho}_\mu(t)\hat{H}_\mu, \tag{6.1}$$

where $\hat{H}_\mu$ denotes the Hamiltonian operators of the μ-th phonons. If $h_\mu = Op_\hbar^{-1}(\hat{H}_\mu)$ is the symbol associated with $\hat{H}_\mu$, then, from Eq.s (6.1), we obtain the *Wigner equation* for each phonon species

$$i\hbar\partial_t g_\mu(\mathbf{x}, \mathbf{q}, t) = \{h_\mu, g_\mu(\mathbf{x}, \mathbf{q}, t)\}_* := h_\mu * g_\mu(\mathbf{x}, \mathbf{q}, t) - g_\mu(\mathbf{x}, \mathbf{q}, t) * h_\mu. \tag{6.2}$$

If we neglect, temporarily, the phonon-phonon interactions, the Hamiltonian symbol for each phonon branch is given by

$$h_\mu(\mathbf{q}) = \varepsilon_\mu(\mathbf{q}) \quad \mu = LA, TA, \dots. \tag{6.3}$$

By using the Moyal calculus, one can expand the second members of the previous Wigner equations. Up to first order in $\hbar^2$, we have

$$\partial_t g_\mu(t) + S[h_\mu]g_\mu(t) = 0, \quad \mu = LA, TA, \dots, \tag{6.4}$$

where[1]

$$S[h_\mu]g_\mu(\mathbf{x},\mathbf{q},t) := \mathbf{c}_\mu \cdot \nabla_{\mathbf{x}} g_\mu(\mathbf{x},\mathbf{q},t) - \frac{\hbar^2}{24}\frac{\partial^3 h_\mu(\mathbf{q})}{\partial q_i \partial q_j \partial q_k}\frac{\partial^3 g_\mu(\mathbf{x},\mathbf{q},t)}{\partial x_i \partial x_j \partial x_k} + O(\hbar^4) \tag{6.5}$$

The previous equations describe only ballistic transport and include only the harmonic contribution to the Hamiltonian. In order to describe also intra and inter-branch phonon-phonon interactions, an additional anharmonic term $\hat{H}_{int}$ encompassing the high order correction to the Hamiltonian operator must be added. So doing, one gets the so-called Wigner-Boltzmann equations

$$\partial_t g_\mu(\mathbf{x},\mathbf{q},t) + S[h_\mu]g_\mu(\mathbf{x},\mathbf{q},t) = C_\mu(\mathbf{x},\mathbf{q},t), \quad \mu = LA, TA, \ldots, \tag{6.6}$$

In the quantum case the expression of C_μ is rather cumbersome. For electron transport in semiconductors the interested reader can see [32]. In certain regimes it is justified to retain the same form of the semiclassical collision operator as the semiclassical case [3].

The equation (6.6) represents our starting point for the phonon transport. Note that for the optical phonons under the Einstein approximation for the energy bands one has formally the same transport equation as the semiclassical case because the group velocity vanishes.

An alternative derivation of (6.6) can be obtained by explicitly writing the von Neumann equation (see [17, 27] for the details). One obtains

$$S[h_\mu]g_\mu(t) = \frac{i}{\hbar(2\pi)^d}\int_{\mathbb{R}^{2d}}\left[\varepsilon_\mu\left(\mathbf{q}+\frac{\hbar}{2}\boldsymbol{\nu},t\right) - \varepsilon_\mu\left(\mathbf{q}-\frac{\hbar}{2}\boldsymbol{\nu},t\right)\right]\times \\ g_\mu(\mathbf{x}',\mathbf{q},t)\exp(-i(\mathbf{x}'-\mathbf{x})\cdot\boldsymbol{\nu})d\mathbf{x}'d\boldsymbol{\nu}, \tag{6.7}$$

whose expansion is of course in agreement with the Moyal calculus.

6.2 Phonon Moment equations

Getting analytical solutions to equation (6.6) is a daunting task. Therefore, viable approaches are numerical solutions based on finite differences or finite elements [1] or stochastic solutions, e.g. those obtained with a suitable modification of the Monte Carlo methods for the semiclassical Boltzmann equation [2]. However, it is possible to have simpler, even if approximate, models resorting to the moment method for the expectation values of interest. In fact, it is well known that, although not positive definite, the Wigner function is real and the expectation values of an operator can be formally obtained as an average of the corresponding symbol with respect to $g_\mu(\mathbf{x},\mathbf{q},t)$. So, for any regular enough weight function

[1] Summation over repeated indices is understood from 1 to d.

$\Psi(\mathbf{q})$, let us introduce the short notation

$$\langle \Psi \rangle_\mu(\mathbf{x}, t) := \frac{1}{(2\pi)^d} \int_{\mathbb{R}^d} \Psi(\mathbf{q}) g_\mu(\mathbf{x}, \mathbf{q}, t) d\mathbf{q}, \tag{6.8}$$

which represents a partial average with respect to the phonon momentum $\mathbf{q}$.

More in general, if $a = a(\mathbf{x}, \mathbf{q})$ is a smooth *symbol* then it is possible to prove that the expectation of the (hermitian) operator $A = Op_\hbar(a)$ satisfies[2]

$$\mathbb{E}[A] = \mathrm{tr}(\hat{\rho} A) = \int_{\mathbb{R}^{2d}} \rho(\mathbf{x}, \mathbf{y}, t) k_A(\mathbf{x}, \mathbf{y}) d\mathbf{x} d\mathbf{y} = \frac{1}{(2\pi)^d} \int_{\mathbb{R}^{2d}} a(\mathbf{x}, \mathbf{q}) g_\mu(\mathbf{x}, \mathbf{q}, t) d\mathbf{x} d\mathbf{q}$$
$$= \int_{\mathbb{R}^d} \langle a \rangle_\mu(\mathbf{x}, t) d\mathbf{x},$$

where $k_A(\mathbf{x}, \mathbf{y})$ is the kernel of A.

We want to consider a minimum set of moments whose physical meaning is well clear. In particular, we shall consider the phonon energy density and energy flux density of each branch

$$W_\mu(\mathbf{x}, t) = \langle h_\mu \rangle_\mu(\mathbf{x}, t), \quad \mathbf{Q}_\mu(\mathbf{x}, t) = \langle h_\mu \mathbf{c}_\mu \rangle_\mu(\mathbf{x}, t). \tag{6.9}$$

Note that the latter is directly related to the heat flux.

The evolution equations for $W_\mu(\mathbf{x}, t)$ and $\mathbf{Q}_\mu(\mathbf{x}, t)$ are obtained by multiplying the relative Wigner equation by $h_\mu(\mathbf{q})$, and $h_\mu(\mathbf{q})\mathbf{c}_\mu$ and integrating with respect to $\mathbf{q}$

$$\begin{aligned} &\partial_t W_\mu(\mathbf{x}, t) + \frac{1}{(2\pi)^d} \int_{\mathbb{R}^d} h_\mu(\mathbf{q}) S[h_\mu] g_\mu \, d\mathbf{q} = \frac{1}{(2\pi)^d} \int_{\mathbb{R}^d} h_\mu(\mathbf{q}) C_\mu \, d\mathbf{q}, \\ &\partial_t \mathbf{Q}_\mu(\mathbf{x}, t) + \frac{1}{(2\pi)^d} \int_{\mathbb{R}^d} h_\mu(\mathbf{q}) \mathbf{c}_\mu S[h_\mu] g_\mu \, d\mathbf{q} = \frac{1}{(2\pi)^d} \int_{\mathbb{R}^d} h_\mu(\mathbf{q}) \mathbf{c}_\mu C_\mu \, d\mathbf{q}. \end{aligned} \qquad \mu = LA, TA, \ldots \tag{6.10}$$

We implicitly assume that the resulting integrals there exist, at least in the principal value sense. In order to get some global insight from eq.s (6.10), we formally assume the following expansions for each phonon branch[3]

$$g_\mu(\mathbf{x}, \mathbf{q}, t) = g_\mu^{(0)}(\mathbf{x}, \mathbf{q}, t) + \hbar^2 g_\mu^{(2)}(\mathbf{x}, \mathbf{q}, t) + o(\hbar^2). \tag{6.11}$$

It is possible to prove, at least formally [7], that the semiclassical Boltzmann equation is recovered from the Wigner equation as $\hbar \to 0^+$. Therefore, $g_\mu^{(0)}(\mathbf{x}, \mathbf{q}, t)$ can be considered as the solution f_μ of the semiclassical transport equation. Accordingly, we write

$$W_\mu = W_\mu^{(0)} + \hbar^2 W_\mu^{(2)} + o(\hbar^2), \quad \mathbf{Q}_\mu = \mathbf{Q}_\mu^{(0)} + \hbar^2 \mathbf{Q}_\mu^{(2)} + o(\hbar^2), \tag{6.12}$$

[2]Here we are considering a fixed instant of time.

[3]The coefficients of the odd powers in $\hbar$ are assumed zero in according to the previous Moyal expansion.

where

$$W_\mu^{(0)} = \frac{1}{(2\pi)^d}\int_{\mathbb{R}^d} h_\mu g_\mu^{(0)}(\mathbf{x},\mathbf{q},t)d\mathbf{q}, \quad W_\mu^{(2)} = \frac{1}{(2\pi)^d}\int_{\mathbb{R}^d} h_\mu g_\mu^{(2)}(\mathbf{x},\mathbf{q},t)d\mathbf{q},$$
$$\mathbf{Q}_\mu^{(0)} = \frac{1}{(2\pi)^d}\int_{\mathbb{R}^d} h_\mu \mathbf{c}_\mu g_\mu^{(0)}(\mathbf{x},\mathbf{q},t)d\mathbf{q}, \quad \mathbf{Q}_\mu^{(2)} = \frac{1}{(2\pi)^d}\int_{\mathbb{R}^d} h_\mu \mathbf{c}_\mu g_\mu^{(2)}(\mathbf{x},\mathbf{q},t)d\mathbf{q}.$$

Regarding the moments of the collision terms, only with drastic simplifications analytical expressions can be deduced. In analogy with the time relaxation approximation, we assume that the r.h.s. of eq.s (6.10) are expressed as relaxation time terms

$$\frac{1}{(2\pi)^d}\int_{\mathbb{R}^d} h_\mu(\mathbf{q})C_\mu\, d\mathbf{q} = -\frac{W_\mu - W_\mu^{LE}}{\tau_\mu^W} = -\frac{W_\mu^{(0)} - W_\mu^{(0)LE}}{\tau_\mu^W} - \hbar^2\frac{W_\mu^{(2)} - W_\mu^{(2)LE}}{\tau_\mu^W} + o(\hbar^2),$$
$$\frac{1}{(2\pi)^d}\int_{\mathbb{R}^d} h_\mu(\mathbf{q})\mathbf{c}_\mu C_\mu\, d\mathbf{q} = -\frac{\mathbf{Q}_\mu}{\tau_\mu^{\mathbf{Q}}} = -\frac{\mathbf{Q}_\mu^{(0)} + \hbar^2\mathbf{Q}_\mu^{(2)}}{\tau_\mu^{\mathbf{Q}}} + o(\hbar^2),$$

where

$$W_\mu^{LE} = \frac{1}{(2\pi)^d}\int_{\mathbb{R}^d} h_\mu(\mathbf{q}) g_\mu^{LE}\, d\mathbf{q}.$$

Note that we have used the fact that the local equilibrium values of the energy-flux $\mathbf{Q}_\mu^{LE}$ vanishes. The energy and energy-flux relaxation times, τ_μ^W and $\tau_\mu^{\mathbf{Q}}$ respectively, are assumed to depends on the temperature, which will be defined in the next section, of the relative branch. (see for example [33]).

Altogether, the resulting model is made of the following fluid-type equations

$$\begin{cases} \partial_t W_\mu + \dfrac{\partial(\mathbf{Q}_r)_\mu}{\partial x_r} - \dfrac{\hbar^2}{24}\dfrac{\partial^3(\mathbf{T}_{ijk})_\mu}{\partial x_i\partial x_j\partial x_k} = -\dfrac{W_\mu^{(0)} - W_\mu^{(0)LE}}{\tau_\mu^W} - \hbar^2\dfrac{W_\mu^{(2)} - W_\mu^{(2)LE}}{\tau_\mu^W} + o(\hbar^2) \\ \\ \partial_t(\mathbf{Q}_r)_\mu + \dfrac{\partial(\mathbf{J}_{ri})_\mu}{\partial x_i} - \dfrac{\hbar^2}{24}\dfrac{\partial^3(\mathbf{U}_{rijk})_\mu}{\partial x_i\partial x_j\partial x_k} = -\dfrac{(\mathbf{Q}_r^{(0)})_\mu + \hbar^2(\mathbf{Q}_r^{(2)})_\mu}{\tau_\mu^{\mathbf{Q}}} + o(\hbar^2), \end{cases} \tag{6.13}$$

where $\mathbf{J}_\mu = \mathbf{J}_\mu^{(0)} + \hbar^2\mathbf{J}_\mu^{(2)}$ with components

$$(\mathbf{J}_{ri}^{(0)})_\mu = \frac{1}{(2\pi)^d}\int_{\mathbb{R}^d} (\mathbf{c}_\mu)_r(\mathbf{c}_\mu)_i h_\mu(\mathbf{q}) g_\mu^{(0)}(\mathbf{x},\mathbf{q},t)d\mathbf{q},$$
$$(\mathbf{J}_{ri}^{(2)})_\mu = \frac{1}{(2\pi)^d}\int_{\mathbb{R}^d} (\mathbf{c}_\mu)_r(\mathbf{c}_\mu)_i h_\mu(\mathbf{q}) g_\mu^{(2)}(\mathbf{x},\mathbf{q},t)d\mathbf{q},$$

and the complete symmetric tensors $\mathbf{T}_\mu$ and $\mathbf{U}_\mu$ have components

$$(\mathbf{T}_{ijk})_\mu = \frac{1}{(2\pi)^d}\int_{\mathbb{R}^d} h_\mu(\mathbf{q})\frac{\partial^3 h_\mu(\mathbf{q})}{\partial q_i\partial q_j\partial q_k} g_\mu^{(0)}(\mathbf{x},\mathbf{q},t)d\mathbf{q},$$
$$(\mathbf{U}_{rijk})_\mu = \frac{1}{(2\pi)^d}\int_{\mathbb{R}^d} (\mathbf{c}_\mu)_r h_\mu(\mathbf{q})\frac{\partial^3 h_\mu(\mathbf{q})}{\partial q_i\partial q_j\partial q_k} g_\mu^{(0)}(\mathbf{x},\mathbf{q},t)d\mathbf{q}.$$

If we split into zero and first order in $\hbar^2$, the evolution equations read

$$\partial_t W_\mu^{(0)} + \nabla_{\mathbf{x}} \cdot \mathbf{Q}_\mu^{(0)} = -\frac{W_\mu^{(0)} - W_\mu^{(0)LE}}{\tau_\mu^W} \tag{6.14}$$

$$\partial_t W_\mu^{(2)} + \nabla_{\mathbf{x}} \cdot \mathbf{Q}_\mu^{(2)} - \frac{1}{24}\left(\mathbf{T}_{ijk}\right)_\mu = -\frac{W_\mu^{(2)} - W_\mu^{(2)LE}}{\tau_\mu^W}, \tag{6.15}$$

$$\partial_t (\mathbf{Q}_r^{(0)})_\mu + \frac{\partial (\mathbf{J}_{ri}^{(0)})_\mu}{\partial x_i} = -\frac{(\mathbf{Q}_r^{(0)})_\mu}{\tau_\mu^{\mathbf{Q}}}, \tag{6.16}$$

$$\partial_t (\mathbf{Q}_r^{(2)})_\mu + \frac{\partial (\mathbf{J}_{ri}^{(2)})_\mu}{\partial x_i} - \frac{1}{24}(\mathbf{U}_{rijk})_\mu = -\frac{(\mathbf{Q}_r^{(2)})_\mu}{\tau_\mu^{\mathbf{Q}}}. \tag{6.17}$$

The zero order equations are the model already investigated in several papers [8, 30] (for specific materials see also [34, 35]), where is proved that it is a hyperbolic system of conservation law, while the first order corrections in $\hbar^2$ introduce dispersive terms. This is not surprising on account of the nonlocal character of the quantum evolution equations.

6.3 QMEP for the closure relations

The evolution equations (6.14)-(6.17) do not form a closed system of balance laws. If we assume the energies W_μ and the energy-fluxes $\mathbf{Q}_\mu$ as the main fields, in order to get a set of closed equations we need to express the additional fields $\mathbf{J}_\mu$, $\mathbf{T}_\mu$ and $\mathbf{U}_\mu$ as functions of W_μ and $\mathbf{Q}_\mu$. A successful approach in a semiclassical setting is that based on the Maximum Entropy Principle (MEP) (see also [17] for a complete review) which is based on a pioneering paper of Jaynes [23, 24] who also proposed a way to extend the approach to the quantum case (see Section 4.5).

Therefore, we take as entropy a generalization of the classical one for bosons. The entropy of the μ-th phonon branch reads

$$S(\hat{\rho}_\mu) = \mathrm{tr}\{s(\hat{\rho}_\mu)\}$$

which can be viewed as a quantum Bose-Einstein entropy.

According to MEP, we estimate $\hat{\rho}_\mu$ with $\hat{\rho}_\mu^{MEP}$ which is obtained by maximizing $S(\hat{\rho}_\mu)$ under the constraints that some expectation values have to be preserved. In the semiclassical point case, one maximizes the entropy preserving the values of the moments we have taken as basic field variables

$$\begin{aligned}(W_\mu(\mathbf{x},t), \mathbf{Q}_\mu(\mathbf{x},t)) &= \frac{1}{(2\pi)^d}\int_{\mathbb{R}^d} \mathbf{\Psi}_\mu(\mathbf{q}) g_\mu(\mathbf{x},\mathbf{q},t) d\mathbf{q} = \\ &= \frac{1}{(2\pi)^d}\int_{\mathbb{R}^d} \mathbf{\Psi}_\mu(\mathbf{q}) g_\mu^{MEP}(\mathbf{x},\mathbf{q},t) d\mathbf{q},\end{aligned} \tag{6.18}$$

where

$$\mathbf{\Psi}_\mu(\mathbf{q}) = (h_\mu(\mathbf{q}), \mathbf{c}_\mu h_\mu(\mathbf{q})) \tag{6.19}$$

is the vector of the weight functions and g_μ^{MEP} is the Wigner function associated with $\hat{\rho}_\mu^{MEP}$. In the previous relations the time t and position $\mathbf{x}$ must be considered as fixed.

The quantum formulation of MEP is given in terms of expectation values

$$E_1(t) = \mathrm{tr}\left\{\hat{\rho}_\mu Op_\hbar(h_\mu(\mathbf{q}))\right\}(t), \quad \mathbf{E}_2(t) = \mathrm{tr}\left\{\hat{\rho}_\mu Op_\hbar(\mathbf{c}_\mu h_\mu(\mathbf{q}))\right\}(t),$$

as follows: for fixed t

$$\hat{\rho}_\mu^{MEP} = \text{argument max}\, S(\hat{\rho}_\mu) \tag{6.20}$$

under the constraints

$$\mathrm{tr}\{\hat{\rho}_\mu^{MEP} Op_\hbar(h_\mu(\mathbf{q}))\} = E_1(t), \quad \mathrm{tr}\{\hat{\rho}_\mu^{MEP} Op_\hbar(\mathbf{c}_\mu h_\mu(\mathbf{q}))\} = \mathbf{E}_2(t) \tag{6.21}$$

in the space of the Hilbert-Schmidt operators on $L^2(\mathbb{R}^d, \mathbb{C})$ which are positive, with trace one and such that the previous expectation values there exist. Note that we are applying the maximization of the entropy for each phonon branch separately. In other words, we are requiring the additivity of the entropy.

If we introduce the vector of the Lagrange multipliers

$$\boldsymbol{\eta}_\mu = (\eta_{0\mu}(\mathbf{x}, t), \boldsymbol{\eta}_{1\mu}(\mathbf{x}, t)), \tag{6.22}$$

the vector of the moments

$$\mathbf{m}[\rho_\mu](\mathbf{x}, \mathbf{t}) := \mathbf{m}_\mu(\mathbf{x}, t) = \frac{1}{(2\pi)^d} \int_{\mathbb{R}^d} \mathbf{\Psi}_\mu(\mathbf{q}) g_\mu(\mathbf{x}, \mathbf{q}, t) d\mathbf{q}, \tag{6.23}$$

and the vector of the moments which must be considered as known

$$\mathbf{M}_\mu(\mathbf{x}, t) := (W_\mu(\mathbf{x}, t), \mathbf{Q}_\mu(\mathbf{x}, t)), \tag{6.24}$$

the constrained optimization problem (6.20)-(6.21) can be rephrased as a saddle-point problem for the Lagrangian

$$\begin{aligned} \mathcal{L}_\mu(\hat{\rho}_\mu, \boldsymbol{\eta}_\mu) &= S(\hat{\rho}_\mu) - \int_{\mathbb{R}^d} \boldsymbol{\eta}_\mu \cdot (\mathbf{m}_\mu(\mathbf{x}, t) - \mathbf{M}_\mu(\mathbf{x}, t))\, d\mathbf{x} \\ &= S(\hat{\rho}_\mu) - \mathrm{tr}\left\{\hat{\rho}_\mu Op_\hbar(\boldsymbol{\eta}_\mu \cdot \mathbf{\Psi}_\mu(\mathbf{q}))\right\} + \int_{\mathbb{R}^d} \boldsymbol{\eta}_\mu \cdot \mathbf{M}_\mu(\mathbf{x}, t)\, d\mathbf{x} \end{aligned} \tag{6.25}$$

in the space of the admissible $\hat{\rho}_\mu$ and smooth function $\boldsymbol{\eta}_\mu$.

If the Lagrangian $\mathcal{L}_\mu(\hat{\rho}_\mu, \boldsymbol{\eta}_\mu)$ is Gâteaux-differentiable with respect to $\hat{\rho}_\mu$, the first order optimality conditions require

$$\delta\mathcal{L}_\mu(\hat{\rho}_\mu, \boldsymbol{\eta}_\mu)(\delta\hat{\rho}) = 0$$

for each Hilbert-Schmidt operators $\delta\hat{\rho}$ on $L^2(\mathbb{R}^d, \mathbb{C})$ which is positive, with trace one and such that the previous expectation values there exist.

Using the results presented in Subsection 4.5.1, the operator solving the first order optimality condition reads

$$\hat{\rho}^*_\mu = (s')^{-1}(Op_\hbar(\boldsymbol{\eta}_\mu \cdot \boldsymbol{\Psi}_\mu)) = \frac{1}{\exp(Op_\hbar(\boldsymbol{\eta}_\mu \cdot \boldsymbol{\Psi}_\mu)) - 1}. \tag{6.26}$$

where we have rescaled the Lagrange multipliers including the factor $1/k_B$. Moreover, such an operator is a point of maximum for the Lagrangian.

Now, to complete the program we have to determine, among the smooth functions, the Lagrange multipliers $\boldsymbol{\eta}_\mu$ by solving the constraint

$$\mathrm{tr}\,\{\hat{\rho}_\mu Op_\hbar(\boldsymbol{\eta}_\mu \cdot (h_\mu(\mathbf{q}), \mathbf{c}_\mu h_\mu(\mathbf{q}))\} - \int_{\mathbb{R}^d} \boldsymbol{\eta}_\mu \cdot \mathbf{M}_\mu(\mathbf{x}, t)\, d\mathbf{x} = 0. \tag{6.27}$$

If such an equation has a solution $\boldsymbol{\eta}^*_\mu$, altogether the MEP density operator reads

$$\hat{\rho}^{MEP}_\mu = \frac{1}{\exp\left[Op_\hbar\left(\eta^*_{0\mu}(\mathbf{x}, t)h_\mu(\mathbf{q}) + \boldsymbol{\eta}^*_{1\mu}(\mathbf{x}, t) \cdot \mathbf{c}_\mu h_\mu(\mathbf{q})\right)\right] - 1}. \tag{6.28}$$

To determine conditions under which the equation (6.27) admits solutions is a very difficult task. Even in the semiclassical case there are examples (see [36]) of sets of moments that cannot be moments of a MEP distribution.

We will directly find out the solution at least up to first order in $\hbar^2$.

Once the MEP density function has been determined, the MEP Wigner function is given by

$$g^{MEP}_\mu(\mathbf{x}, \mathbf{q}, t) = Op^{-1}_\hbar(\hat{\rho}^{MEP}_\mu)$$

which can be used to get the necessary closure relations by evaluating the additional fields with g_μ replaced by g^{MEP}_μ.

We remark that the constraints (6.27) can be more conveniently expressed as

$$\frac{1}{(2\pi)^d} \int_{\mathbb{R}^{2d}} \boldsymbol{\eta}_\mu \cdot \boldsymbol{\Psi}_\mu(\mathbf{x}, t) g^{MEP}_\mu(\mathbf{x}, \mathbf{q}, t)\, d\mathbf{q}\, d\mathbf{x} - \int_{\mathbb{R}^d} \boldsymbol{\eta}_\mu \cdot \mathbf{M}_\mu(\mathbf{x}, t)\, d\mathbf{x} = 0$$

and indeed we will require, in analogy with the semiclassical case, the stronger conditions

$$\frac{1}{(2\pi)^d} \int_{\mathbb{R}^d} \boldsymbol{\Psi}_\mu(\mathbf{x}, t) g^{MEP}_\mu(\mathbf{x}, \mathbf{q}, t)\, d\mathbf{q} = \mathbf{M}_\mu(\mathbf{x}, t),$$

where the Lagrange multipliers enter through $g^{MEP}_\mu(\mathbf{x}, \mathbf{q}, t)$.

6.3.1 Determination of the Lagrange Multipliers

For the sake of making lighter the notation, let us consider a single branch and drop the index μ in the Wigner function in this section. We look formally for a solution in powers of $\hbar$

$$g^{MEP} = g^{MEP}_0 + \hbar g^{MEP}_1 + \hbar^2 g^{MEP}_2 + ... \tag{6.29}$$

firstly without taking into account the dependence of the Lagrange multipliers on $\hbar$.

Of course, on account of the properties of the Weyl quantization, g_0^{MEP} is equal to the semiclassical counterpart [13]

$$g_0^{MEP} = \frac{1}{\exp(\xi) - 1}$$

where

$$\xi = \eta_0(\mathbf{x}, t)h(\mathbf{q}) + \boldsymbol{\eta}_1(\mathbf{x}, t) \cdot \mathbf{c}h(\mathbf{q}).$$

In order to determine the higher order terms g_k^{MEP}, $k \geq 1$, given a symbol $a(\mathbf{x}, \mathbf{q})$ let us introduce the so-called *quantum exponential* $Exp(a)$ defined as

$$Exp(a) = Op_\hbar^{-1}[\exp(Op_\hbar(a))]$$

which can be expanded as

$$Exp(a) = Exp_0(a) + \hbar Exp_1(a) + \hbar^2 Exp_2(a) + ... \tag{6.30}$$

Proposition Let $a(\mathbf{x}, \mathbf{q})$ be a smooth symbol. Then the following expansion is valid

$$\begin{aligned} Exp(a) = \exp(a) - \frac{\hbar^2}{8}\exp(a)\Bigg(&\frac{\partial^2 a}{\partial x_i \partial x_j}\frac{\partial^2 a}{\partial q_i \partial q_j} - \frac{\partial^2 a}{\partial x_i \partial q_j}\frac{\partial^2 a}{\partial q_i \partial x_j} + \frac{1}{3}\frac{\partial^2 a}{\partial x_i \partial x_j}\frac{\partial a}{\partial q_i}\frac{\partial a}{\partial q_j} \\ &- \frac{2}{3}\frac{\partial^2 a}{\partial x_i \partial q_j}\frac{\partial a}{\partial q_i}\frac{\partial a}{\partial x_j} + \frac{1}{3}\frac{\partial^2 a}{\partial q_i \partial q_j}\frac{\partial a}{\partial x_i}\frac{\partial a}{\partial x_j}\Bigg) + O(\hbar^4) \end{aligned} \tag{6.31}$$

where Einstein's convention has been used.

The proof can be found for example in [26].

By using what is proved in [29], we have

$$g_{2n+1}^{MEP} = 0, \quad n \geq 0, \tag{6.32a}$$

$$g_{2n}^{MEP} = -\sum_{m=0}^{n-1} \sum_{k+l+m=n} \frac{Exp_{2k}(\xi) *_{2l} g_{2m}^{MEP}}{\exp(\xi) - 1}, \quad n \geq 1 \tag{6.32b}$$

where $*_{2l}$ are the even terms of the Moyal product expansion.

In particular

$$g_1^{MEP} = 0$$

and

$$\begin{aligned} g_2^{MEP} \;=\; & -\frac{1}{8}\frac{\exp(\xi)}{(\exp(\xi) - 1)^3}\Bigg[(\exp(\xi) + 1)\left(\frac{\partial^2 \xi}{\partial x_i \partial x_j}\frac{\partial^2 \xi}{\partial q_i \partial q_j} - \frac{\partial^2 \xi}{\partial x_i \partial q_j}\frac{\partial^2 \xi}{\partial q_i \partial x_j}\right) \\ & - \frac{(\exp(2\xi) + 4\exp(\xi) + 1)}{3(\exp(\xi) - 1)}\left(\frac{\partial^2 \xi}{\partial x_i \partial x_j}\frac{\partial \xi}{\partial q_i}\frac{\partial \xi}{\partial q_j} - 2\frac{\partial^2 \xi}{\partial x_i \partial q_j}\frac{\partial \xi}{\partial q_i}\frac{\partial \xi}{\partial x_j} + \frac{\partial^2 \xi}{\partial q_i \partial q_j}\frac{\partial \xi}{\partial x_i}\frac{\partial \xi}{\partial x_j}\right)\Bigg] \end{aligned}$$

Therefore, up to first order in $\hbar^2$ we have

$$g^{MEP} = g_0^{MEP} + \hbar^2 g_2^{MEP}.$$

and the constraints for each phonon branch read

$$W = \frac{1}{(2\pi)^d}\int_{\mathbb{R}^d}\frac{h(\mathbf{q})}{\exp(\xi)-1}d\mathbf{q} + \hbar^2\frac{1}{(2\pi)^d}\int_{\mathbb{R}^d} h(\mathbf{q})g_2^{MEP}d\mathbf{q}, \quad (6.33)$$

$$\mathbf{Q} = \frac{1}{(2\pi)^d}\int_{\mathbb{R}^d}\frac{\mathbf{c}h(\mathbf{q})}{\exp(\xi)-1}d\mathbf{q} + \hbar^2\frac{1}{(2\pi)^d}\int_{\mathbb{R}^d} \mathbf{c}h(\mathbf{q})g_2^{MEP}d\mathbf{q}. \quad (6.34)$$

The previous equations form a nonlinear system of PDEs for the Lagrange multipliers whose analytical solution seems very difficult to get. Indeed, the situation is even more cumbersome because in a numerical scheme the inversion of the constraints should be performed at each time step.

A viable strategy is to use the Lagrange multipliers as field variables by rewriting the evolution equations (6.13) in the form

$$\frac{\partial W}{\partial \eta_k}\frac{\partial \eta_k}{\partial t} + \frac{\partial \mathbf{Q}_i}{\partial \eta_k}\frac{\partial \eta_k}{\partial x_i} - \frac{\hbar^2}{24}\left(\frac{\partial}{\partial \eta_k}\frac{\partial^2 \mathbf{T}_{ijk}}{\partial x_j \partial x_k}\right)\frac{\partial \eta_k}{\partial x_i} = -\frac{W - W^{LE}}{\tau^W}, \quad (6.35)$$

$$\frac{\partial \mathbf{Q}_i}{\partial \eta_k}\frac{\partial \eta_k}{\partial t} + \frac{\partial \mathbf{J}_{ir}}{\partial \eta_k}\frac{\partial \eta_k}{\partial x_r} - \frac{\hbar^2}{24}\left(\frac{\partial}{\partial \eta_h}\frac{\partial^2 \mathbf{U}_{ijkr}}{\partial x_k \partial x_r}\right)\frac{\partial \eta_h}{\partial x_j} = -\frac{Q_i}{\tau^{\mathbf{Q}}}, \quad (6.36)$$

getting a highly nonlinear system of PDEs.

A further simplification can be obtained by expanding the Lagrange multipliers as

$$\boldsymbol{\eta} = \boldsymbol{\eta}^{(0)} + \hbar^2\boldsymbol{\eta}^{(2)} + o(\hbar^2).$$

Therefore, the basic fields are also expanded with respect to $\hbar^2$

$$W = W^{(0)} + \hbar^2 W^{(2)} + o(\hbar^2), \quad \mathbf{Q} = \mathbf{Q}^{(0)} + \hbar^2\mathbf{Q}^{(2)} + o(\hbar^2)$$

where

$$W^{(0)} = \frac{1}{(2\pi)^d}\int_{\mathbb{R}^d}\frac{h(\mathbf{q})}{\exp(\xi^{(0)})-1}d\mathbf{q},$$

$$W^{(2)} = -\frac{1}{(2\pi)^d}\boldsymbol{\eta}^{(2)}\cdot\int_{\mathbb{R}^d}\exp(\xi^{(0)})\frac{h(\mathbf{q})\boldsymbol{\Psi}}{\left(\exp(\xi^{(0)})-1\right)^2}d\mathbf{q} + \frac{1}{(2\pi)^d}\int_{\mathbb{R}^d} h(\mathbf{q})g_2^{MEP}(\boldsymbol{\eta}^{(0)})d\mathbf{q},$$

$$Q_i^{(0)} = \frac{1}{(2\pi)^d}\int_{\mathbb{R}^d}\frac{c_i h(\mathbf{q})}{\exp(\xi^{(0)})-1}d\mathbf{q},$$

$$Q_i^{(2)} = -\frac{1}{(2\pi)^d}\boldsymbol{\eta}^{(2)}\cdot\int_{\mathbb{R}^d}\frac{c_i\boldsymbol{\Psi}\exp(\xi^{(0)})h(\mathbf{q})}{(\exp(\xi^{(0)})-1)^2}d\mathbf{q} + \frac{1}{(2\pi)^d}\int_{\mathbb{R}^d} c_i h(\mathbf{q})g_2^{MEP}(\boldsymbol{\eta}^{(0)})d\mathbf{q},$$

with $\xi^{(0)} = \boldsymbol{\eta}^{(0)}\cdot\boldsymbol{\Psi}$.

The balance equations become

$$\nabla_{\boldsymbol{\eta}^{(0)}} W^{(0)} \frac{\partial}{\partial t}(\boldsymbol{\eta}^{(0)})^T + \sum_{i=1}^{d} \left[\nabla_{\boldsymbol{\eta}^{(0)}} Q_i^{(0)} \frac{\partial}{\partial x_i}(\boldsymbol{\eta}^{(0)})^T \right] = -\frac{W^{(0)} - W^{(0)LE}}{\tau^W}, \tag{6.37}$$

$$\nabla_{\boldsymbol{\eta}^{(0)}} Q_i^{(0)} \frac{\partial}{\partial t}(\boldsymbol{\eta}^{(0)})^T + \sum_{j=1}^{d} \left[\nabla_{\boldsymbol{\eta}^{(0)}} J_{ij}^{(0)} \frac{\partial}{\partial x_j}(\boldsymbol{\eta}^{(0)})^T \right] = -\frac{Q_i^{(0)}}{\tau^{\mathbf{Q}}}, \tag{6.38}$$

$$\partial_t W^{(2)} + \nabla_{\mathbf{x}} \cdot \mathbf{Q}^{(2)} - \frac{1}{24} \frac{\partial^3}{\partial x_i \partial x_j \partial x_k} \mathbf{T}_{ijk}^{(0)} = -\frac{W^{(2)} - W^{(2)LE}}{\tau^W}, \tag{6.39}$$

$$\partial_t \mathbf{Q}_i^{(2)} + \nabla_{\mathbf{x}} \cdot \mathbf{J}_{ir}^{(2)} - \frac{1}{24} \frac{\partial^3}{\partial x_i \partial x_j \partial x_k} \mathbf{U}_{rijk}^{(0)} = -\frac{\mathbf{Q}_i^{(2)}}{\tau^{\mathbf{Q}}}. \tag{6.40}$$

with

$$\mathbf{T}_{ijk}^{(0)} = -\frac{1}{(2\pi)^d} \int_{\mathbb{R}^d} h(\mathbf{q}) g_0^{MEP}(\boldsymbol{\eta}^{(0)}) \frac{\partial^3}{\partial q_i \partial q_j \partial q_k} h(\mathbf{q}) d\mathbf{q}$$

$$\mathbf{U}_{rijk}^{(0)} = -\frac{1}{(2\pi)^d} \int_{\mathbb{R}^d} \mathbf{c}_r h(\mathbf{q}) g_0^{MEP}(\boldsymbol{\eta}^{(0)}) \frac{\partial^3}{\partial q_i \partial q_j \partial q_k} h(\mathbf{q}) d\mathbf{q}$$

We observe that the equations (6.37)-(6.38) decouple. Once they are solved, one can get the second order term of the Lagrange multipliers from (6.39)-(6.40) which form a linear system for $\boldsymbol{\eta}^{(2)}$. This is rather beneficial from a computational point of view

Proposition 10 *At zero order in $\hbar^2$ the map $\boldsymbol{\eta} \to \mathbf{M}(\boldsymbol{\eta})$ is (locally) invertible.*

Proposition 11 *The equations (6.37)-(6.38) form a symmetric hyperbolic system of balance laws.*

The proofs can be found in [17].

6.4 Local equilibrium temperature

The concept of temperature out of equilibrium is a subtle topic and still a matter of debate. In the case of charge transport in semiconductors often the phonons are considered as a thermal bath and under some reasonable assumptions one can hypothesize that the electrons are in thermal equilibrium with the bath. In general if the dynamics of the phonons must be included, a thermal bath for these does not exist, unless a thermostated system is considered. Therefore, we need to introduce a local equilibrium temperature for the overall phonon system.

In statistical mechanics, one of the most reasonable and adopted ways to generalize the concept of temperature in a non-equilibrium state is that of relating it to the Lagrange multipliers associated with the energy constraint. For the phonon transport in graphene, an approach based on the Lagrange multipliers was followed in [30] (which the interested reader is referred to for the details).

Let us recall here the main features. At equilibrium, the phonon temperatures and the corresponding Lagrange multipliers are related by

$$k_B\, T_\mu(\mathbf{x}) = \frac{1}{\eta_{0,\mu}(\mathbf{x})} = \frac{1}{\eta^{(0)}_{0,\mu}(\mathbf{x})} - \hbar^2 \frac{\eta^{(2)}_{0,\mu}(\mathbf{x})}{(\eta^{(0)}_{0,\mu}(\mathbf{x}))^2} + o(\hbar^2).$$

If we assume that such relations hold, even out of equilibrium, the definition of the local temperature can be given in terms of the Lagrangian multipliers as follows.

Definition 11 *The local temperature of a system of two or more branches of phonons is* $T_{LE} := \frac{1}{k_B \eta_0^{LE}(\mathbf{x})}$, *where* $\eta_0^{LE}(\mathbf{x})$ *is the common Lagrange multiplier that the occupation numbers of the branches, taken into account, would have if they were in the local thermodynamic equilibrium corresponding to their total energy density, that is, the following:*

$$W(\eta_0^{LE}(\mathbf{x})) := \sum_\mu W_\mu(\eta_{0,\mu}(\mathbf{x})) = \sum_\mu W_\mu(\eta_0^{LE}(\mathbf{x})), \tag{6.41}$$

where the sum runs over all the phonon branches.

At *global equilibrium* the temperature is constant $T = \bar{T}$ and the Wigner function reduced to the Bose -Einstein distribution

$$g_\mu = \left[\exp(h_\mu(\mathbf{q})/k_B\bar{T}) - 1\right]^{-1}, \tag{6.42}$$

with the same temperature for each phonon branch.

Let us consider a small perturbation $\delta T_\mu(\mathbf{x})$ of the temperature in the sense that $\delta T_\mu(\mathbf{x})/\bar{T} \ll 1$. We can expand g_μ^{MEP} in powers of $\delta T_\mu(\mathbf{x})/\bar{T}$

$$\begin{aligned} g_\mu^{MEP} &= \left[\exp(h_\mu(\mathbf{q})/k_B\bar{T}) - 1\right]^{-1} + \left[\exp(h_\mu(\mathbf{q})/k_B\bar{T}) - 1\right]^{-2} \exp(h_\mu(\mathbf{q})/k_B\bar{T}) \frac{h_\mu(\mathbf{q})}{k_B\bar{T}} \frac{\delta T_\mu(\mathbf{x})}{\bar{T}} \\ &\quad + \hbar^2 \bar{T} \frac{\partial g^{MEP}_{2,\mu}(\bar{T})}{\partial T} \frac{\delta T_\mu}{\bar{T}} + o\left(\frac{\delta T_\mu}{\bar{T}} + \hbar^2 + \hbar^2 \frac{\delta T_\mu}{\bar{T}}\right). \end{aligned}$$

Note that $g^{MEP}_{2,\mu}(\bar{T})$ is zero because $\dfrac{\partial \xi}{\partial x_i} = \dfrac{\partial \xi}{\partial T}\dfrac{\partial T}{\partial x_i} = 0$ in the case of uniform temperature.

6.5 Heat flux in the stationary regime

In order to have a guess of the main features of the constitutive relations deduced with QMEP, we would like to get some asymptotic expression for the heat flux which can be compared with that in the semiclassical case. In particular, in order to devise a suitable coefficient of thermal conductivity, we try to put $(\mathbf{Q}_r)_\mu$ in form as close as possible to the Fourier one. Since in the semiclassical case, the

Fourier form is obtained from the hyperbolic balance equations in the stationary regime, we consider a steady state.

In such a case the time derivatives can be dropped and one gets

$$\mathbf{Q}_\mu = -\tau^{\mathbf{Q}} \left[\nabla_{\mathbf{x}} \cdot \mathbf{J}_\mu - \frac{\hbar^2}{(2\pi)^d} \frac{\partial^3}{\partial x_i \partial x_j \partial x_k} \int_{\mathbb{R}^d} \mathbf{c}_\mu \frac{h_\mu(\mathbf{q})}{24} g_{0,\mu}^{MEP}(\boldsymbol{\eta}_\mu^{(0)}) \frac{\partial^3 h_\mu(\mathbf{q})}{\partial q_i \partial q_j \partial q_k} d\mathbf{q} \right] + o(\hbar^2). \tag{6.43}$$

The relation between the Lagrange multipliers and the basic fields, as seen, can hardly be inverted analytically but a numerical procedure is necessary. However, if we consider a situation where the system is not too far from the equilibrium an expansion of the Lagrange multipliers around the equilibrium state can be performed. At equilibrium g_μ^{MEP} is isotropic and therefore $\boldsymbol{\eta}_{1,\mu}^{equil} = \mathbf{0}$ and in a neighborhood of the equilibrium $\boldsymbol{\eta}_{1,\mu}$ remains *small*.

More in general, in the spirit of Levermore theory of moments [37], we can consider the distribution depending on both energy density and energy-flux density as a perturbation of the distribution when only W_μ is the macroscopic field variable. Consistently, we assume that $\boldsymbol{\eta}_{1,\mu}$ remains *small*. Formally we introduce an anisotropy parameter $0 < \delta \ll 1$ and require

$$\boldsymbol{\eta}_\mu = \left(\frac{1}{k_B T_\mu}, \delta \boldsymbol{\eta}_{1,\mu} \right). \tag{6.44}$$

Note that in this way we are not necessarily restricted to situation close to equilibrium. So the temperature can vary without any constraints. By expanding in power of δ, one gets, at zero order in $\hbar^2$,

$$g_{0,\mu}^{MEP} = [\exp(h_\mu(\mathbf{q})/k_B T_\mu) - 1]^{-1} - \delta \left[\exp(h_\mu(\mathbf{q})/k_B T_\mu) - 1\right]^{-2} \exp(h_\mu(\mathbf{q})/k_B T_\mu) h_\mu(\mathbf{q}) \boldsymbol{\eta}_{1,\mu} \cdot \mathbf{c}_\mu + O(\hbar^2 + \delta^2).$$

We remark that the higher order terms do not enter the constitutive relation for $\mathbf{Q}_\mu$ and observe that $\forall \mathbf{n} \in S^d$

$$\int_{S^d} n_{i_1} n_{i_2} \cdots n_{i_r} d\Omega = 0 \quad \text{if } r \quad \text{odd},$$

S^d being the unit sphere in $\mathbb{R}^d$.

The previous relation implies

$$\int_{\mathbb{R}^d} \underbrace{\mathbf{c}_\mu \otimes \mathbf{c}_\mu \otimes \cdots \otimes \mathbf{c}_\mu}_{r \text{ times}} h_\mu(\mathbf{q}) \left[\exp(h_\mu(\mathbf{q})/k_B T_\mu) - 1\right]^{-1} d\mathbf{q} = \mathbf{0}$$

if r is odd because the Bose-Einstein distribution is isotropic(remember that the dispersion relation is assumed isotropic).

At the zero order in $\hbar^2$ we have

$$\begin{aligned}\mathbf{Q}_\mu^{(0)} &= -\tau^{\mathbf{Q}}\nabla_{\mathbf{x}}\cdot\mathbf{J}_\mu^{(0)} = -\frac{\tau^{\mathbf{Q}}}{(2\pi)^d}\nabla_{\mathbf{x}}\int_{\mathbb{R}^d}\mathbf{c}_\mu\otimes\mathbf{c}_\mu h_\mu(\mathbf{q})g_{0,\mu}^{MEP}(\boldsymbol{\eta}^{(0)}(\mathbf{x},\mathbf{q},t))d\mathbf{q}+o(\delta)\\ &= -\frac{\tau^{\mathbf{Q}}}{(2\pi)^d}\nabla_{\mathbf{x}}\int_{\mathbb{R}^d}\mathbf{c}_\mu\otimes\mathbf{c}_\mu h_\mu(\mathbf{q})\left[\exp(h_\mu(\mathbf{q})/k_BT_\mu)-1\right]^{-1}d\mathbf{q}+o(\delta)\\ &= -\frac{\tau^{\mathbf{Q}}}{(2\pi)^d}\int_{\mathbb{R}^d}\mathbf{c}_\mu\otimes\mathbf{c}_\mu h_\mu(\mathbf{q})\frac{\partial}{\partial T_\mu}\left[\exp(h_\mu(\mathbf{q})/k_BT_\mu)-1\right]^{-1}d\mathbf{q}\,\nabla_{\mathbf{x}}T_\mu+o(\delta)\\ &= -\frac{\tau^{\mathbf{Q}}}{(2\pi)^dk_BT_\mu^2}\int_{\mathbb{R}^d}\mathbf{c}_\mu\otimes\mathbf{c}_\mu h_\mu^2(\mathbf{q})\frac{\exp(h_\mu(\mathbf{q})/k_BT_\mu)}{\left(\exp(h_\mu(\mathbf{q})/k_BT_\mu)-1\right)^2}d\mathbf{q}\,\nabla_{\mathbf{x}}T_\mu+o(\delta),\end{aligned}$$

which can be written in the Fourier form

$$\mathbf{Q}_\mu^{(0)} = -\mathbf{K}_\mu^{(0)}\nabla_{\mathbf{x}}T_\mu$$

with the thermal conductivity tensor given by

$$\mathbf{K}_\mu^{(0)} = \frac{\tau^{\mathbf{Q}}}{(2\pi)^dk_BT_\mu^2}\int_{\mathbb{R}^d}\mathbf{c}_\mu\otimes\mathbf{c}_\mu h_\mu^2(\mathbf{q})\frac{\exp(h_\mu(\mathbf{q})/k_BT_\mu)}{\left(\exp(h_\mu(\mathbf{q})/k_BT_\mu)-1\right)^2}d\mathbf{q}.$$

It is evident that $\mathbf{K}_\mu^{(0)}$ is positive definite.

Therefore, if $h_\mu(\mathbf{q})$ is isotropic then $\mathbf{K}_\mu^{(0)}$ is isotropic as well

$$\mathbf{K}_\mu^{(0)} = \frac{1}{d}k^{(0)}\mathbf{I},$$

with $\mathbf{I}$ identity matrix of order d and $k^{(0)}$ the zero order trace

$$k^{(0)} = \frac{\tau^{\mathbf{Q}}}{(2\pi)^dk_BT_\mu^2}\int_{\mathbb{R}^d}|\mathbf{c}_\mu|^2 h_\mu^2(\mathbf{q})\frac{\exp(h_\mu(\mathbf{q})/k_BT_\mu)}{\left(\exp(h_\mu(\mathbf{q})/k_BT_\mu)-1\right)^2}d\mathbf{q}.$$

The second order correction in $\hbar^2$ reads

$$\begin{aligned}&\mathbf{Q}_\mu^{(2)} = -\frac{\tau^{\mathbf{Q}}}{(2\pi)^d}\nabla_{\mathbf{x}}\int_{\mathbb{R}^d}\mathbf{c}_\mu\otimes\mathbf{c}_\mu h_\mu(\mathbf{q})g_{2,\mu}^{MEP}(\boldsymbol{\eta}^{(0)}(\mathbf{x},\mathbf{q},t))d\mathbf{q}\\ &+\delta\frac{\tau^{\mathbf{Q}}}{(2\pi)^d}\frac{\partial^3}{\partial x_i\partial x_j\partial x_k}\int_{\mathbb{R}^d}\mathbf{c}_\mu\frac{h_\mu(\mathbf{q})}{24}\left[\exp(h_\mu(\mathbf{q})/k_BT_\mu)-1\right]^{-2}\exp(h_\mu(\mathbf{q})/k_BT_\mu)h_\mu(\mathbf{q})\boldsymbol{\eta}_{1,\mu}\\ &\cdot\mathbf{c}_\mu\frac{\partial^3}{\partial q_i\partial q_j\partial q_k}h_\mu(\mathbf{q})d\mathbf{q}+o(\delta).\end{aligned}$$

Indeed, if we are close to equilibrium the last term in the previous relation is of order $\hbar^2\delta$ and can be considered negligible for small deviations from local equilibrium. In any case the remaining part gives a highly nonlinear correction which cannot be put in a Fourier form.

In the next subsections we will analyze the quantum corrections in the most relevant phonon branches. Of course the optical phonons, and in particular the K-phonons in graphene, have a zero group velocity in the Einstein approximation and, as a consequence, they do not contribute directly to the thermal diffusion even if they play an indirect role on account of the scattering with the acoustic branches.

6.5.1 Acoustic phonons

In this subsection and in the next one only the zero order terms in δ are considered. In the case of the longitudinal and transversal acoustic phonons in the Debye approximation for a single branch the corresponding symbol of the phonon Hamiltonian reads $c_{ac}|\mathbf{q}|$ and therefore

$$\begin{aligned} k_{ac}^{(0)} &= \frac{\tau^{\mathbf{Q}}}{(2\pi)^d k_B T^2}\int_{\mathbb{R}^d} c_{ac}^4|\mathbf{q}|^2\frac{\exp(c_{ac}|\mathbf{q}|/k_BT)}{\left(\exp(c_{ac}|\mathbf{q}|/k_BT)-1\right)^2}d\mathbf{q} \\ &= \frac{\tau^{\mathbf{Q}}c_{ac}^4}{(2\pi)^d k_B T^2}\mathrm{meas}(S_d)\int_0^{+\infty}|\mathbf{q}|^{d+1}\frac{\exp(c_{ac}|\mathbf{q}|/k_BT)}{\left(\exp(c_{ac}|\mathbf{q}|/k_BT)-1\right)^2}d|\mathbf{q}| \\ &= \frac{k_B\tau^{\mathbf{Q}}c_{ac}^{2-d}}{(2\pi)^d}\mathrm{meas}(S_d)\,(k_BT)^d\int_0^{+\infty}\xi^{d+1}\frac{\exp(\xi)}{\left(\exp(\xi)-1\right)^2}d\,\xi \qquad (6.45) \end{aligned}$$

with now $\xi = c_{ac}|\mathbf{q}|/k_BT$ and

$$\mathrm{meas}(S_d) = \frac{2\pi^{d/2}}{\Gamma(d/2)}$$

the measure of S_d, $\Gamma(x)$ being the Euler gamma function. The previous integral is convergent for any $d \in \mathbb{N}$. Observe that we get a dependence on the temperature proportional to T^d.

We observe that

$$\begin{aligned} g_2^{MEP} = -\frac{1}{8}\frac{c_{ac}^2\exp(\xi)}{(\exp(\xi)-1)^3}\Bigg\{\frac{(\exp(\xi)+1)}{k_B^2T(\mathbf{x},t)^4}\left[2|\nabla_{\mathbf{x}}T|^2 - T\Delta_{\mathbf{x}}T + n_in_j\left(T\frac{\partial^2T}{\partial x_i\partial x_j} - 3\frac{\partial T}{\partial x_i}\frac{\partial T}{\partial x_j}\right)\right] \\ -\frac{c_{ac}(\exp(2\xi)+4\exp(\xi)+1)|\mathbf{q}|}{3k_B^3(\exp(\xi)-1)T(\mathbf{x},t)^5}\left[(\delta_{ij}-n_in_j)\frac{\partial T}{\partial x_i}\frac{\partial T}{\partial x_j} - n_in_jT\frac{\partial^2T}{\partial x_i\partial x_j}\right]\Bigg\}. \end{aligned}$$

and, therefore, the second order correction to the heat flux is given by

$$\mathbf{Q}^{(2)} = -\tau^{\mathbf{Q}}\nabla_{\mathbf{x}}\cdot\mathbf{J}^{(2)}$$

with

$$\mathbf{J}^{(2)} = \frac{1}{(2\pi)^d}\int_{\mathbb{R}^d}\mathbf{c}_{ac}\otimes\mathbf{c}_{ac}h(\mathbf{q})g_2^{MEP}d\mathbf{q} = \frac{c_{ac}^2}{(2\pi)^d}\int_{\mathbb{R}^d}n_hn_kh(\mathbf{q})g_2^{MEP}d\mathbf{q}\,\mathbf{e_h}\otimes\mathbf{e_k} := \mathbf{J}_{hk}^{(2)}\mathbf{e_h}\otimes\mathbf{e_k}$$

$(\mathbf{e_1},\mathbf{e_2},\cdots,\mathbf{e_d})$ being an orthonormal basis of $\mathbb{R}^d$.

By taking into account the well-known formulas

$$\begin{aligned} &\int_{S_d}n_hn_k d\Omega = \frac{\mathrm{meas}(S_d)}{d}\delta_{hk}, \\ &\int_{S_d}n_in_jn_hn_k d\Omega = \frac{\mathrm{meas}(S_d)}{d(d+2)}(\delta_{ij}\delta_{hk}+\delta_{ih}\delta_{jk}+\delta_{ik}\delta_{jh}), \end{aligned}$$

the components of $\mathbf{J}^{(2)}$ read

$$
\begin{aligned}
&\mathbf{J}^{(2)}_{hk} = -\frac{c_{ac}^5}{8(2\pi)^d}\frac{\mathrm{meas}(S_d)}{d}\frac{1}{k_B^2 T^4(\mathbf{x},t)}\left(\frac{k_B T}{c_{ac}}\right)^{d+1}\\
&\left\{\left[\left(\frac{2d+1}{d+2}I_1(d) - \frac{d+1}{3(d+2)}I_2(d)\right)|\nabla_x T|^2 - \left(\frac{d+1}{d+2}I_1(d) - \frac{I_2(d)}{3(d+2)}\right)T\Delta_x T\right]\delta_{hk}\right.\\
&\left. + \frac{2}{3(d+2)}\left[\left(I_2(d) - 9I_1(d)\right)\frac{\partial T}{\partial x_h}\frac{\partial T}{\partial x_k} + \left(3I_1(d) + I_2(d)\right)T\frac{\partial^2 T}{\partial x_h \partial x_k}\right]\right\},
\end{aligned}
$$

where

$$
\begin{aligned}
I_1(d) &= \int_0^{+\infty}\frac{\exp(\xi)(\exp(\xi)+1)}{(\exp(\xi)-1)^3}\xi^d d\xi,\\
I_2(d) &= \int_0^{+\infty}\frac{\exp(\xi)(\exp(2\xi)+4\exp(\xi)+1)}{(\exp(\xi)-1)^4}\xi^{d+1} d\xi.
\end{aligned}
$$

From the above results one gets the second order correction to the energy flux density

$$
\begin{aligned}
&(\mathbf{Q}^{(2)})_h = \frac{\tau^{\mathbf{Q}}}{8(2\pi)^d}c_{ac}^{4-d}\frac{\mathrm{meas}(S_d)}{d}k_B^{d-1}T^{d-4}(\mathbf{x},t)\\
&\left\{(d-3)\left(\frac{2d-5}{d+2}I_1(d) - \frac{d-1}{3(d+2)}I_2(d)\right)|\nabla_x T|^2\frac{\partial T}{\partial x_h}\right.\\
&-\left(\frac{d^2-d+4}{d+2}I_1(d) - \frac{d}{3(d+2)}I_2(d)\right)T\frac{\partial T}{\partial x_h}\Delta_x T\\
&\left.+\left(\frac{6d-8}{d+2}I_1(d) - \frac{4}{3(d+2)}I_2(d)\right)T\frac{\partial^2 T}{\partial x_h \partial x_k}\frac{\partial T}{\partial x_k} + \left(\frac{1-d}{d+2}I_1(d) + \frac{1}{d+2}I_2(d)\right)T^2\frac{\partial \Delta_x T}{\partial x_h}\right\}.
\end{aligned}
\tag{6.46}
$$

The integrals $I_1(d)$ and $I_2(d)$ are divergent in the cases $d = 1$ and $d = 2$. As a consequence, the quantum corrections are valid only in the bulk ($d = 3$) case where $I_1(3) = \pi^2, I_2(3) = 4\pi^2$. This peculiarity is physically related to the density of states and the form of the energy dispersion relations and cannot be ascribed to the approximation of the FBZ with all $\mathbb{R}^d$ because the singularity appears as the momentum tends to zero, that is at the center Γ of the FBZ. Since this pathology is not present for quadratic dispersion relations (see the next subsection) such as for Z-phonons, to overcome the divergence of the integrals $I_1(d)$ and $I_2(d)$ a viable way could be to quadratically regularize the dispersion relation in a suitable small neighborhood of the Γ point of the FBZ and matching it with a linear function for higher energies.

6.5.2 Quadratic dispersion relations and Z-phonons.

The Z-phonons have a quadratic dispersion relation $h_{ZA}(\mathbf{q}) = \bar{\alpha}|\mathbf{q}|^2$, which is also a rather common approximation in a neighborhood of a energy minimum, and the group velocity is $\mathbf{c}_{ZA}(\mathbf{q}) = 2\bar{\alpha}\mathbf{q}$.

One gets the following zero order thermal conductivity

$$k_{ZA}^{(0)} = \frac{2k_B\tau^{\mathbf{Q}}}{(2\pi)^d}\frac{(k_BT)^{\frac{d}{2}+1}}{\bar{\alpha}^{\frac{d}{2}-1}}\mathrm{meas}(S_d)\int_0^{+\infty}\frac{\exp(\xi)}{(\exp(\xi)-1)^2}\xi^{\frac{d}{2}+2}d\xi \quad (6.47)$$

with $\xi = \dfrac{\bar{\alpha}|\mathbf{q}|^2}{k_BT}$. Observe that previous integral is always convergent for any d and that $k_{ZA}^{(0)}$ depends on the temperature as $T^{\frac{d}{2}+1}$.

The second order correction to the distribution function reads

$$\begin{aligned} g_2^{MEP} = & -\frac{1}{4}\frac{\bar{\alpha}\xi}{k_BT^3}\left[\frac{\exp(\xi)(\exp(\xi)+1)}{(\exp(\xi)-1)^3}\left(2|\nabla_x T|^2 - T\Delta_x T - 2\frac{\partial T}{\partial x_i}\frac{\partial T}{\partial x_j}n_in_j\right)\right. \\ & \left. + \frac{\exp(\xi)(\exp(2\xi)+4\exp(\xi)+1)}{3(\exp(\xi)-1)^4}\xi\left(2T\frac{\partial^2 T}{\partial x_i\partial x_j}n_in_j - |\nabla_x T|^2\right)\right] \end{aligned}$$

and one gets

$$\begin{aligned} &\mathbf{J}_{hk}^{(2)} = -\frac{\bar{\alpha}^{2-\frac{d}{2}}k_B^{\frac{d}{2}+1}T^{\frac{d}{2}-1}}{(2\pi)^d}\frac{\mathrm{meas}(S_d)}{2d} \\ &\left\{\left[\left(\frac{2d+2}{d+2}H_1(d) - \frac{1}{3}H_2(d)\right)|\nabla_x T|^2 - \left(H_1(d) - \frac{2}{3(d+2)}H_2(d)\right)T\Delta_x T\right]\delta_{hk}\right. \\ &\left. -\frac{4}{d+2}\left[H_1(d)\frac{\partial T}{\partial x_h}\frac{\partial T}{\partial x_k} - \frac{1}{3}H_2(d)T\frac{\partial^2 T}{\partial x_h\partial x_k}\right]\right\} \end{aligned}$$

where

$$\begin{aligned} H_1(d) &= \int_0^{+\infty}\frac{\exp(\xi)(\exp(\xi)+1)}{(\exp(\xi)-1)^3}\xi^{\frac{d}{2}+2}d\xi, \\ H_2(d) &= \int_0^{+\infty}\frac{\exp(\xi)(\exp(2\xi)+4\exp(\xi)+1)}{(\exp(\xi)-1)^4}\xi^{\frac{d}{2}+3}d\xi. \end{aligned}$$

Note that the integrals $H_1(d)$ and $H_2(d)$ are convergent in the two and three dimensional cases which are the relevant ones from a physical point of view. For $d = 1$ they diverge but this case can be considered as an oversimplification.

By evaluating the divergence of the completely symmetric second order tensor $\mathbf{J}^{(2)}$ one finds out the second order correction to the energy-flux density

$$\begin{aligned} &\left(\mathbf{Q}^{(2)}\right)_h = \tau^{\mathbf{Q}}\frac{\bar{\alpha}^{2-\frac{d}{2}}k_B^{\frac{d}{2}+1}}{(2\pi)^d}\frac{\mathrm{meas}(S_d)}{2d}T^{\frac{d}{2}-2} \\ &\left\{\left[\frac{d^2-3d+2}{d+2}H_1(d) - \frac{d-2}{6}H_2(d)\right]\frac{\partial T}{\partial x_h}|\nabla_x T|^2 - \left[\frac{d^2+2d+8}{2(d+2)}H_1(d) - \frac{d}{3(d+2)}H_2(d)\right]T\frac{\partial T}{\partial x_h}\Delta_x T + \right. \\ &\left.\left[\frac{4d}{d+2}H_1(d) - \frac{4}{3(d+2)}H_2(d)\right]T\frac{\partial T}{\partial x_k}\frac{\partial^2 T}{\partial x_h\partial x_k} - \left[H_1(d) - \frac{2}{d+2}H_2(d)\right]T^2\frac{\partial}{\partial x_h}\Delta_x T\right\} \end{aligned}$$

Chapter 7

Quantum MEP hydrodynamical model for charge transport

In this chapter we use the same method of the previous one to develop a transport model for electrons. We remark that the results of this chapter are original and they are under review.

A way to study quantum transport is to resort to the Wigner function which leads to a description resembling the classical or semiclassical transport models. In fact, the mean values can be evaluated as expectation values with respect to the Wigner function as it were a probability density. The Wigner equation has been intensively investigated both from an analytical and numerical point of view (the interested reader is referred to [1–3] and references therein) but it is almost exclusively assumed a quadratic dispersion relation for the energy while semiconductors or semimetal, e.g. graphene, obey different dispersion relations [4, 7, 8]. Quantum hydrodynamical models for charge transport in silicon have been devised in [9] starting from the Wigner transport equation in the case of parabolic bands, and in [10] the case of electrons moving in graphene has been tackled including quantum effects as second order corrections in the scaled Planck constant arising from the equilibrium Wigner function at the same temperature of a thermal bath of phonons.

Quantum hydrodynamical models are obtained as moment equations of Wigner equation and as in the classical case, one gets a system of balance equations which need some closure relations, that is one has to express the additional fields appearing in the moment equations in terms of a set of fundamental variables. A sound way to accomplish this task is resorting to a quantum formulation of the maximum entropy principle [24]. The quantum formulation

of the maximum entropy principle was already given by Jaynes [23]. Recently, a more formal theory has been developed in series of papers [25, 26] with several applications, for example for charge transport in semiconductors [9, 27–29]. The interested reader is also referred to [7, 17].

Here we consider a general dispersion relation and formulate a hydrodynamic model for charge transport which is valid also beyond the parabolic band approximation. We apply QMEP to the moment equations deduced from the Wigner one assuming as basic fields those typical of a hydrodynamical model, that is the density, energy density and momentum density of charge carriers. Expanding up to second order in $\hbar$, quantum corrections to the semiclassical case [30] are deduced (see (3.8) for details about the justification of the expansion in $\hbar$). Specific constitutive relations are explicitly obtained, with the aid of the Moyal calculus, for charge transport in silicon and graphene including the main electron-phonon scatterings. The results for graphene improve those obtained in [27] in what concerns the expression for the Lagrange multipliers of energy, no longer assumed to be that of a local thermal equilibrium with a bath of phonons. With a similar approach phonon transport has been tackled in [31].

The plan of the chapter is as follows. In section 7.1 we write down the Wigner equations for charge transport. Section 7.2 is dedicated to deducing the moment equations whose closure relations are achieved by QMEP in section 7.3. Specific examples of hydrodynamical models for charge transport in bulk semiconductors and in graphene are presented in sections 7.4 and 7.5 respectively. In the last section quantum corrections to mobilities are obtained.

7.1 Electron Wigner equation

The starting point of our derivation is the one-particle Wigner function. For the system under consideration, given the density operator $\hat{\rho}$, i.e. a bounded non-negative operator with unit trace, acting on $L^2(\mathbb{R}^d, \mathbb{C})$, the associated Wigner function, $w = w(\mathbf{x}, \mathbf{p}, t)$, evaluated at position $\mathbf{x}$, momentum $\mathbf{p}, (\mathbf{x},\ \mathbf{p}) \in \mathbb{R}^{2d}$, and time $t > 0$, is the inverse Weyl quantization of $\hat{\rho}$,

$$w = Op_\hbar^{-1}(\hat{\rho}). \tag{7.1}$$

We recall that the Weyl quantization of a phase-space function (a *symbol*) $a = a(\mathbf{x}, \mathbf{p})$ is the (Hermitian) operator $Op_\hbar(a)$ formally defined by [13]

$$Op_\hbar(a)\psi(\mathbf{x}) = \frac{1}{(2\pi\hbar)^d} \int_{\mathbb{R}^{2d}} a\left(\frac{\mathbf{x}+\mathbf{y}}{2}, \mathbf{p}\right) \psi(\mathbf{y}) e^{i(\mathbf{x}-\mathbf{y})\cdot\mathbf{p}/\hbar} d\mathbf{y}\, d\mathbf{p} \tag{7.2}$$

for any $\psi \in L^2(\mathbb{R}^d, \mathbb{C})$. The inverse quantization of $\hat{\rho}$ can be written as the *Wigner transform*

$$w(\mathbf{x}, \mathbf{p}) = \frac{1}{\hbar^d} \int_{\mathbb{R}^d} \rho(\mathbf{x} + \xi/2, \mathbf{x} - \xi/2) e^{i\mathbf{p}\cdot\xi/\hbar} d\xi, \tag{7.3}$$

of the kernel $\rho(\mathbf{x}, \mathbf{y})$ of the density operator.

The dynamics of the time-dependent Wigner function $w(\mathbf{x}, \mathbf{p}, t)$ steams directly from the dynamics of the corresponding density operator $\hat{\rho}(t)$, i.e. from the Von Neumann or quantum Liouville equation

$$i\hbar\partial_t\hat{\rho}(t) = [\hat{H}, \hat{\rho}(t)] := \hat{H}\hat{\rho}(t) - \hat{\rho}(t)\hat{H}, \tag{7.4}$$

where $\hat{H}$ denotes the Hamiltonian operator and $[\cdot, \cdot]$ the commutator. If $h = Op_\hbar^{-1}(\hat{H})$ is the symbol associated with $\hat{H}$, then, from Eq.s (7.4), we obtain the *Wigner equation*

$$i\hbar\partial_t w(\mathbf{x}, \mathbf{p}, t) = \{h, w(\mathbf{x}, \mathbf{p}, t)\}_\# := h\#w(\mathbf{x}, \mathbf{p}, t) - w(\mathbf{x}, \mathbf{p}, t)\#h. \tag{7.5}$$

With the symbol $\#$ we have denoted the Moyal (or *twisted*) product which translates the product of operators at the level of symbols according to

$$a\#b = Op_\hbar^{-1}(Op_\hbar(a)Op_\hbar(b)), \tag{7.6}$$

for any pair of symbols a and b. Here, we do not tackle the analytical issues which guarantee the existence of the previous relations but limit ourselves to remark that if two operators are in the Hilbert-Schmidt class, that is the trace there exists and it is not negative and bounded, then the product is still Hilbert-Schmidt and the Moyal calculus is well defined. In the sequel, we will suppose that such conditions are valid.

Let us consider the standard Hamiltonian symbol

$$h(\mathbf{x}, \mathbf{p}) = \epsilon(\mathbf{p}) - q\Phi(\mathbf{x}) \tag{7.7}$$

where $\epsilon(\mathbf{p})$ is the energy band in terms of the crystal momentum $\mathbf{p} = \hbar\mathbf{k}$ and $\Phi(\mathbf{x})$ the electrostatic potential, which is assumed to be real. We do not assume for the moment a specific form of $\epsilon(\mathbf{p})$. We have

$$h\#w - w\#h = -i\hbar(S[\epsilon]w - q\Theta[\Phi]w)$$

where

$$i\hbar S[\epsilon]w = w\#\epsilon(\mathbf{p}) - \epsilon(\mathbf{p})\#w, \tag{7.8}$$

$$i\hbar q\Theta[\Phi]w = q(w\#\Phi(\mathbf{x}) - \Phi(\mathbf{x})\#w). \tag{7.9}$$

If we express the Moyal product as a power series

$$\epsilon(\mathbf{p})\#w = \sum_{n=0}^{\infty} \hbar^n \epsilon(\mathbf{p})\#_n w$$

we get (for the details see [29, 31])

$$S[\epsilon]w = \nabla_{\mathbf{p}}\epsilon(\mathbf{p}) \cdot \nabla_{\mathbf{x}} w - \frac{\hbar^2}{24}\partial_{\mathbf{p}}^3\epsilon(\mathbf{p})\partial_{\mathbf{x}}^3 w + O(\hbar^4), \tag{7.10}$$

$$\Theta[\Phi]w = -\nabla_{\mathbf{x}}\Phi(\mathbf{x}) \cdot \nabla_{\mathbf{p}} w + \frac{\hbar^2}{24}\frac{\partial^3\Phi(\mathbf{x})}{\partial x_i \partial x_j \partial x_k}\frac{\partial^3 w}{\partial p_i \partial p_j \partial p_k} + O(\hbar^4). \tag{7.11}$$

Altogether, the Wigner equation reads

$$\frac{\partial}{\partial t}w(\mathbf{x},\mathbf{p},t) + S[\epsilon]w(\mathbf{x},\mathbf{p},t) - q\Theta[\Phi]w(\mathbf{x},\mathbf{p},t) = 0, \tag{7.12}$$

By adding a collision term, one has the the Wigner-Boltzmann equation

$$\frac{\partial}{\partial t}w(\mathbf{x},\mathbf{p},t) + S[\epsilon]w(\mathbf{x},\mathbf{p},t) - q\Theta[\Phi]w(\mathbf{x},\mathbf{p},t) = C(w). \tag{7.13}$$

We suppose that the expansion

$$w = w^{(0)}(\mathbf{x},\mathbf{p},t) + \hbar^2 w^{(2)}(\mathbf{x},\mathbf{p},t) + O(\hbar^4) \tag{7.14}$$

holds. Since formally as $\hbar \to 0$ the semiclassical Boltzmann equation is recovered from the Wigner equation, $w^{(0)}(\mathbf{x},\mathbf{p},t)$ has to solve the first one while $w^{(2)}(\mathbf{x},\mathbf{p},t)$ is solution of the equation[1]

$$\frac{\partial}{\partial t}w^{(2)}(\mathbf{x},\mathbf{p},t) + \nabla_{\mathbf{p}}\epsilon(\mathbf{p})\cdot\nabla_{\mathbf{x}}w^{(2)}(\mathbf{x},\mathbf{p},t) - \frac{1}{24}\frac{\partial^3\epsilon(\mathbf{p})}{\partial p_i\partial p_j\partial p_k}\frac{\partial^3 w^{(0)}(\mathbf{x},\mathbf{p},t)}{\partial x_i\partial x_j\partial x_k} \tag{7.15}$$

$$+q\left(\nabla_{\mathbf{x}}\Phi(\mathbf{x})\cdot\nabla_{\mathbf{p}}w^{(2)}(\mathbf{x},\mathbf{p},t) - \frac{1}{24}\frac{\partial^3\Phi(\mathbf{x})}{\partial x_i\partial x_j\partial x_k}\frac{\partial^3 w^{(0)}(\mathbf{x},\mathbf{p},t)}{\partial p_i\partial p_j\partial p_k}\right) = C^{(2)}(w) \tag{7.16}$$

The explicit form of $C^{(2)}(w)$ will be specified later in the chapter.

7.2 Moment equations

One of the most interesting properties of the Wigner function is that its moments have a direct physical interpretation in terms of macroscopic fluid quantities, which makes Wigner function an ideal tool for the derivation of quantum fluid equations. Analogously to previous works [17, 27], in this chapter we shall write equations involving the following moments to devise a quantum hydrodynamical model:

- the density

$$n(\mathbf{x},t) = y\int_{\mathbb{R}^d} w(\mathbf{x},\mathbf{p},t)d\mathbf{p}, \tag{7.17}$$

- the momentum density

$$\mathbf{J}(\mathbf{x},t) = y\int_{\mathbb{R}^d} \mathbf{v}w(\mathbf{x},\mathbf{p},t)d\mathbf{p}, \tag{7.18}$$

- the energy density

$$W(\mathbf{x},t) = y\int_{\mathbb{R}^d} \epsilon(\mathbf{p})w(\mathbf{x},\mathbf{p},t)d\mathbf{p}, \tag{7.19}$$

[1] Th Einstein convention on the repeated index is understood.

where $y = \dfrac{g_s g_v}{(2\pi\hbar)^d}$, g_s and g_v being spin and valley degeneracy, respectively.

The resulting moment system is obtained by taking the moments of the Wigner equation. Integrating with respect to $\mathbf{p}$ the Wigner equation (7.12) we have the following equation for the density [2]

$$\frac{\partial}{\partial t} y \int_{\mathbb{R}^d} w(\mathbf{x},\mathbf{p},t)d\mathbf{p} + y\int_{\mathbb{R}^d} S[\epsilon]w(\mathbf{x},\mathbf{p},t)d\mathbf{p} - qy\int_{\mathbb{R}^d}\Theta[\Phi]w(\mathbf{x},\mathbf{p},t)d\mathbf{p} = 0,$$

Multiplying by $\epsilon(\mathbf{p})$ and integrating with respect to $\mathbf{p}$ the (7.12) we obtain the equation for the energy density W

$$\frac{\partial}{\partial t} y \int_{\mathbb{R}^d} \epsilon(\mathbf{p}) w(\mathbf{x},\mathbf{p},t)d\mathbf{p} + y\int_{\mathbb{R}^d} \epsilon(\mathbf{p}) S[\epsilon]w(\mathbf{x},\mathbf{p},t)d\mathbf{p} - qy\int_{\mathbb{R}^d}\epsilon(\mathbf{p})\Theta[\Phi]w(\mathbf{x},\mathbf{p},t)d\mathbf{p} = y\int_{\mathbb{R}^d}\epsilon(\mathbf{p})C d\mathbf{p}.$$

while multiplying by $\mathbf{v}$ and integrating with respect to $\mathbf{p}$ the equation (7.12) we obtain the equation for the momentum density $\mathbf{J}$

$$\frac{\partial}{\partial t} y \int_{\mathbb{R}^d} \mathbf{v} w(\mathbf{x},\mathbf{p},t)d\mathbf{p} + y\int_{\mathbb{R}^d} \mathbf{v} S[\epsilon]w(\mathbf{x},\mathbf{p},t)d\mathbf{p} - qy\int_{\mathbb{R}^d}\mathbf{v}\Theta[\Phi]w(\mathbf{x},\mathbf{p},t)d\mathbf{p} = y\int_{\mathbb{R}^d}\mathbf{v}C d\mathbf{p}.$$

Observe that up to terms of order in $\hbar^2$, $n = n^{(0)} + \hbar^2 n^{(2)}$, where

$$n^{(0)} = y\int_{\mathbb{R}^d} w^{(0)}(\mathbf{x},\mathbf{p},t)d\mathbf{p} \quad \text{and} \quad n^{(2)} = y\int_{\mathbb{R}^d} w^{(2)}(\mathbf{x},\mathbf{p},t)d\mathbf{p}.$$

Similarly $W = W^{(0)} + \hbar^2 W^{(2)}$ and $\mathbf{J} = \mathbf{J}^{(0)} + \hbar^2\mathbf{J}^{(2)}$ with obvious meaning of the symbols.

The moment equations split into zero and first order in $\hbar^2$ read

$$\frac{\partial}{\partial t} n^{(0)}(\mathbf{x},t) + \nabla_{\mathbf{x}}\mathbf{J}^{(0)}(\mathbf{x},t) = y\int_{\mathbb{R}^d} C^{(0)} d\mathbf{p}, \tag{7.20}$$

$$\frac{\partial}{\partial t} W^{(0)} + \nabla_{\mathbf{x}}\mathbf{S}^{(\mathbf{0})} - q\nabla_{\mathbf{x}}\Phi(\mathbf{x})\cdot\mathbf{J}^{(\mathbf{0})} = y\int_{\mathbb{R}^d}\epsilon(\mathbf{p})C^{(0)}d\mathbf{p}, \tag{7.21}$$

$$\frac{\partial}{\partial t}\mathbf{J}^{(0)} + y\nabla_{\mathbf{x}}\int_{\mathbb{R}^d}\mathbf{v}\otimes\mathbf{v}\, w^{(0)}(\mathbf{x},\mathbf{p},t)d\mathbf{p} - yq\nabla_{\mathbf{x}}\Phi(\mathbf{x})\int_{\mathbb{R}^d} w^{(0)}(\mathbf{x},\mathbf{p},t)\nabla_{\mathbf{p}}\mathbf{v}d\mathbf{p} = y\int_{\mathbb{R}^d}\mathbf{v}C^{(0)}d\mathbf{p}, \tag{7.22}$$

$$\frac{\partial}{\partial t} n^{(2)}(\mathbf{x},t) + \nabla_{\mathbf{x}}\mathbf{J}^{(2)}(\mathbf{x},t) - y\frac{1}{24}\frac{\partial^3}{\partial x_i\partial x_j\partial x_k}\int_{\mathbb{R}^d} w^{(0)}(\mathbf{x},\mathbf{p},t)\frac{\partial^3\epsilon(\mathbf{p})}{\partial p_i\partial p_j\partial p_k}d\mathbf{p} = y\int_{\mathbb{R}^d} C^{(2)}d\mathbf{p}, \tag{7.23}$$

$$\begin{aligned}&\frac{\partial}{\partial t} W^{(2)} + \nabla_{\mathbf{x}}\mathbf{S}^{(2)} - q\nabla_{\mathbf{x}}\Phi(\mathbf{x})\cdot\mathbf{J}^{(2)} - \frac{y}{24}\frac{\partial^3}{\partial x_i\partial x_j\partial x_k}\int_{\mathbb{R}^d}\epsilon(\mathbf{p})\frac{\partial^3\epsilon(\mathbf{p})}{\partial p_i\partial p_j\partial p_k}w^{(0)}(\mathbf{x},\mathbf{p},t)d\mathbf{p}\\ &+q\frac{y}{24}\frac{\partial^3\Phi(\mathbf{x})}{\partial x_i\partial x_j\partial x_k}\int_{\mathbb{R}^d} w^{(0)}(\mathbf{x},\mathbf{p},t)\frac{\partial^3\epsilon(\mathbf{p})}{\partial p_i\partial p_j\partial p_k}d\mathbf{p} = y\int_{\mathbb{R}^d}\epsilon(\mathbf{p})C^{(2)}d\mathbf{p},\end{aligned} \tag{7.24}$$

$$\begin{aligned}&\frac{\partial}{\partial t}\mathbf{J}^{(2)} + y\left(\nabla_{\mathbf{x}}\int_{\mathbb{R}^d}\mathbf{v}\otimes\mathbf{v}w^{(2)}(\mathbf{x},\mathbf{p},t)d\mathbf{p} - \frac{1}{24}\frac{\partial^3}{\partial x_i\partial x_j\partial x_k}\int_{\mathbb{R}^d}\mathbf{v}\frac{\partial^3\epsilon(\mathbf{p})}{\partial p_i\partial p_j\partial p_k}w^{(0)}(\mathbf{x},\mathbf{p},t)d\mathbf{p}\right)\\ &-qy\nabla_{\mathbf{x}}\Phi(\mathbf{x})\int_{\mathbb{R}^d} w^{(2)}(\mathbf{x},\mathbf{p},t)\nabla_{\mathbf{p}}\mathbf{v}d\mathbf{p} + q\frac{y}{24}\frac{\partial^3\Phi(\mathbf{x})}{\partial x_i\partial x_j\partial x_k}\int_{\mathbb{R}^d}\frac{\partial^3\mathbf{v}}{\partial p_i\partial p_j\partial p_k}w^{(0)}(\mathbf{x},\mathbf{p},t)d\mathbf{p}\\ &= y\int_{\mathbb{R}^d}\mathbf{v}C^{(2)}d\mathbf{p},\end{aligned} \tag{7.25}$$

[2] in the unipolar case the density production term is zero for the conservation of charge.

where

$$\mathbf{S}^{(0)} = y\int_{\mathbb{R}^d} \epsilon(\mathbf{p})\mathbf{v}w^{(0)}(\mathbf{x},\mathbf{p},t)d\mathbf{p} \quad \text{and} \quad \mathbf{S}^{(2)} = y\int_{\mathbb{R}^d} \epsilon(\mathbf{p})\mathbf{v}w^{(2)}(\mathbf{x},\mathbf{p},t)d\mathbf{p}.$$

are the zeroth and fist order terms in $\hbar^2$ of the energy flux.

7.3 QMEP for the closure relations

The evolution equations do not form a closed system of balance laws. We need to express the additional fields as functions of n, W and $\mathbf{J}$. To this aim the quantum version of the maximum entropy principle (QMEP) will be adopted.

Since electrons are fermions, let us introduce the operator

$$s(\hat{\rho}) = -k_B[\hat{\rho}\ln\hat{\rho} + (1-\hat{\rho})\ln(1-\hat{\rho})], \tag{7.26}$$

which must be intended in the sense of the functional calculus. Here k_B is the Boltzmann constant. The entropy of the electrons reads

$$S(\hat{\rho}) = \mathrm{Tr}\{s(\hat{\rho})\}$$

which can be viewed as a quantum Fermi-Dirac entropy.

According to MEP, we estimate $\hat{\rho}$ with $\hat{\rho}^{MEP}$ which is obtained by maximizing $S(\hat{\rho})$ under the constraints that some expectation values have to be preserved. In particular, in view of formulating hydrodynamical models we require that the following average values must be preserved

$$y\int_{\mathbb{R}^d} \boldsymbol{\psi}(\mathbf{p})w^{MEP}(\mathbf{x},\mathbf{p},t)d\mathbf{p} = (n(\mathbf{x},t), W(\mathbf{x},t), \mathbf{J}(\mathbf{x},t)) := y\int_{\mathbb{R}^d} \boldsymbol{\psi}(\mathbf{p})w(\mathbf{x},\mathbf{p},t)d\mathbf{p}, \tag{7.27}$$

where

$$\boldsymbol{\psi}(\mathbf{p}) = (1, \epsilon(\mathbf{p}), \epsilon(\mathbf{p})\mathbf{v})$$

is the vector of the weight functions and w^{MEP} is the Wigner function associated with $\hat{\rho}^{MEP}$ while w is the Wigner function associated to $\hat{\rho}$. In the previous relations the time t and position $\mathbf{x}$ must be considered as fixed. In the moment conditions (7.27), the first relation is a set of constraints while the second one is just a definition.

The quantum formulation of MEP is given in terms of expectation values. By taking into account that for a weight function $\psi(\mathbf{p})$ regular enough,

$$\mathrm{tr}\left\{\hat{\rho}Op_\hbar(\psi(\mathbf{p}))\right\}(t) = y\int_{\mathbb{R}^d} \psi(\mathbf{p})w(\mathbf{x},\mathbf{p},t)d\mathbf{p},$$

with the choice done above, the constrains read

$$E_1(t) = \mathrm{tr}\left\{\hat{\rho}Op_\hbar(1)\right\}(t), \quad E_2(t) = \mathrm{tr}\left\{\hat{\rho}Op_\hbar(\epsilon(\mathbf{p}))\right\}(t), \quad \mathbf{E}_3(t) = \mathrm{tr}\left\{\hat{\rho}Op_\hbar(\mathbf{v})\right\}(t),$$

and therefore, for fixed t,

$$\hat{\rho}^{MEP} = \text{argument max}\, S(\hat{\rho}) \tag{7.28}$$

under the constraints

$$\text{tr}\{\hat{\rho}^{MEP} Op_\hbar(1)\} = E_1(t), \quad \text{tr}\{\hat{\rho}^{MEP} Op_\hbar(\epsilon(\mathbf{p}))\} = E_2(t), \quad \text{tr}\{\hat{\rho}^{MEP} Op_\hbar(\mathbf{v})\} = E_3(t) \tag{7.29}$$

in the space of the Hilbert-Schmidt operators on $L^2(\mathbb{R}^d, \mathbb{C})$ which are positive, with trace one and such that the previous expectation values there exist.

If we introduce the vector of the Lagrange multipliers

$$\boldsymbol{\eta} = (\eta_0(\mathbf{x}, t), \eta_1(\mathbf{x}, t), \boldsymbol{\eta}_2(\mathbf{x}, t)), \tag{7.30}$$

the vector of the moments

$$\mathbf{m}[\rho](\mathbf{x}, \mathbf{t}) := \mathbf{m}(\mathbf{x}, t) = y \int_{\mathbb{R}^d} \boldsymbol{\psi}(\mathbf{p}) w(\mathbf{x}, \mathbf{p}, t) d\mathbf{p}, \tag{7.31}$$

and the vector of the moments which must be considered as known

$$\mathbf{M}(\mathbf{x}, t) := (n(\mathbf{x}, t), W(\mathbf{x}, t), \mathbf{J}(\mathbf{x}, t)), \tag{7.32}$$

the constrained optimization problem (7.28)-(7.29) can be rephrased as a saddle-point problem for the Lagrangian

$$\begin{aligned} \mathcal{L}(\hat{\rho}, \boldsymbol{\eta}) &= S(\hat{\rho}) - \int_{\mathbb{R}^d} \boldsymbol{\eta} \cdot (\mathbf{m}(\mathbf{x}, t) - \mathbf{M}(\mathbf{x}, t))\, d\mathbf{x} \\ &= S(\hat{\rho}) - \text{tr}\left\{\hat{\rho} Op_\hbar(\boldsymbol{\eta} \cdot (1, \epsilon(\mathbf{p}), \mathbf{v}))\right\} + \int_{\mathbb{R}^d} \boldsymbol{\eta} \cdot \mathbf{M}(\mathbf{x}, t)\, d\mathbf{x} \end{aligned} \tag{7.33}$$

in the space of the admissible $\hat{\rho}$ and smooth function $\boldsymbol{\eta}$.

If the Lagrangian $\mathcal{L}(\hat{\rho}, \boldsymbol{\eta})$ is Gâteaux-differentiable with respect to $\hat{\rho}$, the first order optimality condition requires

$$\delta\mathcal{L}(\hat{\rho}, \boldsymbol{\eta})(\delta\hat{\rho}) = 0$$

for each Hilbert-Schmidt operator $\delta\hat{\rho}$ on $L^2(\mathbb{R}^d, \mathbb{C})$ which is positive, with trace one and such that the previous expectation values there exist.

The existence of the first order Gâteaux derivative is a consequence of the following Lemma

Lemma 3 *If $r(x)$ is a continuously differentiable increasing function on $\mathbb{R}^+$ then $tr\{r(\hat{\rho})\}$ is Gâteaux-differentiable in the class of the Hermitian Hilbert-Schmidt positive operators on $L^2(\mathbb{R}^d, \mathbb{C})$. The Gâteaux derivative along $\delta\rho$ is given by*

$$\delta tr\{r(\hat{\rho})\}(\delta\hat{\rho}) = tr\{r'(\hat{\rho})\delta\hat{\rho}\}. \tag{7.34}$$

The extremality conditions for the unconstrained maximization problem (7.28)-(7.29) are similar to that of the semiclassical case, as expressed by the following lemma.

Lemma 4 *The first order optimality condition for the maximization problem (7.28)-(7.29) is equivalent to*

$$\hat{\rho} = (s')^{-1}(Op_\hbar(\boldsymbol{\eta} \cdot \boldsymbol{\psi})) \tag{7.35}$$

where $(s')^{-1}$ *is the inverse function of the first derivative of* s*.*

$$\delta\mathcal{L}(\hat{\rho}, \boldsymbol{\eta})(\delta\hat{\rho}) = \mathrm{tr}\left\{\left(s'(\hat{\rho}) - Op_\hbar(\boldsymbol{\eta} \cdot \boldsymbol{\psi})\right)\delta\hat{\rho}\right\}$$

$\forall \delta\hat{\rho}$ perturbation in the class of the Hermitian Hilbert-Schmidt positive operators on $L^2(\mathbb{R}^d, \mathbb{C})$. This implies

$$s'(\hat{\rho}) = Op_\hbar(\boldsymbol{\eta} \cdot \boldsymbol{\psi}).$$

□

Since the function $s(x)$ is concave, $s'(x)$ is invertible. Explicitly we have

$$(s')^{-1}(z) = \frac{1}{e^{z/k_B} + 1}$$

and the operator solving the first order optimality condition reads

$$\hat{\rho}^* = (s')^{-1}(Op_\hbar(\boldsymbol{\eta} \cdot \boldsymbol{\psi})) = \frac{1}{e^{Op_\hbar(\boldsymbol{\eta} \cdot \boldsymbol{\psi})} + 1}. \tag{7.36}$$

Moreover, such an operator is a point of maximum for the Lagrangian. □

Now, to complete the program we have to determine, among the smooth functions, the Lagrange multipliers $\boldsymbol{\eta}$ by solving the constraint

$$\mathrm{tr}\left\{\hat{\rho} Op_\hbar(\boldsymbol{\eta} \cdot (1, \epsilon(\mathbf{p}), \mathbf{v})\right\} - \int_{\mathbb{R}^d} \boldsymbol{\eta} \cdot \mathbf{M}(\mathbf{x}, t)\, d\mathbf{x} = 0. \tag{7.37}$$

If such an equation admits a solution $\boldsymbol{\eta}^*$, the MEP density operator reads

$$\hat{\rho}^{MEP} = \frac{1}{\exp\left[Op_\hbar\left(\eta_0^*(\mathbf{x}, t) + \eta_1^*(\mathbf{x}, t)\epsilon(\mathbf{p}) + \boldsymbol{\eta}_2^*(\mathbf{x}, t) \cdot \mathbf{v}\right)\right] + 1}, \tag{7.38}$$

where we have rescaled the Lagrange multipliers by the factor $1/k_B$.

To determine conditions under which the equation (7.37) admits solutions is a very difficult task. Even in the semiclassical case there are examples of sets of moments that cannot be moments of a MEP distribution.

We will look for the solution up to first order in $\hbar^2$. Once the MEP density function has been determined, the MEP Wigner function is given by

$$w^{MEP}(\mathbf{x}, \mathbf{p}, t) = Op_\hbar^{-1}(\hat{\rho}^{MEP})$$

which can be used to get the necessary closure relations by evaluating the additional fields with w replaced by w^{MEP}.

We remark that the constraints (7.37) can be more conveniently expressed as

$$y\int_{\mathbb{R}^{2d}}\boldsymbol{\eta}\cdot\boldsymbol{\psi}(\mathbf{x},t)w^{MEP}(\mathbf{x},\mathbf{p},t)\,d\mathbf{p}\,d\mathbf{x}-\int_{\mathbb{R}^{d}}\boldsymbol{\eta}\cdot\mathbf{M}(\mathbf{x},t)\,d\mathbf{x}=0$$

but we require, in analogy with the semiclassical case, the stronger conditions

$$y\int_{\mathbb{R}^{d}}\boldsymbol{\psi}(\mathbf{x},t)w^{MEP}(\mathbf{x},\mathbf{p},t)\,d\mathbf{p}=\mathbf{M}(\mathbf{x},t),$$

where the Lagrange multipliers enter through $w^{MEP}(\mathbf{x},\mathbf{p},t)$.

7.3.1 Determination of the Lagrange Multipliers

We look formally for a solution in powers of $\hbar$

$$w^{MEP}=w_0^{MEP}+\hbar w_1^{MEP}+\hbar^2 w_2^{MEP}+... \tag{7.39}$$

firstly without taking into account the dependence of the Lagrange multipliers on $\hbar$.

Of course, on account of the properties of the Weyl quantization, w_0^{MEP} is equal to the semiclassical counterpart

$$w_0^{MEP}=\frac{1}{1+\exp(\xi)} \tag{7.40}$$

with

$$\xi=\eta_0(\mathbf{x},t)+\eta_1(\mathbf{x},t)\epsilon(\mathbf{p})+\boldsymbol{\eta}_2(\mathbf{x},t)\cdot\mathbf{v}$$

where the Lagrange multipliers have been rescaled by the factor $1/k_B$.

On account of the properties of Moyal product [29], $w_1^{MEP}=0$ and

$$w_2^{MEP}(\xi)=\frac{e^{\xi}}{8(e^{\xi}+1)^3}\left[(1-e^{\xi})\left(\frac{\partial^2\xi}{\partial x_i\partial x_j}\frac{\partial^2\xi}{\partial p_i\partial p_j}-\frac{\partial^2\xi}{\partial x_i\partial p_j}\frac{\partial^2\xi}{\partial x_j\partial p_i}\right)\right.$$
$$\left.+\left(\frac{\partial^2\xi}{\partial x_i\partial x_j}\frac{\partial\xi}{\partial p_i}\frac{\partial\xi}{\partial p_j}-2\frac{\partial^2\xi}{\partial x_i\partial p_j}\frac{\partial\xi}{\partial p_i}\frac{\partial\xi}{\partial x_j}+\frac{\partial^2\xi}{\partial p_i\partial p_j}\frac{\partial\xi}{\partial x_i}\frac{\partial\xi}{\partial x_j}\right)\frac{(e^{2\xi}-4e^{\xi}+1)}{3(e^{\xi}+1)}\right]. \tag{7.41}$$

Consistently, if we also expand the Lagrange multipliers as

$$\boldsymbol{\eta}=\boldsymbol{\eta}^{(0)}+\hbar^2\boldsymbol{\eta}^{(2)}+o(\hbar^2), \tag{7.42}$$

one has

$$w_2^{MEP}(\xi^{(0)},\xi^{(2)})\simeq-\frac{e^{\xi^{(0)}}}{(e^{\xi^{(0)}}+1)^2}\xi^{(2)}+\frac{e^{\xi^{(0)}}}{8(e^{\xi^{(0)}}+1)^3}\left[(1-e^{\xi^{(0)}})\left(\frac{\partial^2\xi^{(0)}}{\partial x_i\partial x_j}\frac{\partial^2\xi^{(0)}}{\partial p_i\partial p_j}-\frac{\partial^2\xi^{(0)}}{\partial x_i\partial p_j}\frac{\partial^2\xi^{(0)}}{\partial x_j\partial p_i}\right)\right.$$
$$\left.+\left(\frac{\partial^2\xi^{(0)}}{\partial x_i\partial x_j}\frac{\partial\xi^{(0)}}{\partial p_i}\frac{\partial\xi^{(0)}}{\partial p_j}-2\frac{\partial^2\xi^{(0)}}{\partial x_i\partial p_j}\frac{\partial\xi^{(0)}}{\partial p_i}\frac{\partial\xi^{(0)}}{\partial x_j}+\frac{\partial^2\xi^{(0)}}{\partial p_i\partial p_j}\frac{\partial\xi^{(0)}}{\partial x_i}\frac{\partial\xi^{(0)}}{\partial x_j}\right)\frac{(e^{2\xi^{(0)}}-4e^{\xi^{(0)}}+1)}{3(e^{\xi^{(0)}}+1)}\right], \tag{7.43}$$

where

$$\xi^{(0)} = \eta_0^{(0)}(\mathbf{x},t) + \eta_1^{(0)}(\mathbf{x},t)\epsilon(\mathbf{p}) + \boldsymbol{\eta}_2{}^{(0)}(\mathbf{x},t)\cdot\mathbf{v}, \tag{7.44}$$

$$\xi^{(2)} = \eta_0^{(2)}(\mathbf{x},t) + \eta_1^{(2)}(\mathbf{x},t)\epsilon(\mathbf{p}) + \boldsymbol{\eta}_2{}^{(2)}(\mathbf{x},t)\cdot\mathbf{v}. \tag{7.45}$$

Let us suppose now a small anisotropy in the distribution by assuming that $\boldsymbol{\eta}_2$ is a quantity of order δ with $|\delta| \ll 1$. This can be also justified by observing that at equilibrium $\boldsymbol{\eta}_2 \approx \mathbf{0}$. Therefore we formally write

$$\begin{aligned}\xi^{(0)} &= \eta_0^{(0)}(\mathbf{x},t) + \eta_1^{(0)}(\mathbf{x},t)\epsilon(\mathbf{p}) + \delta\boldsymbol{\eta}_2^{(0)}(\mathbf{x},t)\cdot\mathbf{v} := \xi_0^{(0)} + \delta\boldsymbol{\eta}_2^{(0)}(\mathbf{x},t)\cdot\mathbf{v},\\ \xi^{(2)} &= \eta_0^{(2)}(\mathbf{x},t) + \eta_1^{(2)}(\mathbf{x},t)\epsilon(\mathbf{p}) + \delta\boldsymbol{\eta}_2^{(2)}(\mathbf{x},t)\cdot\mathbf{v} := \xi_0^{(2)} + \delta\boldsymbol{\eta}_2^{(2)}(\mathbf{x},t)\cdot\mathbf{v}.\end{aligned} \tag{7.46}$$

Expanding also with respect to δ, we get

$$w_0^{MEP} = \frac{1}{e^{\xi_0^{(0)}+\delta\boldsymbol{\eta}_2^{(0)}\cdot\mathbf{v}}+1} \simeq \frac{1}{e^{\xi_0^{(0)}}+1} - \frac{e^{\xi_0^{(0)}}}{(e^{\xi_0^{(0)}}+1)^2}\delta\boldsymbol{\eta}_2^{(0)}\cdot\mathbf{v} \simeq w_{0,0}^{MEP} + \delta w_{0,1}^{MEP}, \tag{7.47}$$

$$w_2^{MEP} = w_{2,0}^{MEP} + \delta w_{2,1}^{MEP}, \tag{7.48}$$

where

$$\begin{aligned}w_{2,0}^{MEP} = &-\frac{e^{\xi_0^{(0)}}}{(e^{\xi_0^{(0)}}+1)^2}\xi_0^{(2)} + \frac{e^{\xi_0^{(0)}}}{8(e^{\xi_0^{(0)}}+1)^3}\left[(1-e^{\xi_0^{(0)}})\left(\frac{\partial^2\xi_0^{(0)}}{\partial x_i\partial x_j}\frac{\partial^2\xi_0^{(0)}}{\partial p_i\partial p_j} - \frac{\partial^2\xi_0^{(0)}}{\partial x_i\partial p_j}\frac{\partial^2\xi_0^{(0)}}{\partial x_j\partial p_i}\right)\right.\\ &\left.+\left(\frac{\partial^2\xi_0^{(0)}}{\partial x_i\partial x_j}\frac{\partial\xi_0^{(0)}}{\partial p_i}\frac{\partial\xi_0^{(0)}}{\partial p_j} - 2\frac{\partial^2\xi_0^{(0)}}{\partial x_i\partial p_j}\frac{\partial\xi_0^{(0)}}{\partial p_i}\frac{\partial\xi_0^{(0)}}{\partial x_j} + \frac{\partial^2\xi_0^{(0)}}{\partial p_i\partial p_j}\frac{\partial\xi_0^{(0)}}{\partial x_i}\frac{\partial\xi_0^{(0)}}{\partial x_j}\right)\frac{e^{2\xi_0^{(0)}}-4e^{\xi_0^{(0)}}+1}{3(e^{\xi_0^{(0)}}+1)}\right],\end{aligned} \tag{7.49}$$

$$
\begin{aligned}
w_{2,1}^{MEP} &= -\frac{e^{\xi_0^{(0)}}}{(e^{\xi_0^{(0)}}+1)^2}\delta\boldsymbol{\eta}_2^{(2)}\cdot\mathbf{v}+\frac{e^{\xi_0^{(0)}}}{(e^{\xi_0^{(0)}}-1)^2}\xi_0^{(2)}\delta\boldsymbol{\eta}_2^{(0)}\cdot\mathbf{v}\\
+ &\quad \frac{e^{\xi_0^{(0)}}}{8(e^{\xi_0^{(0)}}+1)^3}\left\{\left(1-e^{\xi_0^{(0)}}\right)\left(\frac{\partial^2\xi_0^{(0)}}{\partial x_i\partial x_j}\delta\boldsymbol{\eta}_2^{(0)}\cdot\frac{\partial^2\mathbf{v}}{\partial p_i\partial p_j}+\frac{\partial^2\xi_0^{(0)}}{\partial p_i\partial p_j}\delta\frac{\partial^2\boldsymbol{\eta}_2^{(0)}}{\partial x_i\partial x_j}\cdot\mathbf{v}\right.\right.\\
- &\quad \frac{\partial^2\xi_0^{(0)}}{\partial x_j\partial p_i}\delta\frac{\partial\boldsymbol{\eta}_2^{(0)}}{\partial x_j}\cdot\frac{\partial\mathbf{v}}{\partial p_i}-\frac{\partial^2\xi_0^{(0)}}{\partial x_j\partial p_i}\delta\frac{\partial\boldsymbol{\eta}_2^{(0)}}{\partial x_i}\cdot\frac{\partial\mathbf{v}}{\partial p_j}\Bigg)-e^{\xi_0^{(0)}}\delta\boldsymbol{\eta}_2^{(0)}\cdot\mathbf{v}\left(\frac{\partial^2\xi_0^{(0)}}{\partial x_i\partial x_j}\frac{\partial^2\xi_0^{(0)}}{\partial p_i\partial p_j}\right.\\
- &\quad \left.\frac{\partial^2\xi_0^{(0)}}{\partial x_i\partial p_j}\frac{\partial^2\xi_0^{(0)}}{\partial x_j\partial p_i}\right)+\left[2\frac{\partial^2\xi_0^{(0)}}{\partial x_i\partial x_j}\frac{\partial\xi_0^{(0)}}{\partial p_i}\delta\boldsymbol{\eta}_2^{(0)}\cdot\frac{\partial\mathbf{v}}{\partial p_j}+\frac{\partial\xi_0^{(0)}}{\partial p_i}\frac{\partial\xi_0^{(0)}}{\partial p_j}\delta\frac{\partial^2\boldsymbol{\eta}_2^{(0)}}{\partial x_i\partial x_j}\cdot\mathbf{v}\right.\\
- &\quad 2\left(\frac{\partial^2\xi_0^{(0)}}{\partial x_i\partial p_j}\frac{\partial\xi_0^{(0)}}{\partial p_i}\delta\frac{\partial\boldsymbol{\eta}_2^{(0)}}{\partial x_j}\cdot\mathbf{v}+\frac{\partial^2\xi_0^{(0)}}{\partial x_i\partial p_j}\frac{\partial\xi_0^{(0)}}{\partial x_j}\delta\boldsymbol{\eta}_2^{(0)}\cdot\frac{\partial\mathbf{v}}{\partial p_i}+\frac{\partial\xi_0^{(0)}}{\partial p_i}\frac{\partial\xi_0^{(0)}}{\partial x_j}\delta\frac{\partial\boldsymbol{\eta}_2^{(0)}}{\partial x_i}\cdot\frac{\partial\mathbf{v}}{\partial p_j}\right)\\
+ &\quad \left.2\frac{\partial^2\xi_0^{(0)}}{\partial p_i\partial p_j}\frac{\partial\xi_0^{(0)}}{\partial x_i}\delta\frac{\partial\boldsymbol{\eta}_2^{(0)}}{\partial x_j}\cdot\mathbf{v}+\frac{\partial\xi_0^{(0)}}{\partial x_i}\frac{\partial\xi_0^{(0)}}{\partial x_j}\delta\boldsymbol{\eta}_2^{(0)}\cdot\frac{\partial\mathbf{v}}{\partial p_i\partial p_j}\right]\frac{e^{2\xi_0^{(0)}}-4e^{\xi_0^{(0)}}+1}{3(e^{\xi_0^{(0)}}+1)}\\
+ &\quad \frac{e^{\xi_0^{(0)}}(e^{2\xi_0^{(0)}}+2e^{\xi_0^{(0)}}-5)}{3(e^{\xi_0^{(0)}}+1)^2}\delta\boldsymbol{\eta}_2^{(0)}\cdot\mathbf{v}\left(\frac{\partial^2\xi_0^{(0)}}{\partial x_i\partial x_j}\frac{\partial\xi_0^{(0)}}{\partial p_i}\frac{\partial\xi_0^{(0)}}{\partial p_j}-2\frac{\partial^2\xi_0^{(0)}}{\partial x_i\partial p_j}\frac{\partial\xi_0^{(0)}}{\partial p_i}\frac{\partial\xi_0^{(0)}}{\partial x_j}\right.\\
+ &\quad \left.\left.\frac{\partial^2\xi_0^{(0)}}{\partial p_i\partial p_j}\frac{\partial\xi_0^{(0)}}{\partial x_i}\frac{\partial\xi_0^{(0)}}{\partial x_j}\right)\right\}\\
+ &\quad \frac{e^{\xi_0^{(0)}}(1-2e^{\xi_0^{(0)}})}{8(e^{\xi_0^{(0)}}+1)^4}\delta\boldsymbol{\eta}_2^{(0)}\cdot\mathbf{v}\left[(1-e^{\xi_0^{(0)}})\left(\frac{\partial^2\xi_0^{(0)}}{\partial x_i\partial x_j}\frac{\partial^2\xi_0^{(0)}}{\partial p_i\partial p_j}-\frac{\partial^2\xi_0^{(0)}}{\partial x_i\partial p_j}\frac{\partial^2\xi_0^{(0)}}{\partial x_j\partial p_i}\right)\right.\\
+ &\quad \left.\left(\frac{\partial^2\xi_0^{(0)}}{\partial x_i\partial x_j}\frac{\partial\xi_0^{(0)}}{\partial p_i}\frac{\partial\xi_0^{(0)}}{\partial p_j}-2\frac{\partial^2\xi_0^{(0)}}{\partial x_i\partial p_j}\frac{\partial\xi_0^{(0)}}{\partial p_i}\frac{\partial\xi_0^{(0)}}{\partial x_j}+\frac{\partial^2\xi_0^{(0)}}{\partial p_i\partial p_j}\frac{\partial\xi_0^{(0)}}{\partial x_i}\frac{\partial\xi_0^{(0)}}{\partial x_j}\right)\frac{e^{2\xi_0^{(0)}}-4e^{\xi_0^{(0)}}+1}{3(e^{\xi_0^{(0)}}+1)}\right]
\end{aligned}
$$

The constraints

$$
\begin{aligned}
n(\mathbf{x},t) &= y\int_{\mathbb{R}^d} w^{MEP}(\mathbf{x},\mathbf{p},t)d\mathbf{p},\\
W(\mathbf{x},t) &= y\int_{\mathbb{R}^d} \epsilon(\mathbf{p})w^{MEP}(\mathbf{x},\mathbf{p},t)d\mathbf{p},\\
\mathbf{J}(\mathbf{x},t) &= y\int_{\mathbb{R}^d} \mathbf{v}(\mathbf{p})\ w^{MEP}(\mathbf{x},\mathbf{p},t)d\mathbf{p}.
\end{aligned}
$$

can be split into two systems: one at zero order in $\hbar^2$

$$
n^{(0)}(\mathbf{x},t) = y\int_{\mathbb{R}^d} w_0^{MEP}(\xi_0^{(0)}(\mathbf{x},t),\mathbf{p})d\mathbf{p}, \tag{7.50}
$$

$$
W^{(0)}(\mathbf{x},t) = y\int_{\mathbb{R}^d} \epsilon(\mathbf{p})w_0^{MEP}(\xi_0^{(0)}(\mathbf{x},t),\mathbf{p})d\mathbf{p}, \tag{7.51}
$$

$$
\mathbf{J}^{(0)}(\mathbf{x},t) = y\int_{\mathbb{R}^d} \mathbf{v}(\mathbf{p})\ w_0^{MEP}(\xi_0^{(0)}(\mathbf{x},t),\mathbf{p})d\mathbf{p}, \tag{7.52}
$$

and one at first order in $\hbar^2$

$$n^{(2)} = y\int_{\mathbb{R}^d} w_2^{MEP}(\xi^{(0)}(\mathbf{x},t),\xi^{(2)}(\mathbf{x},t),\mathbf{p})\,d\mathbf{p}, \tag{7.53}$$

$$W^{(2)} = y\int_{\mathbb{R}^d} \epsilon(\mathbf{p}) w_2^{MEP}(\xi^{(0)}(\mathbf{x},t),\xi^{(2)}(\mathbf{x},t),\mathbf{p})\,d\mathbf{p}, \tag{7.54}$$

$$\mathbf{J}^{(2)} = y\int_{\mathbb{R}^d} \mathbf{v}\; w_2^{MEP}(\xi^{(0)}(\mathbf{x},t),\xi^{(2)}(\mathbf{x},t),\mathbf{p})\,d\mathbf{p}. \tag{7.55}$$

The system (7.50)-(7.52) is a set of nonlinear algebraic equations; the system (7.53)-(7.55) form a nonlinear system of PDEs for the Lagrange multipliers whose analytical solution seems very difficult to get. Indeed, the situation is even more cumbersome because in a numerical scheme the inversion of the constraints should be performed at each time step.

It is possible to prove the following properties (see for example [9])

Proposition 1 *At zero order in $\hbar^2$ the map $\boldsymbol{\eta} \to \mathbf{M}(\boldsymbol{\eta})$ defined by the system (7.50)-(7.52) is (at least locally) invertible.*

Proposition 2 *The equations (7.20)-(7.22) form a symmetric hyperbolic system of balance laws when the closure relation is that given by MEP.*

In order to have an analytical guess about the solution of the system (7.50)-(7.52) we adopt the same strategy used in [9, 27, 31] and expand the equations (7.50)-(7.52) up to first order in δ

$$n^{(0)} \simeq y\int_{\mathbb{R}^d} \frac{1}{e^{\xi_0^{(0)}}+1} d\mathbf{p}, \tag{7.56}$$

$$W^{(0)} \simeq y\int_{\mathbb{R}^d} \frac{\epsilon(\mathbf{p})}{e^{\xi_0^{(0)}}+1} d\mathbf{p}, \tag{7.57}$$

$$\mathbf{J}^{(0)} \simeq -y\int_{\mathbb{R}^d} \mathbf{v}\frac{e^{\xi_0^{(0)}}\boldsymbol{\eta}_2(\mathbf{x},t)\cdot\mathbf{v}}{\left(e^{\xi_0^{(0)}}+1\right)^2} d\mathbf{p} \tag{7.58}$$

Since we are requiring that for $\hbar = 0$ one recovers the semiclassical distribution, the approximation is valid provided

$$0 \le w_0^{MEP} \le 1 \iff 0 \le \frac{1}{e^{\xi_0^{(0)}}+1} - \frac{e^{\xi_0^{(0)}}\boldsymbol{\eta}_2(\mathbf{x},t)\cdot\mathbf{v}}{\left(e^{\xi_0^{(0)}}+1\right)^2} \le 1. \tag{7.59}$$

Now we can not apply directly proposition 1 because of the expansion.

However, the Jacobian matrix

$$\frac{\partial\left(n^{(0)},W^{(0)}\right)}{\partial\left(\eta_0^{(0)},\eta_1^{(0)}\right)}=\begin{pmatrix} -y\int_{\mathbb{R}^d}\frac{e^{\xi_0^{(0)}}}{\left(e^{\xi_0^{(0)}}+1\right)^2}d\mathbf{p} & -y\int_{\mathbb{R}^d}\frac{e^{\xi_0^{(0)}}\epsilon(\mathbf{p})}{\left(e^{\xi_0^{(0)}}+1\right)^2}d\mathbf{p} \\ -y\int_{\mathbb{R}^d}\frac{e^{\xi_0^{(0)}}\epsilon(\mathbf{p})}{\left(e^{\xi_0^{(0)}}+1\right)^2}d\mathbf{p} & -y\int_{\mathbb{R}^d}\frac{e^{\xi_0^{(0)}}\epsilon^2(\mathbf{p})}{\left(e^{\xi_0^{(0)}}+1\right)^2}d\mathbf{p} \end{pmatrix}$$

is negative defined and therefore, by taking into account that the third equation is linear in $\boldsymbol{\eta}_2^{(0)}$, we have what follows.

Proposition 3 *The constraints (7.56)-(7.58) are at least locally invertible.*

Once the equations (7.50)-(7.52) or the approximated equations (7.56)-(7.58) are solved, the equations (7.53)-(7.55) are a linear sytems for the second order correction in $\hbar$ to the Lagrange mltipliers.

In the next section we will investigate some specific examples.

7.4 Hydrodynamical model for charge transport in semiconductors

Let us consider a bulk (3d) semiconductor whose energy band in each valley can be approximated by the Kane dispersion relation

$$\epsilon(\mathbf{p})\left(1+\alpha\epsilon(\mathbf{p})\right)=\frac{p^2}{2m^*},\quad \mathbf{k}\in B,$$

where B is the first Brillouin zone, expanded to all $\mathbb{R}^3$, α is the non parabolicity parameter and m^* is the effective mass. The previous parameter depends on the specific material one are dealing with, e.g. silicon, GaAs, etc.. Sometimes the simple parabolic approximation ($\alpha=0$) is adopted.

The group velocity is given by

$$\mathbf{v}=\frac{1}{m^*\sqrt{1+\dfrac{2\alpha}{m^*}p^2}}\mathbf{p}.$$

Note that it is limited; indeed

$$|\mathbf{v}|\le v_\infty=\frac{1}{\sqrt{2m^*\alpha}}.$$

In the sequel we first study the first order terms and then the second order corrections in $\hbar^2$.

Proposition 4 *For the Kane dispersion relation a sufficient condition to satisfy (7.59) is*

$$|\boldsymbol{\eta}_2|\le\frac{\left(e^{\xi_0}+1\right)}{v_\infty e^{\xi_0^{(0)}}} \tag{7.60}$$

Proof. First we observe that

$$\frac{1}{e^{\xi_0^{(0)}}+1}-\frac{e^{\xi_0^{(0)}}\boldsymbol{\eta}_2(\mathbf{x},t)\cdot\mathbf{v}}{\left(e^{\xi_0^{(0)}}+1\right)^2}\geq 0 \iff \boldsymbol{\eta}_2(\mathbf{x},t)\cdot\mathbf{v}\leq\frac{e^{\xi_0^{(0)}}+1}{e^{\xi_0^{(0)}}},$$

which is satisfied if (7.60) is true.

On the other hand

$$\frac{1}{e^{\xi_0^{(0)}}+1}-\frac{e^{\xi_0^{(0)}}\boldsymbol{\eta}_2(\mathbf{x},t)\cdot\mathbf{v}}{\left(e^{\xi_0^{(0)}}+1\right)^2}\leq 1 \iff -\boldsymbol{\eta}_2(\mathbf{x},t)\cdot\mathbf{v}\leq e^{\xi_0^{(0)}}+1,$$

which surely holds if

$$|\boldsymbol{\eta}_2|\leq\frac{e^{\xi_0^{(0)}}+1}{v_\infty}. \tag{7.61}$$

Since $\dfrac{\left(e^{\xi_0^{(0)}}+1\right)}{v_\infty e^{\xi_0^{(0)}}}\leq\dfrac{e^{\xi_0^{(0)}}+1}{v_\infty}$, the proposition is proved. □

By taking into account the density of state for the Kane dispersion relation, one has

$$d\mathbf{p}=p^2dp\sin\theta\,d\theta\,d\phi=(m^*)^{3/2}(1+2\alpha\epsilon)\sqrt{2\epsilon(1+\alpha\epsilon)}d\epsilon\sin\theta\,d\theta\,d\phi,\quad \epsilon\in[0,+\infty[,\theta\in[0,\pi],\phi\in[0,2\pi].$$

By using the relation

$$\int_{S_2}\mathbf{n}\otimes\mathbf{n}\,d\,S_2=\frac{4\pi}{3}\mathbf{I}$$

where S_2 is the unit sphere of $\mathbb{R}^3$ and $\mathbf{I}$ the identity tensor, and by taking into account that

$$\int_{S_2}\underbrace{\mathbf{n}\otimes\mathbf{n}\cdots\otimes\mathbf{n}}_{k\quad\text{times}}\,d\,S_2=\mathbf{0}\quad\text{if}\quad k\quad\text{odd},$$

the constraints read

$$n^{(0)} = 4\pi y\int_0^{+\infty}(m^*)^{3/2}\frac{1+2\alpha\epsilon}{\exp\left(\eta_0^{(0)}+\eta_1^{(0)}\epsilon\right)+1}\sqrt{2\epsilon(1+\alpha\epsilon)}d\epsilon, \tag{7.62}$$

$$W^{(0)} = 4\pi y\int_0^{+\infty}(m^*)^{3/2}\frac{\epsilon(1+2\alpha\epsilon)}{\exp\left(\eta_0^{(0)}+\eta_1^{(0)}\epsilon\right)+1}\sqrt{2\epsilon(1+\alpha\epsilon)}d\epsilon, \tag{7.63}$$

$$\mathbf{J}^{(0)} = -\frac{8\pi}{3}y\int_0^{+\infty}\frac{\exp\left(\eta_0^{(0)}+\eta_1^{(0)}\epsilon\right)}{\left[\exp\left(\eta_0^{(0)}+\eta_1^{(0)}\epsilon\right)+1\right]^2}\frac{\epsilon(1+\alpha\epsilon)(1+2\alpha\epsilon)}{1+4\alpha\epsilon(1+\alpha\epsilon)}\sqrt{2m^*\epsilon(1+\alpha\epsilon)}d\epsilon\,\boldsymbol{\eta}_2^{(0)} \tag{7.64}$$

The first two equations are a nonlinear system for the Lagrange multipliers η_0 and η_1 while the third equation gives $\boldsymbol{\eta}_2$ which results proportional to $\mathbf{J}^{(0)}$.

Thanks to proposition 3 equations (7.62), (7.63) are locally invertible.

Once we have obtained the Lagrange multipliers (likely with a numerical procedure), we can evaluate the additional tensorial quantities appearing in eqs.

(7.20)-(7.22). Regarding the energy-flux, the pressure tensor and the tensor gradient of the velocity, one has

$$\mathbf{S}^{(0)} = y\int_{\mathbb{R}^3}\epsilon(\mathbf{p})\mathbf{v}(\mathbf{p})\,w_0^{MEP}(\mathbf{x},\mathbf{p},t)d\mathbf{p} =$$
$$-\frac{8\pi}{3}y\int_0^{+\infty}\frac{\exp\left(\eta_0^{(0)}+\eta_1^{(0)}\epsilon\right)}{\left[\exp\left(\eta_0^{(0)}+\eta_1^{(0)}\epsilon\right)+1\right]^2}\frac{\epsilon^2(1+\alpha\epsilon)(1+2\alpha\epsilon)}{1+4\alpha\epsilon(1+\alpha\epsilon)}\sqrt{2m^*\epsilon(1+\alpha\epsilon)}d\epsilon\,\boldsymbol{\eta}_2^{(0)}. \quad (7.65)$$

$$\int_{\mathbb{R}^3}\mathbf{v}\otimes\mathbf{v}\,w_0^{MEP}(\mathbf{x},\mathbf{p},t)d\mathbf{p} = \frac{8\pi}{3}y\int_0^{+\infty}\frac{\epsilon(1+\alpha\epsilon)(1+2\alpha\epsilon)}{1+4\alpha\epsilon(1+\alpha\epsilon)}\frac{\sqrt{2m^*\epsilon(1+\alpha\epsilon)}}{\exp\left(\eta_0^{(0)}+\eta_1^{(0)}\epsilon\right)+1}d\epsilon\,\mathbf{I} \quad (7.66)$$

$$\int_{\mathbb{R}^3}w_0^{MEP}(\mathbf{x},\mathbf{p},t)\nabla_{\mathbf{p}}\mathbf{v}d\mathbf{p} =$$
$$4\pi\sqrt{m^*}y\int_0^{+\infty}\frac{(1+2\alpha\epsilon)\sqrt{2\epsilon(1+\alpha\epsilon)}}{(\exp\left(\eta_0^{(0)}+\eta_1^{(0)}\epsilon\right)+1)\sqrt{1+4\alpha\epsilon(1+\alpha\epsilon)}}\left[1-\frac{4\alpha\epsilon(1+\alpha\epsilon)}{3(1+4\alpha\epsilon(1+\alpha\epsilon))}\right]d\epsilon\,\mathbf{I} \quad (7.67)$$

In the parabolic band approximation the constraints can be written in terms of the Fermi integrals of order k

$$\mathcal{F}_k(\eta) = \frac{1}{\Gamma(k+1)}\int_0^{+\infty}\frac{\chi^k}{1+e^{\chi-\eta}}\,d\,\chi,$$

with $\Gamma(x)$ Euler gamma function, as

$$n^{(0)} = 4\pi y\int_0^{+\infty}(m^*)^{3/2}\frac{\sqrt{2\epsilon}}{\exp\left(\eta_0^{(0)}+\eta_1^{(0)}\epsilon\right)+1}d\epsilon = \frac{y^*}{2\left(\eta_1^{(0)}\right)^{3/2}}F_{1/2}(-\eta_0^{(0)}/\eta_1^{(0)}), \quad (7.68)$$

$$W^{(0)} = 4\pi y\int_0^{+\infty}(m^*)^{3/2}\frac{\epsilon\sqrt{2\epsilon}}{\exp\left(\eta_0^{(0)}+\eta_1^{(0)}\epsilon\right)+1}d\epsilon = \frac{3y^*\sqrt{\pi}}{4\left(\eta_1^{(0)}\right)^{5/2}}F_{3/2}(-\eta_0^{(0)}/\eta_1^{(0)}), \quad (7.69)$$

$$\mathbf{J}^{(0)} = -\frac{8\pi}{3}y\int_0^{+\infty}\frac{\exp\left(\eta_0^{(0)}+\eta_1^{(0)}\epsilon\right)}{\left[\exp\left(\eta_0^{(0)}+\eta_1^{(0)}\epsilon\right)+1\right]^2}\epsilon\sqrt{2m^*\epsilon}d\epsilon\,\boldsymbol{\eta}_2^{(0)}. \quad (7.70)$$

where $y^* = 4\pi y(m^*)^{3/2}\sqrt{2}$.

Once the Lagrange multipliers have been determined at the zero order in $\hbar$, the constraints (7.53)-(7.55) are a linear system for $\boldsymbol{\eta}^{(2)}$. In fact we can write

$$w_2^{MEP} = -\frac{e^{\xi_0^{(0)}}}{(e^{\xi_0^{(0)}}+1)^2}\left(\xi_0^{(2)}+\boldsymbol{\eta}_2^{(2)}\cdot\mathbf{v}\right)+\frac{e^{\xi_0^{(0)}}}{(e^{\xi_0^{(0)}}-1)^2}\xi_0^{(2)}\delta\boldsymbol{\eta}_2^{(0)}\cdot\mathbf{v}+\Psi(\boldsymbol{\eta}^{(0)},\nabla\boldsymbol{\eta}^{(0)}).$$

for a suitable scalar function Ψ. Note that also the derivatives of $\boldsymbol{\eta}^{(0)}$ enter the system. So, at variance with the semiclassical case, the constraints are nonlocal even by expanding in power of $\hbar$.

The equations (7.53)-(7.55) give

$$y\int_{\mathbb{R}^3}\frac{e^{\xi_0^{(0)}}}{(e^{\xi_0^{(0)}}+1)^2}\left(\eta_0^{(2)}+\eta_1^{(2)}\epsilon(\mathbf{p})\right)d\mathbf{p}=-n^{(2)}+y\int_{\mathbb{R}^3}\Psi(\boldsymbol{\eta}^{(0)},\nabla\boldsymbol{\eta}^{(0)})d\mathbf{p}, \tag{7.71}$$

$$y\int_{\mathbb{R}^3}\epsilon(\mathbf{p})\frac{e^{\xi_0^{(0)}}}{(e^{\xi_0^{(0)}}+1)^2}\left(\eta_0^{(2)}+\eta_1^{(2)}\epsilon(\mathbf{p})\right)d\mathbf{p}=-W^{(2)}+y\int_{\mathbb{R}^3}\epsilon(\mathbf{p})\Psi(\boldsymbol{\eta}^{(0)},\nabla\boldsymbol{\eta}^{(0)})d\mathbf{p}, \tag{7.72}$$

$$\left(y\int_{\mathbb{R}^3}\frac{e^{\xi_0^{(0)}}}{(e^{\xi_0^{(0)}}+1)^2}\mathbf{v}\otimes\mathbf{v}\;d\mathbf{p}\right)\;\boldsymbol{\eta}_2^{(2)}=-\mathbf{J}^{(2)}+y\int_{\mathbb{R}^3}\mathbf{v}\;\Psi(\boldsymbol{\eta}^{(0)},\nabla\boldsymbol{\eta}^{(0)})d\mathbf{p}. \tag{7.73}$$

Proposition 5 *The constraints relations (7.71)-(7.72) are invertible.*

Proof. In fact, the matrix of the coefficients of the subsystem for $\eta_0^{(2)}$ and $\eta_1^{(2)}$ is the same of that appearing in Proposition 3 and therefore invertible. Moreover the tensor

$$\int_{\mathbb{R}^3}\frac{e^{\xi_0^{(0)}}}{(e^{\xi_0^{(0)}}+1)^2}\mathbf{v}\otimes\mathbf{v}\;d\mathbf{p}$$

is positive defined. □

Regarding the collisions, we require the conservation of charge in the unipolar case[3]. The general form of the scattering terms is rather cumbersome and very difficult to tackle. So, some simplification is adopted also in direct numerical integrations of the Wigner-Boltzmann equation. An approach is to consider the collisions as semiclassical, that is the correction in $\hbar^2$ is neglected (an analysis about the validity of such an approximation can be found in [3]).

The main scattering mechanism in semiconductors is that between electrons and phonons. If the latter are considered as a thermal bath, and therefore obeying a Bose-Einstein statistics with lattice temperature T_L, the corresponding scattering has the expression

$$C(w)\simeq\frac{1}{(2\pi)^3}\int_{\mathbb{R}^3}\left[P(\tilde{\mathbf{p}},\mathbf{p})w_0^{MEP}(\tilde{\mathbf{p}})\left(1-w_0^{MEP}(\mathbf{p})\right)-P(\mathbf{p},\tilde{\mathbf{p}})w_0^{MEP}(\mathbf{p})\left(1-w_0^{MEP}(\tilde{\mathbf{p}})\right)\right]\;d\tilde{\mathbf{p}} \tag{7.74}$$

where $P(\tilde{\mathbf{p}},\mathbf{p})$ is the transition probability per unit time to change the state of momentum $\tilde{\mathbf{p}}$ into that of momentum $\mathbf{p}$. The terms $\left(1-w_0^{MEP}(\mathbf{p})\right)$ and $\left(1-w_0^{MEP}(\tilde{\mathbf{p}})\right)$ account for the Pauli exclusion principle. Note that w_0^{MEP} is the semiclassical distribution, so the collision term is well defined.

The general expression of the transition rate reads

$$P(\tilde{\mathbf{p}},\mathbf{p})=\mathcal{G}(\tilde{\mathbf{p}},\mathbf{p})\left[(N_B+1)\,\delta\left(\epsilon(\mathbf{p})-\epsilon(\tilde{\mathbf{p}})+\hbar\omega\right)+N_B\delta\left(\epsilon(\mathbf{p})-\epsilon(\tilde{\mathbf{p}})-\hbar\omega\right)\right]$$

where $\mathcal{G}(\tilde{\mathbf{p}},\mathbf{p})$ is the so-called overlap factor, which enjoys the symmetry property $\mathcal{G}(\tilde{\mathbf{p}},\mathbf{p})=\mathcal{G}(\mathbf{p},\tilde{\mathbf{p}})$, and N_B is the Bose-Einstein distribution

$$N_B=\frac{1}{\exp(\hbar\omega/k_BT_L)-1},$$

[3]in the bipolar case the presence of generation and recombination terms should be included.

k_B being the Boltzmann constant and δ the Dirac distribution. The first term represents an emission process of a quantum of energy $\hbar\omega$, the second one represents an absorption process of a quantum of energy $\hbar\omega$.

In the specific case of silicon, one has $\mathcal{G}(\tilde{\mathbf{p}}, \mathbf{p}) = \Lambda = \text{constant}$[4] and one gets the following expressions for the moments of the optical collision term C_{op} in the Einstein approximation ($\hbar\omega = \text{constant}$)

$$
\begin{aligned}
&C_n = 0,\\
&C_W = \frac{4y\Lambda\hbar\omega m^{*3} N_B}{\pi}\int_0^{+\infty}\left[f_i(\epsilon,\epsilon+\hbar\omega) - f_i(\epsilon+\hbar\omega,\epsilon)e^{\hbar\omega/k_BT}\right](1+2\alpha\epsilon)(1+2\alpha(\epsilon+\hbar\omega))\\
&\sqrt{\epsilon(\epsilon+\hbar\omega)(1+\alpha\epsilon)(1+\alpha(\epsilon+\hbar\omega))}\,d\epsilon,\\
&C_{\mathbf{V}} = \frac{y\Lambda m^{*3} N_B}{3\pi^2}\int_0^{+\infty}(1+2\alpha\epsilon)(1+2\alpha(\epsilon+\hbar\omega))\sqrt{\epsilon(\epsilon+\hbar\omega)(1+\alpha\epsilon)(1+\alpha(\epsilon+\hbar\omega))}\\
&\left[(E(\epsilon+\hbar\omega)F_1(\epsilon,\epsilon+\hbar\omega) - E(\epsilon)F_2(\epsilon,\epsilon+\hbar\omega)) + e^{\hbar\omega/k_BT}\left(E(\epsilon)F_1(\epsilon+\hbar\omega,\epsilon) - E(\epsilon+\hbar\omega)F_2(\epsilon+\hbar\omega,\epsilon)\right)\right]\\
&\delta\boldsymbol{\eta}_2^{(0)},
\end{aligned}
$$

with

$$
\begin{aligned}
f_i(\tilde{\epsilon},\epsilon) &= \frac{1}{e^{\eta_0^{(0)}+\eta_1^{(0)}\tilde{\epsilon}}+1}\,\frac{e^{\eta_0^{(0)}+\eta_1^{(0)}\epsilon}}{e^{\eta_0^{(0)}+\eta_1^{(0)}\epsilon}+1},\\
F_1(\tilde{\epsilon},\epsilon) &= \frac{e^{\eta_0^{(0)}+\eta_1^{(0)}\epsilon}}{(e^{\eta_0^{(0)}+\eta_1^{(0)}\tilde{\epsilon}}+1)(e^{\eta_0^{(0)}+\eta_1^{(0)}\epsilon}+1)^2},\\
F_2(\tilde{\epsilon},\epsilon) &= \frac{e^{\eta_0^{(0)}+\eta_1^{(0)}\tilde{\epsilon}}}{e^{\eta_0^{(0)}+\eta_1^{(0)}\tilde{\epsilon}}+1}\left(\frac{1}{(e^{\eta_0^{(0)}+\eta_1^{(0)}\epsilon}+1)^2} - \frac{1}{e^{\eta_0^{(0)}+\eta_1^{(0)}\tilde{\epsilon}}}\right),\\
E(\epsilon) &= \sqrt{\frac{2\epsilon(1+\alpha\epsilon)}{m[1+4\alpha\epsilon(1+\alpha\epsilon)]}}
\end{aligned}
$$

In the limit $\hbar\omega \to 0$, one recovers the contribution to the production terms in the elastic approximation, often used for the acoustic phonons.

Remark 1 *We remark that the use of MEP adopted here differs from the way it has been used in [25, 26, 28]. Indeed, in the quoted references the collision terms of the Wigner equations are written in a relaxation time form with a local equilibrium distribution which is estimated by MEP. This along with a Chapmann-Ensgok expansion allows to get macroscopic models like drift-diffusion, energy-transport or hydrodynamical ones. Here, we fix a set of fundamental variables and apply MEP to express the Wigner function in terms of the Lagrange multipliers. The resulting estimation is used to get closure relations both for the additional fluxes and production terms, without assuming for the latter a relaxation time form.*

[4]More in detail for the optical phonon scattering $\Lambda = Z_{if}\dfrac{\pi(D_TK)^2}{\rho\omega}$, where Z_{if} is the degeneracy of the final valley, ρ is the density of the material, D_TK the optical coupling constant, ω the phonon angular frequency.

7.5 Hydrodynamical model for charge transport in graphene

Now we apply the theory developed above to devise a hydrodynamical model for charge transport in graphene which is a 2D semimetal.

Let us assume the following dispersion relation

$$\varepsilon(\mathbf{p}) = v_F \tilde{p} \tag{7.75}$$

where $\tilde{p} = \sqrt{|\mathbf{p}|^2 + c^2}$ with $\mathbf{p} \in \mathbb{R}^2$, c being a positive constant that represents a possible half gap between the valence and the conduction band. Usually the gapless dispersion relation ($c = 0$) is considered but apparently a (even if small) gap could be present from the general point of view [42].

The group velocity reads

$$\mathbf{v} = \nabla_{\mathbf{p}} \varepsilon(\mathbf{p}) = \frac{v_F}{\tilde{p}} \mathbf{p}. \tag{7.76}$$

The Proposition 4 is still valid with v_F instead of v_∞.

Assuming also in this case small anisotropy, we get the same expansions as for bulk (3d) semiconductors. The closure relations for the energy-flux, pressure tensor and tensor gradient of the velocity at the zeroth order $\hbar^2$ in are given by

$$\begin{aligned}
&\mathbf{S}^{(0)} = -y\pi \int_{v_F c}^{+\infty} \frac{e^{\xi^{(0)}}}{(e^{\xi^{(0)}}+1)^2} (\epsilon^2 - v_F^2 c^2) d\epsilon \, \delta \boldsymbol{\eta}_0^{(0)}, \\
&\int_{\mathbb{R}^2} \mathbf{v} \otimes \mathbf{v} w_0^{MEP}(\mathbf{x}, \mathbf{p}, t) = \pi \int_{v_F c}^{+\infty} \frac{\epsilon^2 - v_F^2 c^2}{\epsilon^2} \frac{1}{e^{\xi^{(0)}}+1} \, d\epsilon \, \mathbf{I}, \\
&\int_{\mathbb{R}^2} w_0^{MEP}(\mathbf{x}, \mathbf{p}, t) \nabla_{\mathbf{p}} \mathbf{v} = \pi \int_{v_F}^{+\infty} \left(2 - \frac{\epsilon^2 - v_F^2 c^2}{\epsilon^2}\right) \frac{1}{e^{\xi^{(0)}}+1} d\epsilon \, \mathbf{I}.
\end{aligned}$$

The second order corrections can be obtained with the same procedure for bulk semiconductors as well.

Regarding the production terms, the main scattering mechanisms in graphene are those of electrons with acoustic, optical and K phonons (see [**?**]). By using the MEP estimation of the Wigner function one can evaluate the closure relations for the production terms.

For the acoustic phonons one finds

$$\begin{aligned}
&C_n^{(ac)} = 0, \\
&C_W^{(ac)} = 0, \\
&C_{\mathbf{V}}^{(ac)} = -\frac{y A^{(ac)}}{4\pi v_F^2} \int_{v_F c}^{+\infty} \epsilon \sqrt{\frac{\epsilon^2}{v_F^2} - c^2} \frac{e^{\eta_0^{(0)} + \eta_1^{(0)} \epsilon}}{(e^{\eta_0^{(0)} + \eta_1^{(0)} \epsilon} + 1)^2} d\epsilon \boldsymbol{\eta}_2^{(0)},
\end{aligned}$$

with $A^{(ac)} = \frac{2\pi D_{ac}^2 k_B T}{\sigma \hbar v_{ac}^2}$ where D_{ac}^2 is the acoustic phonon coupling constant, v_{ac} is the sound speed in graphene, σ is the graphene areal density and T_L is the graphene lattice temperature.

For the optical phonons we have

$$
\begin{aligned}
&C_n^{(opt)} = 0,\\
&C_W^{(opt)} = \frac{2yD_\Gamma^2}{\sigma\omega v_F^4} N_B \hbar\omega \int_{v_F C}^{+\infty} \epsilon(\epsilon+\hbar\omega)\left[f_i(\epsilon,\epsilon+\hbar\omega) - e^{\frac{\hbar\omega}{k_B T}} f_i(\epsilon+\hbar\omega,\omega)\right] d\epsilon,\\
&C_{\mathbf{V}}^{(opt)} = \frac{yD_\Gamma^2 N_B}{4\sigma\omega\pi v_F^2}\\
&\left\{\int_{v_F C}^{+\infty} e^{\frac{\hbar\omega}{k_B T}} \left[F_1(\epsilon+\hbar\omega,\epsilon)G(\epsilon+\hbar\omega,\epsilon) - F_2(\epsilon+\hbar\omega,\epsilon)G(\epsilon,\epsilon+\hbar\omega)\right] d\epsilon\right.\\
&\left.+\int_{v_F C}^{+\infty} \left[F_1(\epsilon,\epsilon+\hbar\omega)G(\epsilon,\epsilon+\hbar\omega) - F_2(\epsilon,\epsilon+\hbar\omega)G(\epsilon+\hbar\omega,\epsilon)\right] d\epsilon\right\} \delta\boldsymbol{\eta}_2^{(0)},
\end{aligned}
$$

with

$$
\begin{aligned}
f_i(\tilde{\epsilon},\epsilon) &= \frac{1}{e^{\eta_0^{(0)}+\eta_1^{(0)}\tilde{\epsilon}}+1} \frac{e^{\eta_0^{(0)}+\eta_1^{(0)}\epsilon}}{e^{\eta_0^{(0)}+\eta_1^{(0)}\epsilon}+1},\\
F_1(\tilde{\epsilon},\epsilon) &= \frac{e^{\eta_0^{(0)}+\eta_1^{(0)}\epsilon}}{(e^{\eta_0^{(0)}+\eta_1^{(0)}\tilde{\epsilon}}+1)(e^{\eta_0^{(0)}+\eta_1^{(0)}\epsilon}+1)^2},\\
F_2(\tilde{\epsilon},\epsilon) &= \frac{e^{\eta_0^{(0)}+\eta_1^{(0)}\tilde{\epsilon}}}{e^{\eta_0^{(0)}+\eta_1^{(0)}\tilde{\epsilon}}+1}\left(\frac{1}{(e^{\eta_0^{(0)}+\eta_1^{(0)}\epsilon}+1)^2} - \frac{1}{e^{\eta_0^{(0)}+\eta_1^{(0)}\tilde{\epsilon}}}\right),\\
G(\tilde{\epsilon},\epsilon) &= \frac{\tilde{\epsilon}}{\epsilon}(\epsilon^2 - v_F^2 C^2),
\end{aligned}
$$

where D_Γ^2 is the optical phonon coupling constant, N_B is the Bose-Einstein distribution

$$N_B = \frac{1}{e^{\hbar\omega/k_B T_L}-1}$$

with $\hbar\omega$ the phonon energy (here assumed the same for LO and TO branches).

At last, the production terms given due to the optical K-phonons reads

$$
\begin{aligned}
&C_n^{(K)} = 0,\\
&C_W^{(K)} = \frac{yD_K^2}{2\sigma\omega v_F^4} N_B \hbar\omega \int_{v_F C}^{+\infty} \epsilon(\epsilon+\hbar\omega)\left[f_i(\epsilon,\epsilon+\hbar\omega) - e^{\frac{\hbar\omega}{k_B T}} f_i(\epsilon+\hbar\omega,\omega)\right] d\epsilon,\\
&C_{\mathbf{V}}^{(K)} = \frac{yD_K^2 N_B}{4\sigma\omega\pi v_F^2}\\
&\left\{\int_{v_F C}^{+\infty} e^{\frac{\hbar\omega}{k_B T}} \left[F_1(\epsilon+\hbar\omega,\epsilon)G(\epsilon+\hbar\omega,\epsilon) - F_2(\epsilon+\hbar\omega,\epsilon)G(\epsilon,\epsilon+\hbar\omega)\right] d\epsilon\right.\\
&\left.+\int_{v_F C}^{+\infty} \left[F_1(\epsilon,\epsilon+\hbar\omega)G(\epsilon,\epsilon+\hbar\omega) - F_2(\epsilon,\epsilon+\hbar\omega)G(\epsilon+\hbar\omega,\epsilon)\right] d\epsilon\right\} \delta\boldsymbol{\eta}_2^{(0)},
\end{aligned}
$$

where D_K^2 is the K-phonon coupling constant.

7.6 Quantum correction to mobility

The model devised in the previous sections allow us to get corrections to the mobilities due to quantum effects. As well known, mobilities are crucial for the design of electron devices and, therefore, it is a crucial question to investigate the influence of quantum effects on them.

In Sec.s 7.4 and 7.5, the collisions have been considered as semiclassical, neglecting the terms in $\hbar^2$. To face with the complete second order correction of the collision operator in the Wigner equation is a formidable task, so, in view of getting highlights on the mobilities, we adopt the following approach. The $\hbar^2$ correction of the production term of the momentum balance equation (7.25) is modeled in a relaxation time form

$$y \int_{\mathbb{R}^d} \mathbf{v} C d\mathbf{p} = -\frac{\mathbf{J}}{\tau}$$

where τ is a relaxation time which can be obtained from (7.22) by imposing

$$-\frac{\mathbf{J}^{(0)}}{\tau} = y \int_{\mathbb{R}^d} \mathbf{v} C^{(0)} d\mathbf{p}$$

Moreover, let us suppose to have a homogenous semiconductor undergoing a constant electric field, i.e. $\nabla_{\mathbf{x}}\Phi(\mathbf{x}) = \text{constant}$, while the other spacial derivatives are zero. Under such an hypothesis, the momentum balance equation up to order $\hbar^2$ reads

$$\frac{\partial}{\partial t}\mathbf{J} - qy \int_{\mathbb{R}^d} \left[w^{(0)}(\mathbf{x}, \mathbf{p}, t) + \hbar^2 w^{(2)}(\mathbf{x}, \mathbf{p}, t) \right] \nabla_{\mathbf{p}} \mathbf{v} d\mathbf{p}\, \mathbf{E} = -\frac{\mathbf{J}}{\tau}.$$

In a long time scaling, one reaches a steady state and therefore

$$-\tau q y \mathbf{E} \int_{\mathbb{R}^d} \left[w^{(0)}(\mathbf{x}, \mathbf{p}, t) + \hbar^2 w^{(2)}(\mathbf{x}, \mathbf{p}, t) \right] \nabla_{\mathbf{p}} \mathbf{v} d\mathbf{p} = \mathbf{J}. \tag{7.77}$$

Recalling that the mobility $\boldsymbol{\mu}$, which is in general a tensor, is defined from the relation[5]

$$\mathbf{v} = \boldsymbol{\mu} : \mathbf{E},$$

and that

$$\mathbf{J} = n\boldsymbol{\mu} : \mathbf{E}. \tag{7.78}$$

We expand the latter as

$$\begin{aligned} \mathbf{J}^{(0)} + \hbar^2 \mathbf{J}^{(2)} &= \left(n^{(0)} + \hbar^2 n^{(2)} \right) \left(\boldsymbol{\mu}^{(0)} + \hbar^2 \boldsymbol{\mu}^{(2)} \right) : \mathbf{E}, \\ &= n^{(0)} \boldsymbol{\mu}^{(0)} : \mathbf{E} + \hbar^2 \left(n^{(0)} \boldsymbol{\mu}^{(2)} + n^{(2)} \boldsymbol{\mu}^{(0)} \right) : \mathbf{E} + o(\hbar^2). \end{aligned}$$

so

$$\begin{aligned} \mathbf{J}^{(0)} &= n^{(0)} \boldsymbol{\mu}^{(0)}, \\ \mathbf{J}^{(2)} &= n^{(0)} \boldsymbol{\mu}^{(2)} + n^{(2)} \boldsymbol{\mu}^{(0)}. \end{aligned}$$

[5] We denote with $\boldsymbol{\mu} : \mathbf{E}$ the vector whose components are $v_k = \mu_{kh} E_h$.

From (7.77) one finds

$$\begin{aligned}
\boldsymbol{\mu}^{(0)} &= -\frac{\tau q y}{n^{(0)}} \int_{\mathbb{R}^d} w_0^{MEP} \nabla_{\mathbf{p}} \mathbf{v} d\mathbf{p}, \\
\boldsymbol{\mu}^{(2)} &= -\frac{n^{(2)}}{n^{(0)}} \boldsymbol{\mu}^{(0)} - \frac{\tau q y}{n^{(0)}} \int_{\mathbb{R}^d} w_2^{MEP} \nabla_{\mathbf{p}} \mathbf{v} d\mathbf{p}.
\end{aligned}$$

Specifically, the contributions to mobility in the case of Kane dispersion relation reads

$$\begin{aligned}
\boldsymbol{\mu}^{(0)} &= -\frac{\tau q y}{n^{(0)}} 4\pi \sqrt{m^*} y \int_0^{+\infty} \frac{(1+2\alpha\epsilon)\sqrt{2\epsilon(1+\alpha\epsilon)}}{(\exp(\eta_0^{(0)} + \eta_1^{(0)}\epsilon) + 1)\sqrt{1+4\alpha\epsilon(1+\alpha\epsilon)}} \left[1 - \frac{4\alpha\epsilon(1+\alpha\epsilon)}{3(1+4\alpha\epsilon(1+\alpha\epsilon))}\right] d\epsilon \, \mathbf{I}, \\
\boldsymbol{\mu}^{(2)} &= -\frac{n^{(2)}}{n^{(0)}} \boldsymbol{\mu}^{(0)} - \frac{\tau q y}{n^{(0)}} 4\pi \left\{ \int_0^{\infty} \frac{e^{\xi_0^{(0)}}}{e^{\xi_0^{(0)}} + 1} \xi_0^{(2)} \sqrt{\frac{2m^*\epsilon(1+\alpha\epsilon)}{1+4\alpha\epsilon(1+\alpha\epsilon)}} (1+2\alpha\epsilon) d\epsilon \right. \\
&\quad \left. -\frac{1}{3} \int_0^{\infty} \frac{e^{\xi_0^{(0)}}}{e^{\xi_0^{(0)}} + 1} \xi_0^{(2)} \left[2m^*\epsilon(1+\alpha\epsilon)\right]^{5/2} m^*(1+2\alpha\epsilon) d\epsilon \right\} \mathbf{I},
\end{aligned}$$

while in the case of graphene we get

$$\begin{aligned}
\boldsymbol{\mu}^{(0)} &= -\frac{\tau q y}{n^{(0)}} \pi \int_{cv_F}^{+\infty} \left(2 - \frac{\epsilon^2 - v_F^2 c^2}{\epsilon^2}\right) \frac{1}{e^{\xi^{(0)}} + 1} d\epsilon \, \mathbf{I}, \\
\boldsymbol{\mu}^{(2)} &= -\frac{n^{(2)}}{n^{(0)}} \boldsymbol{\mu}^{(0)} - \frac{\tau q y}{n^{(0)}} \frac{\pi}{v_F} \int_{cv_F}^{\infty} \frac{e^{\xi_0^{(0)}}}{e^{\xi_0^{(0)}} + 1} \xi_0^{(2)} \left(2 - \frac{\epsilon^2 - c^2 v_F^2}{\epsilon^2}\right) \sqrt{\epsilon^2 - c^2 v_F^2} \, d\epsilon \mathbf{I}.
\end{aligned}$$

Conclusions and acknowledgements

The Wigner equation for electrons moving in a d-dimensional crystal has been written in the case of a generic dispersion relation. Moment equations have been deduced and closed by QMEP taking into account the Fermi-Dirac statistics. Explicit closure relations have been obtained for bulk semiconductors and for graphene under a suitable expansion both in $\hbar$ and in a parameter measuring the anisotropy of the Wigner functions. The devised models seem very useful for the simulation of charge transport in regime where quantum effects cannot be neglected.

Chapter 8

Optimized Quantum Drift Diffusion Model for a Resonant Tunneling Diode

In this chapter an optimized Quantum Drift Diffusion model (QDD) [29, 54, 55] is presented. Comparing it with the Boltzmann-Wigner Transport Equation (BWTE) [56] solved using a signed Monte Carlo method [57], an improved QDD model will be obtained. A situation of high non equilibrium regime is investigated: electron transport in a Resonant Tunneling Diode (RTD) made of GaAs with two potential barriers in GaAlAs. The range of the suitable voltage bias applied to the RTD is analyzed.

We find an acceptable agreement between QDD model and BWTE when the applied bias is low or moderate with a threshold of about 0.225 V over a length of 150 nm; it is found out that the use of a field dependent mobility is crucial for getting a good description of the negative differential conductivity in such a range. At higher bias voltages, we expect that QDD model loses accuracy.

We remark that the results presented in this chapter are original and have been published in [58].

8.1 Introduction

The RTD has been widely studied because of its importance in the field of nanoelectronic science and technology and its potential applications in very high speed/functionality devices and circuits [59]. Usually in engineering design a QDD model is adopted to describe the charge transport in a RTD. The approaches based on the BWTE are physically more accurate but computationally very expensive and not suitable for CAD purposes. A RTD represents a situation

of high non thermodynamical equilibrium and therefore it is interesting, both from a theoretical and an applicative point of view, to investigate the validity of QDD models.

We consider a RTD in GaAs with two potential barriers in GaAlAs. The QDD model is given by the continuity equation for the charge in the unipolar case (in the investigated situation the current due to the holes is negligible) coupled to the Poisson equation; in the constitutive relation for the current, the quantum effect is given by the Bohm potential. The scattering terms are taken into account through the expression of the mobility. A mobility model based on that proposed in [60] has been used. The interested reader can find articles related to QDD model for example in [54, 55, 61, 62]. An application of a QDD model to two dimensional materials can be found in [63].

The more accurate BWTE has been solved by using a signed Monte Carlo method (see [57] for the details on the approach) as in [56, 64–66]. In order to make a fair comparison, some parameters of the QDD model present in the expression of the mobility and in the Bohm potential have been optimized by comparing the characteristic curves obtained with the BWTE and QDD model.

We find two different situations when the QDD model and BWTE are compared, depending on the values of applied bias voltage. There is a good agreement for low or moderate fields, roughly below 15 kV/cm. It is found out that the use of a field dependent mobility is crucial for getting a good description of the negative differential conductivity in such a range of applied fields. At higher fields more sophisticated models should be employed, e.g. quantum energy-transport or more general models based on the moment method and the quantum version of the maximum entropy principle (see [27, 29]).

The plan of the chapter is as follows. In Sec. 8.2 the BWTE is introduced and the signed Monte Carlo method is sketched while in Sec. 8.3 the QDD equations together with the mobility model are presented. In Sec. 8.4 the RTD considered for the comparison is described. In Sec. 8.5 the numerical scheme used to solve the QDD model is introduced. In the last section the optimization procedure is explained and the numerical results are discussed.

8.2 The Boltzmann-Wigner transport equation

An accurate way to deal with quantum transport phenomena is to resort to the BWTE [3]

$$\frac{\partial}{\partial t} f_w(t, \mathbf{x}, \mathbf{k}) + \frac{\hbar}{m^*} \mathbf{k} \cdot \nabla_{\mathbf{x}} f_w(t, \mathbf{x}, \mathbf{k}) + \frac{e}{\hbar} \nabla_{\mathbf{x}} \phi \cdot \nabla_{\mathbf{k}} f_w(t, \mathbf{x}, \mathbf{k}) = \mathcal{Q}(f_w) + \mathcal{C}(f_w)\,, \tag{8.1}$$

where $f_w(t, \mathbf{x}, \mathbf{k})$ is the Wigner quasi-distribution function which generalises the semiclassical Boltzmann distribution function, $\mathbf{x} = (x^1, x^2, x^3) \in \mathbb{R}^3$ and

$\hbar\mathbf{k} = (\hbar k^1, \hbar k^2, \hbar k^3) \in \mathbb{R}^3$ are the electron position and momentum respectively, m^* is the electron effective mass, $\hbar$ is the reduced Planck constant and $e > 0$ is the elementary charge; indeed $\mathbf{k}$ belongs to the first Brillouin zone but we will adopt analytical approximation for the energy bands. In eq. (8.1) $\nabla_{\mathbf{x}}$ denotes the gradient with respect to $\mathbf{x}$ while $\nabla_{\mathbf{k}}$ denotes the gradient with respect to $\mathbf{k}$. ϕ is the slowly-varying potential satisfying the Poisson equation

$$\nabla_{\mathbf{x}} \cdot [\epsilon_0 \epsilon_r \nabla_{\mathbf{x}} \phi(\mathbf{x})] = -e(N_D - N_A - n)\,, \tag{8.2}$$

ϵ_0 the vacuum dielectric constant, ϵ_r the relative dielectric constant. N_D, N_A are the donors and acceptors doping profiles and n is the particle density which is related to the Wigner function as

$$n(t, \mathbf{x}) = \int f_w(t, \mathbf{x}, \mathbf{k})\, d\mathbf{k}. \tag{8.3}$$

$\mathcal{C}(f_w)$ is the collision term, whose formulation is itself a very complex problem. In this paper the effects of scattering with phonons are taken into account via a semiclassical Boltzmann collision operator, which employs transition rates calculated by using Fermi's golden rule. In the not-degenerate case we have [67]

$$\mathcal{C}(f_w) = \int [w_s(\mathbf{k}', \mathbf{k}) f_w(\mathbf{k}') - w_s(\mathbf{k}, \mathbf{k}') f_w(\mathbf{k})]\, d\mathbf{k}'\,, \tag{8.4}$$

where $w_s(\mathbf{k}, \mathbf{k}')$ is the rate of the scatterings with phonons and impurities electrons undergo. In the evolution the quantum effect is given by the term

$$\mathcal{Q}(f_w) = \int V_w(\mathbf{x}, \mathbf{k} - \mathbf{k}') f_w(t, \mathbf{x}, \mathbf{k}')\, d\mathbf{k}'. \tag{8.5}$$

Here V_w is the Wigner potential

$$V_w(\mathbf{x}, \mathbf{k}) = -e \frac{1}{i\hbar(2\pi)^3} \int d\mathbf{x}'\, e^{-i\mathbf{k}\cdot\mathbf{x}'} \left[B\left(\mathbf{x} + \frac{\mathbf{x}'}{2}\right) - B\left(\mathbf{x} - \frac{\mathbf{x}'}{2}\right) \right], \tag{8.6}$$

and $-eB(\mathbf{x})$ is the rapidly-varying term of the potential energy, which models the potential barriers in hetero-junctions and is a prescribed function of the position.

A parabolic band will be adopted according to which the electron energy ε is assumed to be similar to that of a classical free particle,

$$\varepsilon(\mathbf{k}) = \frac{\hbar^2 |\mathbf{k}|^2}{2m^*}, \tag{8.7}$$

where m^* is the effective electron mass. Therefore, the electron group velocity is

$$\mathsf{v}(\mathbf{k}) = (v^1, v^2, v^3) = \frac{1}{\hbar} \nabla_{\mathbf{k}} \varepsilon = \frac{\hbar \mathbf{k}}{m^*}. \tag{8.8}$$

Solving the BWTE, from the numerical point of view, is a quite difficult task. The main complication, arising in the direct solution based on finite-difference

schemes or finite elements, is the discretization of the diffusion term $\mathbf{k} \cdot \nabla_{\mathbf{x}} f_w$ due to the typically fast variation in the phase space. Particle based Monte Carlo techniques do not require the discretization of this term, but they need costly computational times.

According to the so-called *Signed particle Monte Carlo approach* developed initially in [68], the quantum evolution term (8.5) looks like the *Gain* term of a collisional operator in which the *Loss* term is missing. However, since the Wigner potential (8.6) is not always positive, (8.5) cannot be considered a real scattering term. For this reason, it is separated into positive and negative parts V_w^+, V_w^- such that

$$V_w = V_w^+ - V_w^-, \quad V_w^+, V_w^- \geq 0. \tag{8.9}$$

In this way, we can define an integrated scattering probability per unit time as

$$\gamma(\mathbf{x}) = \int d\mathbf{k}' \, V_w^+(\mathbf{x}, \mathbf{k} - \mathbf{k}') = \int d\mathbf{k}' \, V_w^-(\mathbf{x}, \mathbf{k} - \mathbf{k}') \tag{8.10}$$

(not that the two integrals are equal) and rewrite the quantum evolution term as the difference between *Gain* and *Loss* terms, i.e.

$$\mathcal{Q}(f_w) = \int d\mathbf{k}' w(\mathbf{k}', \mathbf{k}) f_w(t, \mathbf{x}, \mathbf{k}') - \gamma(\mathbf{x}) f_w(t, \mathbf{x}, \mathbf{k}) \tag{8.11}$$

$$w(\mathbf{k}', \mathbf{k}) = V_w^+(\mathbf{x}, \mathbf{k} - \mathbf{k}') - V_w^-(\mathbf{x}, \mathbf{k} - \mathbf{k}') + \gamma(\mathbf{x}) \delta(\mathbf{k} - \mathbf{k}'). \tag{8.12}$$

The term $w(\mathbf{k}', \mathbf{k})$ is interpreted as a scattering rate which produces, from the old particle, a pair of new particles having weights u and $-u$. This interpretation gives rise to the following scheme: an initial parent particle (with sign) evolves on a free-flight trajectory and, according to a generation rate given by the function $\gamma(\mathbf{x})$, two new signed particles are generated in the same position having weight u and $-u$ respectively. The momentum of the new particles is generated with probability $V_w^+(\mathbf{x}, \mathbf{k})/\gamma(\mathbf{x})$. However this procedure suffers from an efficiency issue in particle generation, because γ usually is a rapidly oscillating function and leads to an exponential growth of the number of particles. In order to contain the particle number, a cancellation procedure is introduced: if the total number of particles exceeds a certain bound N_{canc} , then pairs of particles with similar positions and wave-vectors, but with opposite signs, are removed from the system. For details about the procedure the interested reader is referred to [56]. In the sequel, for the simulation of the RTD, we have used ohmic boundary conditions, assuming carriers are in thermal equilibrium at the contacts. At level of Monte Carlo approach this is obtained as follows. When a carrier flows out the contact another particle is injected into the device in order to ensure charge neutrality. The wave-vector $\mathbf{k}$ of the incoming particle is chosen randomly with a probability density given by a Fermi-Dirac distribution.

8.3 Quantum Drift-Diffusion Model

Although very accurate, the BWTE is not suited for CAD purposes and usually for the design of electron devices simpler macroscopic models are used. Among these, the most known is the quantum drift-diffusion model which, in the unipolar case, is given by the continuity equation for the electron density n

$$\frac{\partial n}{\partial t} + \nabla_{\mathbf{x}} \cdot \mathbf{J} = 0, \tag{8.13}$$

coupled to the Poisson equation (8.2) and supplemented with a constitutive relation for the current density $\mathbf{J}$, which is expressed as the sum of a diffusion and a drift

$$\mathbf{J} = -\mu \frac{k_B T}{e} \nabla_{\mathbf{x}} n + n\mu \nabla_{\mathbf{x}} (\phi + Q + B), \tag{8.14}$$

where k_B is the Boltzmann constant, T is the lattice temperature kept at equilibrium, μ is the high field mobility and B is the potential barrier. The quantum effects are encoded in the presence of the Bohm potential Q, given by

$$Q = \frac{\hbar^2}{\beta m^* e \sqrt{n}} \Delta_{\mathbf{x}} (\sqrt{n}). \tag{8.15}$$

In the original Magdelung quantum fluid model $\beta = 2$ but often in semiconductors one takes $\beta = 6$. In commercial simulators β is considered as a fitting parameter, usually assumed to vary from two to six. The mobility μ is taken as a function of the modulus of the electric field $\mathbf{E} = -\nabla_{\mathbf{x}} \phi$. We adopt the mobility model proposed in [60], that is

$$\mu(|\mathbf{E}|) = \frac{\mu_0 + v_{sat}(|\mathbf{E}|^{\delta-1}/E_c^{\delta})}{1 + \alpha(|\mathbf{E}|/E_c)^{\gamma} + (|\mathbf{E}|/E_c)^{\delta}}. \tag{8.16}$$

where μ_0 is the low field mobility, v_{sat} is the saturation speed, E_c is the critical electric field. These parameters, along with $\alpha, \delta, \gamma, \beta$ will be used like fitting parameters to optimize the QDD model.

The drift-diffusion model (8.13)-(8.14) must be supplemented with boundary conditions. Ohmic contacts and zero quantum effects at the edges of the diode are assumed [69], that is

$$n(0) = N_D(0), \quad n(L) = N_D(L), \quad Q(0) = Q(L) = 0, \tag{8.17}$$

where we have identified the device with the interval $[0, L]$.

The derivation of the QDD model assumes that electrons are in thermal equilibrium with the phonon bath of the crystal and the validity of the Einstein relation for the diffusion coefficient. Moreover, for the evaluation of the density the Fermi-Dirac distribution function or the limiting Maxwell-Boltzmann one in the non-degenerate case is adopted. The QDD model can be regarded as the minimal set of moment equations arising from the BWTE with phenomenological

closure relations based on the previous assumptions. Therefore, it is interesting from a thermodynamic point of view to investigate the range of validity of the QDD model.

Before proceeding, it is useful to rewrite our system in a scaled form. The scaling has the advantage to emphasize the singularly perturbed nature of the equations. Since the device that we will consider is 1-d in space, if we denote by x the only relevant abscissa, our choice for the scaling parameters is as follows: $n \mapsto \dfrac{n}{\overline{n}} = \tilde{n}$, $t \mapsto \dfrac{t}{\bar{t}} = \tilde{t}$, $\phi \mapsto \dfrac{\phi}{k_B T/e} = \tilde{\phi}$, $Q \mapsto \frac{Q}{k_B T/e} = \tilde{Q}$, $B \mapsto \dfrac{B}{k_B T/e} = \tilde{B}$, $x \mapsto \dfrac{x}{\overline{x}} = \tilde{x}$ and $\mu \mapsto \mu \dfrac{k_B T \bar{t}}{e \overline{x}^2} = \tilde{\mu}$ where $\overline{n}$ is the low doping concentration ($10^3 \mu m^{-3}$), $\bar{t} = 1$ ps, $\overline{x} = 1 \mu m$.

The significant component of the electric field and the current density is only that along x and non-dimensional form of equation (8.13) reads

$$\frac{\partial \tilde{n}}{\partial \tilde{t}} + \frac{\partial \tilde{J}}{\partial \tilde{x}} = 0, \tag{8.18}$$

where

$$\tilde{J} = -\tilde{\mu} \frac{\partial \tilde{n}}{\partial \tilde{x}} + \tilde{\mu} \tilde{n} \frac{\partial}{\partial \tilde{x}} \left(\tilde{\phi} + \tilde{Q} + \tilde{B} \right), \tag{8.19}$$

$$\tilde{Q} = \frac{\hbar^2}{\beta m^* k_B T \overline{x}^2 \sqrt{\tilde{n}}} \frac{\partial^2}{\partial \tilde{x}^2} \left(\sqrt{\tilde{n}} \right), \tag{8.20}$$

$$\tilde{\mu}(|\mathbf{E}|) = \frac{k_B T}{e} \left(\frac{\mu_0 + v_{sat}(|\mathbf{E}|^{\delta - 1}/E_c^{\delta})}{1 + \alpha(|\mathbf{E}|/E_c)^{\gamma} + (|\mathbf{E}|/E_c)^{\delta}} \right). \tag{8.21}$$

The non-dimensional Poisson equation reads

$$\left(\frac{\epsilon_0 k_B T}{e^2 \overline{x}^2 \overline{n}} \right) \frac{\partial}{\partial \tilde{x}} \left(\epsilon_r \frac{\partial \tilde{\phi}}{\partial \tilde{x}} \right) = (\tilde{n} - \tilde{c}(\tilde{x})), \tag{8.22}$$

where $\tilde{c}(\tilde{x}) = \dfrac{N_D - N_A}{\overline{n}}$. In the following sections, for the sake of simplifying the notation, we will omit the tilde symbol in the non-dimensional quantities.

8.4 Resonant Tunneling Diode

We consider the RTD structure introduced in [65], but with a simplified physical setup. The device simulated is 1-d in space and its total length is $L = 150$ nm. It consists of two barriers with width $a = 3$ nm and height $B = -0.3$ V surrounding a quantum well with width $b_w = 5$ nm, see Fig.8.1. The barrier structure is centered in a 30 nm lightly doped ($N_D = 10^{16}$ cm^{-3}) spacer region that is connected to 60 nm highly doped ($N_D = 10^{18}$ cm^{-3}) drift regions in either side.

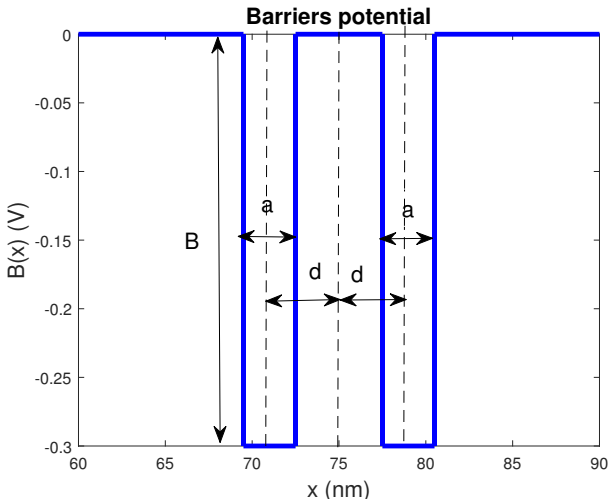

Figure 8.1: Quantum well region.

The quantum well region is symmetric with respect to the mid-point $L/2$, as shown in Fig.8.1, where the distance between each barrier center and the mid-point is

$$|d| = \frac{a + b_w}{2} = 4\,\text{nm}.$$

The barrier potential can be expressed as a piecewise constant function, as follows:

$$B(x) = \begin{cases} -0.3\,\text{V} & 69.5\,\text{nm} < x < 72.5\,\text{nm} \vee 77.5\,\text{nm} < x < 80.5\ \text{nm} \\ 0 & \text{otherwise} \end{cases} \tag{8.23}$$

The scattering mechanisms include polar optical phonons within a single Γ valley band [67]. The parameter ϵ_r is taken constant and equal to that for GaAs. The temperature is 300 K. The effective electron mass is $m^* = 0.067 m_e$, where m_e is the bare electron mass. The schematic of the considered device is depicted in Fig.8.2.

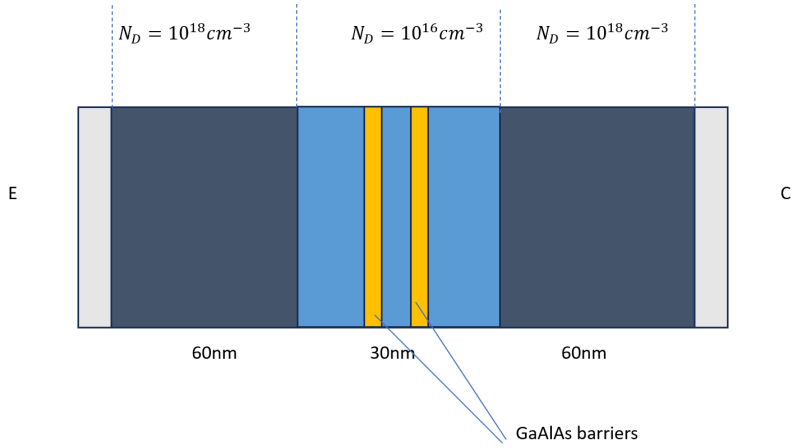

Figure 8.2: Simulated resonant tunneling diode.

8.5 Numerical Schemes for the QDD model

In order to compare the characteristic curves obtained with the BWTE and QDD models we will consider the stationary solutions. To solve the steady QDD equations, one needs numerical approximations for the continuity and the Poisson equations. We start with the discretization of Poisson's equation.

Let us consider a uniform spatial grid $0 = x_1 < x_2 < ... < x_N = L$, where $\Delta x = x_{i+1} - x_i$, $\forall i = 1, ..., N-1$, and discretize the second derivatives in the Poisson equation with standard central differencing

$$\phi_{xx}(x_i) = \frac{\phi_{i-1} - 2\phi_i + \phi_{i+1}}{\Delta x^2} + o(\Delta x). \tag{8.24}$$

By substituting into the scaled Poisson equation and by taking into account that $\epsilon = \epsilon_0 \epsilon_r$ is piecewise constant, we obtain

$$\phi_{i-1} - 2\phi_i + \phi_{i+1} = \frac{e\Delta x^2}{\epsilon}(n_i - c_i), \quad \forall i = 2, ..., N-1 \tag{8.25}$$

with boundary conditions: $\phi_1 = 0$ and $\phi_N = V_b$ where V_b is the bias voltage.

In order to discretize the continuity equation and to get a second order numerical scheme, we need also the intermediate grid points $x_{i+1/2} = x_i + \frac{\Delta x}{2}$. We set $n_i \approx n(x_i)$ and $J_i \approx J(x_i)$. The stationary continuity equation (8.13) is discretized as

$$\frac{J_{i+1/2} - J_{i-1/2}}{\Delta x} = 0 \tag{8.26}$$

In order to approximate J we expand respect to the space variable x

$$J(x) = J_{i+1/2} + (x - x_{i+1/2}) \left(\frac{\partial J}{\partial x}\right)_{i+1/2} + o(\Delta x).$$

and introduce the thermal voltage $U_T = \frac{k_B T}{e}$ and the Slotboom variable

$$s = ne^{\left(\frac{-G}{U_T}\right)}$$

where $G = \phi + Q + B$. We take

$$G(0) = \phi(0) + B(0), \quad G(L) = \phi(L) + B(L), \tag{8.27}$$

assuming that the quantum effects are null at the boundary, that is $Q(0) = Q(L) = 0$ [70].

In terms of the Slotboom variable the current reads $J = \mu k_B T e^{G/U_T} \dfrac{\partial s}{\partial x}$ wherefrom

$$\mu k_B T \frac{\partial s}{\partial x} = e^{-G/U_T} J(x) = e^{-G/U_T} \left[J_{i+1/2} + (x - x_{i+1/2}) \left(\frac{\partial J}{\partial x} \right)_{i+1/2} + o(\Delta x) \right]. \tag{8.28}$$

In each interval $[x_i, x_{i+1}]$ we suppose that the mobility and the current are constants

$$\mu(x) \approx \mu_{i+1/2} \quad \forall x \in [x_i, x_{i+1}], \quad J(x) \approx J_{i+1/2} \quad \forall x \in [x_i, x_{i+1}].$$

The potential G is approximated in $[x_i, x_{i+1}]$ by a piecewise linear function

$$G(x) \approx G_i + \frac{x - x_i}{\Delta x}(G_{i+1} - G_i).$$

In particular, we discretize the Bohm potential by using finite difference

$$Q_i = \frac{\hbar^2}{\beta m^* e} \frac{(\sqrt{n_{i+1}} - 2\sqrt{n_i} + \sqrt{n_{i-1}})}{\Delta x^2 \sqrt{n_i}}$$

Integrating over $[x_i, x_{i+1}]$, one has

$$\mu_{i+1/2} k_B T (s_{i+1} - s_i) = \int_{x_i}^{x_{i+1}} e^{-G/U_T} J_{i+1/2} dx + o(\Delta x) =$$

$$= J_{i+1/2} \frac{\Delta x U_T}{G_{i+1} - G_i} \left(e^{-G_i/U_T} - e^{-G_{i+1}/U_T} \right) + o(\Delta x)$$

which after some algebra, gives the Scharfetter-Gummel discretization of the current

$$J_{i+1/2} \approx \frac{U_T \mu_{i+1/2} \sigma_{i+1/2}}{\Delta x} [e(n_{i+1} - n_i) \coth(\sigma_{i+1/2}) - e(n_{i+1} + n_i)] \tag{8.29}$$

where $\sigma_{i+1/2} = \frac{G_{i+1} - G_i}{2U_t}$.

We remark that the barrier is not a regular function and its derivatives must be intended in a distributional sense. Indeed, what we evaluate is a numerical

regularization of B. By substituting this expression of current density in (8.26) we obtain the overall scheme (for more details see [71])

$$\begin{cases} \phi_{i-1} - 2\phi_i + \phi_{i+1} = \dfrac{e\Delta x^2}{\epsilon}(n_i - c_i), \\ \dfrac{\mu_{i+1/2}\sigma_{i+1/2}[(n_{i+1} - n_i)\coth(\sigma_{i+1/2}) - (n_{i+1} + n_i)]}{\Delta x^2}, \\ -\dfrac{\mu_{i-1/2}\sigma_{i-1/2}[(n_i - n_{i-1})\coth(\sigma_{i-1/2}) - (n_{i-1} + n_i)]}{\Delta x^2} = 0, \end{cases} \tag{8.30}$$

$i = 2, ..., N-1$, augmented with the boundary conditions (8.27).

In order to decouple the system we adopt the following iterative scheme.

1. Set as initial guess $n^1(x) = c(x)$.
2. For each iteration $k \geq 1$:
   (a) solve the Poisson equation to find ϕ^{k+1};
   (b) solve the second equation of the system (8.30) to find n^{k+1}.
3. Iterate step 2 until convergence, according to a suitable stopping criterion.

8.6 Optimization procedure and numerical results

For the optimization procedure, we take the current density calculated by the BWTE as reference and introduce the objective function

$$f_{obj}(\mathbf{a}) = \left[\sum_i |J_{QDD}(\mathbf{a}, (V_b)_i) - J_{BWTE}((V_b)_i)|^2\right]^{1/2}. \tag{8.31}$$

Here $J_{BWTE}((V_b)_i)$ is the reference current density given by the BWTE at applied bias $(V_b)_i$ running from 0.025 V to 0.275 V with increment 0.025 V, while $J_{QDD}(\mathbf{a}, (V_b)_i)$ is the current computed with the QDD mode at applied bias $(V_b)_i$ and value

$$\mathbf{a} = [\mu_0, E_c, v_{sat}, \delta, \alpha, \gamma, \beta]$$

of the vector of the parameters to be optimized.

As initial guess we take $\mathbf{a}_0 = [1.066, 5.659, 0.253, 14.93, -0.045, 0.564, 1.775]$ which has been inferred by the original values in [60]. In order to write the set of admissible values equal to $[0, 1]$ for each component of $\mathbf{a}$, we introduce the transformation

$$\begin{aligned} \mu_0 &= 1.5t_1 + 0.5, \quad E_c = 7.5t_2 + 2.5, \quad v_{sat} = 0.38t_3 + 0.12, \\ \delta &= 10t_4 + 10, \quad \alpha = 3t_5, \quad \gamma = t_6, \quad \beta = 2t_7 + 1, \end{aligned}$$

where $\mathbf{t} \in [0,1]^7$ and, consequently, $\mu_0 \in [0.5, 2]$, $E_c \in [2.5, 10]$, $v_{sat} \in [0.12, 0.5]$, $\delta \in [10, 20]$, $\alpha \in [0, 3]$, $\gamma \in [0, 1]$, $\beta \in [1, 3]$. The intervals for the constraints have been chosen in order to have the initial point in the middle of the interval.

The complete formulation of the problem reads as follows:

$$\begin{cases} \min f_{obj}(\mathbf{t}) \\ \mathbf{t}_0 = [0.38, 0.42, 0.35, 0.49, 0.015, 0.56, 0.39]; \\ 0 \leq t_k \leq 1 \qquad k = 1, ..., 7. \end{cases} \tag{8.32}$$

where $f_{obj}(\mathbf{t})$ is obtained from (8.2)-(8.13) which represent PDE constraints.

To solve this constrained optimization problem we have adopted the MATLAB optimization function `fmincon` [78] with tolerance 10^{-6}. The numerical procedure gives the following optimal values for $\mathbf{t}$

$$\mathbf{t}_{min} = [0.955, 0.399, 0.227, 0.363, 0.192, 8.141 \times 10^{-6}, 0.852]$$

to which the optimal value

$$\mathbf{a}_{min} = [1.933 \mu m^2/Vps, 5.493 V/\mu m, 0.206 \mu m/ps, 13.63, 0.576, 8.141 \times 10^{-6}, 2.704]$$

corresponds.

In Fig. 8.3 the reference characteristic curves obtained by solving the BWTE are compared with those deduced from the QDD model with the initial guess of the parameters and with the optimized ones. For applied voltages lower than 0.225 V an acceptable agreement is obtained. The main finding is that at variance with the results presented in [54] it is indeed possible to get a negative differential conductivity even with a QDD model. The lack of such an effect in [54] is presumably ascribable to the use of constant mobility which, although coherent with the derivation of the QDD model expanding around a local equilibrium, is too simplistic for performing accurate simulations at moderate or high fields.

In Figure 8.4 the simulation of the RTD is shown in the case $V_b = 0.175$V. The qualitative behavior is in agreement with the results present in the literature.

Of course, the optimized parameters are calibrated on the specific resonant diode under consideration and cannot be considered as general values for any simulations. To this aim a more extensive campaign of simulations should be performed. However, we would like to remark that in any case several applied electric fields have been considered (those present in the characteristic curve) and also the fitted parameters obtained from experimental data suffer from a lack of generality because they are usually obtained from measures in bulk semiconductors which include only the drift contribution. The diffusive and, more stringently, the quantum effects require the simulation or a set of measures of the specific device under investigation. Therefore, it is intrinsically unavoidable a limitation of any set of optimized parameters. The only theoretical general

way to get *universal* transport coefficient is to deduce them directly from the scattering term in the BWTE but this is a daunting task which goes beyond the scope of the present paper.

We tried to consider also higher fields (see Fig. 8.3) but a certain discrepancy is present both qualitatively and quantitatively, casting doubts on the use of the QDD model in situations of high non-equilibrium. It is likely that thermal effects must be included, e.g. considering an energy-transport or hydrodynamical model.

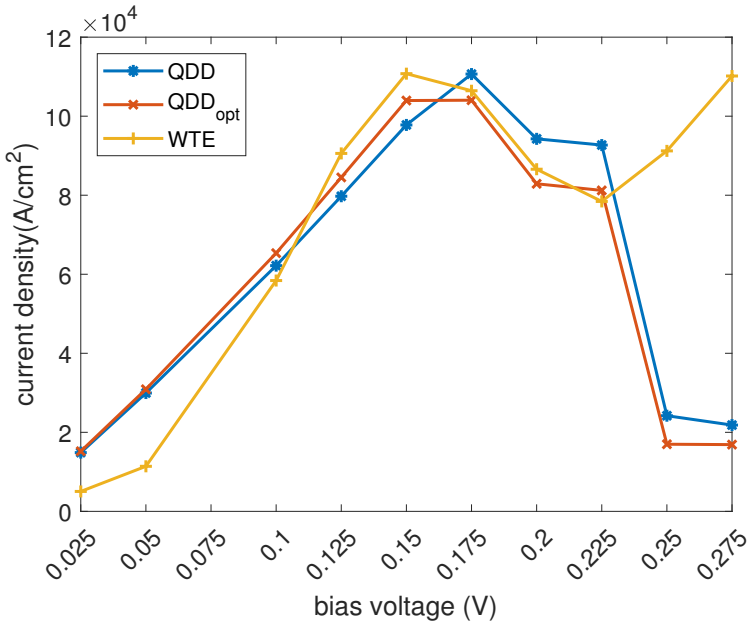

Figure 8.3: Comparison of the characteristic curves.

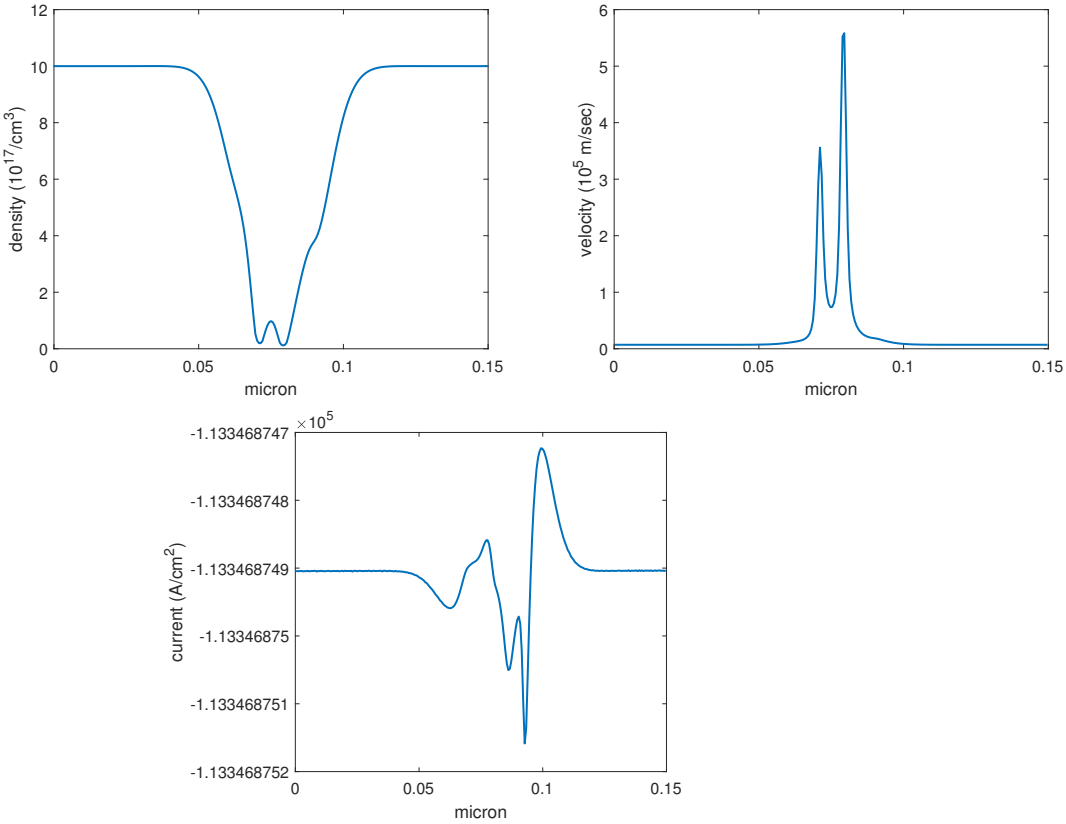

Figure 8.4: Density, velocity and current calculated by the optimized QDD model with $V_b = 0.175V$.

In [72] we improved the optimization adopting the following procedure. As initial guess a_0 we choose the parameters present in the literature,

$$a_0 = (0.85\,\mu\text{m}^2/\text{V ps}, 22.09\,\text{V}/\mu\text{m}, 0.1907\,\mu\text{m/ps}, 7.144, 5.362, 0.783, 2)$$

At variance with reference [58], as second step, we perform a Particle Swarm Optimization (PSO) procedure [73–75]. This algorithm is gradient free and it is designed for large parameter spaces. A candidate optimum a_1 is found. As third step, we perform an unconstrained optimization procedure by means of the Nelder-Mead algorithm [76, 77], starting from a_1 as initial guess. The optimum is obtained at

$$a_{opt} = (1.1393\,\mu\text{m}^2/\text{V ps}, 5.3075\,\text{V}/\mu\text{m}, 0.1878\,\mu\text{m/ps}, 6.8461, 0.0512, 0.8094, 1.6660)$$

About the validity of QDD model, we observe that for high voltages than 0.3 V the QDD model does not predict accurately the value of the current (see Fig. 8.5), even if this improves the results in [58] where the discrepancy was

already evident for applied voltage greater than 0.25 V. In any case, since the underlying hypotheses of the QDD models require that the system is close to equilibrium, it is not surprising a limitation on the applied field in order to guarantee acceptably accurate results. A possible way to improve the simulation, with still computationally feasible computing time, is to adopt more sophisticated models such as quantum energy-transport or hydrodynamical ones.

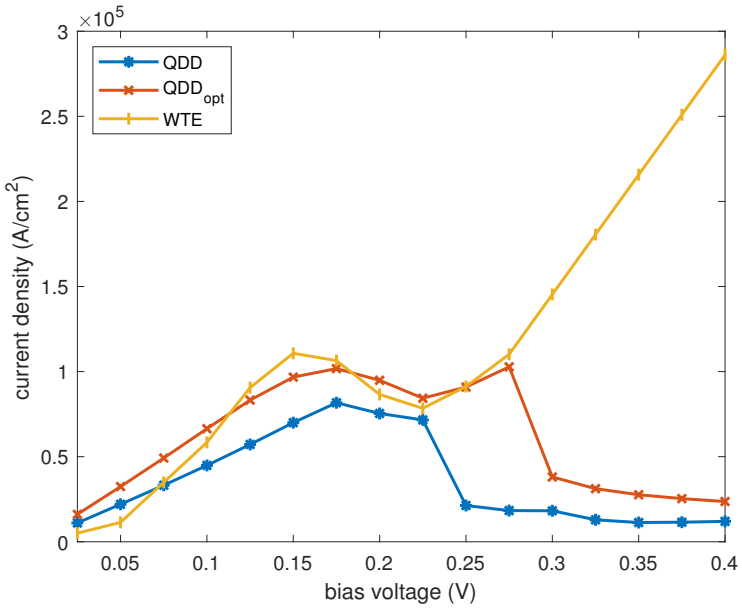

Figure 8.5: New optimization results for high voltages.

Chapter 9

Additional topics

9.1 A time delayed deterministic model for the spread of COVID-19 with calibration on a real dataset

During the evolution of the COVID-19 pandemic, each country has adopted different control measures to contrast the epidemic diffusion. Restrictions to mobility, public transport, and social life in general, have been actuated to contain the spread of the pandemic. In this chapter, we consider the deterministic SIRD model with delays proposed in [79] which is improved by adding the vaccinated compartment V (SIRDV model) and considering a time dependent contact frequency. The three delays take into account the incubation time of the disease, the healing and the death time. The aim of this work is to study the effect of the vaccination campaigns in Great Britain (GBR) and Israel (ISR) during the pandemic period. The different restriction periods are included by fitting the contact frequency on real datasets as a piecewise constant function. As expected, the vaccination campaign reduces the amount of deaths and infected people. Furthermore, for the different levels of restriction policy, we find specific values of the contact frequency, that can be used to predict the trend of the pandemic.

We remark that the results presented in this section are original and have been published in [80].

9.1.1 Introduction

The COVID-19, acronym of COronaVIrus Disease 19, is a respiratory infectious disease caused by the virus called SARS-CoV-2 belonging to the coronavirus family. It has spread rapidly and has taken millions of lives worldwide since the end of 2019 [81].

Epidemic models can be devised with the aim to predict the pandemic evolution. They represent a class of mathematical models that are used not only to study epidemics properly but also to predict social phenomena or the behavior of biological systems and, for these reasons, they have been a branch of interest in applied mathematics for several years. Epidemic models can help the governments to decide the best restriction policy to adopt so that the virus spreading can be contained in a better way [82, 83]. The crucial point consists to determine suitable parameters of such models that are able to represent and predict accurately the behavior of the illness.

Regarding the COVID-19 pandemic, many mathematical models have been proposed. Epidemic models based on ordinary differential equations have been introduced in [82, 84, 85]. Stochastic models have been proposed in [79, 86]. For models based on stochastic differential equations see e.g. [87, 88]. A model based on an operatorial approach as in quantum mechanics can be found in [89]. A continuous space-time non-linear probabilistic model has been proposed in [90], where the interpretation is given in analogy with quantum mechanics.

In [79] a deterministic model based on differential equations with time delays has been devised, although it was introduced only to validate the stochastic one and no applications have been provided by using such a model. In [91, 92] mathematical models with only a delay regarding the incubation time are presented. In the present work, we consider a compartmental model consisting in dividing the population in four categories: susceptible S, infected I, recovered R, and dead D (SIRD model). The transitions between classes are governed by a system of differential equations with delays. The adopted model considers three time delays: the incubation time, the healing time, and the death time. The use of time delays allows to include characteristics of the disease under consideration, such as incubation, and also possible delays due to the data communication and recording. Moreover, we provide an application of the model mentioned above to the cases of the COVID-19 spread in Great Britain (GBR) and Israel (ISR). The parameters are extracted from real data collected in [93] by a fitting procedure and a comparison with the policy measures to prevent the pandemic diffusion is done. Furthermore, the effect of vaccination is a key point for the pandemic evolution and therefore several studies are carried out (see e.g. [94]). For this reason, we include in the examined SIRD model the further category of vaccinated people V which time evolution is provided by data, thus defining a SIRDV model. In this way, we include the effect of vaccination in the examined model for the countries under investigation to predict different scenarios depending on whether it is considered or not.

The plan of the chapter is as follows. In Sec. 9.1.2 the SIRD and SIRDV mathematical models are introduced; in Sec. 9.1.2 the numerical approach to simulate the previous models is presented and applied for a specific analysis of

the single country under consideration. In particular, in Subsec. 9.1.3 we perform a data fitting for ISR to obtain the SIRDV model parameters and we get also numerical simulations, and in Subsec. 9.1.3 the same analysis is done for GBR; in Sec. 9.1.4 we perform a comparison between the parameters of the model found for the two countries and we show the results of simulations. Furthermore, we use two statistical tests, i.e. ANOVA and Kruskal-Wallis, to confirm the dependence between the values of the contact frequency and the containment measures.

9.1.2 Mathematical model

The simplest epidemic model is the well-known SIR model [95, 96]. It arises as a deterministic model, that consists of a system of ordinary differential equations, describing the time evolution of three classes: Susceptible (S), Infected (I) and Recovered (R). If the class of Dead (D) people is also considered, the model takes the name of SIRD. Since the COVID-19 has a relevant incubation period [97] and an identifiable period from infection to recovery [98], in [79] a SIRD model with time delays has been proposed as follows.

We suppose that the disease has an incubation time τ_1, a healing time τ_2 and a death time τ_3. Let $t \geq \tau_1$. At time $t + \Delta t$ the number of the susceptibles, $S(t+\Delta t)$, decreases because some of the susceptibles at time t, $S(t)$, get infected. The number of the susceptibles that become infected over the time frame Δt is proportional to $S(t)$ times the fraction of infected people at the previous time $t-\tau_1$, $I(t-\tau_1)/N$, due to the incubation time, where N is the entire population size. The proportionality factor is the contact frequency β of a susceptible individual that leads to an infection. Moreover, for $t < \tau_1$ we suppose that new infections do not occur over the time frame Δt and, to include this assumption, we multiply for $H(t-\tau_1)$, where $H(\cdot)$ is the Heaviside step function. Therefore we have

$$\frac{S(t+\Delta t) - S(t)}{\Delta t} = -\beta S(t) \frac{I(t-\tau_1)}{N} H(t-\tau_1), \tag{9.1}$$

and for Δt going to 0 we get

$$S'(t) = -\beta S(t) \frac{I(t-\tau_1)}{N} H(t-\tau_1).$$

Let α be the mortality rate which is defined as the Infection Fatality Ratio (IFR), i.e. the ratio between the number of deaths from disease and the number of infected individuals. To describe the recovering mechanism we assume that the increase of recovered people at time t is due to the decrease of susceptible people at time $t-\tau_2$ multiplied by $1-\alpha$, that is

$$R'(t) = -(1-\alpha) S'(t-\tau_2).$$

In a similar way, we model the death mechanism, obtaining

$$D'(t) = -\alpha S'(t-\tau_3).$$

Finally, the variation of infected is obtained by the sum of three contributions: the first one is the opposite of the variation of the susceptibles, the second one is the opposite of the variation of the recovereds and the last one is the opposite of the variation of the deads. Indeed, an individual who gets infected leaves the S class and joins the I class; an infected individual that recovers, passes from the I class to the R class; an infected individual that dies passes from the I class to the D class.

From these considerations, the following equations of the SIRD deterministic model are proposed

$$\begin{cases} S'(t) = -\beta S(t)\dfrac{I(t-\tau_1)}{N}H(t-\tau_1), \\ I'(t) = \beta S(t)\dfrac{I(t-\tau_1)}{N}H(t-\tau_1) + (1-\alpha)S'(t-\tau_2) + \alpha S'(t-\tau_3), \\ R'(t) = -(1-\alpha)S'(t-\tau_2), \\ D'(t) = -\alpha S'(t-\tau_3). \end{cases} \tag{9.2}$$

This model falls into the class of differential delay equations with multiple time lags. The theory of time-delayed differential equations is an active research topic. The interested reader can be referred to [99] for an overview. Regarding the specific problem of this chapter, a qualitative theoretical analysis is not provided. Some analytic results valid in a more general class can be found in [100].

By substituting the expression of S' given by the first equation of the system (9.2) in the remaining equations of the system, this latter can be rewritten as

$$\begin{cases} S'(t) = -\beta S(t)\dfrac{I(t-\tau_1)}{N}H(t-\tau_1), \\ I'(t) = \beta S(t)\dfrac{I(t-\tau_1)}{N}H(t-\tau_1) + \\ \qquad -(1-\alpha)\left[\beta S(t-\tau_2)\dfrac{I(t-\tau_1-\tau_2)}{N}H(t-\tau_1-\tau_2)\right] \\ \qquad -\alpha\left[\beta S(t-\tau_3)\dfrac{I(t-\tau_1-\tau_3)}{N}H(t-\tau_1-\tau_3)\right], \\ R'(t) = (1-\alpha)\left[\beta S(t-\tau_2)\dfrac{I(t-\tau_1-\tau_2)}{N}H(t-\tau_1-\tau_2)\right], \\ D'(t) = \alpha\left[\beta S(t-\tau_3)\dfrac{I(t-\tau_1-\tau_3)}{N}H(t-\tau_1-\tau_3)\right]. \end{cases} \tag{9.3}$$

Moreover, to include the effect of the vaccination campaign we improve the model by introducing the variable V which represents the total number of cumulative vaccinated people. The aim of the vaccination campaign is to decrease the number of susceptible individuals and to weaken the pandemic. Let us consider eq. (9.1) and we subtract at the right-hand side the variation of vaccinated people over the time frame Δt, that is

$$\frac{S(t+\Delta t) - S(t)}{\Delta t} = -\beta S(t)\frac{I(t-\tau_1)}{N}H(t-\tau_1) - \frac{V(t+\Delta t) - V(t)}{\Delta t}$$

and for Δt going to 0 we get

$$S'(t) = -\beta S(t)\frac{I(t-\tau_1)}{N}H(t-\tau_1) - V'(t).$$

We do not provide a model for $V(t)$ because in the applications of the next sections we get its values from data. Another improvement of the model consists to consider β as a function of time, whose expression will be explained below.

Therefore, we propose the following SIRDV model

$$\begin{cases} S'(t) = -\beta(t)S(t)\dfrac{I(t-\tau_1)}{N}H(t-\tau_1) - V'(t), \\ I'(t) = \beta(t)S(t)\dfrac{I(t-\tau_1)}{N}H(t-\tau_1) \\ \qquad -(1-\alpha)\left[\beta(t-\tau_2)S(t-\tau_2)\dfrac{I(t-\tau_1-\tau_2)}{N}H(t-\tau_1-\tau_2)\right] \\ \qquad -\alpha\left[\beta(t-\tau_3)S(t-\tau_3)\dfrac{I(t-\tau_1-\tau_3)}{N}H(t-\tau_1-\tau_3)\right], \\ R'(t) = (1-\alpha)\left[\beta(t-\tau_2)S(t-\tau_2)\dfrac{I(t-\tau_1-\tau_2)}{N}H(t-\tau_1-\tau_2)\right], \\ D'(t) = \alpha\left[\beta(t-\tau_3)S(t-\tau_3)\dfrac{I(t-\tau_1-\tau_3)}{N}H(t-\tau_1-\tau_3)\right]. \end{cases} \tag{9.4}$$

In (9.4) the function $\beta(t)$ is modeled as a piecewise constant function, that depends on the more or less restrictive policies along all the days considered, that is

$$\beta(t) = \begin{cases} \beta_0, & T_{min} \le t \le t_0, \\ \beta_1, & t_0 < t \le t_1, \\ \vdots & \vdots \\ \beta_i, & t_{i-1} < t \le t_i, \\ \vdots & \vdots \\ \beta_n, & t_{n-1} < t \le T_{max}, \end{cases} \tag{9.5}$$

where $\beta_0, \beta_1, \cdots, \beta_i, \cdots, \beta_n$ and $t_0, t_1, \cdots, t_i, \cdots, t_{n-1}$ are parameters to be estimated, and T_{min} and T_{max} correspond to the first and last day of the investigated period, respectively. We note that $0 \le \beta(t) \le 1$ and if $\beta(t) \approx 1$ it means that the contact frequency is greater and there are few restrictive measures; on the contrary, if $\beta(t) \approx 0$ it implies a lockdown period.

Upon these considerations, we would like to find the parameters needed in the proposed model by a non-linear optimization procedure based on the Nelder-Mead method , implemented in MATLAB [101]. Some convergence properties of the method in low dimensions can be found in [102]. The target is the minimization of the functional

$$J = \|I - I_d\| + \|R - R_d\| + \|D - D_d\|,$$

where $\|\cdot\|$ is the 2-norm, I, R and D are the numerical solutions of the model and I_d, R_d and D_d are the same quantities given by official data for GBR and

ISR, i.e. the actual number of infected, the cumulative number of recovered and the cumulative number of deaths.

9.1.3 Simulations and results

In this section, the numerical approach is presented and the results of the simulations are reported and commented. We analyze the COVID-19 epidemic behavior in two different countries: ISR and GBR. The time interval goes from the onset of the pandemic and includes several waves of infection. The dataset used for both countries has been taken from [93].

Numerical approach

In order to find numerical solutions of the system (9.4), we adopt a first-order finite differences scheme. Let us fix a temporal grid $T_{min} = t_0 < t_1 < ... < t_M = T_{max}$ of constant time step Δt small enough to guarantee the numerical stability. We introduce the numerical approximations $S_k \approx S(t_k)$, $I_k \approx I(t_k)$, $R_k \approx R(t_k)$, $D_k \approx D(t_k)$, $V_k \approx V(t_k)$, $\beta_k \approx \beta(t_k)$ for $k = 0, 1, ..., M$, and we discretize the system (9.4) as follows

$$\begin{aligned}
S_{k+1} =& S_k - \frac{\Delta t}{N}\beta_k S_k I_{k_1} H(t_k - \tau_1) - (V_{k+1} - V_k),\\
I_{k+1} =& I_k + \frac{\Delta t}{N}\beta_k S_k I_{k_1} H(t_k - \tau_1)\\
&- (1-\alpha)\frac{\Delta t}{N}\beta_{k_2} S_{k_2} I_{k_{12}} H(t_k - \tau_1 - \tau_2)\\
&- \alpha\frac{\Delta t}{N}\beta_{k_3} S_{k_3} I_{k_{13}} H(t_k - \tau_1 - \tau_3),\\
R_{k+1} =& R_k + \frac{\Delta t}{N}(1-\alpha)\beta_{k_2} S_{k_2} I_{k_{12}} H(t_k - \tau_1 - \tau_2),\\
D_{k+1} =& D_k + \alpha\frac{\Delta t}{N}\beta_{k_3} S_{k_3} I_{k_{13}} H(t_k - \tau_1 - \tau_3),
\end{aligned}$$

where the indexes k_1, k_2, k_3, k_{12} and k_{13} are given by

$$k_j = \max\left\{0, \left\lfloor \frac{t_k - \tau_j}{\Delta t} \right\rfloor\right\} \qquad j = 1, 2, 3,$$

$$k_{1m} = \max\left\{0, \left\lfloor \frac{t_k - \tau_1 - \tau_m}{\Delta t} \right\rfloor\right\} \qquad m = 2, 3,$$

with $\lfloor \cdot \rfloor$ the floor function.

ISR analysis

We consider the data in the temporal range that goes from the day of detection of the first infected, i.e. February 21, 2020, until April 30, 2021. For each variable, the dataset contains a value for each of the 435 days, but for the numerical

solutions of the system (9.4) it is needed to fix a temporal grid with a smaller step size Δt. For this reason, we use the spline interpolation of data to have a match with different vector lengths.

In the dataset the number of vaccines is reported, that is the cumulative number of administrated doses. In the proposed model the number of vaccinated people is needed. Therefore, in order to estimate the number of vaccinated people, we divide the number of doses by 1.7, considering the number of people that have received two doses of vaccine.
In Tab. 9.1 the adopted values of $\alpha, \tau_1, \tau_2, \tau_3$ are reported. The value of α is estimated by dividing the number of deaths by the number of infected people and averaging the result.

Parameter	**Value**
α	0.0085
τ_1	5.5 d
τ_2	17 d
τ_3	20 d

Table 9.1: Parameters adopted for the simulation in the case of ISR.

In order to have a more precise agreement between our model and data, we divide the investigated period of time into several periods. In this case, we select four periods: the first one from day 1 until day 98, the second one from day 99 until day 200, the third one from day 201 until day 300, the fourth one from day 301 until day 435. Each period is associated with an epidemic wave in which we recognize a proper number of phases of diffusion depending on the different restriction policies adopted. In particular, stronger restrictions correspond to lower values of $\beta(t)$ and vice versa. More precisely, we consider 2 phases for the first and third wave, and 3 phases for the second and fourth one.

For the optimization procedure, we adopt the following strategy. We find the fitting parameters in each period corresponding to a single epidemic wave. Then the data are merged and the optimization is applied to the entire dataset. The overall results are shown in Fig. 9.1 and the corresponding fitting parameters are reported in Tab. 9.2. We observe that the proposed model is able to keep the several waves of infection. This is primarily due to the fine modeling of $\beta(t)$. We notice a good agreement between the simulated curves and the data.

In order to quantify the importance of vaccines, we compare the results with the solutions of system (9.3), adopting the same parameters of Tab. 9.2. The obtained results are shown in Fig. 9.2. We observe that without vaccines the number of infected and dead people would increase exponentially. This is due to a quite high value of the contact frequency in the last intervals of time. We deduce that an increasing number of vaccinated people allow the governments

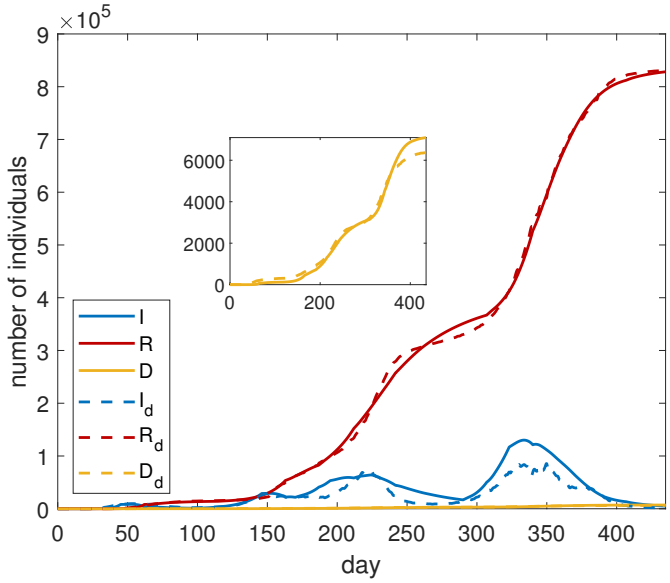

Figure 9.1: Comparison between SIRDV model (system (9.4)) with parameters of Tab.9.2 (continuous lines) and ISR data (dashed lines). In the inset, the curve of the deaths is magnified.

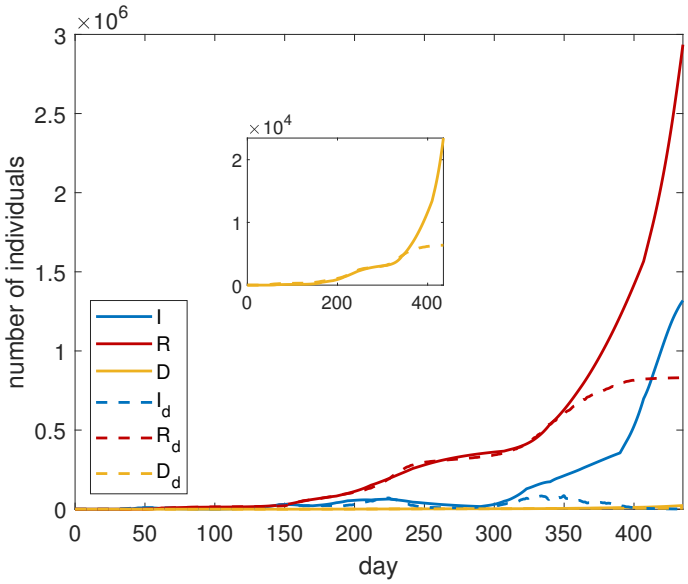

Figure 9.2: Comparison between SIRD model (9.3), with parameters of Tab. 9.2 (continuous lines), and ISR data (dashed lines). In the inset, the curve of the deaths is magnified.

to adopt a less restrictive policy, remarking in this way the importance of the vaccination campaign.

Estimated parameters			
β	**Value**	t	**Value**
β_0	0.72152 d^{-1}	t_0	45.04975 d
β_1	0.026274 d^{-1}	t_1	98.01835 d
β_2	0.14467 d^{-1}	t_2	146.0086 d
β_3	0.046757 d^{-1}	t_3	170.0053 d
β_4	0.0969 d^{-1}	t_4	195.0024 d
β_5	0.0645 d^{-1}	t_5	224.9946 d
β_6	0.0444 d^{-1}	t_6	289.993 d
β_7	0.13793 d^{-1}	t_7	323.0012 d
β_8	0.080843 d^{-1}	t_8	389.9505 d
β_9	0.12619 d^{-1}		

Table 9.2: Fitting parameters for the SIRDV model (9.4) applied to ISR.

Since the crucial point for containing the spread of the disease consists to prevent new cases, some parameters can be defined to provide insight into the state of the pandemic. One of the parameters used for that purpose is the basic reproduction number R_0. It represents the average number of infections generated by a single infected individual if all the individuals are susceptible. In the case of an ongoing outbreak, it is defined the effective reproduction number R_t, which is the average number of new infections generated by a single infected individual at time t considering the part of the population of susceptible individuals. Following [103], we calculate the R_t numerically by using the results of our simulations. In particular, from the first two equations of system (9.2) we get

$$\frac{\mathrm{d}I}{\mathrm{d}S} = -1 + \frac{1}{R_t(t)}.$$

It can be discretized in an interval $[t_i, t_{i+1}]$ where R_t is constant obtaining

$$R_t(t_i) = \frac{1}{\frac{\Delta_i I}{\Delta_i S} + 1},$$

where $\Delta_i I = I(t_i) - I(t_{i-1})$ and $\Delta_i S = S(t_i) - S(t_{i-1})$.

In the case of ISR, we show the results of the numerical evaluation of R_t in Fig. 9.3. It is calculated daily. The plotted time interval starts from April 11, 2020, that is after 50 days from the detection of the first infection. This choice is due to the fact that in the first period the curves are flat, leading to inaccurate evaluation of R_t. We observe that after approximately 300 days the effect of vaccination becomes relevant in order to reduce the R_t values.

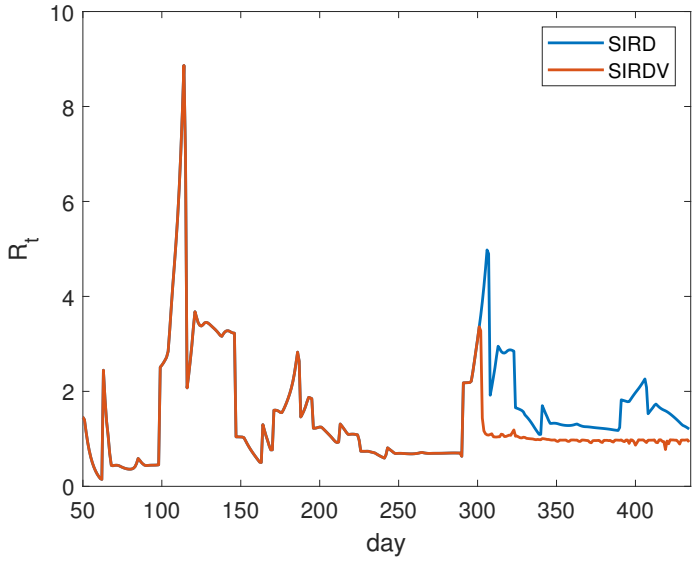

Figure 9.3: Daily trend of R_t for ISR. Both the cases of SIRD and SIRDV models are investigated.

GBR analysis

We consider the data in the temporal range that goes from the day of detection of the first infected, i.e. January 31, 2020, until April 30, 2021. As in the case of ISR, we perform the spline interpolation of the data.

Similar to ISR, to estimate the number of people vaccinated, we divide the number of doses provided by data by 1.45, taking into account the number of people that have received two doses of vaccine. Since GBR does not report the number of people recovered from COVID-19, to obtain the missing data we adopt the following formula

$$R_d(t) = (1 - \alpha) I_d(t - \tau_1 - \tau_2),$$

where $R_d(t)$ represents the number of recovered people at the time t, α represents the mortality rate and I_d represents the number of infected people at previous time $t - \tau_1 - \tau_2$.

In Tab. 9.3 we report the adopted values of $\alpha, \tau_1, \tau_2, \tau_3$ in the simulation. In this case, the value of α is estimated by dividing the number of total deaths by the number of total infected people.

As we have done for ISR, to have a more precise agreement between our model and data, we split the investigated period of time into three parts: the first one from day 1 until day 221, the second one from day 222 until day 318, the third one from day 319 until day 456. Each period is associated with a wave of infection, in which we recognize a proper number of phases of diffusion. More precisely, we consider three phases for the first and the second wave and

Parameter	Value
α	0.0289
τ_1	5.5 d
τ_2	20 d
τ_3	20 d

Table 9.3: Parameters adopted for the simulation in the case of GBR

four phases for the third one. After finding in each period the best parameters thanks to the optimization, the data are merged again and the optimization is applied to the entire dataset. The results are shown in Fig. 9.4 and the final fitting parameters are reported in Tab. 9.4. In this case, a very good agreement between the numerical results and the data is noticeable.

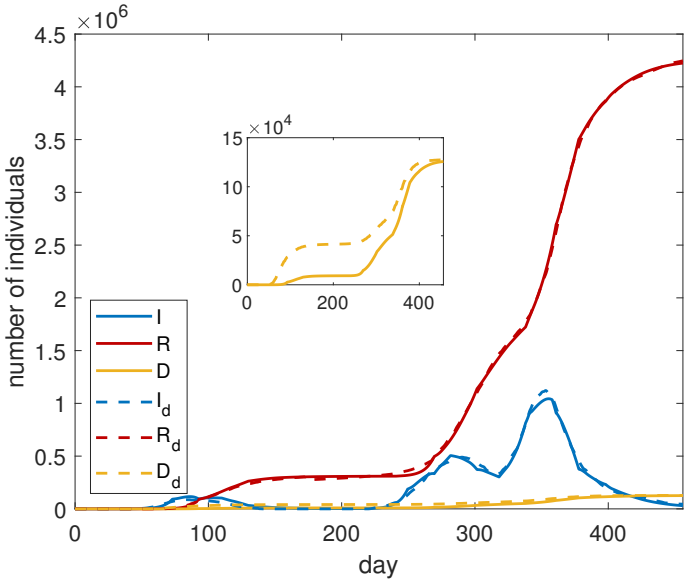

Figure 9.4: Comparison between SIRDV model (9.4) with parameters of Tab. 9.4 (continuous lines) and GBR data (dashed lines). In the inset, the curve of the deaths is magnified.

To understand the importance of vaccines, we solve system (9.3), which does not take into account the presence of vaccines, with the parameters of Tab. 9.4, obtaining the results of Fig. 9.5. We can deduce that without a vaccination campaign the infected curve does not substantially increase in the short time because it is affected by the effects of the last lockdown. However, in the medium and long time, we expect a different behaviour.

The analysis of R_t is performed with the same technique presented in the previous section for ISR. The numerical results are plotted in Fig. 9.6. Here

Estimated parameters			
β	**Value**	t	**Value**
β_0	0.3746 d^{-1}	t_0	73.0302 d
β_1	0.0483 d^{-1}	t_1	110.0003 d
β_2	0.0183 d^{-1}	t_2	220.9293 d
β_3	0.3239 d^{-1}	t_3	249.5555 d
β_4	0.0771 d^{-1}	t_4	281.6010 d
β_5	0.0393 d^{-1}	t_5	318.0524 d
β_6	0.1054 d^{-1}	t_6	340.9996 d
β_7	0.0583 d^{-1}	t_7	357.9999 d
β_8	0.0254 d^{-1}	t_8	377.9999 d
β_9	0.0409 d^{-1}		

Table 9.4: Fitting parameters for the SIRDV model (9.4) applied to GBR.

the considered time interval starts from March 21, 2020, after 50 days from the detection of the first infection. In this case, we notice the presence of high peaks. This is a numerical effect because the peaks correspond to the time periods in which a low number of infections are registered (see Fig. 9.4). In this situation, the numerical estimation of R_t does not result accurate.

9.1.4 Pandemic containment measures effects comparisons

The most influential pandemic containment measure is the vaccination campaign which affects the contact frequency reduction described by the function β.

In ISR the vaccination campaign has been really effective because most of the population has received two doses of vaccine until 30 April 2021. At the same time, the pandemic containment measures during the vaccination period had been less restrictive with respect to the lockdown periods; for these reasons, it is possible to notice a substantial difference between the SIRD and the SIRDV model in ISR. In the SIRD model, the combination of the absence of the vaccination campaign with a high β value caused an additional infection wave.

In GBR the vaccination campaign has been less effective because most of the population has received only one dose of vaccine, while simultaneously the pandemic containment measures have been more stringent than in ISR during the vaccination campaign. From Fig.9.5 we can deduce that without a vaccination campaign the infected curve does not substantially increase in the short time

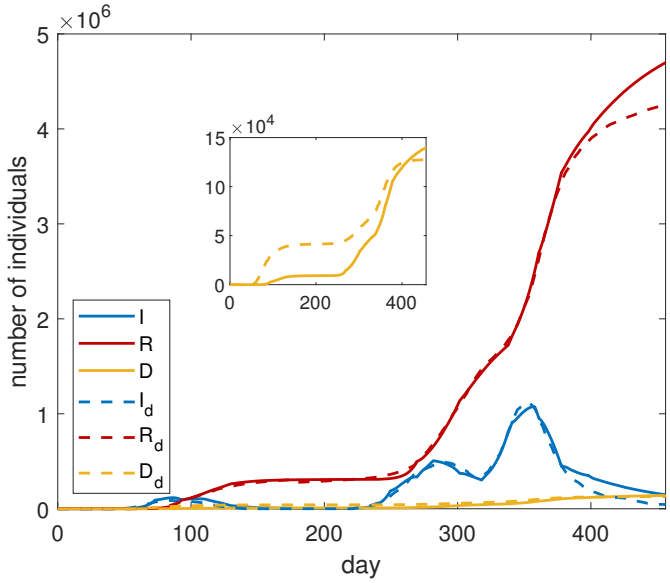

Figure 9.5: Comparison between SIRD model (9.3) with parameters of Tab.9.4 (continuous lines) and GBR data (dashed lines). In the inset, the curve of the deaths is magnified.

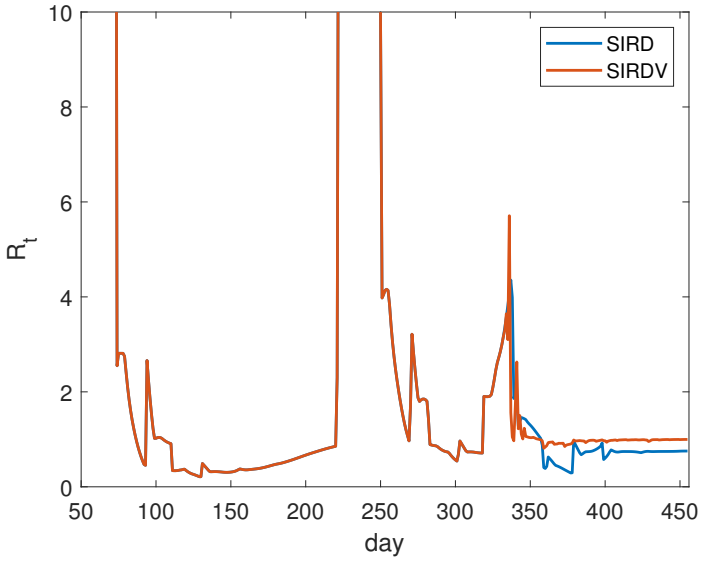

Figure 9.6: Daily trend of R_t for GBR. Both the cases of SIRD and SIRDV models are investigated.

because social distancing measures are still adopted in GBR in such a period, corresponding to a low value for β. However, in medium and long time, we expect a spread increment in both cases with and without vaccination, especially

if restrictions are released.

The crucial issue for the model is the function $\beta(t)$. Its values depend on specific restriction measures. It is possible to recognize four levels of restrictions in each country: total opening, corresponding to an absence of restrictions; partial opening, which implies an opening but controlled phase to isolate the infected individuals; partial closure, describing a restrictive situation but not totally; lockdown, that is the most restrictive level. In Tab. 9.5 we report the values of $\beta(t)$ corresponding to the four restriction levels explained before, for both countries analyzed in this study.

Policy measure	β	**Value**
Total opening	β_0	0.3746 d^{-1}
Partial closure	β_1	0.0483 d^{-1}
Lockdown	β_2	0.0183 d^{-1}
Partial opening	β_3	0.3239 d^{-1}
Partial closure	β_4	0.0771 d^{-1}
Lockdown	β_5	0.0393 d^{-1}
Partial opening	β_6	0.1054 d^{-1}
Partial closure	β_7	0.0583 d^{-1}
Lockdown	β_8	0.0254 d^{-1}
Partial closure	β_9	0.0409 d^{-1}

Policy measure	β	**Value**
Total opening	β_0	0.7215 d^{-1}
Lockdown	β_1	0.0262 d^{-1}
Partial opening	β_2	0.1446 d^{-1}
Partial closure	β_3	0.0467 d^{-1}
Partial opening	β_4	0.0969 d^{-1}
Partial closure	β_5	0.0645 d^{-1}
Lockdown	β_6	0.0444 d^{-1}
Partial opening	β_7	0.1379 d^{-1}
Partial closure	β_8	0.0808 d^{-1}
Partial opening	β_9	0.1261 d^{-1}

Table 9.5: GBR (left table) and ISR (right table) function $\beta(t)$ values related to the restriction measures.

Policy measure	**β values for GBR**	**β values for ISR**
Total opening	0.3746 d^{-1}	0.7215 d^{-1}
Partial opening	0.1054 d^{-1}, 0.3239 d^{-1}	0.0969 d^{-1}, 0.1261 d^{-1}, 0.1379 d^{-1}, 0.1446d^{-1}
Partial closure	0.0409 d^{-1}, 0.0483 d^{-1}, 0.0583 d^{-1}, 0.0771 d^{-1}	0.04675 d^{-1}, 0.0645 d^{-1}, 0.0808 d^{-1}
Lockdown	0.0183 d^{-1},0.0254 d^{-1} , 0.0393 d^{-1}	0.0262 d^{-1}, 0.0444 d^{-1}

Table 9.6: $\beta(t)$ values grouped by total opening, partial opening, partial closure and lockdown for the two countries.

In order to have a confirmation of the dependence between the β values and the policy measures, a one-way ANalysis Of VAriance (ANOVA) is performed. To apply this test the data are organized into several groups representing a sample extracted from a proper population and each population represents the results of a specific factor level.
In this case, both for GBR and ISR, the factor is the policy measure and its levels are: total opening, partial opening, partial closure, and lockdown. Instead of a sample extracted from a certain population, the β values grouped as in Tab. 9.6 have been used.
The Fisher statistic (F) value is computed both for GBR and ISR, and it is compared with the quantile of order 0.95 of the Fisher distribution with (3,6) degrees of freedom ($f^F_{0.95}(3,6) = 4.7571$). The results are reported in Tab. 9.7.

ANOVA test results		
	GBR	**ISR**
p-value	0.0095	$3.61 \cdot 10^{-7}$
F	9.97	362.36

Table 9.7: ANOVA test results for GBR and ISR.

It is evident that there is a strong dependence of the β values on the policy measures, because of a very low significance level (p-value).

Since the number of β values, grouped according to the policy measures, is not so high, we performed the ANOVA test also in a non-parametric way, by means of the Kruskal-Wallis test. The results are reported in Tab. 9.8.

Kruskal-Wallis test results		
	GBR	**ISR**
p-value	0.0424	0.0424
Statistics	8.18	8.18

Table 9.8: Kruskal-Wallis test results for GBR and ISR.

In this case, the dependence of β on the policy measures is still strong but with a higher p-value. We remark that the same values both for GBR and ISR are obtained because the Kruskal-Wallis test works with ranks instead of data and in this case the statistic results are similar.

Thanks to these considerations, the values in Tab. 9.6 can be useful initial guesses to predict the pandemic trend based on the particular policy measures applied by the governments.

9.2 AMBEATion: Analog Mixed-Signal Back-End Design Automation with Machine Learning and Artificial Intelligence Techniques

For the competitiveness of the European economy, automation techniques in the design of complex electronic systems are a prerequisite for winning the global chip challenge. Specifically, while the physical design of digital Integrated Circuits (ICs) can be largely automated, the physical design of Analog-Mixed-Signal (AMS) ICs built with an analog-on-top flow, where digital subsystems are instantiated as Intellectual Property (IP) modules, is still carried out predominantly by hand, with a time-consuming methodology. The AMBEATion consortium, including global semiconductor and design automation companies as well as leading universities, aims to address this challenge by combining classic Electronic Design Automation (EDA) algorithms with novel Artificial Intelligence and Machine Learning (ML) techniques. Specifically, the scientific and technical result expected at the end of the project will be a new methodology, implemented in a framework of scripts for AMS placement, internally making use of state-of-the-art AI/ML models, and fully integrated with Industrial design flows. With this methodology, the AMBEATion consortium aims to reduce the design turnaround-time and, consequently, the silicon development costs of complex AMS ICs.

We remark that the results of this section are original and they have been accepted as a conference paper by DATE2024 Multi-Partner Projects Co-Chairs. The authors are: Giulia Elena Aliffi, Joao Baixinho, Dalibor Barri, Francesco Daghero, Nicola Di Carolo, Gabriele Faraone, Michelangelo Grosso, Daniele Jah-

ier Pagliari, Jiri Jakovenko, Vladimír Janíček, Dario Licastro, Vazgen Melikyan, Matteo Risso, Vittorio Romano, Eugenio Serianni, Martin Štastný, Patrik Vacula, Giorgia Vitanza, Chen Xie. The authors come from different institutions like University of Catania, Czech Technical University, Prague, Politecnico di Torino, STMicroelectronics and Synopsys. Everyone is involved in the AMBEATion project.

9.2.1 Introduction

Improving the development process of electronic systems is an essential factor for the competitiveness of the European economy. In fact, most key technology areas at the forefront of tomorrow's society, including among others the Internet of Things (IoT), Smart Driving, Industry 4.0, and Active Assisted Living (AAL), rely on complex electronic devices. These Smart Systems, are composed of heterogeneous parts, providing different functionalities, including digital and analog blocks, sensors, actuators, power generation and storage, etc. In this context, on-chip heterogeneous integration is fundamental to improve. Therefore, a leading role is held by Analog Mixed-Signal Integrated Circuits (AMS-ICs) where Analog and Digital domains are strictly intertwined.

In AMS ICs, digital blocks usually carry out computational tasks, and their design and physical implementation are highly automated by means of highly specialized flows and optimized standard cell libraries [104]. On the other hand, analog parts realize functionalities. Despite numerous efforts [105–107], automated and universally valid analog physical design flows are not yet available. The reason for this discrepancy is rooted in the inherently higher difficulty of the analog layout problem. In fact, not only are analog circuits more sensitive to noise and variability effects but they also have larger and more complex sets of constraints (e.g., gain, bandwidth, distortion, etc), all of which affect performance [108, 109]. Additionally, different specific classes of analog circuits require different metrics and trade-offs [109].

Machine Learning (ML) and Artificial Intelligence (AI) techniques have been introduced in the Electronic Design Automation (EDA) industry since several years to improve the efficiency and scalability, as well as the Quality of Results (QoR) of design and verification tools. ML has been applied ubiquitously, from synthesis to floorplanning, place&route, timing analysis, analog design and simulation [110, 111]. However, while digital flows greatly benefits from the integration with ML and AI techniques [110, 111], a wide gap still exists in this respect within the analog domain [112].

This paper introduces the Marie Skłodowska-Curie Research and Innovation Staff Exchange project **AMBEAtion** (**A**nalog **M**ixed-signal **B**ack-**E**nd design **A**utoma**tion** with Machine Learning and Artificial Intelligence Techniques). The project aims to improve the quality and productivity of AMS physical design,

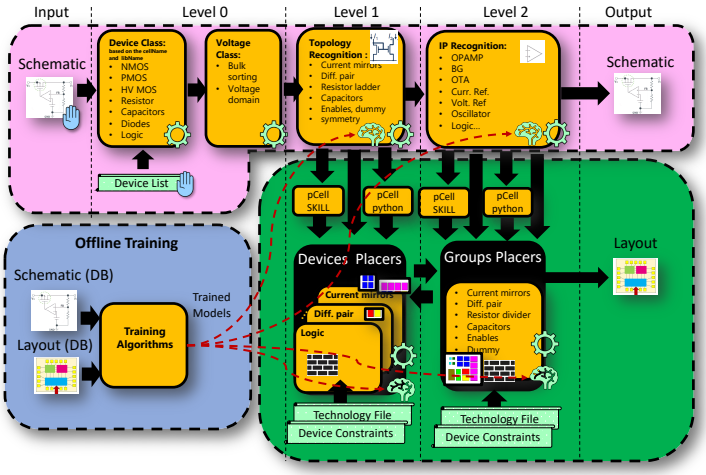

Figure 9.7: The AMBEATion flow.

with particular focus on device placement, by developing a new methodology implemented in a framework of scripts, code parsers, automated processes and simulation tools, internally making use of a combination of classic EDA algorithms, and novel AI and ML models. A further intent of the AMBEATion project is to reach full integration with Industrial Design flows by leading EDA tool providers, thus allowing a seamless addition of the methodology to existing AMS designers' workflows, as well as easing the access to large databases of past designs.

The scientific contributions within the AMBEATion consortium are, therefore, strongly driven by the needs of industrial partners, while academic partners contribute with their expertise on AI/ML. The presence in the consortium of world leaders in EDA, System on Chip (SoC) and System in Package (SiP) design such as Synopsys and STMicroelectronics gives the partners access to a large database of existing designs on which data-driven ML algorithms can be trained. This allows to overcome one of the main limitations of current academic efforts in using AI and ML for back-end, i.e., the very limited availability of training data.

Given that the main goal of the AMBEATion project is the development of a new EDA flow for analog layout, we believe that it fully aligns with the scope of the DATE 2024 conference. With respect to the Call for Paper, the project relates perfectly to tracks DT4 ("Design and Test for Analog and Mixed-Signal Circuits and Systems, and MEMS") and D14 ("Physical Analysis and Design").

The remainder of this paper is organized as follows. In Section II we illustrate the AMBEATion flow concept, providing a general overview of all the steps and abstraction levels involved. Then, Section III, provides an overview on the current implementation of each step. Perspectives, future research directions

and lessons learned from the past months of the project are discussed in Section IV.

9.2.2 The AMBEATion Concept

At the highest level the AMBEATion Back-end flow focuses on the IC AMS placement phase. Therefore, the main element of the flow consists in a placer tool together with a set of supporting tools for realizing auxiliary functions which will be briefly described in the following section. The flow implements a novel mix of *top-down* placement steps, inspired by the techniques used in digital design, and *bottom-up* ones, specific of the analog domain [109].

Specifically, as illustrated in Figure 9.7, the AMBEATion flow is divided into three main sections: the first part processes the IC schematic, and is highlighted in pink; the second, generates the corresponding layout (green); finally, an offline phase is also included (blue) to train ML algorithms on a database of pre-existing designs. The schematic and layout processing sections are further split into five "levels", associated with an input-to-output flow with increasing abstraction levels:

The Input Level deals with the processing of input schematic/netlist and layout database files. Layouts can also be an input to the flow during the training phase of ML algorithms, whereas they are only an output during normal usage. The flow supports several industrial standards in terms of file format for schematic and layouts, including the IC CAD Open Access (OA) database format, as well as Circuit Design Language (CDL) netlists, and GDS-II layouts.

Level 0 contains simple pre-processing scripts aimed at simplifying the subsequent steps of the flow. In particular, it aims to recognize all classes of IC components which are present in the schematic and to differentiate devices based on different voltage classes or bulk connections. This level adds a layer of abstraction that makes the flow at least partially independent from the considered IC technology and device details. After Level 0, the rest of the flow is entirely realized with internal technology-independent netlist and layout database formats, based on JSON.

Level 1 is in charge of the generation of individual devices by processing PCells (or similar), and of their placement onto small topologies (such as current mirrors, differential pairs, capacitor dividers, etc). In order to do so, at the netlist level, a *Topology Recognition* script identifies different elementary functional topologies in the input schematic/netlist. At layout level, a *Device Placer* positions the devices' layouts generated by PCells within each identified topology, by respecting both general technology constraints and additional topology-specific constraints.

Level 2 deals with the placement of devices and elementary topologies identified at Level 1 onto an IP or block. At netlist level, the *IP Recognition* block identifies the parts of the netlist belonging to each IP. At layout level, the *Group Placer* positions them in the layout. This placement process is closely interconnected with the device placement of Level 1, and multiple feedback iterations between the two are foreseen.

The Output Level it's where the final placement layout is produced, as well as and detailed reports on the flow execution.

The of multiple IPs in the top-level circuit, considering signal/supply domains, clock routing for the digital part, etc, as well as packaging and bonding issues, are out of the scope of the automation flow foreseen in the AMBEATion project. However, the flow can be conceptually extended with additional abstraction levels (Level 3, 4, etc) to deal with these aspects in the future. As mentioned, the flow does not simply go from one level to the next in a "linear" way. Rather, the levels provide feedback to each other in an iterative way (e.g., the group placement will depend on the individual topologies placement, but will also influence the latter).

The offline training phase processes databases of human-generated inputs and outputs for any step that needs to be implemented by means of ML techniques, be it related to digital or analog components, and to any abstraction level. The obtained trained models are then used in inference-mode in various schematic- or layout-processing steps of the flow. In particular, Figure 9.7 is annotated with a "brain" icon to identify steps that internally use ML, and with a "wheel" icon to indicate classic rule-based algorithms. As can be seen, for many steps, both classic and ML-based solutions are available, enabling a precise comparative assessment of the benefits of AI in this domain. Lastly, a "hand" icon indicates human-generated inputs. In the next section, we go in more detail on the flow steps implemented at the current state of the project.

9.2.3 Implementation

Similar to industrial EDA tools, the AMBEATion flow can be accessed both with a Command Line Interface (CLI) and with a simple Graphical User Interface (GUI), shown in Figure 9.8. The flow is built as an interconnection of modular software components, to simplify extensibility and maintainability, and to permit an easy swap between multiple implementations of the same step (e.g., classical vs ML-based, for comparison). To this end, all exchange of information between steps occurs through a unified file format based on the JSON standard. At Input Level, the JSON is substantially a translation of a common netlist format (CDL, OA, etc). Then, each step modifies or enriches this internal database, e.g., adding physical device information, placement coordinates, etc. The entire

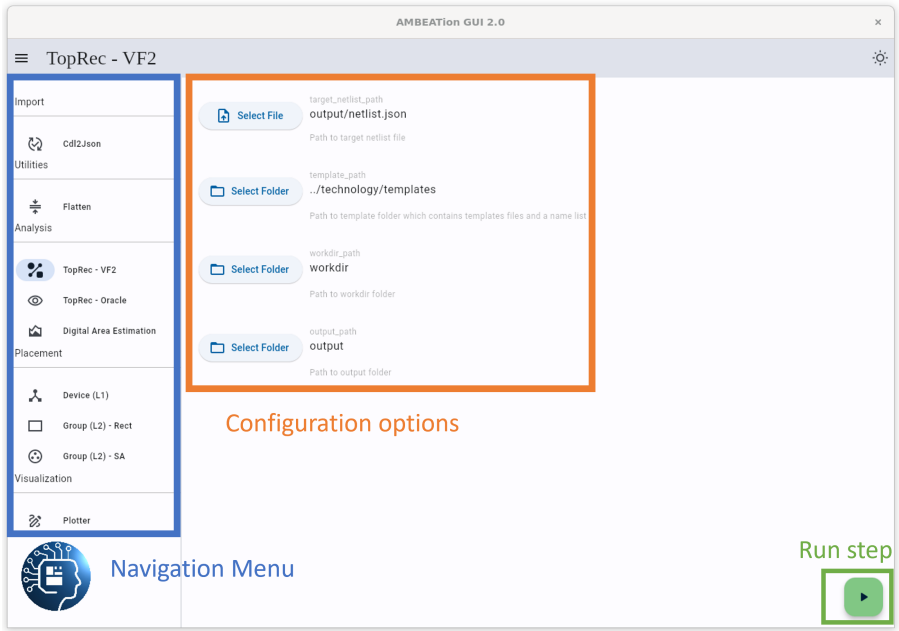

Figure 9.8: An overview of the AMBEAtion GUI with main components highlighted. The navigation pane contains an entry for each pass of the AMBEATion flow currently implemented. Clicking on each item will display a different set of configuration options in the main window, which can then be changed by users. It also permits opening plots, log files, etc.

AMBEATion codebase is written in Python. In the following we briefly illustrate the functionality of each component of the flow.

Level 0 (Schematic): Input Conversion and Pre-processing

To implement Level 0 of Figure 9.7, a set of scripts have been developed to convert standard netlist formats into our internal JSON-based, vendor-independent "lingua franca", and assign each device to its respective class and voltage group, thus reducing the dependency on a specific technology node.

The main entities described in the internal database at this stage include: a) *cells*, i.e., sub-circuit definitions; b) *instances* of elementary devices or other sub-circuits within a cell; c) *libraries*, i.e., sets of cells, usually grouped by common functionality. Each entity contains several attributes, depending on its type. In later stages, the database will be enhanced with new entities, such as *topologies*, i.e., groups of devices identified at Level 1, forming a higher-level structure (e.g., a current mirror). Further, existing entities will receive new attributes, e.g., x/y layout coordinates for each device.

Level 1 (Schematic): Topology Recognition

The objective of this step is to identify functional topologies within the schematic, e.g., current mirrors, differential pairs, etc. This identification process is essential for accurately specifying constraints in the layout placement phase. Topology recognition can be converted to a subgraph isomorphism problem between a template graph (e.g. a current mirror) and the target graph (e.g., an operational amplifier). Namely, following [113], we adopt a bipartite graph representation for netlists, with two sets of nodes, one for devices and one for nets, as shown in Figure 9.9. The AMBEATion flow currently supports two topology recognition implementations: a classical one, based on the VF2 matching algorithm [114] and a ML-based alternative using Relational Graph Convolutional Neural Networks (RGCNs) [113, 115].

The main limitation of the VF2 implementation lies in its complexity, implying very long running time on large flattened netlists. Therefore, the orders of magnitude faster RGCN version can provide significant benefits in terms of efficiency for real world use-cases. On the other hand, the ML-approach can lead to significant accuracy degradations, which can be partially coped with by means of pre- and post-processing steps, as detailed in Section 9.2.4. The output file produced by topology recognition is a JSON database containing the original netlist enriched with the extracted topologies, with their associated type, device group, and nets.

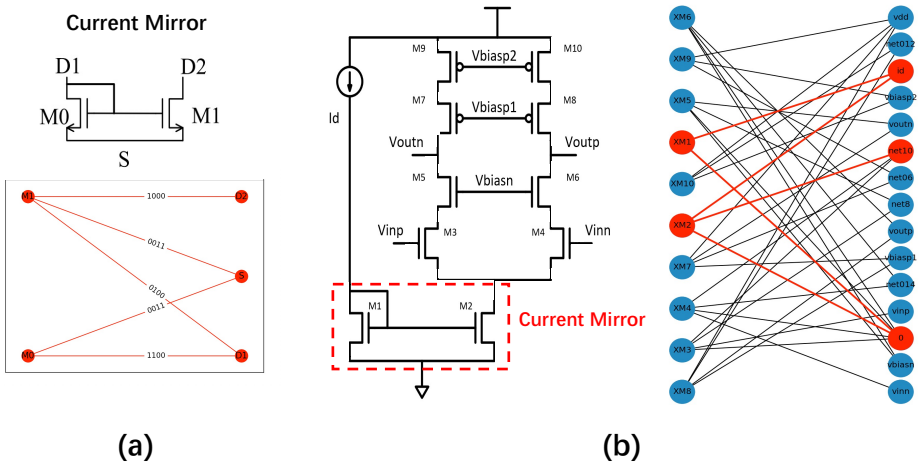

Figure 9.9: Topology recognition. An NMOS current mirror primitive (a) is represented by a pattern graph, where vertices on the left side represent devices M0 and M1 respectively and those on the right side represent nets D1, D2 and S. Similarly, a fully differential Telescopic operational transconductance amplifier (OTA) (b) is converted into a bipartite graph and one subgraph is matched the current mirror pattern graph, highlighted by red.

Level 1 (Layout): PCell Processing and Device Placement

For what concerns the layout processing, Level 2 comprises two main steps: *PCell processing* and *device placement*. The former reconstructs the polygons comprising the device's layers, extracting the correspondence between spatial coordinates in the schematic and layout representations. Additionally, it can incorporate technology-specific constraints, such as spacing requirements, into the design. Currently, AMBEATion supports PCells [116].

The Device Placer then elaborates the internal layout of each topology identified in the corresponding recognition step, using the geometrical information extracted from PCells, as well as technology-dependent constraints from a tech file. Furthermore, this step processes additional inputs relative to the type of dummy insertion required, and to the desired aspect ratio for each topology. The script then positions devices in matrix arrays which respect the user defined constraints. Moreover, to suppress the layout dependent effects (such as WPE, STI-stress etc) it reserves the necessary extra area around the matrix array. The optimization is purely analytical, and aims at approximating as well as possible the target aspect ratio, positioning devices in the appropriate number of rows.

The output of the script is an updated JSON netlist, where each device is annotated with the minimum (x_{min}, y_{min}) and maximum (x_{max}, y_{max}) coordinates of its bounding box within the topology it belongs to (if any). Coordinates are referred to (0,0) for each topology since this module does not deal with

inter-topology placement, which is handled by the Level 2 Group Placer. The Device Placer is designed so that it can be iteratively invoked from within the optimization loop of the higher-level Group Placer, each time with different input parameters (e.g., different target aspect ratios). This gives the Group Placer the freedom to "re-shape" some topologies' bounding boxes to better fit the overall IP layout.

Importantly, digital blocks within an AMS IC are treated separately for what concerns device placement. Namely, they are not placed by the AMBEATion flow directly, but rather, after being identified by topology recognition, they are offloaded to a state-of-the-art digital EDA Place And Route (PnR) tool, given their high level of automation and QoR. Therefore. However, the placer should have the freedom to reshape/resize digital blocks, similarly to the case of analog topologies. To allow this, while avoiding time-consuming iterations including full digital PnR executions, the AMBEATion flow includes a fast ML-based *PnR Fesibility estimator* for digital logic.

Digital PnR Feasibility Estimation

The role of this component is to assess whether a digital block within an AMS design can be accommodated effectively within the designated layout area, without the need of a full PnR run.

In the current version of the AMBEATion flow, the Digital PnR Feasibility module has been implemented with a Decision Tree (DT) ML model, trained to assign a feasibility score to a design, based on high-level netlist and (expected) layout characteristics, as well as technology information. A DT was selected due to its simplicity, explainability, and effectiveness with limited training samples [117]. The model is trained in a supervised way, given examples of both successful and failed back-end executions of past designs. Its inputs are features that influence the chances of successfully closing a PnR, based on domain knowledge, e.g, the layout area hypothesis and its shape factor, the initial row utilization, the number of sequential cells in the design, the clock frequency, and the total number and density of pins. Technology information, such as the number of available routing layers is also provided. Once all features are available, a feature selection step based on cross-validation can then be applied to select the subset that best generalizes on unseen data.

After training, the model learns simple if-then-else rules that assign each new design to a "bin" (leaf node) by recursively comparing its features with learned thresholds. The leaf node value is a feasibility score (in [0:1]), as shown in Figure 9.10.

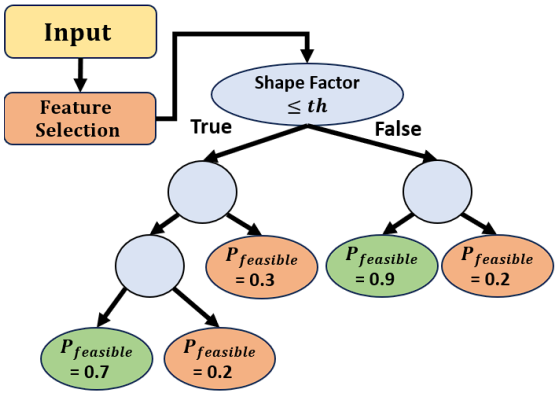

Figure 9.10: Digital Area Estimation flow overview, consisting of a first feature selection step followed by the Decision Tree inference. The output of the flow is a probability of successful PnR.

Level 2 (Schematic): IP Recognition

The goal of IP Recognition is to identify higher level structures in the circuit, such as operational amplifiers, oscillators, etc, and then constrain them accordingly for placement. Currently, this stage is not implemented, but techniques similar to those applied for Topology Recognition can be used for it too. The input, in this case, will include both individual devices and topologies identified at Level 1. ML-based approaches leveraging Graph Neural Networks are expected to work effectively in this case too, as demonstrated in [113].

Level 2 (Layout): Group Placer

The group placer (Level 2) places topology rectangles prepared by the device placer relative to each other. Thus, it forms the complete layout of a single IP block. Two alternative implementations are supported, leveraging respectively Simulated Annealing (SA) [118, 119], and Non-Linear Programming (NLP) [120, 121], two of the optimization methods considered state-of-the-art for this problem.

The SA placer leverages a "Sequence Pair" representation of the layout [122], which identifies virtual non-crossing pathways in the floorplan. Conversely, the NLP solution simply represents the x and y coordinates of the bottom-left corner of each group of devices as floating-point vectors, whose values are to be determined in the optimization process using gradient descent with adaptive estimation of first- and second-order moments [123].

Both placers can support the same optimization objectives, including area minimization, routability (e.g., Half-Perimeter Wire-Length or HWPL), etc. However, they are quite sensitive to their input hyper-parameters, as well as being entirely dependent on the L1 Placer results. To solve this, an agent-based

approach is considered to optimize the placement of each IP. Namely, the group placement process can be controlled by an AI agent (e.g., a neural network trained with Reinforcement Learning, or an Evolutionary Algorithm), which will internally invoke the Device Placers with different input parameters (e.g. aspect ratio targets), and change the hyper-parameters of the SA and NLP optimizers, until all constraints are respected, and a combined objective function is minimized.

At the end, the output layout for each IP is exported both in the internal JSON database format, as well as in the standard GDS-II format. Other Output Layer adapter scripts allow the import of the generated layout into industrial EDA tools, to implement the following design phases (routing, signoff, etc).

Utilities

Besides the main scripts to implement key placement operations, the AMBEATion flow also includes several utilities, including basic scripts such as netlist flattening using the internal JSON format, as well as an interactive layout plotter, and several other import/export and conversion tools.

9.2.4 Conclusions and Future Outlooks

Being a MSCA-RISE action, the main goal of the AMBEATion project is to put in contact European academic staff with leading industries, and vice versa, through the mechanism of secondments. In parallel, the overarching technical objective is to strengthen the competencies on AI-based AMS placement in Europe. To this end, the project takes strong inspiration from other non-EU initiatives, mainly from the U.S. NSF and DARPA programs [106, 107], building upon their work, and trying to further improve it. At the current stage, the main result achieved by the project is that of having built a flexible, modular AMS placement framework, which can function as foundational infrastructure for future research. Not only in the direction of developing new ML-enhanced EDA algorithms, but also in quantitatively and thoroughly comparing existing solutions, and in extensively evaluating them on *real-world* industrial use cases. To this end, the AMBEATion platform has been designed around a rich and easy-to-use language such as Python, and using an open, extensible and human-readable JSON-based database format. The flow is built for usability and extensibility, and is entirely cross platform. While the main evaluations have been performed on BCD8 technology by ST Microelectronics, the platform is also designed with technology independence in mind.

The most interesting results obtained up to the current stage concern the "real-world effectiveness" of ML-based AMS placement techniques. In fact, preliminary validation experiments on the flow revealed interesting insights, and highlighted

key limitations. We report here three of the main issues that have been identified during the project journey. Addressing these issues will also be the main direction of our future research in the remaining years of the project.

Data Quality and Variety while the industrial partners involved in AMBEATion have access to large databases of past designs, the main obstacle towards obtaining highly accurate with ML-based placement approaches is data *quality* rather than quantity. The available datasets are often highly imbalanced, and contain many similar samples, that do not cover the design space entirely. For instance, input graphs used to train our RGCN models for topology recognition, despite including hundreds of thousands of nodes, contain very few examples of "uncommon" topologies (all structures except current mirrors are present in far less than 1% of the total nodes). Despite applying several countermeasures at training level, such as loss function weighting, oversampling, or treating the problem as a one-class anomaly detection, this imbalance still negatively affects performance in many cases. Similarly, the training data used for Digital PnR Feasibility Estimation contains many more examples of *successful* runs than failed ones, because the outputs and logs for the latter are usually not preserved by designers. One solution we envision and we explore in the future, is the use of *synthetic data generation* by means of scripts that create from scratch or modify existing netlists and layouts. This approach has proven effective in several other domains [124]. More broadly, these limitations also provides guidance on possible updates company policies on data storage and management.

Technology Independence Many previous efforts on ML-based AMS layout focused on single technology nodes [106, 107, 113]. In AMBEATion, we found that one of the key issues in applying techniques from the state-of-the-art to build a general tool is that ML-based approaches, and often also classic ones, do not generalize well across technologies. As an example, the template library used by the VF2 algorithm for topology recognition had to be completely rewritten with respect to previous works [113] to make it work on BCD8, and new post-processing rules had to be designed to avoid false positive matches. Similar issues apply to ML models trained on one technology and applied to a different one. Similar to other domains, possible directions to address this issue for ML-based components are domain adaptation and transfer learning [125].

Scalability The main practical limitation of many of the algorithms implemented in the AMBEATion flow is their limited scalability to large designs with hundreds of thousands of devices. Scalability has been addressed in digital design for years, and many of the same solutions (hierarchical placement, parallelization, etc) can be applied on AMS too. However, there are also some peculiarities. For example, the VF2 algorithm for topology recognition scales extremely well if it

is applied independently, and possibly in parallel, to hierarchical blocks of the netlist (most of which correspond to small bipartite graphs). Conversely, it scales poorly on large flattened netlists. However, the hierarchical approach cannot identify topologies spread across multiple sub-circuit blocks, thus it requires designers to fully trust the goodness of their human-made hierarchy. The RGCN approach, conversely, executes fast even on flat netlists. In this sense, here and in many other parts of the flow, ML can be seen more as a way to improve performance by means of computational approximation, rather than a way to solve otherwise unsolvable problems.

Bibliography

[1] Morandi, O.; Schürrer, F. "Wigner model for quantum transport in graphene". *J. Phys. A Math. Theor.* 2011, 44, 265301.

[2] Muscato, O.;Wagner,W. "A class of stochastic algorithms for theWigner equation". *SIAM J. Sci. Comp.* 2016, 38, A1483–A1507.

[3] Querlioz, D.; Dollfus, P. "The Wigner Monte Carlo Method for Nanoelectronic Devices"; *ISTE Wiley: London, UK*, 2010.

[4] Jacoboni, C." Theory of Electron Transport in Semiconductors"; *Springer: Berlin/Heidelberg*, Germany, 2013.

[5] N. Ashcroft, and N. Mermin, Solid State Physics, Holt-Saunders, (1976).

[6] Reed, M., & Simon, B. (1978). IV: Analysis of Operators (Vol. 4). *Elsevier*.

[7] Jüngel, A. "Transport Equations for Semiconductors"; *Springer: Berlin/Heidelberg*, Germany, 2009.

[8] Mascali, G., Romano, V.:"A hierarchy of macroscopic models for phonon transport in graphene". *Physica A*, 548 (2020) 124489. doi: https://doi.org/10.1016/j.physa.2020.124489.

[9] Romano, V. "Quantum corrections to the semiclassical hydrodynamical model of semiconductors based on the maximum entropy principle". *J. Math. Phys.* 2007, 48, 123504.

[10] Luca, L., Romano, V.: "Comparing linear and nonlinear hydrodynamical models for charge transport in graphene based on the Maximum Entropy Principle". *International Journal of Non-Linear Mechanics*, Volume 104, pp. 39-58 (2018) doi:10.1016/j.ijnonlinmec.2018.01.010.

[11] H Weyl, 2 Phys 46 (1927) 1-33; H Weyl, The Theory of Groups and Quantum Mechanics (Dover, New York, 1931)

[12] Quantum Mechanics in Phase Space, An Overview with Selected Papers (2005) World Scientific Pub Co

[13] Hall, B. C.: Quantum theory for Mathematicians, *Springer* (2013).

[14] L.D. Faddeev, O.A. Yakubovskii, Lectures on Quantum Mechanics for Mathematics Students, American Mathematical Society, (2009).

[15] Folland, G. B.: "Harmonic Analysis in Phase Space", *Princeton University Press* (1989).

[16] L.D., Landau, E.M., Lifschitz. Statistical Physics, part 1, vol 5. Pergamon Press, Oxford (1980).

[17] V.D. Camiola, G. Mascali, V. Romano. Charge Transport in Low Dimensional Semiconductor Structures, Springer, (2020). Berlin Heidelberg 2009), DOI 10.1007/978-3-540-89526-8

[18] D. Chandler, Introduction to Modern Statistical Mechanics, Oxford University Press, 1944.

[19] Mikhail I. Katsnelson - Graphene Carbon in Two Dimensions, Cambridge University Press (2012).

[20] Coco, M., Romano, V.: "Simulation of Electron-Phonon Coupling and Heating Dynamics in Suspended Monolayer Graphene Including All the Phonon Branches", *J. Heat Transfer* **140** 092404-1 (2018).

[21] Sellitto, A., Cimmelli, A., Jou, D.: "Mesoscopic theories of heat transport in nanosystems", *Springer*, (2016).

[22] Srivastava, G. P.: "The Physics of Phonons", *Taylor and Francis* (1990).

[23] E. T. Jaynes, "Information Theory and Statistical Mechanics.II", *Phys. Rev.* **108**, 171-190 (1957).

[24] E. T. Jaynes, "Information Theory and Statistical Mechanics", *Phys. Rev.* **106**, 620-630 (1957).

[25] Degond, P. and Ringhofer, C.: "Quantum Moment Hydrodynamics and the Entropy Principle". *Journal of Statistical Physics*, Vol. 112, Nos. 3/4, 587-628 (2003).

[26] Degond, P., Méhats, F., Ringhofer, C.: "Quantum Energy-Transport and Drift-Diffusion Models". *Journal of Statistical Physics*, Vol. 118, Nos. 3/4, 625-667 (2005).

[27] Luca, L., Romano, V.: "Quantum corrected hydrodynamic models for charge transport in graphene". *Annals of Physics*, Volume 406, pp. 30-53 (2019) doi:10.1016/j.aop.2019.03.018.

[28] Barletti, L.: "Hydrodynamic equations for electrons in graphene obtained from the maximum entropy principle", *J. Math. Phys.*, 55, 083303, 21 pp (2014).

[29] Barletti, L., Cintolesi, C.: "Derivation of Isothermal Quantum Fluid Equations with Fermi-Dirac and Bose-Einstein Statistics". *J Stat Phys* 148,353–386 (2012). doi: 10.1007/s10955-012-0535-5.

[30] Mascali, G., Romano, V.:"Charge Transport In Graphene Including Thermal Effects". *SIAM J. APPL. MATH*, Vol. 77, No. 2, pp. 593-613, (2017) Society for Industrial and Applied Mathematics. doi: 10.1137/15M1052573.

[31] Camiola, V.D., Romano, V., Vitanza G.: "Wigner Equations for Phonons Transport and Quantum Heat Flux ". *J. of Nonlinear Science*. 2024, 34:10.

[32] Frommlet, F., Markowich, P., Ringhofer, C.: "A Wigner function Approach to Phonon Scattering", *VLSI Design* **9** (4) 339-350 (1999).

[33] Vallabhaneni, A. K., Singh, D., Bao, H., Murthy, J., and XiuRuan, X.: "Reliability of Raman Measurements of Thermal Conductivity of Single-Layer Graphene Due to Selective Electron-Phonon Coupling: A First-Principles Study," *Phys. Rev B* **93**: 125432 (2016).

[34] Mascali, G.: "Exploitation of the Maximum Entropy Principle in the Study of Thermal Conductivity of Silicon, Germanium and Graphene", *Energies* **15**: 4718. https:// doi.org/10.3390/en15134718 (2022).

[35] Mascali, G.: "Some electric, thermal and thermoelectric properties of suspended monolayer graphene", *SIAM J. on Appl. Math*, **83(2)**: 835 (2023).

[36] Junk, M.: "Domain of definition of Levermore's five moment system, *J. Stat. Physics* **93** 1143-1167 (1998).

[37] Levermore, C.D.: "Moment closure hierarchies for kinetic theories", *J. Stat. Phys.* **83**: 1021–1065 (1996).

[38] Camiola, V.D., Nastasi, G., Romano, V., Vitanza, G. (2022), "Optimized Hydrodynamical Model for Charge Transport in Graphene" In: Ehrhardt, M., Günther, M. (eds) Progress in Industrial Mathematics at ECMI 2021. ECMI 2021. Mathematics in Industry(), vol 39. Springer, Cham. https://doi.org/10.1007/978-3-031-11818-0_37

[39] Camiola, V.D., Romano, V.:" Hydrodynamical Model for Charge Transport in Graphene". *J Stat Phys 157*, 1114–1137 (2014). doi:10.1007/s10955-014-1102-z.

[40] Luca, L., Romano, V.: "Hydrodynamical models for charge transport in graphene based on the Maximum Entropy Principle: the case of moments based on energy powers". *Atti della Accademia Peloritana dei Pericolanti - Classe di Scienze Fisiche, Matematiche e Naturali*, [S.l.], p. A5, (2018) doi: 10.1478/AAPP.96S1A5.

[41] Luca, L., Mascali, G., Nastasi, G., Romano, V.: "Comparing Kinetic and MEP Model of Charge Transport in Graphene", *Journal of Computational and Theoretical Transport*, Volume 49, Issue 7 (2020) doi: 10.1080/23324309.2020.1822870.

[42] Castro Neto, A. H., Geim, A. K., Guinea, F., Novoselov, K. S., Peres, N. M. R.: "The electronic properties of graphene", *Rev. Mod. Phys.*, Vol. 81, pp. 109–162 (2009).

[43] Coco, M., Majorana, A., Romano, V.: "Cross validation of discontinuous Galerkin method and Monte Carlo simulations of charge transport in graphene on substrate". *Ricerche mat 66*, 201–220 (2017) doi: 10.1007/s11587-016-0298-4.

[44] Hwang, E. H., Das Sarma, S.: "Acoustic phonon scattering limited carrier mobility in two-dimensional extrinsic graphene", *Phys. Rev. B*, Volume 77, 115449 (2008).

[45] Majorana, A., Nastasi, G., Romano,V.: "Simulation of Bipolar Charge Transport in Graphene by Using a Discontinuous Galerkin Method". *Commun. Comput. Phys.*, 26 (2019), pp. 114-134. doi: 10.4208/cicp.OA-2018-0052.

[46] MATLAB, 2021. version 9.10.0 (R2021a), Natick, Massachusetts: The MathWorks Inc.

[47] Romano, V., Majorana, A., Coco, M.: "DSMC method consistent with the Pauli exclusion principle and comparison with deterministic solutions for charge transport in graphene". *Journal of Computational Physics*, Volume 302, pp. 267-284 (2015), doi: 10.1016/j.jcp.2015.08.047.

[48] Tomadin, A., Brida, D., Cerullo, G., Ferrari, A. C., Polini, M.,: "Nonequilibrium dynamics of photoexcited electrons in graphene: collinear scattering, Auger processes, and the impact of screening', *Phys. Rev. B*, Volume 88, 035430 (2013).

[49] Jou, D., Restuccia, L.: "Non-Equilibrium Thermodynamics of Heat Transport in Superlattices, Graded Systems, and Thermal Metamaterials with Defects", *Entropy*, **25**: 1091. https://doi.org/ 10.3390/e25071091 (2023).

[50] Mounet, N., and Marzari, N.: "First-Principles Determination of the Structural, Vibrational, and Thermodynamical Properties of Diamond, Graphite, and Derivatives". *Phys. Rev. B* , **71**(20), 205214 (2005).

[51] Nika, D. L., and Balandin, A. A.: "Two-Dimensional Phonon Transport in Graphene". *J. Phys.: Condens. Matter*, **24** (23), p. 233203 (2012).

[52] Pop, E., Varshney, V., and Roy, A. K.: "Thermal Properties of Graphene: Fundamentals and Applications". *MRS Bull.*, **37** (12), p. 1273 (2012).

[53] Nier, F.: "A variational formulation of Schrödinger-Poisson systems in dimension d $\leq$ 3", *Comm. in Partial Differential equations* **18**:7-8 1125-1147.

[54] A. El Ayyadi, A. Jüngel, Semiconductor Simulations Using a Coupled Quantum Drift-Diffusion Schrödinger-Poisson Model, SIAM J. Appl. Math., **66** 2 (2005), 554-72. http://www.jstor.org/stable/4096127.

[55] V. Romano, M. Torrisi, R. Tracinà, Approximate solutions to the quantum drift-diffusion model of semiconductors, J. Math. Phys., **48** (2007), 023501.

[56] O. Muscato, Wigner ensemble Monte Carlo simulation without splitting error of a GaAs resonant tunneling diode, J. Comput. Electron., **20** (2021), 2062–2069.

[57] M. Nedjalkov, H. Kosina, S. Selberherr, C. Ringhofer, D.K. Ferry, Unified particle approach to Wigner-Boltzmann transport in small semiconductor devices, Phys. Rev. B, **70** (2004), 115–319.

[58] Muscato, O., Nastasi, G., Romano, V., Vitanza, G., (2024), "Optimized quantum drift diffusion model for a resonant tunneling diode", Journal of Non-Equilibrium Thermodynamics, 2024. https://doi.org/10.1515/jnet-2023-0059.

[59] J. P. Sun, G. I. Haddad, P. Mazumder and J. N. Schulman, Resonant tunneling diodes: models and properties in: Proceedings of the IEEE, April 1998 **86**(4), 641-660.

[60] L. Yang, Y. Hao, Q. Yao, J. Zhang, Improved negative differential mobility model of GaN and AlGaN for a terahertz Gunn diode, IEEE Trans. Electron Devices, **58** (2011), 1076–1083.

[61] P. Degond, S. Gallego, F. Méhats, An entropic Quantum Drift-Diffusion model for electron transport in resonant tunneling diodes, J. Comput. Phys. (2007), 226-249.

[62] S. Micheletti, R. Sacco, P. Simioni, Numerical Simulation of Resonant Tunneling Diodes with a Quantum Drift Diffusion Model, In: Scientific Computing in Electrical Engineering. Mathematics in Industry, **4** (2004), Springer, Berlin, Heidelberg. https://doi.org/10.1007/978-3-642-55872-6 34

[63] L. Barletti, G. Nastasi, C. Negulescu, V. Romano, Mathematical modelling of charge transport in graphene heterojunctions, Kinetic and Related Models, **14** (2021), 407-427.

[64] O. Muscato, A benchmark study of the Signed-particle Monte Carlo algorithm for the Wigner equation, Commun. Appl. Ind. Math, **8** (1) (2017), 237–250 DOI: 10.1515/caim-2017-0012.

[65] L. Shifren, C. Ringhofer, D. K. Ferry, A Wigner function-based quantum ensemble Monte Carlo study of a resonant tunneling diode, IEEE Trans. Electron Devices, **50**(3) (2003), pp. 769-773.

[66] D. Querlioz, P. Dollfus, V. N. Do, A. Bournel, V. L. Nguyen, An improved Wigner Monte-Carlo technique for the self-consistent simulation of RTDs, J. Comput. Electron. **5** (2006), 443-446, DOI 10.1007/s10825-006-0044-3.

[67] M. Lundstrom, Fundamentals of Carrier Transport. Cambridge Univ. press, Cambridge (2000).

[68] M. Nedjalkov, H. Kosina, S. Selberherr, Ringhofer, D. K. Ferry, Unified particle approach to Wigner-Boltzmann transport in small semiconductor devices, Phys. Rev. B, (2004), **70**, 115319.

[69] A. Jüngel, Quasi-hydrodynamic Semiconductor Equations. Bikhäuser, Basel (2001).

[70] Pinnau, R. (2003, March). *A Scharfetter-Gummel type discretization of the quantum drift diffusion model*. In PAMM: Proceedings in Applied Mathematics and Mechanics (Vol. 2, No. 1, pp. 37-40). Berlin: WILEY-VCH Verlag.

[71] G. Nastasi, V. Romano, A full coupled drift-diffusion-Poisson simulation of a GFET, Commun Nonlinear Sci Numer,**87** (2020), 105-300, https://doi.org/10.1016/j.cnsns.2020.105300.

[72] Muscato, O., Nastasi, G., Romano, V., Vitanza, G., (2024), "Optimized quantum drift-diffusion model for a resonant tunneling diode" (under review)

[73] J. Kennedy, R. Eberhart, Particle Swarm Optimization, Proceedings of the IEEE International Conference on Neural Networks. Perth, Australia, 1995, pp. 1942–1945.

[74] E. Mezura-Montes, C. A. Coello Coello, Constraint-handling in nature-inspired numerical optimization: Past, present and future, Swarm and Evolutionary Computation, 173–194 (2011).

[75] M. E. Pedersen, Good Parameters for Particle Swarm Optimization, Luxembourg: Hvass Laboratories, 2010.

[76] J. A. Nelder, R. Mead, A Simplex Method for Function Minimization, The Computer Journal, **7**, 308–313, (1965).

[77] J. C. Lagarias, J. A. Reeds, M. H. Wright, P. E. Wright, Convergence Properties of the Nelder-Mead Simplex Method in Low Dimensions, SIAM Journal of Optimization, **9**(1), 112–147 (1998).

[78] MATLAB, 2021. version 9.10.0 (R2021a), Natick, Massachusetts: The MathWorks Inc.

[79] F. Calleri, G. Nastasi, and V. Romano, "Continuous-time stochastic processes for the spread of COVID-19 disease simulated via a Monte Carlo approach and comparison with deterministic models", *Journal of Mathematical Biology*, 83, 34 (2021).

[80] Nastasi, G.; Perrone, C.; Taffara, S.; Vitanza, G. "A Time-Delayed Deterministic Model for the Spread of COVID-19 with Calibration on a Real Dataset" Mathematics 2022, 10, 661. https://doi.org/10.3390/math10040661

[81] P. Zhou, X. Yang, X.-G. Wang, B. Hu, L. Zhang, W. Zhang, H.-R. Si, Y. Zhu, B. Li, C.-L. Huang, H.-D. Chen, J. Chen, Y. Luo, H. Guo, R.-D. Jiang, M.-Q. Liu, Y. Chen, X.-R. Shen, and X. Wang, "A pneumonia outbreak associated with a new Coronavirus of probable bat origin", *Nature*, vol. 579, pp. 270–273 (2020).

[82] G. Giordano, F. Blanchini, R. Bruno, P. Colaneri, A. D. Filippo, A. D. D. Matteo, and M. Colaneri, "Modelling the COVID-19 epidemic and implementation of population-wide interventions in Italy", *Nature Medicine*, vol. 26, pp. 855–860 (2020).

[83] F. Brauer, "Mathematical epidemiology: Past, present, and future", *Infectious Disease Modelling*, vol. 2, no. 2, pp. 113–127 (2017).

[84] S. Ansumali, S. Kaushal, A. Kumar, M. K. Prakash, M. Vidyasagar, "Modelling a pandemic with asymptomatic patients, impact of lockdown

and herd immunity, with applications to SARS-CoV-2", *Annual Reviews in Control*, 50, pp. 432–447 (2020).

[85] G. C. Calafiore, C. Novara, C. Possieri, "A time-varying SIRD model for the COVID-19 contagion in Italy", *Annual Reviews in Control*, 50, pp. 361–372 (2020).

[86] Y. Zhang, C. You, Z. Cai, J. Sun, W. Hu, X.-H. Zhou, "Prediction of the COVID-19 outbreak in China based on a new stochastic dynamic model", Scientific Reports, 10, 21522 (2020).

[87] D. Faranda, T. Alberti, "Modeling the second wave of COVID-19 infections in France and Italy via a stochastic SEIR model", *Chaos* 30, 111101 (2020).

[88] F.A. Rihan, H. J. Alsakaji, C. Rajivganthi, "Stochastic SIRC epidemic model with time-delay for COVID-19", *Advances in Difference Equations*, 2020, 502 (2020).

[89] F. Bagarello, F. Gargano, F. Roccati, "Modeling epidemics through ladder operators", *Chaos, Solitons and Fractals*, 140, 110193 (2020).

[90] R. Beneduci, E. Bilotta, P. Pantano, "A unifying nonlinear probabilistic epidemic model in space and time", *Scientific Reports*, 11, 13860 (2021).

[91] Pei, L.; Zhang, M. Long-term predictions of current confirmed and dead cases of COVID-19 in China by the non-autonomous delayed epidemic models. Cogn. Neurodynamics **2021**, 16, 229–238. https://doi.org/10.1007/s11571-021-09701-1.

[92] Pei, L.; Zhang, M. Long-Term Predictions of COVID-19 in Some Countries by the SIRD Model.

[93] D. E. Guidotti, D. Ardia, "COVID-19 data hub", *Journal of Open Source Software 5(51):2376 (2020).*

[94] Usherwood, T.; LaJoie, Z.; Srivastava, V. A model and predictions for COVID-19 considering population behavior and vaccination.Sci. Rep. **2021**, 11, 12051. https://doi.org/10.1038/s41598-021-91514-7.

[95] W. O. Kermack, A. Mckendrick, "A contribution to the mathematical theory of epidemics", *Proceedings of The Royal Society A: Mathematical, Physical and Engineering Sciences*, vol. 115, pp. 700–721 (1927).

[96] I. Cooper, A. Mondal, and C. G. Antonopoulos, "A SIR model assumption for the spread of COVID-19 in different communities", *Chaos, Solitons and Fractals*, vol. 139, p. 110057 (2020).

[97] World Health Organization, Transmission of SARS-CoV-2: implications for infection prevention precautions, Scientific brief, 9 July 2020, WHO Reference Number: WHO/2019-nCoV/Sci_Brief/Transmission_modes/2020.3

[98] World Health Organization, Criteria for releasing COVID-19 patients from isolation, Scientific brief, 17 June 2020, WHO Reference Number: WHO/2019-nCoV/Sci_Brief/Discharge_From_Isolation/2020.1

[99] Richard, J.-P. Time-delay systems: An overview of some recent advances and open problems. Automatica **2003**, 39, 1667–1694. https://doi.org/10.1016/s0005-1098(03)00167-5.

[100] Kiss, G.; Lessard, J.-P. Computational fixed-point theory for differential delayequations with multiple time lags. J. Differ. Equ. **2012**, 252, 3093–3115.

[101] MATLAB, 2021. 9.11.0.1809720 (R2021b); The MathWorks Inc.: Natick, MA, USA, 2021.

[102] Lagarias, J.C.; Reeds, J.A.; Wright, M.H.; Wright, P.E. Convergence Properties of the Nelder—Mead Simplex Method in Low Dimensions. SIAM J. Optim. **1998**, 9, 112–147. https://doi.org/10.1137/s1052623496303470.

[103] Contreras, S.; Villavicencio, H.A.; Medina-Ortiz, D.; Saavedra, C.P. Olivera-Nappa Álvaro Real-Time Estimation of Rt for Supporting Public-Health Policies Against COVID-19. Front. Public Heal. **2020**, 8, 556689. https://doi.org/10.3389/fpubh.2020.556689.

[104] G. D. Micheli, Synthesis and Optimization of Digital Circuits. McGraw-Hill Higher Education, 1994.

[105] E. Malavasi et al., "Automation of ic layout with analog constraints," IEEE TCAD, vol. 15, no. 8, pp. 923–942, 1996.

[106] K. Kunal et al., "ALIGN: Open-Source Analog Layout Automation from the Ground Up," in 56th DAC, 2019.

[107] B. Xu et al., "MAGICAL: Toward Fully Automated Analog IC Layout Leveraging Human and Machine Intelligence: Invited Paper," in 2019 IEEE/ACM ICCAD, 2019, pp. 1–8.

[108] M. P.-H. Lin et al., "Recent research development and new challenges in analog layout synthesis," in ASP-DAC, 2016, pp. 617–622.

[109] J. Scheible and J. Lienig, "Automation of analog ic layout: Challenges and solutions," in ISPD, 2015, p. 33–40.

[110] A. Venkatachar, "Confluence of ai/ml with eda and software engineer- ing," in ISQED, 2021, pp. 13–15.

[111] A. Mirhoseini et al., "A graph placement methodology for fast chip design," Nature, vol. 594, pp. 207 – 212, 2021.

[112] B. Nikoli'c, "Ml for analog design: Good progress, but more to do," in ACM/IEEE MLCAD, 2022, pp. 53–54.

[113] K. Kunal et al., "GANA: Graph Convolutional Network Based Auto- mated Netlist Annotation for Analog Circuits," in DATE, 2020, pp. 55– 60.

[114] L. Cordella et al., "A (sub)graph isomorphism algorithm for matching large graphs," IEEE TPAMI, vol. 26, no. 10, pp. 1367–1372, 2004.

[115] A. Teliti, "Graph neural networks for topology recognition of ams integrated circuits," Master thesis, Politecnico di Torino, 2023.

[116] R. Arora et al., "Virtuoso express pcells for better interoperability and performance on oa," CDNLive! India 2007, 2007.

[117] O. Z. Maimon and L. Rokach, Data mining with decision trees: theory and applications. World scientific, 2014, vol. 81.

[118] Q. Ma et al., "Simultaneous handling of symmetry, common centroid, and general placement constraints," IEEE TCAD, vol. 30, no. 1, pp. 85–95, 2010.

[119] Y. Li et al., "Exploring a machine learning approach to performance driven analog ic placement," in ISVLSI. IEEE, 2020, pp. 24–29.

[120] B. Xu et al., "Device layer-aware analytical placement for analog circuits," in ISPD, 2019, pp. 19–26.

[121] Y. Lin et al., "Are analytical techniques worthwhile for analog ic place- ment?" in 2022. IEEE, 2022, pp. 154–159.

[122] J.-M. Hsu and Y.-W. Chang, "A reusable methodology for non-slicing floorplanning," in ASPCAS, vol. 1, 2004, pp. 165–168 vol.1.

[123] D. P. Kingma and J. Ba, "Adam: A method for stochastic optimization," 2017.

[124] J. Tremblay et al., "Training deep networks with synthetic data: Bridging the reality gap by domain randomization," in CVPR, June 2018.

[125] W. M. Kouw and M. Loog, "An introduction to domain adaptation and transfer learning," arXiv:1812.11806, 2018.